

**DEVELOPMENT OF A NOVEL CO-CULTURE BASED *IN VITRO* MODEL  
SYSTEM TO STUDY THE WOUND HEALING PROCESS**

Submitted to the College of Graduate Studies and Research in partial fulfillment of the

requirements for the degree of

**Doctor of Philosophy**

in the

Department of Anatomy and Cell Biology, College of Medicine,

University of Saskatchewan, Saskatoon

By

**SURAJ ABRAHAM**

© Copyright Suraj Abraham, April 2010. All rights reserved.

## PERMISSION TO USE

In presenting this thesis in partial fulfillment of the requirements for a Doctor of Philosophy degree from the University of Saskatchewan, I agree that the libraries of this university may make it freely available for inspection. I further agree that permission for copying of this thesis in any manner, in whole or in part, for scholarly purposes may be granted by professors who supervised my thesis work or, in their absence, by the Head of the Department or the Dean of the College in which my thesis work was done. It is also understood that any copying or publication or use of this thesis or parts thereof for financial gain shall not be allowed without my written permission. It is also understood that due recognition shall be given to me and to the University of Saskatchewan in any scholarly use which may be made of any materials in my thesis.

Requests for permission to copy or to make other use of material in this thesis in whole or part should be addressed to:

Head of the Department of Anatomy and Cell Biology  
University of Saskatchewan, 107 Wiggins Road  
Saskatoon, Saskatchewan S7N 5E5  
CANADA

## ABSTRACT

Drug development research on wound repair is challenging and inefficient due to the complex nature of wound healing and scarring processes and the limitations of available *in vitro* or *in vivo* models used for preclinical drug testing. Many patients who undergo elective back surgery develop post-surgical complications resulting from excess peridural scarring in and around the site of operation. We tested the effects of two anti-inflammatory compounds, quercetin and L-2-oxothiazolidine-4-carboxylate (OTC), in ameliorating peridural scar formation following spinal laminectomy surgery in laboratory rats. Western blot and immunocytochemical analyses indicated that the peridural scar tissue contained MyoD-positive myoblast cells and expressed prolyl-4-hydroxylase (P4H), a fibroblast marker. Treatment with 1 mM OTC reduced activation of ERK1/2 and p38 mitogen-activated protein kinases (MAPK) at 21 days post-surgery suggesting potential anti-scarring mechanism. However, large animal to animal variation in the expression levels of collagen biosynthesis markers made it difficult to demonstrate any efficacy of quercetin or OTC in reducing peridural scar formation. The shortcomings of this live animal approach led us to develop a novel three-dimensional (3-D) *in vitro* wound repair model for evaluating quercetin and OTC effects. High-density “micromass” co-cultures seeded at a 1:3 ratio of FR 3T3 fibroblast cells and L8 myoblast cells formed 3-D microtissues *in vitro* that expressed MyoD, P4H, and  $\alpha$ -smooth muscle actin. The micromass tissue layer remained adherent to the culture plate when inflicted with a single laceration injury, which allowed monitoring of cell migration into the wound site. Wounded cultures were treated with quercetin, OTC and other agents (TGF- $\beta$ 1, mitomycin, p38 inhibitor SB202190, ERK inhibitor PD184352) to determine their effects on collagen accumulation, wound closure rates, MAPK activation, and gene transcript expression. Both OTC and quercetin treatments reduced collagen biosynthesis in dose-dependent manner. In addition, 1.5 mM OTC accelerated wound closure and significantly reduced p38 MAPK activation without affecting ERK1/2. In contrast, 40  $\mu$ M quercetin delayed wound closure in micromass co-cultures and reduced ERK1/2 activation. Our *in vitro* findings suggest that OTC might have potential as an anti-scarring agent. Importantly, our novel micromass co-culture system shows promise as an improved 3-D scaffold-free *in vitro* model for use in preclinical drug development research.

## ACKNOWLEDGMENTS

I am thankful to my supervisor Prof. William M Kulyk, who provided the necessary guidance and support in my PhD research work. His critical thoughts and constructive criticisms were valuable in preparing this thesis.

I am grateful to my committee members, Profs. Benjamin Rosser (Chair), David Schreyer, Patrick Krone, Adel Mohamed and Baljit Singh (Cognate) who found time in their busy schedules, and provided their scientific insights. I would like to thank Prof. Bernhard Juurlink for providing scientific input and guidance during the period of my research work. I also wish to acknowledge the assistance of our research collaborators, Prof. Kathleen Gough, Richard Wiens and Margaret Rak at the University of Manitoba. I am especially grateful for the opportunity to learn about synchrotron FTIR spectromicroscopy at Dr. Gough's laboratory in Winnipeg.

I must thank Dr. Anne Grahame and Dr. Benoj Varghese for providing their valuable input in critiquing and proof-reading this thesis. I fondly remember my former colleagues, Dr. Brent Bobick and Layne Myhre, for their help and support during the first two years of my PhD studies. I would like to thank my fellow graduate student, Nicole Cox, for providing data pertaining to inflammation aspects of this collaborative project. I wish to thank Dr. Mohsen Basiri, Dr. Jerry Davis, Dr. Hortense Nsoh Tabien, Dr. Rasheed Bani Hammad and Zachery Belak for providing necessary advice and technical information. I would also like to thank many other faculty and staff members of the Department of Anatomy and Cell Biology who have provided necessary help in my graduate studies.

I must thank my beloved wife, Binzy, for her sacrifices, moral support, and encouragement. My appreciation for the love and support of our parents and family back in India and Australia cannot be expressed in words.

I must thank the Natural Sciences Engineering Research Council's Collaborative Health Research Programme (NSERC-CHRP), the College of Medicine, the College of Graduate Studies & Research, and the Department of Anatomy & Cell Biology for their financial support during the period of my PhD research.

Last but not the least; I thank Almighty Lord for providing me the knowledge and opportunity to explore the mysteries of life through this research.

## TABLE OF CONTENTS

PERMISSION TO USE.....	i
ABSTRACT.....	ii
ACKNOWLEDGEMENTS.....	iii
TABLE OF CONTENTS.....	iv
LIST OF TABLES.....	xiii
LIST OF FIGURES.....	xiv
LIST OF ABBREVIATIONS.....	xx
<b>CHAPTER 1. INTRODUCTION.....</b>	<b>1</b>
<b>CHAPTER 2. REVIEW OF PERTINENT LITERATURE.....</b>	<b>4</b>
2.1 Current understanding of the wound healing process.....	4
2.1.1 Types of wound healing response following injury: normal and pathological.....	4
2.1.1.1 Regeneration.....	5
2.1.1.2 Normal Repair.....	6
2.1.1.2.1 Phase-I: Inflammation phase.....	6
2.1.1.2.2 Phase-II: Proliferation or repair phase.....	9
2.1.1.2.3 Phase-III: Tissue remodeling phase.....	11
2.1.1.3 Deficient healing and chronic ulceration.....	13
2.1.1.4 Excessive healing and fibrosis-keloids and hypertrophic scars.....	14
2.2 Skeletal muscle injury and repair processes.....	16
2.2.1 Phases in skeletal muscle healing.....	19
2.2.1.1 Degeneration of the injured muscle fibres and subsequent inflammation.....	19
2.2.1.1.1 Role of neutrophils in the skeletal muscle repair.....	22

2.2.1.1.2	Role of monocytes and macrophages in skeletal muscle repair.....	23
2.2.1.2	Muscle regeneration and development of fibrosis.....	24
2.3	Biomolecules implicated in tissue repair process.....	26
2.3.1	Role of collagen and prolyl-4-hydroxylase in tissue repair.....	27
2.3.2	Role of fibronectin in tissue repair.....	29
2.3.3	Role of hsp-47 in tissue repair.....	30
2.3.4	Role of hyaluronan in tissue repair.....	31
2.3.5	Role of Vascular endothelial growth factor (VEGF) in tissue repair.....	33
2.3.6	Role of TGF- $\beta$ s in tissue repair.....	34
2.3.7	Role of ERK and p38 MAPK signaling in tissue repair.....	36
2.4	Pharmacotherapeutic approaches in scar reduction research.....	39
2.4.1	Antioxidants and anti-inflammatory molecules.....	41
2.4.1.1.	Quercetin.....	42
2.4.1.2 .	L-2-Oxothiazolidine-4-carboxylate (OTC).....	45
2.5	Experimental models for wound healing studies.....	48
2.5.1.	<i>In vivo</i> models for wound research.....	52
2.5.1.1.	Animal models.....	52
2.5.2.	<i>In vitro</i> models for wound research.....	55
2.6.	Use of co-culture systems in developing functional tissue models <i>in vitro</i> .....	58
2.7.	Micromass culture technology.....	61

2.7.1	Micromass co-culture technology- Potential for <i>in vitro</i> tissue regeneration and drug development research.....	65
2.8.	Experimental objectives of this PhD thesis project.....	66
<b>CHAPTER 3.</b>	<b>MATERIALS &amp; METHODS.....</b>	<b>68</b>
3.1	<i>In vivo</i> studies using a rat spinal laminectomy model.....	68
3.1.1.	Preparation of the animals for spinal laminectomy surgery.....	68
3.1.2	Procedure for spinal laminectomy surgery.....	68
3.1.3	Treatment groups.....	71
3.1.4	Animal perfusion and harvesting of peridural wound and granulation tissue.....	73
3.1.5	Picosirius red- polarization method for histochemical detection of collagen fibril distribution.....	75
3.1.6	Synchrotron FTIR mapping for scar tissue sections.....	77
3.1.7	Total RNA isolation from the scar tissues for mRNA analysis.....	78
3.1.8	RiboGreen RNA quantification assay.....	79
3.1.9	Analysis of gene-specific mRNA transcripts by RNA dot blot and Northern blot hybridization.....	80
3.1.9.1	Primer design & generation of antisense cDNA probes to specific genes of interest using LPCR cloning strategy.....	80
3.1.9.2	Generation of <sup>32</sup> P radio-labeled antisense cDNA probes using LPCR method .....	85
3.1.9.3	Analysis of mRNA transcripts using RNA dot blot analysis.....	87
3.1.10	Analysis of proteins from scar tissue.....	88

3.1.10.1	Tissue preparation for protein analysis.....	88
3.1.10.2	Total protein estimation using filter-paper dye binding assay.....	88
3.1.10.3	SDS-PAGE gel preparation for Western blot analysis.....	90
3.1.10.4	Gel electrophoresis and immunoblotting.....	92
3.1.11	Statistical analysis.....	93
3.2	<i>In vitro</i> studies using micromass co-culture technology.....	96
3.2.1	Cell culture propagation and maintenance.....	96
3.2.2	Preparation of micromass co-cultures.....	97
3.2.3	Wounding the micromass co-cultures.....	98
3.2.4	MTT /Cell viability assay.....	98
3.2.5	Determination of total cellular DNA by fluometric assay.....	100
3.2.6	Histochemistry and Immunostaining.....	100
3.2.6.1	Picrosirius red staining and quantification of total collagen <i>in vitro</i> .....	100
3.2.6.2	Immunostaining for dual phosphorylated p-38, dual phosphorylated ERK 1/2, type I collagen and fibronectin.....	101
3.2.6.3	Actin filament and nuclear staining.....	103
3.2.6.4	Scanning electron microscopy.....	103
3.2.7	DiI and DiO labeling of cells.....	104
3.2.8	Treatment of micromass co-cultures with TGF- $\beta$ 1, Quercetin, L-2-oxothiazolidine-4-carboxylate (OTC), Anisomycin, UO126 and PD 184352.....	105
3.2.9	Gene expression analysis of wounded and unwounded micromass cultures using RT-PCR.....	106
3.2.9.1	Isolation & purification of total RNA from micromass co-cultures.....	106
3.2.9.2	RT-PCR analysis of gene transcript expression.....	107
3.2.10	Western blot analysis for wounded and unwounded micromass co-cultures.....	108

3.2.11	<i>In vitro</i> “micromass” co-culture wound closure assay.....	109
3.2.12	Dual color fluorescent image analysis.....	109
3.2.13	Statistical Analysis.....	112
<b>CHAPTER 4.</b>	<b>RESULTS.....</b>	<b>112</b>
4.1.	Effect of Quercetin and OTC on overall scar formation following experimental spinal laminectomy surgery in rats.....	112
4.2.	Effect of Quercetin and OTC on collagen distribution and biosynthesis in the peridural scar of laminectomized rats.....	118
4.2.1	Correlating Vibrational FTIR spectromicroscopy maps of scar tissue sections with picrosirius red polarized light microscopy images of scar tissue to determine the orientation and distribution of collagen.....	118
4.2.2	Effect of Quercetin and OTC on total collagen distribution in the histological sections of peridural scar tissue of laminectomized rats.....	122
4.2.3	Effect of Quercetin and OTC on extracellular matrix proteins (type I collagen, fibronectin) and markers of collagen biosynthesis (prolyl-4-hydroxylase and heat shock protein (hsp47)).....	126
4.3	Effect of Quercetin and OTC on the expression of potential regulatory molecules such as TGF- $\beta$ 1, TGF- $\beta$ 3, VEGF, ERK and p38 MAPK in the peridural scar tissue homogenates.....	135
4.3.1.	Effect of Quercetin and OTC on TGF- $\beta$ 1 and TGF- $\beta$ 3 mRNA expression levels in 3 day and 21 day scar tissue homogenates..	135
4.3.2.	Effect of Quercetin and OTC on the expression of VEGF protein and myogenic markers in 3 day and 21 day peridural scar tissue.....	139
4.3.3.	Effect of Quercetin and OTC on ERK and p38 MAP kinases expressions in 3 and 21 peridural scar tissue.....	143
4.3.3.1	Effect of Quercetin and OTC on p38 MAPK expression in peridural scar tissue.....	143
4.3.3.2	Effect of Quercetin and OTC on ERK expression in peridural scar tissues.....	145

4.4	Development of a novel co-culture based <i>in vitro</i> wound model to study wound healing process: Method development & validation.....	147
4.4.1.	Introduction.....	147
4.4.1.1.	Method development: Characterization of “micromass” co-culture technology as a 3-D scaffold free <i>in vitro</i> wound repair model..	148
4.4.1.1.1.	Determination of the proportion of L8 myoblast cells and FR 3T3 fibroblast cells that promote micromass adhesion and withstand wounding manipulation.....	148
4.4.1.1.2.	Microtissue formation and the 3-D nature of the micromass co-culture of 1 part rat fibroblast FR 3T3 cell and 3 part L8 myoblast cells.....	151
4.4.1.1.3.	Optimization of the tissue culture media for high density micromass co-culture of 1 part FR 3T3 cells and 3 part L8 myoblast cells.....	158
4.4.1.1.4.	Muscle specific protein expression pattern in unwounded and wounded 1:3 fibroblast and L8 myoblast micromass co-cultures.....	164
4.4.1.1.5.	Specific gene expression profiling in both unwounded and wounded micromass co-cultures of 1 part FR 3T3 fibroblast cells and 3 part L8 myoblast cells.....	167
4.4.1.1.6.	Determination of the rate of wound closure and the effect of cell proliferation on wound closure pattern on <i>in vitro</i> wound repair.....	171
4.4.1.1.7.	Studies on the migratory pattern of rat skeletal L8 myoblast cells and rat fibroblast FR cells in wounded micromass co-cultures.....	175
4.4.1.1.7.1	Effect of exogenous TGF- $\beta$ 1 treatment on skeletal myoblast cells and fibroblast cells in wounded micromass co-cultures of 1:3 FR fibroblast and L8 myoblast cells.....	180
4.4.1.1.8.	Expression of p38 and ERK1/2 mitogen-activated protein kinases in wounded and unwounded micromass co-cultures of 1 part FR 3T3 fibroblast and 3 parts L8 myoblast cells.....	189

4.4.1.1.8.1	Effect of ERK inhibitor, PD18352, on the wound closure in micromass co-culture of 1:3 FR fibroblast and L8 myoblast cells.....	195
4.4.1.1.8.2	Effect of specific p38 MAPK inhibitor, SB202190, on the wound closure in wounded micromass co-culture of 1:3 FR fibroblast and L8 myoblast cells.....	199
4.4.2	Effects of OTC and Quercetin on both unwounded and wounded micromass co-cultures of 1 part FR fibroblast and 3 part L8 myoblast cells.....	203
4.4.2.1	Effects of OTC on collagen biosynthesis and DNA accumulation in the unwounded 1:3 ratio of FR fibroblast and L8 myoblast micromass co-culture.....	203
4.4.2.2	Effects of Quercetin on collagen biosynthesis and DNA accumulation in the unwounded 1:3 ratio of FR fibroblast and L8 myoblast micromass co-culture.....	208
4.4.2.3	Effects of OTC and Quercetin on wound closure in the wounded micromass co-culture of 1 part FR fibroblast and 3 part L8 myoblast cells.....	212
4.4.2.4	Effect of OTC and Quercetin on p38 MAPK and ERK 1/2 activation in wounded micromass co-culture of 1 part FR fibroblast and 3 part L8 myoblast cells.....	216
4.4.2.5	Effect of OTC and quercetin on the genes involved in tissue repair and regeneration within the wounded micromass co-culture of 1 part FR fibroblast and 3 part L8 myoblast cells.....	220
<b>CHAPTER 5.</b>	<b>DISCUSSION.....</b>	<b>225</b>
5.1.	Outcome of the <i>in vivo</i> studies using rat spinal laminectomy model.....	225
5.1.1.	Characterization of the peridural scar tissue indicates presence of myoblastic cells, VEGF protein, hsp-47, P4H and expression of type I and III collagen.....	225
5.1.2.	Systemic administration of OTC and quercetin might reduce cutaneous scar formation and promote bone regrowth within the spinal laminae of the lumbar laminectomized rats.....	228

5.1.3.	Systemic administration of OTC and quercetin showed no significant treatment effects on collagen biosynthesis and/or abundance in the peridural scar tissue from the rat spinal laminectomy model.....	230
5.1.4.	Systemic administration of OTC and quercetin showed inconclusive results as to their treatment effects on TGF- $\beta$ 1 and TGF- $\beta$ 3 expression with the peridural scar tissue from the rat spinal laminectomy model.....	233
5.1.5.	Effects of systemic administration of OTC and quercetin on mitogen-activated protein kinase signaling. OTC reduced both p38 MAPK and ERK activation in 21 day peridural scar tissue.....	234
5.1.6.	Limitations of the spinal laminectomy wound repair model and possible reasons for the large animal to animal variation encountered.....	237
5.2	Outcome of <i>in vitro</i> wound repair studies in a micromass co-culture model.....	240
5.2.1	Micromass cultures established with a seeding ratio of 1 part FR fibroblast and 3 parts L8 myoblast cells form a 3-D “microtissue” that expresses MyoD and fibroblast marker proteins.....	241
5.2.2	Cell proliferation and preferential migration of fibroblast cells towards the wound site in wounded micromass co-cultures.....	244
5.2.3	Endogenous TGF- $\beta$ 3 gene transcript levels were significantly higher as compared to TGF- $\beta$ 1 gene transcripts in both wounded and corresponding unwounded cultures suggesting possible link to <i>in vivo</i> peridural scar tissue.....	247
5.2.4	Gene and protein expression profiling of the wounded and corresponding unwounded micromass co-culture suggests a potential tool for future drug development studies.....	248
5.2.5	Modulation of p38 MAPK and ERK 1/2 signaling pathways has differential effects on <i>in vitro</i> wound closure.....	251
5.3	Quercetin and OTC treatment of wounded micromass co-culture of 1:3 ratio of fibroblast and L8 myoblast cells suggest that they have differential effect on wound closure through their activity on MAPK signaling pathway, and modulating expression patterns of extracellular matrix gene transcripts.....	254

5.4	As compared to quercetin, OTC might have significant potential as an anti-scarring drug through attenuation of p38 and ERK1/2 MAPK signaling mediated by a cytoprotective gene regulatory pathway.....	258
5.5	Conclusions.....	261
5.6	Future directions.....	264
	<b>REFERENCES.....</b>	<b>269</b>
	<b>APPENDIX 1.....</b>	<b>303</b>
	<b>APPENDIX 2.....</b>	<b>309</b>
	<b>APPENDIX 3.....</b>	<b>315</b>
	<b>APPENDIX 4.....</b>	<b>317</b>

<b>LIST OF TABLES</b>	<b>Page</b>
Table.1 a Current <i>in vivo</i> wound model systems available for wound healing research.....	50
Table.1 b Current <i>in vitro</i> wound model systems available for wound healing research.....	51
Table.2 Co-cultures of differentiated skeletal muscle cells with a second differentiated cell type used in tissue engineering studies.....	60
Table.3 Examples of methods reported to have utilized scaffold free cell culture method for reaggregation of cells to form microtissue.....	63-64
Table.4 Synthetic oligonucleotide PCR forward and reverse primer design.....	83
Table.5 Primary antibodies used for Western blotting and immunohistochemistry.....	94-95
Table.6 Total wet weight, RNA yield and protein yield of the scar tissue samples harvested from Saline, OTC and quercetin treated animals.....	116
Table.7 Effect of OTC and quercetin treatment on the relative gene transcript levels in the wounded micromass co-culture.....	224

<b>LIST OF FIGURES</b>		<b>Page</b>
Figure.1	Role of Calcium ion in skeletal muscle repair.....	21
Figure.2	Chemical structure of quercetin and L-2-oxothiazolidine-4-carboxylate.....	43
Figure.3	Location of spinal laminectomy in adult male wistar rat.....	70
Figure.4	Systemic administration of L-2-oxothiazolidine-4-carboxylate (OTC) and quercetin.....	72
Figure.5	Specificity of the cDNA probes developed.....	86
Figure.6	Regression line analysis.....	91
Figure.7	Illustration showing the setting up of micromass co-culture of FR 3T3 fibroblast and L8 myoblast cells based on the modification of Ahrens <i>et al</i> 's method.....	99
Figure.8	Illustration of the regions of the wounded micromass co-culture imaged to determine cell migration pattern at the wound site (red) and the periphery (blue).....	111
Figure.9	Images of cutaneous scar from Saline, OTC and quercetin treated laminectomized rats.....	114
Figure.10	Picrosirius red polarization method showing 21 day scar tissue sections of Saline, OTC and quercetin treated animals.....	119
Figure.11	Correlation of Picrosirius red polarization images with vibrational FTIR spectromicroscopy maps for oriented collagen fibres in 21 day scar tissue regions.....	121
Figure.12	Picrosirius red polarization images showing the corresponding 3 day scar tissue regions of Saline, OTC and quercetin treated animals.....	123
Figure.13	Picrosirius red polarization images showing the corresponding 21 day scar tissue regions of Saline, OTC and quercetin treated animals.....	124
Figure.14	Picrosirius red polarization image analysis using Image J software for total Sirius red stainable collagen area in 3 day and 21 day post-surgical scar tissue sections of animals treated with Saline, OTC and quercetin.....	125

Figure.15	Western blot analysis of peridural scar tissue homogenates from 3 day post-surgical animals showing relative levels of fibronectin, type I collagen, prolyl-4-hydroxylase, heat shock protein-47 and GAPDH following treatment with Saline, OTC and quercetin.....	128
Figure.16	Western blot analysis of peridural scar tissue homogenates from 21 day post-surgical animals showing relative levels of fibronectin, type I collagen, prolyl-4-hydroxylase, heat shock protein-47 and GAPDH following treatment with Saline, OTC and quercetin.....	129
Figure.17	Relative expression levels of type I collagen, prolyl-4-hydroxylase, heat shock protein-47 and fibronectin proteins in 3 day peridural scar tissue homogenate.....	130
Figure.18	Relative expression levels of type I collagen, prolyl-4-hydroxylase, heat shock protein-47 and fibronectin proteins in 21 day peridural scar tissue homogenate.....	131
Figure.19	RNA dot blot autoradiograph showing signal intensity for Col 1( $\alpha$ 2), Col 3( $\alpha$ 1), Col 4( $\alpha$ 1) with respect to GAPDH signals for peridural scar tissues isolated at 3 day and 21 days following spinal laminectomy surgery.....	132
Figure.20	Relative expression levels of collagen 1( $\alpha$ 2), collagen 3( $\alpha$ 1) and collagen 4( $\alpha$ 1) mRNA in 3 day and 21 day peridural scar tissue homogenates...	133
Figure.21	RNA dot blot autoradiograph showing signal intensity for TGF- $\beta$ 1, TGF- $\beta$ 3 and GAPDH mRNAs for peridural scar tissues isolated at 3 day and 21 day following spinal laminectomy surgery.....	136
Figure.22	Relative expression levels of TGF- $\beta$ 1 and TGF- $\beta$ mRNA in 3 day and 21 day peridural scar tissue homogenates.....	137
Figure.23	Western blot analysis of peridural scar tissue homogenates from 3 day and 21 day post-surgical animals showing relative levels of MyHC, MyoD, VEGF and GAPDH following treatment with Saline, OTC and quercetin.....	140
Figure.24	Relative expression levels of VEGF and MyoD protein in 3 day and 21 day peridural scar tissue homogenates.....	141
Figure.25	Western blot analysis for dual phosphorylated p38 mitogen activated protein kinases (MAPK) and total p38 MAPK, in 3 day and 21 day post-surgical scar tissue homogenates obtained from Saline, OTC and quercetin treated animals.....	144

Figure.26	Western blot analysis for dual phosphorylated ERK1/2 and total ERK1/2, in 3 day and 21 day post-surgical scar tissue homogenates obtained from Saline, OTC and quercetin treated animals.....146
Figure.27	Micromass and micromass co-culture of FR 3T3 fibroblast cells and L8 myoblast cells.....149
Figure.28	Determination of the best seeding ration of FR3T3 fibroblast and L8 myoblast cells that could withstand wound manipulation.....150
Figure.29	Scanning electron micrograph of the intact micromass co-culture of 1 part FR 3T3 fibroblast and 3 part L8 myoblast cells.....153
Figure.30	Scanning electron micrograph (SEM) of 5 min and 8 day post-wounded micromass cultures.....154
Figure.31	Picosirius red and Alcian blue (pH 2.5) staining of 4 day wounded and unwounded micromass co-cultures of 1 part FR 3T3 and L8 myoblast cells.....155
Figure.32	Localization pattern of type I collagen and fibronectin in the wounded micromass co-cultures of 1 part FR 3T3 and L8 myoblast cells.....157
Figure.33	Total DNA levels of wounded and corresponding unwounded micromass co-cultures of 1 part FR 3T3 fibroblast and 3 part L8 myoblast cells....159
Figure.34	Metabolic activity of wounded and corresponding unwounded micromass co-cultures of 1 part FR 3T3 fibroblast and 3 part L8 myoblast cells.....160
Figure.35	Optimization of the propagation media that were used for all cell culture experiments involving micromass cultures.....162
Figure.36	Expression pattern of muscle specific proteins and fibroblast specific protein ( $\alpha$ -sma) in micromass cultures of FR fibroblast alone, L8 myoblast alone and 1:3 co-culture of FR fibroblast: L8 myoblast cells.....165
Figure.37	Determination of the effect of wounding on the expression of muscle specific proteins and osteopontin in the wounded 1:3 ratio of FR fibroblast and L8 myoblast micromass co-culture.....166
Figure.38	RT-PCR DNA gels showing relative band intensities for collagen type 1 ( $\alpha$ 2), collagen type 3( $\alpha$ 1), collagen type 4( $\alpha$ 1). hyaluronan synthase 1, hyaluronan synthase 2, hyaluronan synthase 3, RHAMM, CD 44, TGF- $\beta$ 1, TGF- $\beta$ 3, hsp-47 and GAPDH.....169

Figure.39	Gene expression profile of various genes implicated in tissue repair and regeneration.....	170
Figure.40	Wound closure as function of time in micromass co-culture of 1 part FR fibroblast cells and 3 part L8 myoblast cells.....	173
Figure.41	Effect of cell proliferation on the wound closure in the wounded micromass co-culture of 1 part FR 3T3 fibroblast and 3 part L8 myoblast cells.....	174
Figure.42	Distribution and localization of FR fibroblast and L8 myoblast cells in the 3 day post wounded 1:3 ratio of FR fibroblast and L8 myoblast cell micromass co-cultures and corresponding unwounded cultures.....	177
Figure.43	Quantitative analysis of fluorescence intensities of DiI labeled FR fibroblast cell and DiO labeled L8 myoblast cells at the wounded region and peripheral regions of the micromass co-culture.....	178
Figure.44	Presence of DiI labeled FR 3T3 fibroblast cells and DiO labeled L8 myoblast cells at the wound gap and wound edges.....	179
Figure.45	Dose response effects of Transforming growth factor- $\beta$ 1 on the micromass co-culture of 1 part FR 3T3 fibroblast and 3 part L8 myoblast cells.....	183
Figure.46	Dose response effects of Transforming growth factor- $\beta$ 1 on FR 3T3 fibroblast micromass cultures.....	184
Figure.47	Dose response effects of Transforming growth factor- $\beta$ 1 on L8 myoblast micromass cultures.....	185
Figure.48	Effect of TGF- $\beta$ 1 on wound closure in the wounded micromass co-culture of 1 part FR 3T3 and 3 part L8 myoblast cells.....	186
Figure.49	Effect of Transforming growth factor- $\beta$ 1 on wound migration pattern...	187
Figure.50	Migratory pattern of FR 3T3 fibroblast cell and L8 myoblast cells to the wound gap and wound edges following treatment with 0.1 ng/mL TGF- $\beta$ 1.....	188
Figure.51	Effects of Transforming growth factor- $\beta$ 1 on the migratory pattern of myoblast cells and fibroblast cells at the wound site.....	190
Figure.52	Expression of dual phosphorylated ERK1/2 in wounded micromass co-culture and corresponding unwounded micromass co-cultures.....	191

Figure.53	Localization of dual phosphorylated and total ERK1/2 mitogen activated protein kinases in wounded micromass co-culture.....	193
Figure.54	Expression of dual phosphorylated p38 mitogen activated protein kinases (p38 MAPK) in wounded micromass co-culture.....	194
Figure.55	Localization of dual phosphorylated and total p38 mitogen activated protein kinases (p38MAPK) in wounded micromass co-culture.....	196
Figure.56	Western blot analysis to detect total ERK 2 and dual phosphorylated ERK1/2 in the wounded micromass co-culture of 1 part FR 3T3 fibroblast cells and 3 part L8 myoblast cells treated with 2 $\mu$ M PD184352, 10 $\mu$ M SB202190 and 100 ng/mL Anisomycin.....	197
Figure.57	Effect of PD184352 on wound closure pattern in the micromass co-culture of 1 part FR 3T3 fibroblast and 3 part L8 myoblast cells.....	198
Figure.58	Effect of PD184352 on the rate of wound closure in the micromass co-culture of 1 part FR 3T3 fibroblast and 3 part L8 myoblast cells.....	200
Figure.59	Western blot analysis to detect total and dual phosphorylated p38 MAPK on wound closure in the micromass co-culture of 1 part FR 3T3 fibroblast and 3 part L8 myoblast cells treated with 2 $\mu$ M PD184352, 10 $\mu$ M SB202190 and 100 ng/mL Anisomycin.....	201
Figure.60	Effect of SB202190 treatment on the rate of wound closure in the micromass co-culture of 1 part FR 3T3 fibroblast and 3 part L8 myoblast cells.....	202
Figure.61	Effect of OTC on micromass co-culture of 1 part FR 3T3 fibroblast and 3 part L8 myoblast cells.....	205
Figure.62	Effect of OTC on FR 3T3 fibroblast micromass cultures.....	206
Figure.63	Effect of OTC on L8 myoblast micromass cultures.....	207
Figure 64	Effect of quercetin on the micromass co-culture of 1 part FR 3T3 fibroblast and 3 part L8 myoblast cells.....	209
Figure.65	Effect of quercetin on FR 3T3 fibroblast micromass cultures.....	210
Figure.66	Effect of quercetin on L8 myoblast micromass cultures.....	211
Figure.67	Effect of OTC and quercetin on wound closure in the wounded micromass co-culture of 1 part FR 3T3 and 3 part L8 myoblast cells.....	213

Figure.68	Effect of OTC and quercetin on wound closure pattern.....	214
Figure.69	Effect of the mixture of quercetin and OTC on wounded micromass co-culture of 1 part FR 3T3 fibroblast and 3 part L8 myoblast cells.....	215
Figure.70	Effect of OTC and quercetin on the expression of dual phosphorylated p38 MAPK in the 5 min post-wounded micromass co-culture of 1 part FR 3T3 and 3 part L8 myoblast cells.....	218
Figure.71	Effect of OTC and quercetin on the expression of dual phosphorylated ERK 1/2 in the 5 min post-wounded 1 part FR 3T3 fibroblast and 3 part L8 myoblast micromass co-cultures.....	219
Figure.72	RT-PCR DNA agarose gels showing relative band intensities for collagen type 1( $\alpha$ 2), collagen type 3( $\alpha$ 1), collagen type 4( $\alpha$ 1), hyaluronan synthase 1, hyaluronan synthase 2, hyaluronan synthase 3, RHAMM, CD 44, TGF- $\beta$ 1, TGF- $\beta$ 3, hsp-47 and GAPDH in the unwounded and wounded micromass co-cultures treated with and without 1.5 mM OTC and 40 $\mu$ M quercetin.....	222
Figure.73	Effect of quercetin and OTC on the genes involved in tissue repair and regeneration in the wounded micromass co-cultures of 1 part FR fibroblast and 3 part L8 myoblast cells.....	223

## LIST OF ABBREVIATIONS

2-D	Two dimensional
3-D	Three dimensional
8-OH-dG	8-hydroxy-2'-deoxyguanosine
μL	Microliter
μm	Micrometer
μM	Micromolar
ADME	Absorption, distribution, metabolism and excretion
ANOVA	Analysis of variance
ATCC	American type cell culture
ATP	Adenosine triphosphate
<i>b.i.d</i>	<i>bis in die</i> , twice daily
BSA	Bovine serum albumin
bFGF	Basic fibroblast growth factor
bp	Base pairs
cAMP	Cyclic adenosine mono phosphate
CCD	Closed circuit digital
CD	Conserved domain
cDNA	Complementary deoxyribonucleic acid
Cl	Chlorine
cm	Centimeter
CO <sub>2</sub>	Carbon dioxide
Col	Collagen
COX	Cyclooxygenase
Cs-Gel-HA	Chitosan-Gelatin-hyaluronic acid
CTGF	Connective tissue growth factor
CTP	Cytosine triphosphate
d	Day
DNA	Deoxyribonucleic acid

DiI	1,1'-dioctadecyl-3,3',3'-tetramethylindocarbocyanine perchlorate
DiO	3,3'-dioctadecyloxacarboyanine perchlorate
DMSO	Dimethyl Sulphoxide
ECM	Extracellular matrix
EDTA	Ethylene diamine tetra acetic acid
EGF	Epidermal growth factor
ERK	Extracellular signal-regulated kinases
EtBr	Ethidium bromide
FBSS	Failed back surgery syndrome
Fe	Iron
FGF	fibroblast growth factor
FR	Fischer rat
FITC	Fluorescein isothiocyanate
FTIR	Fourier transformed infra red
GAG	Glycosaminoglycan
GAPDH	Glyceraldehyde -3-phosphate dehydrogenase
GGT	Galactosylhydroxyllysyl glucosyl transferase
GSH	Glutathione
h	Hour
H&E	Hematoxylin & Eosin
HAS	Hyaluronan synthase
HB-EGF	Heparin-binding epidermal growth factor
HPMC	Human peritoneal mesothelial cells
Hsp	Heat shock protein
ICH	International Conference on Harmonization
IFN	Interferons
IGF	Insulin-like growth factor
IgG	Immunoglobulin G
IHC	Immunohistochemistry
IL	Interleukin

i.p.	Intraperitoneal
I/R	Ischemic Perfusion
IR	Infrared
JAK	Janus kinase
JNK	C-jun-N-terminal kinase
kb	Kilo base
KCl	Potassium chloride
kDa	Kilo Dalton
kg	Kilogram
L1/L3	Lumbar vertebra 1 / Lumbar vertebra 3
LIF	Leukemia inhibitory factor
MALDI	Matrix-assisted laser desorption ionization
MAPK	Mitogen-activated protein kinase
MCC	Micromass co-culture
MDSC	Muscle-derived stem cells
MgCl <sub>2</sub>	Magnesium chloride
MKK	Mitogen-activated protein kinase kinase
MKP	Mitogen-activated protein kinase phosphatases
MPO	Myeloperoxidase
mg	Milligram
min	Minute
mL	Milliliter
mM	Millimolar
mm	Millimeter
mmol	Millimoles
MMP	Matrix metalloproteinase
mRNA	Messenger RNA
MTT	3-(4,5-Dimethylthiazol-2-yl)-2,5-diphenyltetrazolium bromide
MyHC	Myosin heavy chain
n	Sample size

N	Normal (units)
NaCl	Sodium chloride
NaOH	Sodium hydroxide
ng	Nanogram
NGF	Nerve growth factor
nm	Nanometer
Na	Sodium
NADPH	Nicotinamide adenine dinucleotide phosphate
NCE	New Chemical Entities
NF- $\kappa$ $\beta$	Nuclear factor kappa-beta
NSAID	Non-steroidal anti-inflammatory drugs
OD	Optical density
OPN	Osteopontin
OTC	L-2-oxothiazolidine-4-carboxylate
$^{32}$ P	Radio-active phosphorous
P4H	Prolyl-4-hydroxylase
PA	Polyacrylamide
PAGE	Polyacrylamide gel electrophoresis
PBS	Phosphate buffered saline
PBT	Polybutylene terephthalate
PCR	Polymerase chain reaction
PDEGF	Platelet derived epidermal growth factor
PDGF	Platelet derived growth factor
PEGT	Polyethylene glycol terephthalate
PPARs	Peroxisome proliferators activated receptors
pmol	Picomoles
RHAMM	receptor for hyaluronan mediated motility
RNA	Ribonucleic acid
ROI	Region of interest
rpm	Revolutions per minute
rt-PCR	Reverse transcriptase polymerase chain reaction

SA-beta-Gal	Senescence-associated beta galactosidase
SAPK	Stress-activated protein kinase
Sca	Stem cell antigen
SD	Standard deviation
SDS	Sodium docedyl sulfate
siRNA	Small interfering RNA
SEM	Scanning electron microscopy
SMA	Smooth muscle actin
SOD	Superoxide dismutase
U	Unit
UV	Ultraviolet
TBS	Tris buffered saline
TBST	Tris buffered saline supplemented with tween-20
TE	Tris-EDTA buffer
TGF	Transforming growth factor
TIMP	Tissue inhibitors of metalloproteinases
TNF	Tumor necrosis factor
TTP	Thymidine triphosphate
V	Volt
VEGF	Vascular endothelial growth factor
v/v	Volume to volume
WAF	Wound angiogenesis factor
WB	Western blotting
w/v	weight to volume

## CHAPTER 1. INTRODUCTION

Wound healing is a normal biological response to any type of tissue injury. It is a complex process involving cells, cellular products, and extracellular components that act in concert to restore the structural and functional integrity of the tissue (Lazarus *et al.*, 1994). The normal wound healing response involves a sequence of functionally coordinated events comprised of cell proliferation, synthesis and release of extracellular matrix proteins, production of growth factors, cell-substratum interactions mediated by cell surface receptors, and cytoskeletal reorganizations accompanied by cell motility (Bhalla, 1999). This combination of cellular and molecular interactions usually results in the formation of a transient fibrous scar. The scar tissue formed will have a different texture and be of inferior functional quality compared to the original tissue (Clark, 1996; Diegelmann and Evans, 2004) . For example, scar tissue in the skin does not have sweat glands or hair follicles, and due to reduced skin pigmentation, is more susceptible to UV damage

Excessive scar formation following injury can sometimes lead to pathological complications that have serious medical and cosmetic implications (Clark, 1996). For example, excessive peridural scar formation frequently occurs in human patients recovering from elective spinal surgery. A prolonged fibrotic healing process is triggered in which the hematoma from the surgical act and traumatized paravertebral muscles invade the posterior dural tissue overlying the spinal cord (Hinton *et al.*, 1995; Taylor *et al.*, 2005). The invading fibrous tissue compresses the adjacent nerve roots, which leads to the post-surgical complication known as “failed back surgery syndrome” (FBSS). FBSS is characterized by debilitating back pain and numbness of the lower extremities.

As a result, clinicians and orthopedic surgeons are in need of effective therapeutic modalities to mitigate peridural fibrosis following elective spinal surgery. Anti-scarring drug development research has been directed towards identifying potential cellular mechanisms that can be effectively targeted for the prevention or reduction of fibrosis (Nanney *et al.*, 2006), and also towards the isolation of appropriate pharmacologically active agents that can be safely administered during the post-operative period.

Our current understanding of the wound healing process is predominantly based on the widely studied models of cutaneous wound healing. Moreover, most research on anti-scarring drug therapies has been directed towards cutaneous wound healing rather than skeletal muscle scarring. Although certain mechanisms of wound repair are common to both cutaneous and skeletal muscle healing, there are also important differences in the nature of wound environment and the tissues response to injury. A cutaneous wound is exposed to atmospheric oxygen that plays a crucial role in determining healing outcome, while skeletal muscle repair involves interaction with components of the immune system that may play a vital role in activating satellite cells and muscle derived stem cells (MDSCs). In addition, the interaction of skeletal muscle cells with fibroblasts from surrounding connective tissue may play an important role in the development of muscle fibrosis (Ambrosio *et al.*, 2008; Jankowski *et al.*, 2002; Clark, 1996; Lehto *et al.*, 1985a; Lehto *et al.*, 1985b; Sasse *et al.*, 1981).

The inherent complexities of the wound healing process, in which multiple cell types interact to regenerate normal tissue structure make it difficult to predict the potential efficacy of candidate wound modulatory drugs (Nanney *et al.*, 2006). Thus wound healing based drug discovery and pre-clinical drug screening is an expensive and

time-consuming process. A large number of new chemical entities (NCEs) tested for a range of therapeutic applications fail to reach the market because the NCEs are either unexpectedly toxic or prove to be ineffective during clinical trials. Current practice in drug development studies involves preliminary drug screening and dose optimization based on pre-clinical *in vitro* studies using monolayer cell culture systems as well as *in vivo* live animal models (Gottrup *et al.*, 2000; Nanney *et al.*, 2006). Increased ethical and social concerns about conducting drug research on animals and humans have led to more strictly enforced animal rights legislation and increasingly stringent human clinical trial procedures based on International Conference on Harmonization (ICH) regulations (Garthoff, 2005). This has placed immense pressure on drug development researchers to reduce, as much as possible, their dependence on laboratory animals in early drug screening studies. These concerns along with a desire to reduce the heavy costs involved in the overall drug development process have created a critical need for improved *in vitro* experimental models that better mimic *in vivo* conditions.

Most currently available *in vitro* models for studying the wound healing process utilize monolayer cell culture systems (Gottrup *et al.*, 2000). These have obvious limitations, as a monolayer system cannot mimic cell-cell interactions, cell-matrix associations and cell migration in the three-dimensional (3-D) context of *in vivo* wound repair. Some *in vitro* 3-D model systems are commercially available; however they are expensive and usually employ artificial scaffolds. The synthetic materials that are used in these artificial scaffolds may have immunogenic or toxicological properties that affect cell phenotype, which is undesirable for drug development studies.

The next chapter reviews the complex sequence of cellular changes that lead to wound repair and scar formation, the pharmacotherapeutic approaches to ameliorate this scarring process, and the potential utility of micromass co-culture technology in developing a novel 3-D scaffold-free *in vitro* wound model for drug evaluation studies.

## **CHAPTER 2. REVIEW OF PERTINENT LITERATURE**

### **2.1 Current understanding of the wound healing process**

Wound healing is a natural biological response to any form of tissue trauma (Clark, 1996). The disruption of intact tissue architecture can elicit four distinct types of wound healing response, which may culminate either in complete tissue repair or pathological changes at the site of injury.

#### **2.1.1 Types of wound healing response following injury: normal and pathological**

According to Diegelmann and Evans (2004), the four basic categories of healing response are:

- i.) Regeneration
- ii.) Normal repair
- iii.) Deficient healing/ Chronic ulceration
- iv.) Excessive healing/ Fibrosis

The following sections describe the characteristic features of different wound healing responses.

### 2.1.1.1 Regeneration

Regeneration is an advanced type of wound healing, in which an entire organ or a major portion of a body structure that has been lost due to injury or surgical excision is able to re-grow and restore the original structure with full functionality. Many invertebrate groups (e.g. echinoderms, arthropods, coelenterates, etc.) have extensive abilities for organ regeneration. Among vertebrates, regeneration capacities are highest in the urodele amphibians (salamanders and newts) and some lizard species that are able to regenerate entire limbs, tails and other body parts following amputation. Recent studies in amphibians have highlighted a set of genes that appears to play important roles in regeneration through regulation of cellular plasticity. Three such genes are *Msx1*, *BMP4*, and *Notch1* which encode, respectively, a transcriptional repressor, a signaling ligand, and a signaling cell surface receptor (Poss *et al.*, 2002; Raya *et al.*, 2003; Simon *et al.*, 1995).

Although mammals have a much lower overall regenerative ability compared to lower animal forms, certain mammalian tissues exhibit limited regenerative capacity as individual components within the body. In humans, the liver, epidermis, and to some extent, peripheral nerves, can be partially regenerated after injury (Diegelmann and Evans, 2004). In addition, the tips of the digits, skeletal muscle tissue, the urinary bladder and bone tissue (Muneoka *et al.*, 2008) have some regenerative properties. The regenerating mammalian tissue is often derived from a population of progenitor cells associated with that tissue, such as prechondrocytic cells of bone and cartilage, hepatic progenitor cells of liver, and satellite cells involved in skeletal muscle repair.

### **2.1.1.2 Normal repair**

Normal repair (sometimes known as “acute wound healing”) is the typical wound healing response that becomes activated in mammalian tissue following most types of injury such as lacerations, burns and crush injuries (Lazarus *et al.*, 1994). It is an intricate physiological process that can be subdivided into three distinct but overlapping temporal phases: the inflammatory phase, the proliferative phase and the tissue-remodeling phase (Clark, 1996; Diegelmann and Evans, 2004).

The following sections will summarize the features of these wound repair phases in the system where they have been most extensively studied, cutaneous wound repair.

#### **2.1.1.2.1 Phase-I: Inflammatory phase**

Inflammation is the initial phase of the normal wound repair process which occurs immediately following injury and persists until approximately 4 days post-injury (Clark, 1996). The purpose of the inflammatory response is to destroy, dilute or isolate the injurious agent and the injured tissues. Inflammation is characterized by pain, heat, redness, swelling and temporary loss of function at the wound site (Clark, 1996). These signs can be observed after any type of tissue injury and are exacerbated by the presence of an infection or a foreign body in the wound site.

The inflammatory phase begins following injury when changes in  $\text{Na}^+$  and  $\text{Cl}^-$  ions within the cells of the tissue create a difference in ionic potential across the edges of the wound (Ojha *et al.*, 2008; Ojingwa and Isseroff, 2003; Reid *et al.*, 2005). This change in ionic potential acts as the stimulant for a plasma based enzyme of the serine protease class, Hageman Factor XII, which initiates a clotting cascade and leads to clot formation

(Leaper *et al.*, 1996). The effector systems within this response, such as the plasminogen cascade, the complement cascade, and the kinin cascade, may interlink to control infection and eventually promote regeneration of tissue (Leaper *et al.*, 1996). The infiltrated leukocytes and platelets become engulfed in the clot triggering the release of chemical mediators such as complement C5a, fibrin degradation factors, platelet activity factors and vasoconstrictors such as histamine and serotonin (Leaper *et al.*, 1996).

Local vasoconstriction followed by activation, adhesion and aggregation of platelets at the site of injury prevents excessive loss of blood following injury. The platelet membrane provides a surface to which serum-derived thrombin is bound and activated. The activated thrombin in turn accelerates the clotting cascade by converting fibrinogen to fibrin. The activated platelets also stimulate the intrinsic coagulation system that converts soluble fibrinogen into a fibrin mesh that produce a thrombus (clot), which stabilizes the initial platelet plug (Bennett and Schultz, 1993). The provisional matrix created by the clotting process described above also entraps blood components including mast cells and platelets, providing bulk to the clot (Clark *et al.*, 1982; O'Leary and Wood, 2003).

Several growth factors such as platelet derived growth factor (PDGF), platelet derived epidermal growth factor (PDEGF), epidermal growth factor (EGF), transforming growth factors (TGF- $\alpha$  and TGF- $\beta$ ), heparin binding epidermal growth factor (HB-EGF), insulin-like growth factor-1 (IGF-1) and vascular endothelial growth factor (VEGF) are also released by the platelets (Kiritsy *et al.*, 1993). PDGF and TGF- $\beta$  stimulate the recruitment of neutrophils and monocytes from the vasculature, further exacerbating the

inflammatory response and stimulating fibroblast cell proliferation and migration at the injured site.

A breakdown fragment generated from complement C5a protein and the bacterial waste product f-Met-Leu-Phe, provide chemotactic signals for the recruitment of neutrophils to the site of injury. VEGF, TGF- $\alpha$  and basic fibroblast growth factor (bFGF) are released from the neutrophils and the surrounding uninjured tissue (Clark *et al.*, 1982; Clark *et al.*, 1997; Clark, 1996). These biomolecules may activate endothelial cells to initiate angiogenesis and also stimulate the orderly migration of cells (additional neutrophils, followed by macrophages and then fibroblasts) into the wound site (Kiritsy *et al.*, 1993). Fibroblasts are then activated by PDGF, released by clot entrapped platelets, initiating production of collagen, glycosaminoglycans (GAGs) and other extracellular matrix (ECM) proteins that augment the provisional matrix and further facilitate cellular migration.

Neutrophils recruited along with macrophages ingest cell debris and bacteria by phagocytosis. Though neutrophils have a very short life, they are capable of producing superoxides and hypochlorous acid that further stimulate the inflammatory response and may promote the differentiation of macrophages from infiltrated monocytes (Martin and Leibovich, 2005).

Macrophages modulate the immune response by generating interleukin-1 $\beta$  (IL-1 $\beta$ ) (Bates and Jones, 2003) and lipoxygenase products through the arachidonic acid cascade (Thuillier *et al.*, 2002; Xaymardan *et al.*, 2002). Macrophages may play an important role in the process of fibrosis or scarring (Martin and Leibovich, 2005). It is shown that when the number of macrophages was reduced fibroblast migration ceased.

Macrophages produce TGF- $\beta$  which directs fibroblasts to proliferate and synthesize collagen (Ghassemifar *et al.*, 1995). The resolution of inflammation is characterized by a gradual reduction in the number of inflammatory cells (macrophages and neutrophils) and an increase in fibroblast cells in the wound site. This heralds the next stage of healing process, the proliferative phase.

#### **2.1.1.2.2** Phase –II: Proliferation or repair phase

The proliferative phase usually starts 2 or 3 days post-injury and may persist for 4 weeks (Clark, 1996). The initial stage of the proliferative phase involves angiogenesis, i.e the restoration of vascular integrity through the migration, proliferation and organization of endothelial cells. This initial stage is influenced by the following growth factors: acidic fibroblast growth factor (aFGF), tumor necrosis factor- $\beta$  (TNF- $\beta$ ), wound angiogenesis factor (WAF), VEGF and EGF (Kiritsy *et al.*, 1993).

Capillaries formed by endothelial budding lead to formation of a capillary-rich fibrous connective tissue known as granulation tissue, which eventually fills the wound and replaces the fibrin clot (Clark, 1996) . Besides new blood vessels, the granulation tissue also contains macrophages, fibroblasts and loose connective tissue. The regeneration of capillaries and arterioles continues until an equilibrium of arterial and venous blood pressure is attained within the microcirculation of the granulation tissue (Bloch *et al.*, 2000).

Cytokines such as TGF- $\alpha$ , TGF- $\beta$ , interleukin-4 (IL-4), and PDGF, along with chemoattractants such as EGF and FGF, and ECM molecules such as hyaluronan, have been proposed as causes of granulation tissue induction (Krummel *et al.*, 1988; Mustoe *et*

*al.*, 1987). The provisional ECM of the fibrin clot promotes granulation tissue formation by providing a collagen-rich and fibronectin-rich scaffold for contact guidance, a reservoir for cytokines, a low impedance hyaluronan-rich matrix for cell mobility and direct signals to cells through integrin receptors (Damsky and Werb, 1992).

Increased deposition of ECM components during the proliferative phase leads to the formation of fibrous tissue at the site of injury. This occurs after the migration of fibroblasts into the wound site, which proliferate and synthesize collagen, fibronectin, hyaluronan and other extracellular matrix components. The collagen-rich and fibronectin-rich fibrous tissue mass provides a further scaffold or conduit for cell migration (Clark, 1988; Clark *et al.*, 1982). In fact, the appearance of the fibronectin and the appropriate integrin receptors on fibroblasts which bind fibronectin and fibrin may act as a rate-limiting step in the formation of granulation tissue (Clark, 1988; Aota *et al.*, 1991, Clark *et al.*, 2004).

Both PDGF and TGF- $\beta$  upregulate integrin receptors (Hertle *et al.*, 1992) and stimulate fibroblast migration (Seppa *et al.*, 1982). Expression of  $\alpha 4\beta 1$  integrin is believed to promote fibroblast migration into the wound space while a switch to expression of  $\alpha 5\beta 1$  ceases their migration, and establishes links to granulation tissue (Hertle *et al.*, 1992). *In vitro* studies indicate that fibroblast migration is also enhanced by a variety of chemoattractants such as IL-4, FGFs, fragments of complement c5a, type I, II and III collagen-derived peptides, fibronectin fragments, and elastin derived peptides (Clark *et al.*, 1982; Clark *et al.*, 2004; Clark *et al.*, 1997).

After the granulation tissue has been established, angiogenesis ceases and many of the newly formed blood vessels disintegrate through apoptosis. In cutaneous healing,

re-epithelization occurs whereby the epithelial cells from the wound edges migrate and proliferate to cover the granulation tissue, thus forming a barrier between the wound and the external environment. The completion of granulation tissue formation and re-epithelization act as the template for the last stage of the wound healing process – tissue remodeling.

### **2.1.1.2.3** Phase-III: Tissue remodeling phase

The remodeling phase usually starts 2 weeks post-injury and can last for months or years. Once the fibroblasts have migrated into the wound, their migratory phenotype is supplanted by a profibrotic phenotype characterized by an abundant endoplasmic reticulum and golgi apparatus filled with procollagen protein (Clark, 1996). The fibroblasts express high levels of the TGF- $\beta$ 1 growth factor that stimulates further synthesis of collagen, which accumulates within the granulation tissue. The production of IL-4 by mast cells, a blood component trapped within the fibrotic tissue, can also induce modest increase in type I and III collagens as well as fibronectin. Once the collagen matrix has been deposited in the wound, the fibroblasts cease collagen production despite continued expression of TGF- $\beta$  (Clark *et al.*, 1997). From this point onwards collagen remodeling occurs, leading to replacement of granulation tissue with fibrotic scar tissue. Any disruption during the remodeling process may also lead to excessive scar tissue formation through continued collagen synthesis and catabolism of collagen at a low rate. Matrix metalloproteinases (MMPs) which are secreted by macrophages, epidermal and endothelial cells, as well as fibroblasts, catalyze the degradation of collagen in the wound (Clark *et al.*, 1997). Studies have shown that IL-4 and IL-10 down regulate expression of

matrix metalloproteinase in macrophages while IL-1 and TNF- $\alpha$  up regulate expression of matrix metalloproteinase (Agren *et al.*, 1998; Liu *et al.*, 2009; Nwomeh *et al.*, 1998). The rate of collagenolytic activity is further regulated by tissue inhibitors of metalloproteinases (TIMP-1), released by neutrophils and fibroblasts.

A relatively acellular scar gradually replaces the fibroblast-rich granulation tissue. The fibroblast cells within the wound undergo apoptosis in response to cellular signals that are not clearly understood (Clark, 1996; Lee *et al.*, 2005a). It has been proposed that interferon gamma (IFN- $\gamma$ ) released by activated T-lymphocytes could be one of the factors responsible for the down-regulation of fibroblast proliferation and fibroblast-collagen synthesis (Falanga, 1993; Lee *et al.*, 2005a).

The final stage of the tissue-remodeling phase consists of wound contraction. This involves a complex and well-orchestrated interaction of cells, extracellular matrix and cytokines. During the second week of cutaneous wound healing, fibroblasts acquire a myofibroblast phenotype characterized by the presence of large bundles of actin microfilaments beneath the plasma membrane of the cells (Moulin *et al.*, 2000). The appearance of the myofibroblasts promotes tissue compaction and therefore wound contraction.

The contraction probably requires stimulation by TGF- $\beta$ 1 or TGF- $\beta$ 2 and PDGF, attachment of fibroblasts to the collagen matrix through integrin receptors, and formation of cross-links between bundles of collagen (Clark *et al.*, 1997; Cox, 1995). Contraction continues until the wound edges are pulled together and there may be continued deposition of type III and type I collagen, while the hyaluronic acid within the resulting scar matrix is replaced by chondroitin sulfate (Chen and Abatangelo, 1999; Fraser *et al.*,

1997; Lovvorn *et al.*, 1998; Maytin *et al.*, 2004; Spicer and McDonald, 1998; Thibeault *et al.*, 2004; Toole, 1990).

Eventually the myofibroblast cells undergo apoptosis under the influence of TGF- $\beta$ 1 and PDGF (Clark, 1996). The maturation of collagen fibrils occurs when levels of collagen production and degradation become equalized within the scar tissue. Collagen maturation is an oxidative deamination process, whereby collagen peptidyl-lysyl residues are converted to semialdehyde, generating an intermolecular cross-link that leads to collagen fibril aggregation and stabilization (Fukae and Mechanic, 1980). The overall maturation process may last for years following injury. The maturation of collagen and contraction of the scar tissue is a gradual time-dependent process resulting in scar tissue that has a tensile strength close to 80% of the original tissue (Clark *et al.*, 1997; Cox, 1995). The scar tissue formed might persist for years or eventually contract to be replaced by normal tissue.

The overall normal wound healing cascade is a well-orchestrated interaction of cellular and molecular components in a time-dependent manner that eventually leads to restoration of the injured tissue. However, anomalies may occur within any of the above tissue repair phases that can lead to pathological healing responses, as discussed in the next section.

### **2.1.1.3 Deficient healing and chronic ulceration**

Deficient healing refers to a situation where there is insufficient deposition of connective tissue matrix at the wound repair site so that the tissue is weakened to the point where it could disintegrate. Chronic non-healing dermal ulcers, such as decubitus

ulcers, exemplify deficient healing (Keller *et al.*, 2002). Excessive neutrophil infiltration in these ulcers appears to be a significant biological marker, and is responsible for chronic inflammation, which is characteristic of ulcers (Diegelmann and Evans, 2004). The neutrophils release significant amounts of enzymes such as collagenase (MMP-8), which are responsible for destruction of the connective tissue matrix (Nwomeh *et al.*, 1999; Nwomeh *et al.*, 1998), along with elastase which is capable of destroying important healing factors such as PDGF and TGF- $\beta$  (Yager *et al.*, 1996). Presence of excessive reactive oxygen species is another factor that further damages the cells and healing tissues (Wenk *et al.*, 2001). Hence, chronic ulcers will not heal until the inflammation is reduced. Chronic ulcers will not respond to the current treatment practice of using skin substitutes and topical cytokines such as PDGF, unless the wound bed is debrided of any underlying infection or inflammatory stimulus (Falanga, 1993; Robson *et al.*, 1998).

#### **2.1.1.4. Excessive healing and fibrosis- keloids and hypertrophic scars**

Fibrosis, strictures, adhesions and contractures are examples of excessive healing. Fibrosis can be defined as the replacement of the normal structural elements of the tissue by distorted, non-functional and excessive scar tissue. Unlike normal fibrous connective tissue found in the body, which is of high tensile strength and elasticity, fibrotic tissue has low tensile strength and is inelastic in nature (Bock and Mrowietz, 2002; Rahban and Garner, 2003).

Contraction is part of the normal process of healing, but if excessive it becomes pathologic and is then termed a contracture (Nedelec *et al.*, 2000). A contracture is developed when normal elastic connective tissues are replaced by inelastic fibrotic tissue

that prevents stretching and normal movement. Contractures may occur in skin, muscle, tendons, and joints.

Many clinical problems are associated with excessive scar formation such as tendon adhesions that immobilize joints, esophageal strictures and urethral strictures, capsule formation around breast implants, liver fibrosis and cirrhosis, and fibrotic non-union in bone (Kovacs, 1991). Both hypertrophic dermal scars and keloids are clinical examples of fibrotic skin healing that result from an extended inflammatory phase in the wound repair process which leads to excessive collagen deposition (Rahban and Garner, 2003; Shaffer *et al.*, 2002). Fibroblasts isolated from keloids produce 2 to 3 times more collagen compared to fibroblasts isolated from normal skin of the same patient (Clark, 1996). Keloids exhibit increased expression of TGF- $\beta$ 1 and also an up-regulation of TGF- $\beta$ 1 receptors (Babu *et al.*, 1992; Chin *et al.*, 2001). Hypertrophic scars are also characterized by excessive accumulation of collagen. A biological marker that distinguishes keloids from hypertrophic scars is the absence of myofibroblast cells in keloids and an abundance of these contractile cells in hypertrophic scars (Ehrlich *et al.*, 1994).

Most conditions of fibrosis are characterized by an increased density of mast cells (Gruber, 2003; LeRoy *et al.*, 1990). Mast cells contain enzymes such as chymase and tryptase are capable of processing procollagen to abnormal collagen fragments. It has been suggested that the production of these abnormal collagen peptides stimulates excessive collagen synthesis in fibroblasts, resulting in fibrosis (Kofford *et al.*, 1997). Therefore, the extracellular matrix collagen accumulation in fibrotic scarring is a logical

target for pharmacological intervention and many researchers have attempted to modify collagen synthesis and degradation pathways (Meier and Nanney, 2006a).

Another clinical condition that results from excessive fibrotic healing is “failed back surgery syndrome” (FBSS) in humans. FBSS is a post-operative complication, that occurs as a result of excessive peridural scarring in patients who have undergone spinal surgery to treat spinal cord trauma, or lumbar disc herniation surgery (Taylor *et al.*, 2005). Following surgery, a hematoma is formed at the site of surgery and the dissected paraspinal and paravertebral muscles start to heal, gradually forming granulation tissue that invades the posterior and lateral aspects of the spinal foramina reaching the dural sac and nerve roots (Hinton *et al.*, 1995; Taylor *et al.*, 2005). The granulation tissue gradually matures into dense fibrous scar. An excessive deposition of ECM proteins occurs following interaction of the connective tissue fibroblasts with injured paraspinal and paravertebral muscles, which further contributes to invasiveness of the peridural scar tissue (Almeida *et al.*, 2008; Taylor *et al.*, 2005). This fibrous scar tissue invades the spinal processes and compresses the nerve roots, leading to FBSS. The key symptom of FBSS is chronic back pain, although some individual patients also experience disabling pain in the hip, thigh and leg, or numbness in the lower extremities.

In the subsequent sections, I will review the process of skeletal muscle repair following injury and the potential molecular interactions that may play a critical role in peridural fibrosis.

## **2.2. Skeletal muscle injury and repair processes**

Skeletal muscle tissue is composed of long, cylindrical multinucleated muscle fibre cells surrounded by a fibrous endomysium. Anatomically, parallel muscle fibres are

grouped into fascicles enclosed in a perimysium, while another connective tissue layer, the epimysium, surrounds the entire muscle. These connective tissue layers carry the blood supply to the tissue and have rich capillary networks that surround the muscle fibres.

Skeletal muscle fibres contain contractile proteins, myosin and actin, which are arranged in repeating units known as sarcomeres (Garrett, 1990; Schiaffino and Reggiani, 1994, Smerdu *et al.*, 1994). Human muscles contain a mixture of physiologically distinct type I and type II muscle fibre cells. Type I fibres have a relatively slow contraction rate, a high resistance to fatigue, and rely largely on aerobic metabolism. Type II fibres are used for both short- and long-term anaerobic activities. Type IIa fibres have a moderately fast contraction rate and fairly high fatigue resistance. Type IIb fibres have a faster contraction rate and lower resistance to fatigue. Type IIx fibres exhibit a fast contraction rate with intermediate fatigue resistance (Smerdu *et al.*, 1994). There is a correlation between the function of each specific skeletal muscle and its relative fiber type composition. Muscles involved in rapid activities have a greater percentage of type II fibres than type I fibres.

Mature skeletal muscle fibres are terminally differentiated and contain post-mitotic nuclei. In order to restore muscle function after injury, the damaged muscle fibres must be replaced with regenerated fibres and this is primarily a function of satellite cells. Lying in close apposition to the plasmalemma of muscle fibres are the satellite cells. These are muscle stem cells that are committed to the myogenic lineage. Satellite cells can differentiate into myoblasts, which subsequently fuse to form myotubes and mature into new multinucleated muscle fibres. The satellite cells are characterized by their

expression of the proto-oncogene, c-Met, the cell surface protein, CD34, and the transcription factor, Pax 7 (Ambrosio *et al.*, 2008; Jankowski *et al.*, 2002; Seale *et al.*, 2000). Another characteristic of satellite cells is their capacity for self-renewal, i.e. the ability to undergo numerous cell division cycles while maintaining the undifferentiated state (Kaufmann *et al.*, 1999). The self-renewal of satellite cells can occur via mechanisms dependent or independent of muscle regulatory factors (MRFs), such as Myf5 and MyoD. The Myf5 and MyoD may show either a simultaneous or alternating expression pattern during the self-renewal process. It has been suggested that their expression may represent a developmental stage of satellite cell division (Kaufmann *et al.*, 1999). It has also been proposed that it is Myf5 alone that drives the self-renewal phase of satellite cells (Seale *et al.*, 2000) .

Recent studies indicate that skeletal muscle tissue also contains a population of multipotent muscle-derived stem cells (MDSC) that are distinct from satellite cells and may also play an important role in muscle tissue regeneration (Jankowski *et al.*, 2002). The MDSCs are considered to be a predecessor to the committed satellite cells, however they also have the capability to differentiate into other mesodermal cell types such as fat, bone and cartilage *in vitro* on stimulation with the synthetic glucocorticoid, dexamethasone (Williams *et al.*, 1999). Conflicting claims have been made that MDSCs typically express CD34 and myogenic regulatory factors (MRFs) such as MyoD, Myf-5, myogenin and MRF4 (Bosch *et al.*, 2000; Jackson *et al.*, 1999; Jankowski *et al.*, 2002; Okada *et al.*, 1992). It has been shown that MDSCs consistently express stem cell antigen-1 (Sca-1) which is absent in committed satellite cells (Bosch *et al.*, 2000; Jackson *et al.*, 1999; Jankowski *et al.*, 2002; Okada *et al.*, 1992). However, Sca-1 is expressed in

myoblasts that arise from Sca-1 negative satellite cells. Also, Sca-1 levels increase following differentiation of myoblasts *in vivo* (Mitchell *et al.*, 2005).

Muscle injuries fall into a number of categories; muscle strain involving complete or partial tears, lacerations, contusions, exercise-induced soreness and compartment syndrome. Compartment syndrome is an acute condition caused by inflammation in a confined region of the body. Muscles with a greater percentage of type II fibres, those which cross two joints and those working eccentrically, are more susceptible to strain injuries (Almekinders and Gilbert, 1986; Garrett, 1990; Nikolaou *et al.*, 1986). Elevated blood levels of creatinine kinase, lactate dehydrogenase, hydroxyproline and myoglobin are clinical indices for skeletal muscle injury. These components are often released into the blood stream following trauma to skeletal muscle tissue.

Many of the events pertaining to skeletal muscle tissue repair are common to the cutaneous wound healing phases discussed in **Section 2.1.1.2.1**. However, muscle healing also involves some unique features such as activation of satellite cells, fusion of satellite cells into muscle fibres, degeneration of the injured muscle fibres and development of fibrosis as discussed below.

## **2.2.1 Phases in skeletal muscle healing.**

### **2.2.1.1 Degeneration of the injured muscle fibres and subsequent inflammation.**

Skeletal muscle injury involves disruption of the muscle fibres, their plasma membrane, and the surrounding connective tissue. This disruption leads to leakage of calcium ions into the extracellular space, resulting in an intracellular serine protease enzyme activation and focal necrosis of the myofibres through autodigestion (Jones *et al.*,

1984). This response occurs within hours to a few days from the time of injury (Jones *et al.*, 1984). To prevent the autodigestion of surrounding healthy muscle tissues, a response known as “contraction zone” formation occurs at the boundary of injury (Hurme *et al.*, 1991; Rantanen *et al.*, 1995). Histologically, the contraction zone is observed as retraction of ruptured muscle fibres that serve as a physical mechanism to limit the area of autodigestion. This response is usually visible within 12 hours following injury.

Muscle fibre degeneration is accompanied by local swelling and hematoma. The injured area is infiltrated with activated macrophages, mononuclear cells and T-lymphocytes (Hurme *et al.*, 1991; Rantanen *et al.*, 1995). The macrophages phagocytose the muscle debris and release factors such as IL-6, IL-8 and TNF- $\alpha$  causing increased vascular permeability thus further stimulating inflammation. The phagocytosis of the injured region results in a “moth eaten appearance” of the muscle tissue, which establishes the scaffold-like framework necessary for subsequent muscle fibre regeneration (Hill *et al.*, 2003).

A calcium ion influx that results from disruption of the myofibre’s structure causes activation of a calcium-dependent protease, calpain, that leads to proteolysis of the myofibrillar apparatus (Dedieu *et al.*, 2002). Activation of calpain is also implicated in the activation of quiescent MDSCs which are involved in muscle regeneration (Raynaud *et al.*, 2004). A schematic representation suggesting the role of calcium ions in the mechanism of muscle repair process is shown in **Figure 1**.

The influx of calcium ions within damaged muscle fibres also initiates the subsequent release of phospholipase A2. Phospholipase A2 promotes the breakdown of membrane phospholipids into arachidonic acid, which is then transformed into

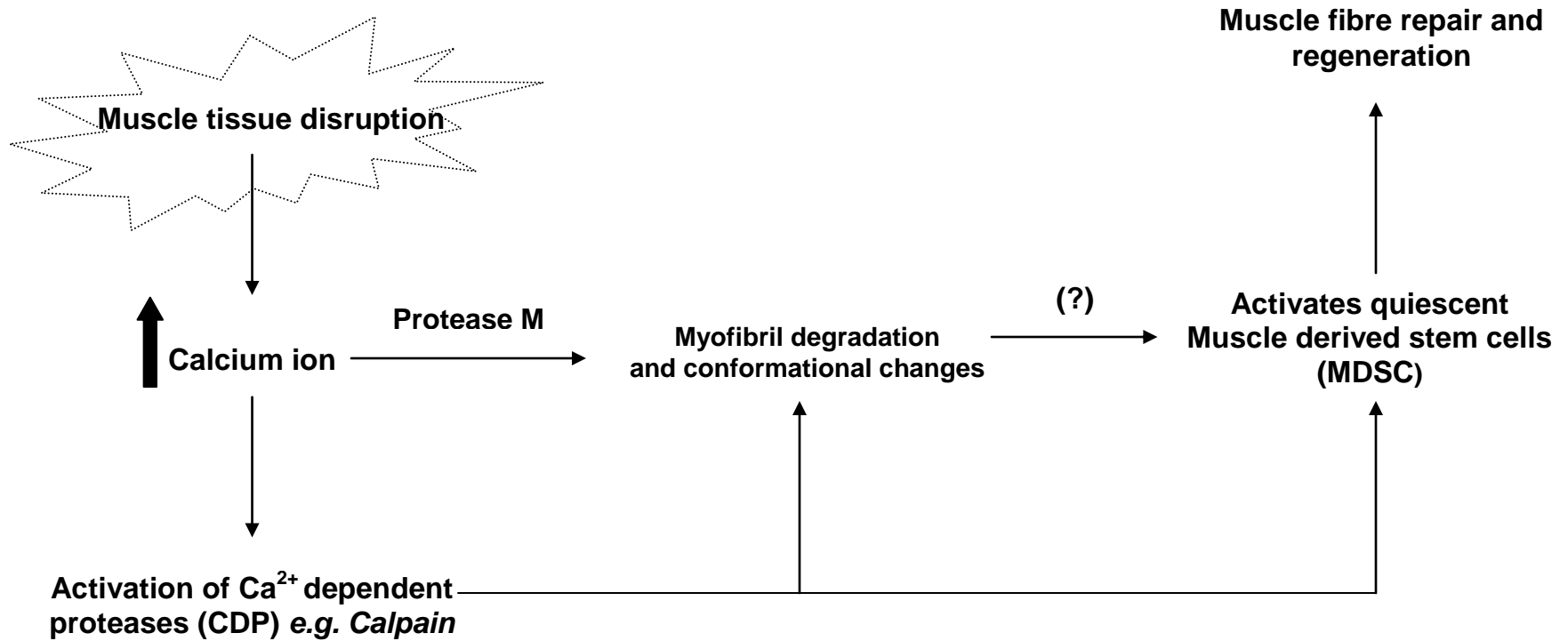


**Figure 1. Role of Calcium ions in skeletal muscle repair.** Following muscle tissue injury, the ruptured muscle fibre cells release calcium ions to the injured site. The increased extracellular calcium ion level activates the calcium-dependent protease, calpain in the adjacent uninjured muscle cells. The activated calpain further activates quiescent MDSCs. Myofibril degradation within the injured muscle fibre cells is initiated through an extra-lysosomal degradation pathway involving a serine protease, Protease M, which causes conformational changes in myofibril structure. It is postulated that this helps to activate the quiescent MDSCs, though the mechanism is not fully understood. (Figure adapted and modified from Ambrosio et al. 2008)

prostaglandins by the cyclooxygenase pathway. The prostaglandins formed induce inflammation by activating peroxisome proliferator-activated receptor (PPAR) transcription factors that are involved in regulation of macrophage and endothelial cell responses (Clark, 2002) and modulation of the cAMP signaling pathway (Horsley and Pavlath, 2003; Shen *et al.*, 2006). Other mediators of the inflammatory response are blood borne neutrophils, activated macrophages and T-lymphocytes that occur in the hematoma formed following injury.

#### **2.2.1.1.1** Role of neutrophils in skeletal muscle repair.

Neutrophils are the first inflammatory cells to respond to the chemoattractants released by platelets during the coagulation cascade following injury. They serve as the first line of defense against infection through phagocytosis of bacteria and removal of foreign bodies and necrotic tissue. Neutrophils rapidly invade injured muscle tissue and their activation by chemoattractants stimulates elastase and collagenase release. They also attract monocytes to the site of injury, and the monocytes in turn amplify the inflammatory response by releasing pro-inflammatory cytokines subsequently transforming into macrophages.

Neutrophils can undergo a respiratory burst and degranulation which generates reactive oxygen species (Ambrosio *et al.*, 2008). Although the neutrophils assist in removal of damaged tissue, this oxidizing reaction may inflict collateral damage to healthy muscle during the early inflammatory period. Neutrophils can generate hypochlorous acid from hydrogen peroxide via a myeloperoxidase (MPO)-mediated reaction and superoxide ( $O_2^-$ ) via NADPH oxidase that has the potential to further

attenuate muscle damage (Horikawa *et al.*, 1999). MPO is commonly used as a marker of neutrophil accumulation within tissue, although macrophages and monocytes also express small amounts of MPO (Tidball, 1995). Superoxide is a mild oxidant that can be rapidly removed by reaction with other free radicals or converted to hydrogen peroxide by superoxide dismutase (SOD) (Horikawa *et al.*, 1999).

The majority of evidence for *in vivo* neutrophil-mediated myofibre damage comes from ischaemia-reperfusion (I/R) studies in which animals are rendered leukopenic using anti-neutrophil serum, anti-tumor agents, radiation or leukopak filters (Korthuis *et al.*, 1988; Lescaudron *et al.*, 1999). Neutrophil depletion prior to I/R can attenuate histologically detectable damage by up to 40% in certain cases (Korthuis *et al.*, 1988; Kosonen *et al.*, 2000; Toumi *et al.*, 2006). Neutrophil-mediated damage during I/R and muscle stretch is largely mediated by free radicals. Reactive oxygen species (ROS) and reactive nitrogen species (RNS) also contribute to skeletal muscle injury and necrosis associated with muscular dystrophies (Rando, 2001) as well as contraction-induced muscle injury (Reid and MacGowan, 1998).

#### **2.2.1.1.2**      Role of monocytes and macrophages in the skeletal muscle repair.

Macrophages are the largest immune cell population present in the injured muscle at 12 hours post injury. They release chemokines, such as CXCL16, that promote a satellite cell response (Merly *et al.*, 1999; Warren *et al.*, 2004). During the proliferative phase, circulating monocytes are attracted to the wound site by growth factors released by neutrophils and platelets, and the monocytes differentiate into macrophages. As platelets are gradually removed from the wound site, the activated macrophages take over the

regulatory role during tissue repair process (Arnold *et al.*, 2007). The macrophages also remove debris by phagocytosis and secrete cytokines that promote further wound healing events (McLennan, 1996; Pimorady-Esfahani *et al.*, 1997).

Studies using rats have shown that ED1+ macrophages are associated with muscle necrosis (McLennan, 1996), while ED2+ macrophages are associated with myofibre regeneration after necrotic tissue is removed (St Pierre and Tidball, 1994). ED2+ macrophages sustain myogenic differentiation and myofibre growth in addition to their protective effect on differentiating myotubes (Sonnet *et al.*, 2006) and subsequent fibre membrane repair (Tidball and Wehling-Henricks, 2007). The macrophages can release heparin-binding EGF-like growth factor that induces terminal myotubes to differentiate (Miyagawa *et al.*, 1995) and promotes muscle cell survival in a high oxidative stress condition (Horikawa *et al.*, 1999). Monocyte derived macrophages also release chemotactic factors such as VEGF, macrophage derived chemokine, monocyte chemoattractant protein-1 (MCP-1), and fractalkine (CX3CL1) that help arouse satellite cells from quiescence (Chazaud *et al.*, 2003) and protect them from apoptosis (Chazaud *et al.*, 2003; Sonnet *et al.*, 2006). The invasion of muscle by macrophages, particularly the ED2+ subpopulation, is essential for satellite cell activation and satellite cell-mediated muscle repair (Merly *et al.*, 1999).

#### **2.2.1.2 Muscle regeneration and development of fibrosis.**

Regeneration of damaged muscle is initially triggered through the interaction of macrophages and satellite cells following injury. The interaction of VLA-4 expressed on the macrophage cell surface with VCAM1, a cell adhesion molecule expressed by

quiescent satellite cells (Seale and Rudnicki, 2000), serves to activate the quiescent satellite cells.

The process of muscle regeneration usually takes place seven to ten days post-injury and begins once the phagocytic cells have ingested the necrotic tissue and the quiescent satellite cells have been activated by macrophages (Hill *et al.*, 2003). Various growth factors such as basic fibroblast growth factor (bFGF), nerve growth factor (NGF), hepatocyte growth factor (HGF), leukemia inhibitory factor (LIF) and IGF-1 have also been shown to promote or enhance self-renewal and differentiation of satellite cells into myoblasts *in vitro* (Kami and Senba, 2002; Menetrey *et al.*, 2000). LIF was found to not only induce satellite cell proliferation but also myoblast cell fusion (Engert *et al.*, 1996). In contrast myostatin, a growth factor belonging to the TGF-beta superfamily and expressed in skeletal muscle, is a negative regulator of skeletal muscle regeneration that blocks satellite cell activation (McCroskery *et al.*, 2003; McCroskery *et al.*, 2005). Myostatin levels are often elevated in muscle atrophy (Carlson *et al.*, 1999). HGF is released from the basal lamina following muscle damage, interacts with its receptor c-Met, in quiescent satellite cells (Seale and Rudnicki, 2000) and may promote satellite cell activation by downregulating myostatin production (McCroskery *et al.*, 2005). Satellite cell activation results in expression of MyoD and/or Myf5 which promotes their differentiation into myoblasts (Seale and Rudnicki, 2000; Seale *et al.*, 2000). The subsequent differentiation of myoblasts into myotubes is coordinated by several growth factors, although IGF-1 is particularly critical in this process (Engert *et al.*, 1996).

While attempting to regenerate the damaged muscle fibres, the injured tissue provides temporary tensile resistance through scar formation. Even in the absence of

muscle loading, such as conditions of immobilization, some fibrosis develops (Menetrey *et al.*, 2000). Fibrosis usually occurs between the second and third week post injury. The ECM of the resulting scar is largely composed of types I and III collagen and its synthesis is increased following skeletal muscle injury (Lehto *et al.*, 1985a; Lehto *et al.*, 1985b; Sasse *et al.*, 1981). Fibrosis decreases the muscle contractility and energy absorbing capacity predisposing the healed muscle to re-injury (Croisier, 2004).

TGF- $\beta$ 1 is the major profibrotic cytokine involved in skeletal muscle fibrosis (Li *et al.*, 2004). TGF- $\beta$ 1 is released by lymphocytes, macrophages and fibroblasts which infiltrate the injured site during the inflammatory response. The release of TGF- $\beta$ 1 activates connective tissue growth factor (CTGF)-mediated synthesis of collagen and prevents the degradation of ECM proteins through induction of tissue inhibitor of matrix metalloproteases (TIMP). Muscle regeneration is the body's natural response to skeletal muscle injury; however this repair is often incomplete. A study in a mouse model demonstrated the presence of large areas of non-regenerated muscle with fibrotic scar tissue even at 35 days post-injury (Kasemkijwattana *et al.*, 1998; Ochoa *et al.*, 2007).

### **2.3. Biomolecules implicated in tissue repair process**

This section will review several biomolecules that have been shown to play crucial roles in tissue repair and scarring processes. These include extracellular matrix molecules such as collagen, fibronectin, and hyaluronans; growth factors such as TGF- $\beta$ s and VEGF; and downstream signal transduction proteins, such as the mitogen-activated protein kinases (MAPKs).

### **2.3.1 Role of collagen and prolyl-4-hydroxylase in tissue repair**

As mentioned before, collagen is necessary for muscle tissue repair. It forms a sheath around fusing myoblasts and also during myotube formation (Allbrook, 1973; Bailey *et al.*, 1979). However, when a large volume of muscle is devitalized by major trauma, the proliferation of fibroblasts may lead to rapid formation of scar tissue which then acts as a dense mechanical barrier to the regenerating muscle fibres (McMinn, 1967).

Both type I and type III collagen are important components of the wound healing process and the balance in the relative amount of these collagen types determines the nature of scar formation. In the early stages of tissue repair, type III collagen levels increase around the site of the wound. This is perhaps due to the migrating endothelial and epithelial cells that are capable of synthesizing this collagen. As the repair process progresses to later stages of healing, there is an increased predominance of type I collagen (McMinn, 1967; Clark 1996; Kinbara *et al.*, 2002).

Biosynthesis of collagen is a complex process involving multiple post-translational modifications that are catalyzed by specific enzymes. Prolyl-4-hydroxylase (P4H) and galactosylhydroxylysyl glucosyltransferase (GGT) are two of the critical enzymes involved in post-translational modifications of collagen. P4H catalyzes the hydroxylation of proline residues in newly synthesized procollagen chains, which is important for their assembly into tropocollagen triple helices. P4H is a tetramer composed of two  $\alpha$  and two  $\beta$  subunits. The  $\beta$ -subunits of P4H, which are identical to the chaperone protein, disulfide isomerase (Kivirikko and Pihlajaniemi, 1998; Myllyharju, 2003) are required to maintain the  $\alpha$ -subunit in a soluble configuration (Lumb and

Bulleid, 2002). The  $\alpha$ -subunits of P4H contain its catalytic domains and are rate limiting in the formation of active P4H (Kivirikko *et al.*, 1990). Three different  $\alpha$ -subunit isoenzymes are known to exist, designated P4H (I), (II), and (III) (Myllyharju, 2003). The type I $\alpha$ -subunit is the most abundant form in most cells, except chondrocytes and endothelial cells (Annunen *et al.*, 1998). Nevertheless, the enzymatic properties of types I–III isoenzymes are very similar (Annunen *et al.*, 1997; Kukkola *et al.*, 2003). Increased P4H levels are associated with increased collagen protein expression in tissues. Therefore, P4H is a potential target for anti-scarring pharmacological intervention (Meier and Nanney, 2006a).

Other post-translational modifications of collagen include hydroxylation of lysyl residues as well as glucosylation and galactosylation of lysyl and hydroxylysyl residues. The collagen hydroxylation process is regulated by iron (Fe) ions, 2-oxoglutarate, and oxygen (O<sub>2</sub>) (Kivirikko and Pihlajaniemi, 1998). Ascorbate is essential for maintaining the iron in its biologically active Fe<sup>2+</sup> form and for maintaining the P4H activity during the hydroxylation process by protecting the enzyme from inactivation by 2-oxoglutarate and O<sub>2</sub> (Nietfeld and Kemp, 1981). Moreover, ascorbate acts as an alternative oxygen acceptor in the uncoupled decarboxylation cycles in which 2-oxoglutarate is decarboxylated without subsequent hydroxylation of the collagen peptide substrate (Myllyharju and Kivirikko, 1997).

After intracellular post-translational modifications and assembly of procollagens into triple helices, the tropocollagen molecules are secreted into the extracellular space where the procollagen propeptides are removed by N- and C- procollagen peptidases. The tropocollagen molecules are then aggregated into fibrils that are stabilized by the

formation of intermolecular cross-links catalyzed by lysyl oxidase (Fukae and Mechanic, 1980; Myllyharju and Kivirikko, 1997). This process is known as collagen maturation as mentioned earlier in **Section 2.1.1.2.3**.

### **2.3.2 Role of fibronectin in tissue repair**

Fibronectin is closely associated with the newly synthesized collagen fibrils and also found during the initial phases of wound healing along with type III collagen. Fibronectin is a high molecular weight dimeric glycoprotein that interacts strongly with other ECM components such as collagen, fibrin and sulfated proteoglycans. Two types of fibronectin have been identified: plasma fibronectin, which is expressed by hepatocytes and secreted in soluble form into the plasma, and cellular fibronectin which is expressed locally by fibroblasts and many other cell types and then deposited in insoluble form into the local ECM (Clark, 1988). Fibronectin is involved in a myriad of biologic processes such as cell adhesion, motility, differentiation, hemostasis and wound repair (Clark *et al.*, 1982; Clark *et al.*, 2004; McKeown-Longo and Mosher, 1984; Tamkun and Hynes, 1983).

Fibronectin plays several key roles in wound healing. In the initial fibrin clot formed after injury, soluble plasma fibronectin and deposits of insoluble cellular fibronectin at the wound site assist in creating a fibrin-fibronectin network (Clark *et al.*, 2004; Knox *et al.*, 1986). This provided scaffold for platelet adhesion and aggregation as well as anchorage for invading fibroblasts (Donaldson and Mahan, 1983). Fibronectin also appear to stimulate migration of epidermal cells such as keratinocytes (Donaldson and Mahan, 1983; Takashima *et al.*, 1986).

It has been found consistently that fibronectin deposition precedes the accumulation of collagen in young granulation tissue (Clark *et al.*, 2004; Clark, 1996). During the subsequent development of granulation tissue the collagenous proteins are organized into bundles and the fibronectin is co-distributed with type I collagen. The fibronectin content gradually diminishes as the granulation tissue is remodeled coincident with a rapid turnover of collagen (Clark *et al.*, 2004; Clark, 1996). Fibronectin may play a vital role in collagen removal by binding to collagen fragments generated by collagenase digestion. The binding of fibronectin to the collagen fragments facilitates the phagocytosis and recycling of collagen proteins by macrophages and fibroblasts (Grinnell *et al.*, 1981).

### **2.3.3 Role of hsp-47 in tissue repair**

The heat shock proteins are a diverse family of proteins with activities that include chaperoning nascent peptides within the cell and the protection of cellular machinery from environmental, physiological and chemically induced stress. Heat shock protein 47 (hsp-47) is a 47 kDa collagen-specific molecular chaperone localized in the endoplasmic reticulum, that plays a critical role in facilitating the correct folding and stabilization of procollagen triple helices within collagen secreting cells. Hsp-47 associates with many types of collagen, including types I and III collagen.

The level of hsp-47 protein is an important determinant of scar formation during wound healing. Numerous studies have shown that there is a strong association between excessive collagen accumulation and increased hsp-47 expression in the scar tissue of human and experimental fibrotic lesions (Naitoh *et al.*, 2001; Razzaque and Taguchi,

1999; Taguchi and Razzaque, 2007). Hsp-47 protein levels were found to be up-regulated during porcine dermal wound healing (Wang *et al.*, 2002). Increased numbers of hsp-47 positive cells were present in injured neonatal rat skin as compared to the normal fetal rat skin (Wang *et al.*, 2002). Hsp-47 levels are also increased in keloid lesions (Naitoh *et al.*, 2001).

Hsp-47 is also involved in skeletal muscle repair (Higuchi *et al.*, 2007). In the histological sections of injured muscle, hsp-47 protein was localized in the basement membrane of the regenerating muscle fibres (Higuchi *et al.*, 2007).

#### **2.3.4 Role of hyaluronan in tissue repair**

Hyaluronan (HA) is a large, non-sulfated extracellular matrix polysaccharide that is abundant in heart valves, skin, skeletal tissue, the vitreous humor of the eye, the umbilical cord and synovial fluid (Fraser *et al.*, 1997). It is also present at lower levels in most other tissues. HA is a linear polymer composed of alternating D-glucuronic acid and N-acetylglucosamine monosaccharides linked together through alternating  $\beta$ -1, 4 and  $\beta$ -1, 3 glycosidic bonds. HA belong to a family of glycosaminoglycans that also includes chondroitin, heparin, heparan sulfate and keratin sulfate.

A significant property of hyaluronan is the capacity to bind huge amounts of water (1000-fold of its own weight). HA functions as a biological lubricant in joints by reducing friction during movement (Engstrom-Laurent, 1997). By creating a hydrating low impedance ECM, HA also functions in promoting cell motility during growth, embryonic development, inflammation and tumor invasion. HA binds to cell-surface receptors such as CD44, and RHAMM (receptor for hyaluronic acid-mediated motility),

and to extracellular matrix proteoglycans including aggrecan and versican (Sherman *et al.*, 1994; Toole, 1990).

HA is synthesized by membrane-bound hyaluronan synthase (HAS) enzymes at the inner surface of the plasma membrane, and the polysaccharide chains are extruded through pore-like structures into the extracellular space (Watanabe and Yamaguchi, 1996). There are three distinct forms of HAS (HAS 1, HAS 2 and HAS 3) that are encoded by separate genes located on different autosomes (Spicer and McDonald, 1998; Spicer and Tien, 2004). HAS 3 synthesizes HA with a molecular weight of  $1 \times 10^5$  to  $1 \times 10^6$  Da, while HAS 1 and HAS 2 synthesize HA with a molecular weight of  $2 \times 10^5$  to  $2 \times 10^6$  Da (Itano *et al.*, 1999). Pro-inflammatory cytokines such as TGF- $\beta$  regulate expression of all three HAS isoforms (Funderburgh *et al.*, 2001).

HA is involved in various phases of the wound healing process. During both the early inflammatory phase of wound repair and the period of granulation tissue formation, the wounded tissue is typically rich in hyaluronan reflecting an increased synthesis of this molecule. This is beneficial for tissue repair processes as HA has been shown to stimulate the production of pro-inflammatory cytokines like TNF- $\alpha$ , IL-1 $\beta$  and IL-8 by endothelial cells (Funderburgh *et al.*, 2001; Funderburgh *et al.*, 2005; Thibeault *et al.*, 2004) and to promote fibroblast cell migration into the wound tissue.

An increased level of HA can negatively influence collagen deposition and it was observed that exogenous hyaluronan promotes scarless healing in several model systems (Funderburgh *et al.*, 2005). Conversely, increased synthesis and expression of dermatan sulfate and heparan sulfate proteoglycans is associated with increased scarring (Lovvorn *et al.*, 1998). HA levels influence epidermal response to injury; an absence of HA causes

terminal differentiation of keratinocytes without disrupting their proliferation (Maytin *et al.*, 2004; Passi *et al.*, 2004). The cell surface hyaluronan receptors, CD44 and RHAMM, have been identified as fibrogenic factors that are required for temporal and spatial regulation of granulation tissue formation and resolution (Tolg *et al.*, 2006). RHAMM is necessary for the recruitment and differentiation of myofibroblasts leading to wound contraction (Tolg *et al.*, 2006) while increased expression of CD44 is associated with scarring (Lovvorn *et al.*, 1998).

### **2.3.5 Role of Vascular endothelial growth factor (VEGF) in tissue repair**

During the proliferative phase of wound healing, new capillary vessels are formed through a process known as angiogenesis (Bates and Jones, 2003). The newly formed vessels will help deliver nutrients and oxygen to proliferating cells at the wound site. VEGF, an important biochemical marker of angiogenesis, is a member of the platelet-derived growth factor super-family. VEGF production in cells is induced under hypoxic conditions. Hypoxic stimuli promote new capillary formation that is characterized by increased VEGF expression, collagen biosynthesis and fibronectin levels at the wound site (Bates and Jones, 2003).

Release of ROS through a respiratory burst from infiltrating neutrophils and macrophages also promotes VEGF production following injury (Sen *et al.*, 2002). In addition, other angiogenic factors released by the macrophages sustain VEGF production in the early phases of wound healing (Bates and Jones, 2003). Fibroblasts produce VEGF under hypoxic conditions and this accounts for its presence during the later phases of wound healing (Takamiya *et al.*, 2002).

A certain level of angiogenesis appears to be required for wound healing, however excess angiogenesis may lead to scar tissue formation (Szpaderska *et al.*, 2005). Excessive angiogenesis was shown to promote scar formation in skin while lesser angiogenesis in oral mucosa led to rapid healing without scar formation (Szpaderska *et al.*, 2003). However, a different study found that anti-angiogenic agents reduced angiogenesis in skin wounds without affecting the quality of healing (Roman *et al.*, 2002).

VEGF has also been shown to influence skeletal muscle repair. VEGF receptors 1 and 2 are present on satellite cells and regenerating muscle fibres (Arsic *et al.*, 2004; Germani *et al.*, 2003). VEGF enhances myoblast migration *in vitro* and prevents apoptosis of myoblasts in cell culture and in skeletal muscle following ischemia (Germani *et al.*, 2003). One study has shown that delayed angiogenesis may lead to impaired skeletal muscle regeneration (Ochoa *et al.*, 2007). Hence, new capillary vessel formation and its associated biochemical factors are a vital component of the healing process.

### **2.3.5 Role of TGF- $\beta$ s in tissue repair**

TGF- $\beta$ s are multifunctional cytokines with diverse effects on cell motility, proliferation, differentiation, cellular apoptosis and expression of ECM proteins (Cox, 1995). The TGF- $\beta$  signaling cascade is initiated after TGF- $\beta$  ligands bind to type II (T $\beta$ II) and type I (T $\beta$ I) TGF- $\beta$  receptors at the cell surface (Soo *et al.*, 2000). The type I and II TGF- $\beta$  receptors heterodimerize and then induce the phosphorylation of receptor-regulated Smad (R-Smad) proteins, such as Smad2 and Smad3. The association of these

phosphorylated R-Smad proteins with co-Smads, such as Smad4, permits their subsequent translocation to the nucleus where they promote the transcription of various target genes (Shi and Massague, 2003). While TGF- $\beta$ s exerts their effects through T $\beta$ I and T $\beta$ II receptors, various modulators such as latent TGF- $\beta$  binding protein-1 (LTBP-1), decorin, biglycan, and fibromodulin may bind and potentially inhibit TGF- $\beta$  activity (Clark, 1996).

TGF- $\beta$ 1 is usually produced in response to injury (Border and Noble, 1994). Both TGF- $\beta$ 1 and TGF- $\beta$ 2 are implicated in promoting scarring (Adzick and Lorenz, 1994; Krummel *et al.*, 1988; Shah *et al.*, 1995) while TGF- $\beta$ 3 was shown to decrease scarring in a rat incisional cutaneous wound model (Shah *et al.*, 1995). TGF- $\beta$ 1 stimulates collagen synthesis, fibroblast proliferation, and angiogenesis, which promote scarring (Cannon and St Pierre, 1998; Ignatz *et al.*, 1987; Massague, 1990). TGF- $\beta$ 1 also prevents collagen degradation through inhibition of matrix metalloprotease-9 (MMP-9) and activation of TIMP. In addition, increased TGF- $\beta$ 1 and TGF- $\beta$ 2 expression is associated with tissue fibrosis in many organ systems (i.e., lung, kidney, skin, liver).

Very high levels of TGF- $\beta$ 1 have been implicated in conditions of excessive scar formation such as keloid and hypertrophic scars (Clark, 1996), while low levels of TGF- $\beta$ 1 expression are associated with deficient wound healing conditions such as diabetic foot ulcers (Liu *et al.*, 2009). TGF- $\beta$ 1 promotes cell proliferation and inhibits cell apoptosis in keloid scars (Chodon *et al.*, 2000).

In skeletal muscle, TGF- $\beta$  has the ability to inhibit myogenic differentiation, myoblast fusion and the expression of various muscle specific proteins (Florini *et al.*, 1991; Liu *et al.*, 2001). Myostatin, a member of the TGF- $\beta$  superfamily, is a negative

regulator of skeletal muscle growth which co-localizes with TGF- $\beta$ 1 in the myofibres in the early stages of muscle tissue injury (Zhu *et al.*, 2007). The combined action of myostatin with TGF- $\beta$ 1 may promote skeletal muscle scarring (Zhu *et al.*, 2007). Use of TGF- $\beta$ 3 which has anti-scarring potential (Occleston *et al.*, 2008) and modulation of the TGF- $\beta$  mediated signaling pathway may be potential targets for pharmacological intervention for anti-scarring properties (Leask and Abraham, 2004)

### **2.3.6 Role of ERK and p38 MAPK signaling in tissue repair**

Various growth factors such as IGF, PDGF, EGF, and FGFs regulate the wound healing process through effects on cell migration, proliferation, apoptosis and protein synthesis (Clark *et al.*, 1997; Clark, 1996) . The mitogen-activated protein kinases (MAPKs) are critical intracellular enzymes in the signal transduction pathways which relay the effects of these growth factors to the cell interior. There are three major types of MAPKs in mammalian cells: the extracellular signal regulated kinases (ERK), c-jun-N-terminal kinases (JNK) and p38 MAPK.

Each MAPK signaling cascade shares an evolutionarily conserved organization and consists of three sequentially acting protein kinases: a MAPK kinase kinase (MAPKKK) which phosphorylates/activates a MAPK kinase (MAPKK) which then phosphorylate/activates a MAPK (Xiao *et al.*, 2002; Bobick and Kulyk, 2004). Within this triple kinase system, each downstream kinase functions as a substrate for the upstream activator and is regulated through phosphorylation within the activation loop of its kinase domain. The MAPK at the bottom of this phosphorylation cascade is selectively activated by dual phosphorylation on specific threonine and tyrosine sites

within a characteristic Thr-X-Tyr motif of its catalytic domain, which is unique for each specific MAPK. ERK 1 and 2 are phosphorylated at a Thr-Glu-Tyr site, while p38 and JNK are activated at Thr-Gly-Tyr and Thr-Pro-Tyr dual phosphorylation motifs respectively.

Following phosphorylation, the activated MAPK regulates cellular responses by phosphorylation of numerous cytosolic and nuclear protein substrate targets, including transcription factors (e.g. Elk-1, Sap1, c-Jun, NF- $\kappa$ B or ATF2), cytoskeletal proteins (e.g. actin, tubulin, neurofilament, vimentin or keratins) and other cytoplasmic protein kinases (e.g. RSK1, cytoplasmic phospholipase A2 or calcium-dependent calmodulin protein kinases).

ERK 1 and ERK 2 (also known as p44 and p42 MAPK, respectively) are typically activated by mitogenic stimuli such as growth factors and some cytokines. The p38 MAPKs consist of four members (p38- $\alpha$ , p38- $\beta$ , p38- $\gamma$ , p38- $\delta$ ) with apparent molecular weights between 38 and 43 kDa. The JNKs consist of 10 isoforms with molecular weights of 46 to 57 kDa which are derived from three different genes, *jnk-1* through *jnk-3*, by alternative splicing. The JNK and p38 pathways are frequently activated in response to stress stimuli including ultraviolet irradiation, heat shock, osmotic shock and tissue injury. However, under non-stress conditions these pathways may also be activated by growth factors, adenosine diphosphate (ADP) and phosphatidyl inositol (Pi).

In a *Drosophila* embryo dorsal wound closure model, JNK signaling plays a crucial role in AP-1 activation at the leading edges of epithelial cells, while the JNK pathway is down-regulated in the amnioserosal substratum that covers the dorsal punch wound (Reed *et al.*, 2001). In both *Drosophila* and mammalian wound repair, it was

found that the JNK mediated AP-1 activation accompanied the re-epithelialization process (Glise and Noselli, 1997; Hou and Perrimon, 1997; Martin and Parkhurst, 2004).

Activation of both p38 MAPK and ERK1/2 was found to suppress the formation of keloid-like scars by promoting apoptosis of keloid fibroblasts (Kuo *et al.*, 2005). The p38 MAPK/ JNK pathway was found to be necessary for mediating human keratinocyte migration on collagen matrix *in vitro* (Li W *et al.*, 2001). Growth factor-stimulated p38 activation induced keratinocyte migration, while ERK1/2 activation induced keratinocytes proliferation (Sharma *et al.*, 2003). During the early phases of corneal wound healing (Imayasu and Shimada, 2003; Sharma *et al.*, 2003), ERK1 and ERK2 activation are involved in the initiation of corneal cell migration and proliferation. Inhibition of either the ERK1/2 or p38 pathway caused a delay in corneal epithelium repair, while a combination of both p38 MAPK and ERK1/2 inhibitor treatments resulted in additional inhibition of the wound healing process (Sharma *et al.*, 2003). Another study involving lipopolysaccharide (LPS)-stimulated macrophage cells reported that TGF- $\beta$  inhibited inflammatory cytokine production through cross-talk between the ERK1/2 and p38 MAPK pathways. ERK-dependent inhibition of p38 MAPK was achieved by up-regulation of MAP kinase phosphatase-1 (MKP-1) (Xiao *et al.*, 2002).

In skeletal muscle, the p38  $\alpha/\beta$  MAPKs are believed to function as a molecular switch for satellite cell activation (Jones *et al.*, 2005). p38  $\alpha/\beta$  MAPK activation promotes the proliferation of satellite cells and their transformation into myoblasts, or myonuclei leading to formation of muscle fibres, and eventually muscle repair (Chen *et al.*, 2007). Conversely, inhibition of p38  $\alpha/\beta$  MAPKs promotes exit of satellite cells from

the cell cycle, prevents their differentiation and insulates these cells from external stimuli to maintain a quiescent state (Jones *et al.*, 2005).

## **2.4 Pharmacotherapeutic approaches in scar reduction research**

Currently available treatment modalities for the management of excessive wound scarring include corrective surgery to remove scar tissue, corticosteroid injections and laser therapy (Meier and Nanney, 2006a; Meier and Nanney, 2006b). These treatments are often inconvenient, painful and have unwanted side effects. The development of optimal therapeutic agents for scar reduction remains an elusive goal for drug development researchers. This is attributed to the intrinsically complex nature of the wound healing process, the high variability of responses between patients during healing, and the multiple genetic factors involved in aberrant scar formation (Meier and Nanney, 2006a).

Most literature pertaining to anti-scarring strategies is focused on improving the healing response rather than the complete elimination of scarring (Clark, 1996; Diegelmann and Evans, 2004). This may be achieved through ameliorating pro-inflammatory events during the initial phase of wound repair that might help to reduce collagen synthesis and deposition.

The ideal anti-scarring drug therapy would be one that is inexpensive, curative in most patients with an existing scar and may be able to prevent excessive scarring by replicating the scarless nature of fetal wound healing (Meier and Nanney, 2006b). It should also lack the adverse side effects seen in currently available treatment options.

Corticosteroids, such as dexamethasone, have been used as anti-fibrotic and anti-inflammatory agents in the therapeutic management of keloid and hypertrophic scars. Intra-lesional administration of corticosteroids is an effective treatment modality for keloidal scarring (reviewed in Jalali and Bayat, 2007). However, the mechanism of ameliorating abnormal scar formation by use of corticosteroids is poorly understood, and their long-term topical use may lead to adverse effects such as hypertrichosis, wound atrophy, altered pigmentation and striae. In addition, topical corticosteroid administration may be associated with adverse systemic effects, including hyperglycemia, glaucoma and adrenal insufficiency. Systemic administration of corticosteroids has been documented to cause a wide range of adverse effects such as heart disease, drug-induced obesity, diabetes mellitus, high blood pressure, myopathy, Cushing's syndrome, and increased risk of infections (Jalali and Bayat, 2007).

Traditional non-steroidal anti-inflammatory drugs (NSAID), such as indomethacin, ibuprofen, ketorolac, diclofenac as well as selective cyclooxygenase-2 (COX-2) inhibitors, such as meloxicam, rofecoxib, parecoxib and valdecoxib, have been used in treating inflammation and associated pain following bone fractures and/or post-operative pain after cardiac and orthopedic procedures (Meier and Nanney 2006a). The use of NSAIDs in anti-scarring therapy is controversial because both beneficial and detrimental effects on wound healing have been reported (Reish and Eriksson, 2008). It was observed that animals treated with COX-2 inhibitors (both selective and non-selective) and transgenic mice which lack COX-2 gene showed impaired or delayed bone fracture repair (Vuolteenaho *et al.*, 2008). Moreover, some of the selective COX-2 inhibitors, such as rofecoxib, parecoxib and valdecoxib, have been reported to cause

cardiac distress in humans, leading to their ban in clinical use by United States Food and Drug administration (US-FDA). Hence, there is a critical need for alternative drug therapies to reduce excessive scar formation following injuries and surgeries.

Research on alternative anti-scarring drugs has been chiefly focused on the following potential drug targets:

- i.) Modulators of extracellular matrix collagen production such as inhibitors of prolyl-4-hydroxylase (Meier and Nanney, 2006a; Meier and Nanney, 2006b).
- ii.) Novel anti-inflammatory and anti-oxidant molecules including certain plant flavanoids such as curcumin, epicatechin, quercetin and cellular glutathione (Davidson and Breyer, 2003; Middleton *et al.*, 2000),
- iii.) Cytokine/growth factors such as TGF- $\beta$  (Meier and Nanney, 2006b; Mustoe *et al.*, 1987), interferon (Lee *et al.*, 2005a), interleukin-10 and imiquimod (Meier and Nanney, 2006a; Meier and Nanney, 2006b; Mustoe *et al.*, 1987)
- iv.) Anti-proliferative agents such as bleomycin, 5-fluorouracil and tamoxifen (Meier and Nanney, 2006a).

#### **2.4.1 Antioxidants and anti-inflammatory molecules.**

Dietary flavanoids, glutathione precursors, and procysteine compounds have both anti-oxidant and anti-inflammatory properties, and may have potential as anti-scarring agents (Juurlink, 2001; Juurlink and Paterson, 1998; Kempuraj *et al.*, 2005). These molecules can inhibit oxidative stress and inflammatory tissue responses by inducing endogenous phase-2 enzymes and promoting cellular glutathione synthesis (Juurlink, 2001; Juurlink and Paterson, 1998; Kempuraj *et al.*, 2005). The following sections will

focus on two candidate anti-inflammatory and antioxidant compounds, specifically quercetin and L-2-oxothiazolidine-4-carboxylate (OTC), which were investigated in my thesis research as potential modulators of wound healing and scar formation.

#### **2.4.1.1 Quercetin.**

Quercetin is a naturally occurring polyphenolic flavonoid, which has anti-inflammatory, anti-oxidant, anti-proliferative and Fe<sup>3+</sup> chelating properties (Davidson and Breyer, 2003; Middleton *et al.*, 2000). The human body cannot synthesize flavanoids including quercetin, therefore the only available sources are through the diet. Dietary quercetin is most abundant in onions (1407 mg/kg), cranberries (121 mg/kg), broccoli (74 mg/kg), apple skin (21 mg/kg), olives (18 mg/kg), red wine (3.5 mg/kg) and green tea (1 mg/kg) (Hertog and Hollman, 1996; Hollman *et al.*, 1995; Rice-Evans and Miller, 1996). Quercetin has a molecular weight of 338.3 Da and is hydrophobic in nature.

Knowledge of the pharmacokinetic parameters of quercetin is still quite limited. It appears that quercetin can undergo extensive biotransformation during metabolism through conjugation reactions by liver and intestinal enzymes leading to the formation of glucuronated, sulfated and methylated quercetin conjugates. Each of these quercetin conjugates has specific physiochemical properties which might exert distinct pharmacological actions (Davidson and Breyer, 2003; Middleton *et al.*, 2000).

Quercetin consists of three ring structures (designated A, B and C) which bear substitutions at specific positions that influence the therapeutic capacity and mechanism of metabolic degradation molecules (**Fig. 2 A**). Structure-activity relationship studies, using both *in vitro* and *in vivo* models, suggest that the presence of an oxy group at position 4 in the quercetin C ring and a double bond between carbon atoms 2 and 3 of the

## FIGURE 2

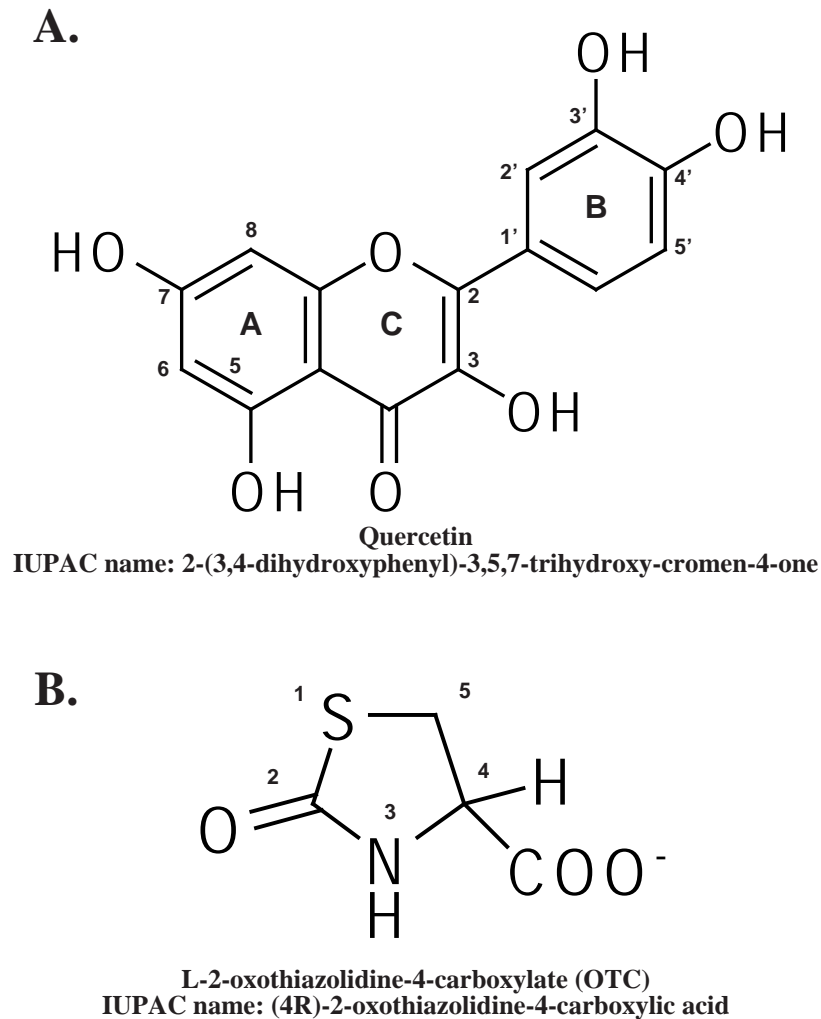


**Figure 2. Chemical structures of Quercetin and L-2-oxothiazolidine-4-carboxylate (OTC) and their International Union of Pure and Applied Chemistry (IUPAC) nomenclature.** (A) Quercetin is a polyphenolic flavanoid containing three ring structures with hydroxyl functional groups at positions that enable the molecule to have anti-inflammatory, anti-oxidant, and iron chelating properties (B) OTC, a procysteine compound, is an analog of 5-oxo-L-proline that has the methylene group replaced with sulphur atom at position 1. Thus OTC act as an excellent substrate for 5-oxoprolinase enzyme that converts it into L-cysteine, a rate limiting aminoacid in cellular glutathione synthesis.

C ring may confer antioxidant properties, enabling quercetin to protect cells from H<sub>2</sub>O<sub>2</sub>-induced oxidative stress and calcium dysregulation (Cotelle, 2001; Hertog and Hollman, 1996; Huk *et al.*, 1998; Theoharides *et al.*, 2001; Wang and Joseph, 1999). The presence of a hydroxyl group at position 3 of ring C could be critical in determining the anti-inflammatory activity of quercetin be critical in determining the anti-inflammatory activity of quercetin (Theoharides *et al.*, 2001).

Studies have demonstrated that quercetin can inhibit inflammation by several different pathways such as inhibition of the Janus Kinase (JAK) pathway (Uchida *et al.*, 1999), myeloperoxidase and xanthine oxidase (Pietta, 2000), certain MAP kinases such as JNK and p38 MAPK (Uchida *et al.*, 1999), as well as by directly scavenging strong oxidants (Middleton *et al.*, 2000).

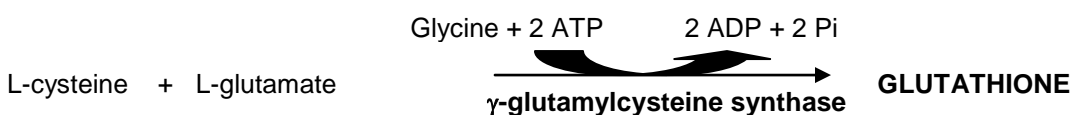
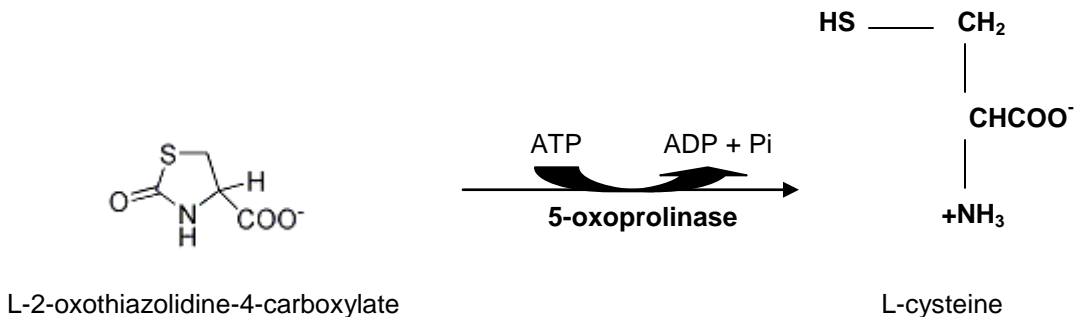
It has been demonstrated that intraperitoneal administration of quercetin promotes partial recovery of the motor functions in rats subjected to an experimentally induced spinal cord injury (Schultke *et al.*, 2003). This study showed that 25 micromoles quercetin (0.025 mmol/kg) was effective in reducing inflammation in spinal cord injury and suggested that this anti-inflammatory activity was due to the Fe<sup>3+</sup> chelating properties of quercetin. In fibroblasts isolated from hypertrophic and keloid scars, treatment with 25 microgram quercetin/mL (0.074 mmol/kg) reduced cell proliferation (Phan *et al.*, 2001) and decreased the production of fibronectin protein (Phan *et al.*, 2003). These authors subsequently demonstrated that quercetin reduced the proliferation of keloid-derived fibroblasts by suppressing TGF-β/ SMAD signaling (Phan *et al.*, 2004). In addition, *in vitro* studies on human dermal fibroblast cells showed that quercetin reduced

both total collagen and total DNA levels in a dose-dependent manner with maximal effect observed at 80 microgram quercetin/mL treatment (Stipcevic *et al.*, 2006).

In skeletal muscle cells, it was observed that quercetin could retard muscle cell differentiation by delaying myogenin expression, and by scavenging superoxide anions and hydroxyl radicals that create conditions conducive for muscle cell differentiation (Orzechowski *et al.*, 2001). Quercetin was also found to inhibit both  $\text{Ca}^{2+}$ -dependent ATP hydrolysis and ATP-dependent  $\text{Ca}^{2+}$  uptake in skeletal muscle fibres (Shoshan *et al.*, 1980). Quercetin was also shown to reduce oxidative stress responses following I/R injury in rabbits (Huk *et al.*, 1998). Quercetin was found to have a positive inotropic effect on rat cardiac tissue, while it inhibited contraction of rat hemidiaphragm muscle (Apisariyakul *et al.*, 1999). At high doses, quercetin was also found to stimulate DNA synthesis in myoblast cells (Orzechowski *et al.*, 2001). The effects of quercetin on collagen synthesis in muscle cells have not been reported.

#### **2.4.1.2 L-2-Oxothiazolidine-4-carboxylate (OTC).**

L-2-Oxothiazolidine-4-carboxylate (OTC) is a synthetic procysteine compound which can act as a precursor for glutathione (GSH) synthesis (**Fig 2 B**). OTC has a molecular weight of 147.15 Da and is hydrophilic in nature. OTC is more stable in solution than cysteine, but is converted to cysteine by 5-oxoprolinase. The reactions mediating conversion of OTC to cysteine and subsequent glutathione formation are shown below.



Since OTC is an excellent substrate of 5-oxoprolinase it may serve as intracellular delivery system for generation of cysteine, a rate-limiting aminoacid for intracellular glutathione (GSH) synthesis. GSH plays an important role in various cellular homeostatic processes such as DNA synthesis, protein synthesis, leukotriene synthesis, enzyme catalysis reactions involving conjugation of xenobiotics, regulation of cellular redox balance, cell growth and cell maturation (Hwang *et al.*, 1992; Kamencic *et al.*, 2001; Lee *et al.*, 2005b; Meister, 1994; Winkler *et al.*, 1994). It has been proposed that treatments which promote synthesis of GSH might be effective in minimizing inflammation following tissue injury. Increased GSH may inactivate oxidstress genes, the NF- $\kappa$  $\beta$  transcription factor and MAP Kinases signaling pathways, that lead to the production of pro-inflammatory molecules (Juurlink, 2001; Juurlink and Paterson, 1998; Kamencic *et al.*, 2001; Lee *et al.*, 2005b; Winkler *et al.*, 1994).

Systemic administration of 1.0 mM OTC was shown to minimize oxidative stress and accompanying inflammation in a rat model of severe spinal cord compression injury

(Kamencic *et al.*, 2001). In this study, the surgically-induced paraplegic rats treated with OTC were able to recover their locomotory abilities significantly better than the corresponding saline-treated control animals.

Unlike N-acetylcysteine, OTC can readily cross the blood-brain barrier and is therefore an appropriate procysteine compound to use when targeting the central nervous system (Hwang *et al.*, 1992; Kamencic *et al.*, 2001; Lee *et al.*, 2005b; Meister, 1994; Winkler *et al.*, 1994). Other studies have shown that OTC administration reduced levels of ROS, VEGF, vascular permeability (Lee *et al.*, 2005b) and decreased airway inflammation in a murine asthma model (Lee *et al.*, 2006). In human peritoneal mesothelial cells which were exposed to a period of hyperglycemia, OTC was found to partially restore glutathione levels and reduce oxidative stress. This was due to reduction in the levels of senescence-associated beta galactosidase (SA-beta-Gal) and 8-hydroxy-2'-deoxyguanosine while diminishing TGF- $\beta$ 1 and fibronectin levels (Ksiazek *et al.*, 2007). Ferreira *et al.* (2009) also demonstrated that OTC increased intracellular GSH levels in myocytes and muscles fibres of diaphragmatic muscle *in vitro*. These OTC treated muscles were protected against muscle fatigue through thiol reduction (Ferreira *et al.*, 2009).

No studies published to date have directly examined OTC effects on collagen biosynthesis and whether OTC might have potential as an anti-fibrotic agent.

## 2.5 Experimental models for wound healing studies

An experimental wound healing model should ideally reproduce the pathogenesis of the trauma in the chosen wound site and it should mimic the sequence of the repair processes in clinically relevant tissue as closely as possible. The choice of an appropriate experimental model system is crucial for efficiency of the drug development process in respect to determining a drug's efficacy (safety, pharmacotherapeutic potential and toxic side effects) in treating a particular pathological condition (e.g. fibrosis, deficient healing). Unfortunately, none of the existing experimental wound repair models fulfill all the ideal criteria or fully replicate the human clinical situation.

The choice of an experimental model in wound healing and drug development research is dependent on several factors, as discussed by Gottrup *et al.* (2000):

- 1.) **Purpose of the investigation:** This includes the type of tissue repair that is being investigated (e.g. bone, cutaneous, liver, kidney, lungs, cardiac and skeletal muscle tissue repair processes); determining the physiological or pathophysiological changes involved in these tissue repair processes; evaluating the efficacy, toxicity and safety of the pharmacological or other bioactive agents, as well as their pharmacokinetic parameters following systemic and local administration.
- 2.) **Type of method:** This includes use of *in vitro* versus *in vivo* models to study acute and chronic wound healing as well as adult and fetal wound healing processes. The choice of method will depend on the type of injury inflicted, such as excisional, incisional, thermal burn, chemical burn or blunt trauma wounds.

- 3.) ***Choice of experimental organism.*** This includes consideration of an appropriate biological species ranging from insects to primates for specific studies. With rare exceptions, the use of humans is generally precluded during the initial stages of drug development study because of ethical and human rights issues. Hence, the choice of a suitable organism and experimental system depends on identifying anatomical, physiological, biochemical or molecular parameters that can be extrapolated to humans. However, in most cases, the use of alternative experimental organisms for drug development studies does not guarantee the efficacy of the drug in humans.
- 4.) ***Outcome of measurement.*** This includes selection of appropriate parameters to assess the outcome of treatment such as wound size (area and volume), wound strength, granulation tissue mass, collagen levels, blood supply, epithelial resurfacing and visual assessment.
- 5.) ***Recruitment criteria.*** This includes determining the effects of conditions such as aging or metabolic disease (e.g diabetes mellitus) on the wound healing process. Moreover, drug development studies often take into consideration sex, species, strain and sample size for uniformity and statistical consideration.

The current wound repair models available can be classified as either *in vitro* or *in vivo* systems. Each group can be further divided into different types of models (see **Table 1 a** and **1 b**).

**Table 1 a. Current *in vivo* wound model system available for wound healing research** (*adapted and modified from Gottrup, 2000*).

	<b>Study parameters</b>	<b>Type of tissue defect/materials</b>	<b>Reference</b>
<u><i>In vivo models</i></u>			
<u><i>Artificial models</i></u>			
Subcutaneous chamber/sponges	Evaluation of growth factor effects, pharmacological agents, granulation tissue studies	Polvinyl alcohol, wire mesh chamber	Woessner et al., 1961 Holm-Pedersen et al., 1964 Hunt et al., 1967 Pallin et al., 1975 Alaish et al., 1995
Subcutaneous implant tubes	Interventional studies to determine the effect of growth factors, collagenase on implants, trauma, surgery.	Expanded polytetrafluoroethylene tubes, viscous sponges soaked in exogenous chemicals within silicone tube (Cellstick).	Viljanto , 1976 Jorgensen et al., 1996 Jorgensen et al., 1998 Arge et al., 1998.
<u><i>Injury models</i></u>			
Excisional wound	Epithelization, wound contraction, dermal reconstitution, inflammation, chemotaxis, angiogenesis, matrix production/organization, evaluation of pharmacological agents for cosmetic and functional outcomes,	Full thickness dermal wound, ear wound models	Kiistala et al., 1964 Jiborn et al., 1978 Ehrlich and Needle, 1983
Incisional wound		Incision in skin, retina, GI-tract	Baker, 1987
Superficial wound		Blister wounds, dermatome wounds	Ahn and Mustoe, 1990
Thermal burn wounds		Partial and full thickness skin	De Vries et al., 1993
Chemical burn wounds			

**Table 1 b. Current *in vitro* wound model system available for wound healing research (adapted and modified from Gottrup, 2000)**

	<b>Study parameters</b>	<b>Cell types &amp; lineages</b>	<b>Reference</b>
<b><i>In vitro model</i></b>			
Single cell monolayer	Cell migration, proliferation, protein synthesis	Keloid & hypertrophic fibroblasts, keratinocytes, Epidermal, endothelial, macrophages	Calderon et al., 1996 Cha et al., 1996 Kheradmand et al., 1994 Ghassemifar et al., 1995
Co-culture monolayer	Cell-Cell interaction, Cell migration, proliferation	Human dermal microvascular endothelial cell and human dermal fibroblast	Oberringer et al., 2007
Three dimensional	Cell matrix interaction, migration, proliferation, protein synthesis and wound contraction.	Fibroblast, keratinocytes, epidermal cells.	Mariappan et al., 1999
<b><i>Organ culture</i></b>			
Explant culture	Epithelialisation, wound contraction, wound margin, wound closure	Intact skin, Cornea	Moll, 2003 Zhao et al., 2006
<b><i>Artificial scaffold-based 3-D culture system</i></b>			
Integra®(artificial bilayer skin substitute)	Re-epithelialisation, wound closure	Tissue engineered proprietary bilayer matrix	(Yannas, 1990) U.S. Patent 4,947,840
Chitosan-Gelatin-hyaluronic acid (skin substitute)	Re-epithelialisation, polysaccharide interaction	Fibroblast cells, keratinocytes,	Liu et al, 2006

### **2.5.1 *In vivo* models for wound research.**

A variety of different *in vivo* models are available for wound research to study various aspects of the healing process. The choice of the *in vivo* model employed is dependent on the type of investigation and the desired outcome. Most studies that have utilized *in vivo* models have focused on three aspects of the wound healing process:

- i.) To study the process of epithelialization, neovascularization and dermal reconstitution in cutaneous tissue healing.
- ii.) To evaluate fibrotic response and scar formation in both normal and pathological wound repair of various tissue types including bone, liver, kidney, skeletal muscle, cardiac muscle and smooth muscle.
- iii.) To assess the formation of granulation tissue and its subsequent contraction during wound repair.

#### **2.5.1.1 Animal models**

Commonly used animal species employed in wound healing research include horses (Cochrane *et al.*, 1996; Gottrup *et al.*, 2000), pigs (Gottrup *et al.*, 2000; Lindblad, 2000; Sullivan *et al.*, 2001), rabbits (Gottrup *et al.*, 2000; Kim *et al.*, 2003), dogs (Gottrup *et al.*, 2000), mice and rats (Dorsett-Martin, 2004; Gottrup *et al.*, 2000). In using pig models, researchers generally acknowledge the fact that porcine dermis has some anatomical similarities to human dermis. Nevertheless, there are certain histological and molecular differences between the skin structures of young adult humans and the skin of adult pigs, such that the latter may not completely replicate age-dependent molecular responses observed in human cutaneous wound healing (Lindblad, 2000).

Small rodents such as rats and mice have been used in various types of wound healing research because of their ready availability, low cost, and small size, which results in a more economical and efficient use of limited laboratory resources and housing facilities (Dorsett-Martin, 2004; Gottrup *et al.*, 2000). The availability of rodent strains with well-defined genetic backgrounds, single gene mutations, and target gene knockouts along with extensive literature correlating biological responses of mice and rats with certain human genetic traits allow them to serve as valuable models in wound healing research (Dorsett-Martin, 2004).

With the advent of transgenic technology, genetically modified mice have been used to study the specific effects of proteins on normal and impaired wound healing in pathological conditions such as diabetes mellitus (Gottrup *et al.*, 2000). This technology has many advantages in terms of simplifying the understanding of wound healing mechanism and also in estimating the effects of NCEs on the gene and protein expressions. However, the use of transgenic mice in drug development studies may increase the overall cost of the drug development process in wound healing research. Moreover, it may be difficult to determine the pharmacokinetics of NCEs using transgenic or knock-out mice, which could have altered systems of drug metabolism, which are not reflective of the NCEs response in normal mice.

Similar to pigs and horses, the tissues of rodents have some differences from human tissues in regard to anatomical, genetic and physiological features. Such differences make it difficult for drug development researchers to directly extrapolate the safety, toxicity and efficacy profiles of pharmaceutical therapies developed in animal models to use in human subjects.

None of the currently available animal models perfectly replicates the biological process occurring in humans during normal wound healing (Gottrup *et al.*, 2000). Nevertheless, researchers have used various animals extensively in wound repair investigations and to test the efficacy of potential wound healing modulators. One disadvantage of the *in vivo* wound model system is that it is difficult to directly examine the response of single tissue components to potential anti-scarring pharmacological agents or NCEs because of the complex composition of natural animal tissues and the multiple cell types involved in the *in vivo* wound healing process (Gottrup *et al.*, 2000; Lindblad, 2000). Animal to animal variability is another factor which makes it difficult to determine the overall outcome of measurement in anti-scarring drug development studies.

In injury models, the normal tissue of the animal forms an integral part of the experimental wound model system, with measurement of outcomes often made discontinuously. There are two types of tissue models that can be described as excisional and incisional wound models. In excisional wound models, a segment of tissue is surgically removed from the animal. An example of an excisional wound model is injuring the skin or ear of an experimental animals (e.g. pig, rat, rabbit, mouse) by taking a small full thickness punch-biopsy (Gottrup *et al.*, 2000). Incisional wound models involve infliction of one or more incisions on the organism. An example is the infliction of full thickness dermal incisions on the back of pigs (Singer and McClain, 2006) or rats (Adamson *et al.*, 1996) using a scalpel. Incisional wound models have also been employed to study wound repair in other organs such as the retina and gastrointestinal tract (**Table 1 a**).

Other types of injury models that have been well studied are thermal burns, chemical burns, blistering skin lesions, and pressure sores (Gottrup *et al.*, 2000). These models are often used to test the efficacy of different types of dressings, dermal substitutes, and drug delivery agents such as medicated ointments and creams. The outcome of measurements applied to these models includes evaluation of wound size, changes in wound area, scar tissue strength and histological changes.

The rat spinal laminectomy wound repair model that was employed in my thesis research is an adaptation of a method that was initially developed to study epidural scar formation following surgically-induced spinal cord trauma (Hinton *et al.*, 1995; Taylor *et al.*, 2005). It involves a combination of both incisional and excisional wound repair features. In this model a dorsal skin incision is made, the underlying muscles retracted and ligaments dissected to expose the bony structures of the spine. The spinal cord and dural sac were exposed by chipping of the laminae of lumbar vertebrae L1 through L3 (as described in **Section 3.1.1**). This procedure induces peridural scar formation that invades the posterior aspect of the dural sac, the surrounding paraspinal musculature, and compressing the nerve roots (Hinton *et al.*, 1995; Taylor *et al.*, 2005). This whole animal wound repair model was employed in the first phase of this project to evaluate the ability of systemically administered quercetin and OTC to ameliorate peridural fibrosis *in vivo*.

### **2.5.2 *In vitro* models for wound research.**

*In vitro* models that have been employed in wound healing studies include both cell culture and organ culture systems (Gottrup *et al.*, 2000). The most commonly investigated cells in wound healing research are fibroblasts, keratinocytes, macrophages,

and endothelial cells. The available *in vitro* model systems can be divided into three types: systems utilizing a single cell type cultured in monolayer or three dimensional formats; multicellular systems utilizing co-cultures of two or more cell types in monolayer or three-dimensional format; and “*ex-vivo*” systems, such as organ and explant cultures utilizing a segment of intact tissue excised from live animals. The outcome of measurements in these systems includes determination of cell proliferation, cell migration, cell-matrix interactions, cell-cell interactions, protein synthesis, wound contraction and expression of specific biochemical and molecular markers appropriate for the cells/tissues under investigation.

Many current *in vitro* models for the study of the wound healing process utilize monolayer cultures of fibroblasts, endothelial cells, or keratinocytes isolated from animal tissues or human wound sites (Bhalla, 1999; Gottrup *et al.*, 2000). Typically, the cells are first cultured to complete confluence and the resulting monolayer is then subjected to local denudation by scraping off the cells from a small portion of the culture (Gottrup *et al.*, 2000; Ronot *et al.*, 2000). This type of *in vitro* assay is often used to determine the effects of exogenous chemical or biological factors on wound closure. The differential expression of proteins such as collagens and cytokines, cell morphology changes such as cell spreading, cell migration and cell contractility, and the metabolic response of cells to exogenous factors following injury are conveniently analyzed using this method. A list of other *in vitro* model systems used for specific wound repair studies is provided in **Table 1 b**.

Specialized *in vitro* wound models such as perfusion cell culture systems have been developed to study specific issues such as the impact of plasminogen on endothelial

cell proliferation and the regulation of MMPs following trauma in the scraped endothelial cell cultures (Hayashi *et al.*, 2009). To study periodontal wound healing, a confluent stratified culture of human periodontal ligament and gingival fibroblasts was subjected to a mechanical wound by removing a 3 mm wide band of the cell layer and then incubating the cells for a defined period of time to determine the wound closure rate (Lackler *et al.*, 2000). However, such systems have significant limitations as they are based on a monolayer configuration and cannot adequately replicate cellular behavior in the three-dimensional (3-D) context of *in vivo* wound repair. Only one cell type is tested in most of these studies, although a recent study examined the interaction between dermal fibroblast cells and microvascular endothelial cells following trauma in a monolayer co-culture system (Oberringer *et al.*, 2007). In another investigation, fibroblast cells were incorporated into a 3-D collagen lattice and a punch biopsy was taken to study fibroblast repopulation at the wound site (O'Leary and Wood, 2003). This study had the limitations of using only one cell type, and relying on an artificial 3-D based scaffold to support cell growth. Artificial 3-D scaffold systems that are currently available are expensive and have the potential problem that the scaffold materials used might have immunogenic properties which could disrupt cell morphology and phenotype (Handschele *et al.*, 2007). One commercially available artificial 3-D scaffold system consists of a tissue engineered bilayer matrix known as Integra<sup>®</sup>, which contains bovine tendon collagen fibrils cross-linked with glycosaminoglycans. The Integra<sup>®</sup> matrix is manufactured to achieve a controlled porosity to enable cells to migrate within the biomaterial matrix and to have a defined matrix degradation rate after the cells populate the pores (Yannas, 1990). The

Integra<sup>®</sup> system has been used clinically as a scaffold for skin regeneration in burn victims.

Another commonly used experimental scaffold system utilizes a chitosan-gelatin-hyaluronic acid (Cs-Gel-HA) hydrogel that has high water binding capacity and biocompatible properties. Fibroblasts and keratinocytes that are co-cultured within this Cs-Gel-HA scaffold have been used to form artificial skin *in vitro* (Liu *et al.*, 2007). A dermal scaffold prepared from a co-polymer of polyethylene glycol-terephthalate (PEGT) and polybutylene-terephthalate (PBT), known as Polyactive, leads to the formation of fully differentiated stratified epidermis and basement membrane (El-Ghalbzouri *et al.*, 2004), which are repopulated with human fibroblasts and keratinocytes.

Integra<sup>®</sup>, Cs-Gel-HA and Polyactive are primarily used as bilayer skin substitutes or tissue scaffolds and have not been reported to be used for anti-scarring based drug development studies. One limitation is that the source and nature of materials used in preparing such scaffolds might potentially cause immunogenic interactions with the cells of interest that make certain 3-D artificial scaffold based *in vitro* models unsuitable for some drug evaluation studies (Handschel *et al.*, 2007).

## **2.6 Use of co-culture systems in developing functional tissue models *in vitro***

Homogenous cultures composed of a single cell type usually behave differently than the same cells under *in vivo* conditions where they are able to interact with cells of other phenotypes. When grown alone, cells in primary culture often lose their ability to proliferate over a period of time and undergo programmed cell death. Alternatively, the cells may undergo more rapid differentiation. Studies have shown that the use of a co-

culture system can be beneficial in maintaining more normal cell functions including proliferation, differentiation and normal physiology (Bhatia *et al.*, 1997; Gerstenfeld *et al.*, 2003; Khetani and Bhatia, 2008).

For example, a microscale culture model of human liver tissue was developed by surrounding hepatocyte cell colonies with various liver or non-liver derived stromal cells to create an *in vitro* liver model that permits heterotypic cell interactions (Khetani and Bhatia, 2008). A novel system of creating micropatterned co-cultures of 3T3-J2 fibroblast cells and human hepatocytes in a microchip format has been developed for application in high throughput drug screening (Khetani and Bhatia, 2008). Similarly, a 3-D culture system utilizing co-cultures of rat hepatocyte spheroids together with NIH/3T3 fibroblasts was reported to promote enhanced hepatocyte function by overcoming the drawbacks of short-term survival and rapid de-differentiation of isolated hepatocytes *in vitro* (Lu *et al.*, 2005).

Examples of co-culture systems of differentiated muscle cells combined with a second differentiated cell type are shown in **Table 2**. In most cases, each cell type helps to maintain the normal physiology and phenotypic features of the other cell type present. A recent study introduced a monolayer co-culture system for the study of wound healing based on the interaction of dermal fibroblast cells and microvascular endothelial cells following trauma (Oberringer *et al.*, 2007). However, this monolayer model did not replicate the interaction of co-cultured cells in the 3-D context of *in vivo* wound healing. Accordingly, cells that are grown in monolayer may behave differently when treated with exogenous chemicals, compared to cells maintained in a 3-D configuration that facilitates cell-cell and cell-matrix interactions.

**Table 2. Co-cultures of differentiated muscle cells with a second differentiated cell type used in tissue engineering studies.**

Tissue	Cell types used for co-culturing		Culture system interaction	Effect of co-culturing on the cell types	Reference
	Cell type I	Cell type II			
Heart	Rat fibroblastic immature ventricular fraction	Immature rat cardiomyocytes	Cell-Cell contact	Cell type I supports the differentiation or physiology of Cell type II	Van Luyn et al., 2002
Heart	Murine mature mesenchymal stem cells	Rat mature cardiomyocytes	Cell-cell contact	Cell type I trans differentiates towards the lineage of the cell type II with which it is co-cultured	Fukuhara et al., 2003
Heart	Human embryonic stem cells	Murine visceral endoderm like cells (embryonic) treated with mitomycin	Cell-cell contact	Cell type I differentiates into a tissue specific lineage which is different from the cell that initiates or enhances the differentiation.	Mummery et al., 2003
Heart	Murine immature cardiomyocytes	Murine mature microvascular endothelial cells	Cell-Cell contact	Both Cell type I and Cell type II support physiology or differentiation of one another.	Narmoneva et al., 2004
Heart	Rat mature mesenchymal stem cells	Rat immature cardiomyocytes	No cell-cell contact	Cell type I trans differentiates towards the lineage of the cell type II with which it is co-cultured	Yoon et al., 2005
Heart	Murine mature bone marrow cells	Avian embryonic cardiac explants	Cell-cell contact	Cell type I trans differentiates towards the lineage of the cell type II with which it is co-cultured	Eisenberg et al., 2006
Muscle	Murine myoblast cell line (C2C12)	Embryonic endothelial cells and HUVEC endothelial cells	Cell-cell contact	Both Cell type I and Cell type II support physiology or differentiation of one another	Levenberg et al., 2005

The *in vitro* model employed in this thesis project combines the strategy of heterotypic cell co-culture together with 3-D “micromass” culture technology to generate an artificial microtissue based wound model for evaluating the effects of quercetin and OTC on collagen deposition and other parameters of wound repair.

## **2.7 Micromass culture technology**

Research has demonstrated that a cellular reaggregation approach using a “micromass” culture technique can promote the formation of *in vitro* microtissues, including myocardial (Zimmermann and Eschenhagen, 2003), hepatic (Kelm and Fussenegger, 2004) and cartilaginous tissues (Ahrens *et al.*, 1977; Cottrill *et al.*, 1987; Edwall-Arvidsson and Wroblewski, 1996; Hattori and Ide, 1984; Hoffman and Kulyk, 1999; Kulyk and Hoffman, 1996; Mello and Tuan, 1999). Ahrens *et al.* (1977) originally developed this technique for studying *in vitro* cartilage differentiation in primary cultures of mesenchymal cells isolated from embryonic chick limb buds.

In the micromass method, “*ex-vivo*” tissue formation is achieved by isolating cells from a tissue or organ of interest then dissociating the cells to create a high density cell suspension, and subsequently plating the cells at superconfluent cell density to encourage their reaggregation to form a 3-D “microtissue”. High density micromass cultures of embryonic limb bud and facial mesenchyme cells from both mouse and chicken embryos have been used to examine the mechanism of cartilage differentiation and to determine the effect of various pharmacological agents on chondrogenesis (Bobick and Kulyk, 2004; Cottrill *et al.*, 1987; Edwall-Arvidsson and Wroblewski, 1996; Hoffman and Kulyk, 1999; Kulyk and Hoffman, 1996; Mello and Tuan, 1999; Motoyama and Eto,

1994). Neuronal and hepatic precursor cells are some of the non-skeletal cell types which have been examined to determine their differentiation potential using micromass culture technology (Boess *et al.*, 2003; Flint, 1983; MacDonald *et al.*, 2003; Pluchino *et al.*, 2003).

In addition, studies have also shown that a high density micromass cultures can be generated using engineered or immortalized lines of cardiac myocytes (HL-1 cells) and chondrogenic progenitor cells (C3H10T1/2 and ATDC5 cell lines) (Denker *et al.*, 1995; van Luyn *et al.*, 2002; Watzka *et al.*, 2000; Zimmermann and Eschenhagen, 2003).

The potential of the “micromass” technology for use in soft tissue regeneration and engineering applications was suggested in a recent publication (Handschel *et al.*, 2007). Micromass technology can be adapted for use in tissue engineering applications because it permits the formation of scaffold-free 3-D microtissues *ex-vivo* (Ahrens *et al.*, 1977; Bobick, 2006; Bobick and Kulyk, 2004; Carlberg *et al.*, 2001; Cottrill *et al.*, 1987; DeLise *et al.*, 2000; Edwall-Arvidsson and Wroblewski, 1996; Handschel *et al.*, 2007; Hattori and Ide, 1984; Hoffman and Kulyk, 1999; Kulyk and Hoffman, 1996; Mello and Tuan, 1999). This technology utilizes the natural extracellular matrix secreted by cells to generate tissue that are devoid of any artificial scaffold materials in order to more closely mimic *in vivo* conditions (Handschel *et al.*, 2007).

Various other methods have been used to generate scaffold-free microtissues *in vitro*, as summarized in **Table 3**. One approach utilizes cell reaggregation in suspension culture to form spheroid- shaped microtissues. For example, autologous spheroid systems have been used to generate transplantable cartilage or bone tissues (Anderer and Libera, 2002). Spheroid systems for cardiac, liver and other cell types have also been developed

**Table 3. Examples of methods reported to have utilized scaffold-free and cell reaggregation based cell culture method to develop microtissue.**

<b>Cell type used</b>	<b>Species</b>	<b>Technology used</b>	<b>References</b>
Cardiomyocytes	Chicken Chicken, rat Mouse	Suspension culture, Stacking of monolayer Static culture	Sperelakis, 1978 Shimizu et al., 2003 Watzka et al., 2000
Hepatocytes	Rat Rat Porcine Human	Spinner flask Eudragit containing culture suspension Spinner flask Rotary cell culture system Stacking of monolayers	Okubo et al., 2002 Kamihira et al., 1997 Sakai et al., 1996 Khaoustov et al., 1999 Harimoto et al., 2002
Chondrocytes	Human Chicken Mouse	Hydrogel coated 96 well plates Pellet culture Gyratory shaker High density “micromass” culture	Anderer and Libera , 2002 Kafienah et al., 2003 Bassleer et al., 1986 Ahrens et al., 1977 Carlberg et al., 2002
Endothelial cells	Human, Bovine	Static culture	Korff and Augustin, 1998
Vascular cells	Human	Stacking of monolayers	Hoerstrup et al., 2002
Dermal fibroblasts	Human	Suspension culture	Furukawa et al., 2001
Pancreatic cells	Human Rat	Tissue fragments of defined size Rotational and static cultures	Hoem et al., 2002 Matta et al., 1994

**Table 3. Examples of methods reported to have utilized scaffold-free and cell reaggregation based cell culture method to develop microtissue (Contd..).**

<b>Cell type used</b>	<b>Species</b>	<b>Technology used</b>	<b>References</b>
Osteoblast	Human Mouse	Static culture Suspension culture	Kale et al., 2000 Keller, 1995
Smooth muscle cells	Human	Static culture Suspension culture	Korff et al., 2001 Bjorkerud et al., 1994
Embryonic retina cells	Chicken	Gyratory shaker	Rothermel and Layer, 2001
Neural precursor cells	Mouse Rat	Static culture “Micromass” culture	Pluchino et al., 2003 Flint, 1983
Spinal cord precursor cells	Mouse	Static culture	MacDonald et al., 2003
Human bone marrow stromal cells	Human	Centrifugation pellet culture	Muraglia et al., 2003
Embryonic stem cells	Human	Suspension culture	Itskovitz-Eldor et al., 2000

(Sperelakis, 1978; Furukawa *et al.*, 2001; Keller, 1995; Bjorkerud *et al.*, 1994; Itskovitz-Eldor *et al.*, 2002). Reaggregated microtissues derived from suspension cultures of tumor cells have been employed in cancer research (Kelm and Fussenegger, 2004).

The multicellular tumor spheroids show increased proliferative activity and drug resistance similar to solid tumors (Kelm and Fussenegger, 2004).

Another scaffold-free high-density culture strategy is to generate microtissues in pellet culture (Kafienah *et al.*, 2003; Muraglia *et al.*, 2003). For example, high-density pellet cultures were established after centrifuging dissociated chondrocytes or bone marrow cell suspensions in a sterile culture tube (Kafienah *et al.*, 2003; Muraglia *et al.*, 2003).

Reaggregated microtissues are becoming increasingly popular as models for neurodegenerative disorders, toxicology, nutrition and environmental monitoring (Bhadriraju and Chen, 2002; Layer *et al.*, 2002). Thus, the engineered tissues from non-skeletal origin confirm that it is feasible to create tissue substitutes based on re-aggregation technology. Examples of these strategies include liver reconstruction, synthesis of an artificial pancreas, restoration of heart valve tissue and cardiac organogenesis *in vitro* (Lu *et al.*, 2005).

### **2.7.1 Micromass co-culture technology – Potential for *in vitro* tissue regeneration and drug development research**

In addition to its use in developmental and tissue engineering studies, micromass culture technology has been utilized for several pharmacological and toxicological evaluation studies. The high-density micromass culture system developed by Ahrens *et al*

(1977) has been used for the evaluation of potential teratogens, pharmacological inhibitors of regulatory signaling pathways and siRNA knock down of gene expression in various cell types (Bobick and Kulyk, 2004; Hoffman and Kulyk, 1999; Jin *et al.*, 2006; Kulyk and Hoffman, 1996; Wang *et al.*, 2005). Several studies have suggested that the experimental approach of generating 3-D microtissues using micromass culture technology could be a valuable tool in the initial screening of chemical or metabolic libraries for therapeutic compounds in a microscale format (Bobick and Kulyk, 2004; Watzka *et al.*, 2000; Cottrill *et al.*, 1987; Edwall-Arvidsson and Wroblewski, 1996; Hoffman and Kulyk, 1999; Kulyk and Hoffman, 1996; Mello and Tuan, 1999; Motoyama and Eto, 1994; Flint, 1983; MacDonald *et al.*, 2003 ).

The micromass culture approach can be adapted for co-culturing two or more distinct cell types at high density to allow formation of heterogeneous microtissues *in vitro* (Muraglia *et al.*, 2003). For example, co-cultures of osteoblasts and endothelial cells were used in one study to form a bi-cellular micromass tissue *in vitro* (Muraglia *et al.*, 2003). Hence, micromass cultures may be a superior replacement for 2D monolayer cultures in classical drug discovery applications. To date, there are no published reports describing the application of micromass technology in wound healing studies.

## **2.8 Experimental objectives of this Ph.D. thesis project**

The main objective of my doctoral research project was to test the hypothesis that quercetin and OTC would reduce scar formation during peridural tissue repair through direct inhibition of collagen biosynthesis and modulation of fibrosis-associated signaling cascades. The specific experimental aims of my project were:

1. To determine the effects of two potential anti-inflammatory compounds, quercetin and OTC, on parameters of peridural fibrosis in an *in vivo* model of peridural scar formation, the rat spinal laminectomy model. The parameters examined include the levels of collagen distribution and biosynthesis along with the changes in potential regulatory molecules such as Transforming Growth Factor- $\beta$ s (TGF- $\beta$ s), fibronectin and mitogen-activated protein kinases (MAPKs).

2. To develop a novel 3-D co-culture based *in vitro* wound healing model system that mimics features of *in vivo* peridural tissue repair.

The second phase of the thesis project involved adapting the micromass culture strategy to generate high-density co-cultures of skeletal myoblast and dermal fibroblast cell lines. The rationale was to encourage the skeletal myoblast and dermal fibroblast cell micromass culture conditions to form a 3-D microtissue layer that mimics *in vivo* peridural scar tissue. This artificial microtissue was then be traumatized to examine the effects of quercetin and OTC treatments on collagen deposition, cell migration, and other aspects of wound repair. This experimental system was chosen because it is a stationary culture that maintains separation of the wound edges following a scrape wound injury and allows for tracking cell migration during the time course.

3. To employ this *in vitro* wound repair model to evaluate the effects of quercetin and OTC on *in vitro* wound closure, and to determine their effects on various molecular parameters of scar formation and wound healing such as TGF- $\beta$ s and MAPKs.

## CHAPTER 3. MATERIALS AND METHODS

### 3.1 *In vivo* studies using a rat spinal laminectomy model

All protocols and procedures involving animals were conducted in accordance with the guidelines of Canadian Council on Animal Care (CCAC), and approved by the Animal Resources Centre at the University of Saskatchewan, Saskatoon, SK, Canada.

Fifty-eight male Wistar rats (~ 150-200 gm body weight) were purchased from Charles River, Laval, QC. The rats were reared in the animal care facility at the College of Medicine on a 12 h light/ 12 h dark cycle. Laboratory chow and water were given *ad libitum* throughout the experiment.

#### 3.1.1 Preparation of the animals for spinal laminectomy surgery

Prior to surgery, each animal was weighed and then anesthetized with 5% halothane (MTC Pharmaceuticals, Cambridge, ON, Canada) in 95% oxygen. The dorsal skin was shaved and disinfected with 2% chlorhexidine gluconate (Hibitane, Wyeth Animal Health, Canada) followed by 70% ethanol, before a surgical incision was made. As a pain management measure, a 0.05 mg/kg dose of buprenorphine (CDMV Inc, St Hyacinthe, QC, Canada) was administered to each rat prior to surgery. Then a maintenance dose of 1.5 - 2.0% halothane in oxygen was administered to prevent animals from regaining consciousness during the surgical procedure.

#### 3.1.2. Procedure for spinal laminectomy surgery

Using a sterile scalpel, an approximately 2 inch long incision was made through the dorsal skin surface overlying the lumbar region of the vertebral column of each rat.

The supraspinous ligaments were cut to expose the spinous processes of vertebral bodies L1 to L3. Using scissors, the adjacent erector spinae muscles were spread away on both sides from the vertebral column and held back using a chest spreader. Using a scalpel, the transversospinalis muscles were bilaterally cut at their point of attachment to the L1-L3 spinous processes, then a blunt flat-head screwdriver was used to spread the detached transversospinalis muscles laterally to permit unobstructed access to the bony spinal process (See **Figure 3 C**).

Due to the small size of the laminae (~ 2 mm), the laminectomy procedure was performed under an operative microscope (Super-Lux 400, Carl Zeiss Inc.). The general location of the spinal laminectomy surgery and the lumbar region is illustrated in **Figure 3 B**. The dorsal portions (spinal laminae along with the spinous process) of lumbar vertebrae L1 through L3 were removed by chipping away the bone using a bone rongeur (**Figure 3 A**). Any bone debris was removed from the surgical site after the laminectomy procedure. The adjacent muscle tissues were then sutured together at the dorsal midline using absorbable 3.0 vicryl sutures and the overlying skin incision was closed using a surgical stapler.

To restore body fluids lost during the surgery, each rat was subcutaneously administered 2 mL of lactated Ringer's solution (Cat #: 07953; Abbott Animal Health, Saint Laurent, QC, Canada) soon after the procedure. For post-surgery pain management, buprenorphine was administered four times at 12 h intervals following surgery for a total of 48 h. A buprenorphine dose of 0.04 mg/kg was initially administered and the dose was decreased by 0.01 mg/kg at each subsequent interval. The suture staples were removed on the seventh day following surgery.

## Figure 3

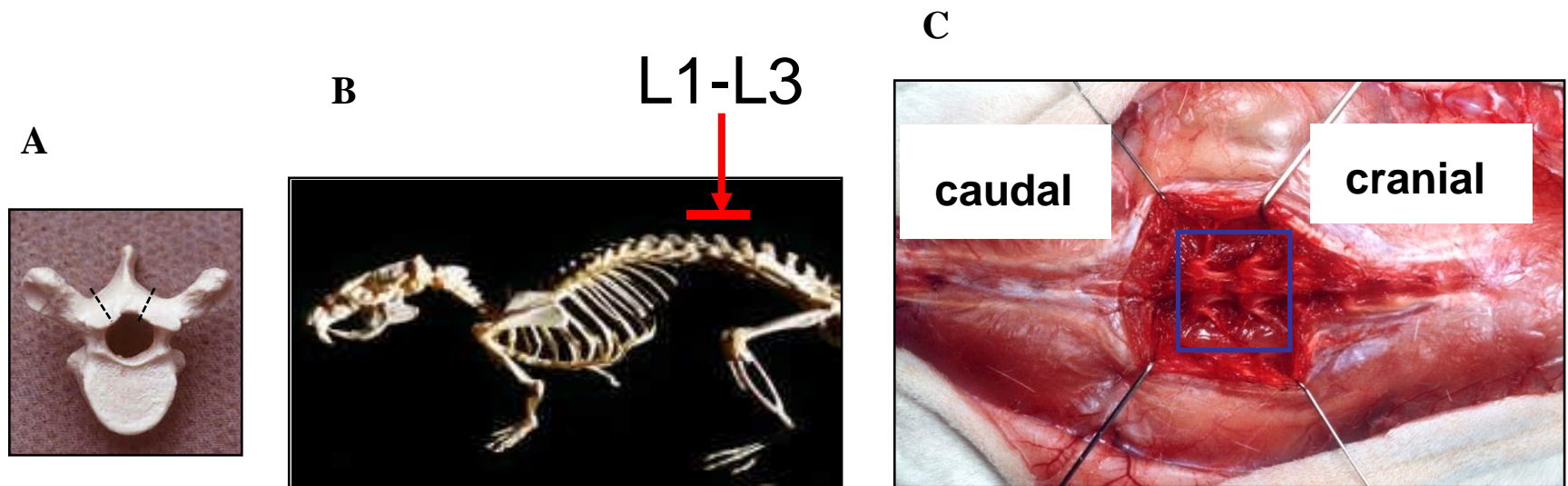


**Figure 3. Location of spinal laminectomy surgery in adult male Wistar rat.** (A) Superior view of lumbar vertebrae shows the segment of lamina between the dotted lines were excised out during spinal laminectomy surgery (B) Rat skeletal system shows the location of region L1-L3 of the rat lumbar spine. (C) shows the exposed L1-L3 region of the rat lumbar spine prior to the laminectomy procedure. The blue square shows the area where the peridural scar tissue is usually formed during the post-surgical recovery period.

### 3.1.3 Treatment groups

Following the laminectomy surgery, animals were randomly assigned to one of the three treatment groups:

**Group A (Saline Control)** animals received intraperitoneal (i.p.) injections of 3 mL normal saline (Cat #: 07983; Abbott Animal Health, St Laurent, QC, Canada) beginning at 30 min post-surgery and repeated every 12 h for a total of either 36 h (for animals sacrificed at 3 days post-surgery, n =10) or 120 h (for animals sacrificed at 21 days or 63 days post surgery, n = 9).

**Group B (OTC-treated)** animals received i.p. injections of 1 mmol/kg of L-2-oxothiazolidine-4-carboxylate (OTC, Cat #: O6254, Sigma Aldrich, St. Louis, MO, USA) dissolved in 3 mL normal saline. The treatment was started at 30 min post-surgery and repeated every 12 h for a total of either 72 h (for animals sacrificed at 3 days post-surgery, n =10) or 120 h (for animals sacrificed at 21 or 63 days post surgery, n = 10).

**Group C (Quercetin-treated)** animals received i.p. injections of 0.025 mmol/kg of quercetin (Cat #: Q-0125, Sigma Aldrich, St. Louis, MO, USA) suspended in 3mL normal saline. The treatment was started at 1 h post-surgery and repeated every 12 h for either 36 h (for animals sacrificed at 3 days post-surgery, n =10) or 120 h (for animals sacrificed at 21 or 63 days post surgery, n = 9).

An illustration of the dosing regimen used for the different treatment groups is shown in **Figure 4**.

**Figure 4**

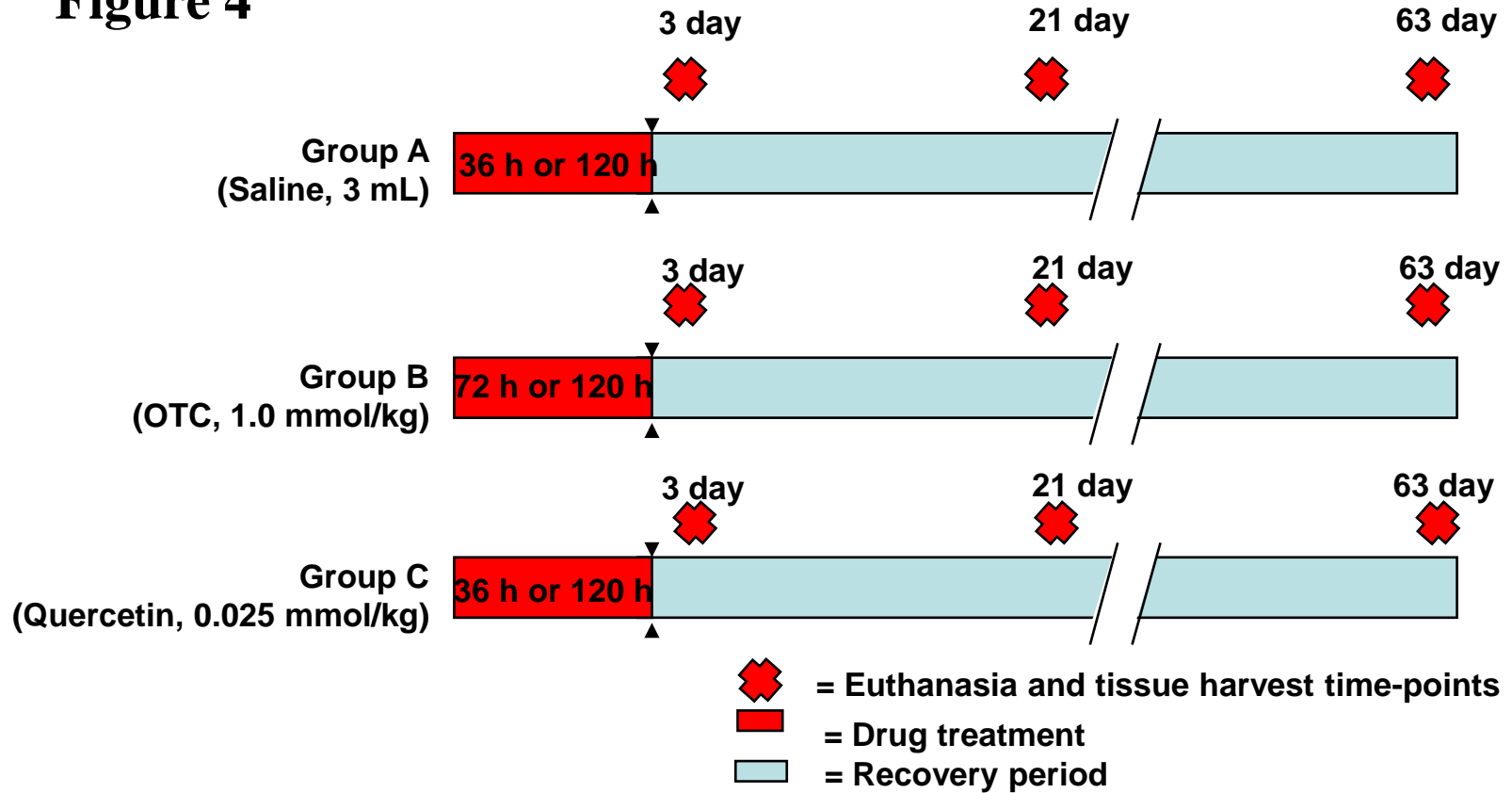


**Figure 4.** Systemic administration of L-2-oxothiazolidine-4-carboxylate (OTC) and Quercetin, shows the dosing regimen used for 3, 21 and 63 day treatment groups. The red bar shows the drug administration period in which 3 mL Saline for 36 h or 120 h (Group A), 1.0 mmol/kg OTC for 72 h or 120 h (Group B) and 0.025 mmol/kg Quercetin (Group C) for 36 h or 120 h were administered intraperitoneally to the laminectomized rats. The 3 day saline and quercetin treated animals had 36 h to recover after drug administration while all 21 day post-surgical treatment groups had 384 h ( approx. 16 days). This dosing regimen and recovery period was followed based on Schultke *et.al* (2003) and Kamenic *et.al* (2001).

### **3.1.4 Animal perfusion and harvesting of peridural wound and granulation tissue**

At representative time points of treatment (3 days, 21 days and 63 days), animals from each of the treatment groups were euthanized for collection of peridural wound tissues. For euthanasia, the rats were first anesthetized using 5% Halothane, and then an incision was made on the anterior region of the abdomen to open up the abdominal cavity. Two further incisions were made laterally through the rib cage and the diaphragm was excised to expose the heart. The left ventricle was punctured using a blunt-end needle, which was connected to an intravenous (IV) line containing cold saline. The needle was passed through the heart until it reached the aorta, held with a hemostat, and then the right atrium of the heart was cut to allow the release of blood. A cold saline drip perfusion was performed until the fluid ran clear through the right atrium of the heart to ensure blood removal from the circulatory system. No fixatives were used in the perfusion procedure to prevent interference with our subsequent tissue analyses (mRNA and protein analyses; Fourier-transformed infra-red [FTIR] spectromicroscopy).

After the perfusion was complete, an incision was made around the skin lateral to the original laminectomy wound site to expose the peridural scar tissue at lumbar region L1 through L3. The scar tissue was excised using surgical scissors. Some spinal bone fragments and healthy skeletal muscle tissue initially surrounded the excised scar. The bone fragments were removed with surgical bone rongeurs, and the healthy muscle tissue was trimmed away using a scalpel blade and fine scissors. Most of the isolated scar tissues (n=34) were weighed, then minced into small pieces (~ 1 mm<sup>3</sup>) using sterile surgical scalpel. Equal portions of the minced tissue fragments were submerged in RNAlater ICE<sup>®</sup> solution (Ambion Inc, Austin TX Cat #: 7031) and kept at -20°C as per

manufacturer's instruction, or transferred into polypropylene tubes, snap frozen in liquid nitrogen and stored at -80°C freezer until needed. The tissue fragments submerged in RNAlater ICE<sup>®</sup> solution were used for RNA analysis, while the snap frozen tissue fragments stored at -80°C were used for western blot protein analysis.

Another group of isolated scar tissues (n = 24) was processed for histological analysis. The excised scar tissues were placed in plastic molds containing O.C.T<sup>®</sup> embedding compound, (VWR Scientific, West Chester, PA) and then flash-frozen by immersion in a bath of iso-pentane cooled with liquid nitrogen. The frozen tissue blocks were serially sectioned at 10-micron thickness in a transverse plane, in a sequence corresponding to successive positions along the animal's rostral-caudal axis.

Most tissue sections were placed on precleaned Superfrost Plus glass microscope slides (VWR Scientific, Westchester, OH), two sections per slide, for a total of forty slides per animal. The slides were numbered in their order of section and stored at -80°C. The pairs of sections that were numbered ten, twelve, thirty and forty were instead mounted on MirrIR slides (Kevley Technologies, Chesterland, OH) and were subsequently used for FTIR spectral analysis of total collagen and sugar distribution by our research collaborators at the University of Manitoba. The sections on slide eleven from each animal were used for histochemical staining of fibrillar collagen using the picrosirius red polarization method (described below).

In addition, contiguous sections from each animal were used by Nicole Cox (Department of Anatomy and Cell Biology, University of Saskatchewan) for standard histological staining (*e.g.* hematoxylin and eosin; toluidine blue) and for

immunocytochemical staining to detect mast cells, activated macrophages, CD4 and CD8 T-lymphocytes (Cox, 2008).

### **3.1.5 Picrosirius red- polarization method for histochemical detection of collagen fibril distribution.**

The picrosirius red-polarization method is a specific histochemical procedure for collagen detection in tissue sections (Junqueira *et al.*, 1979). Sirius red dye binds to interstitial fibrillar collagens at acidic pH and the stained collagen fibrils display birefringence when observed by polarized light microscopy. This procedure is useful for studying total fibrillar collagen distribution in histological sections of routinely fixed and embedded tissues. Moreover, it has been reported that picrosirius red staining may even allow for some discrimination between structurally distinct collagen types in histological sections and reveal collagen fibril orientation in tissue sections. Interstitial type I collagen, which characteristically forms thick fibres, appears as strongly birefringent yellow or red fibres under polarized light when viewed by picrosirius red-polarization method (Montes and Junqueira, 1991; Montes *et al.*, 1980). In contrast, collagen type III, which forms loosely dispersed thin fibrils, displays a weaker birefringence of greenish hue. Type II collagen fibrils within hyaline and elastic cartilage exhibit weak birefringence of varying color (Junqueira and Montes, 1983). The spatial distribution and orientation of collagen fibrils in tissue sections are more prominently revealed when the stained sections are visualized under circularly polarized light.

For picrosirius red staining, cryosections of peridural scar tissues on glass slides were thawed, fixed with 10% buffered formalin, and washed twice with 1X PBS

(Phosphate Buffered Saline). The sections were stained for 90 min in 0.1% Sirius Red (Gurr<sup>®</sup>, C.I 35780; BDH Laboratory Supplies, England) dissolved in saturated picric acid solution, then washed three times for 2 min each in 5% glacial acetic acid, followed by two 5 min washes in 0.001N hydrochloric acid (method of Junqueira *et al.*,1979). Finally, the sections were dehydrated in a graded series of ethanol solutions, cleared with xylene and mounted under glass coverslips in Entellan<sup>®</sup> mounting medium (EM Science, NJ, USA; Lot #: OB 103602).

Stained slides were examined on a Nikon Optiphot.1 light microscope (Nikon, NJ, USA) equipped with two polarizing filters to yield a circularly polarized light. The lower polarizing filter was aligned such that a uniform dark background was obtained in absence of a mounted slide. The entire area of each tissue section was systematically photographed at 4X magnification using a digital camera (Nikon Coolpix 995, Nikon, NJ, USA) in a series of contiguous fields of view.

The total amount of picrosirius red positive birefringent collagen in a given area of scar tissue was quantified using Image J 1.37 G software following the image analysis protocol described in the website of the Department of Cardiovascular Physiology, University of California, San Diego, CA, ([http://cardprint.ucsd.edu/CV\\_Lab\\_Web\\_Page/HowToDocs/ImageJProtocol.pdf](http://cardprint.ucsd.edu/CV_Lab_Web_Page/HowToDocs/ImageJProtocol.pdf)) and using the automated threshold macros obtained from this source. A total of 12 separate fields of view for each scar tissue section were photographed and digitized to determine the area of picrosirius red-positive collagen within the total cross-sectional area of the scar tissue sections.

In brief, the individual digitized raw images obtained from picosirius red polarization microscopy were imported into Image J 1.37 G software. The raw images (2048 X 1536 pixel dimension) were opened in Adobe Photoshop Elements 3.0, then converted to grayscale mode and saved in high quality jpeg format. The resulting grayscale images were opened in NIH Image J software and segmented using the *Image > Adjust image > threshold* function. The threshold values were selected as “*auto*” and the area of each image containing picosirius red-positive pixels were then calculated using the *Analyze > Set Measurement* function in the Image J software and selecting the *Area* (i.e number of picosirius red positive pixels within the threshold range), *min and max gray values*, *Area Fraction* (i.e. % of total field of view containing picosirius red) data output options. Finally, the “*measure*” function was selected to output data. The resulting measurement was expressed as the “collagen area fraction”, which is the picosirius red positive area divided by the total tissue area multiplied by 100.

### **3.1.6 Synchrotron FTIR mapping for scar tissue sections**

Synchrotron FTIR mapping was performed in collaboration with Dr Gough’s laboratory at the University of Manitoba. The Synchrotron FTIR data collection and collagen spectral analysis in scar tissue sections are described in Wiens *et al* (2007). In brief, 8 to 10 maps were generated for each tissue section. Synchrotron FTIR maps were generated from histological sections using a Nicolet 860 FTIR instrument with a continuum microscope (National Synchrotron Light source, Brookhaven National laboratory, NY, USA) or Nicolet Magna 500 FTIR instrument with a Nic-Plan microscope (Synchrotron Radiation Center, Stoughton, WI, USA). All spectra were

collected at  $4\text{ cm}^{-1}$  spectral resolution with a  $12 \times 12\ \mu\text{m}$  aperture and  $10\ \mu\text{m}$  step size. Nicolet OMNIC/Altus software was used for all data acquisition and map analyses.

### **3.1.7 Total RNA isolation from the scar tissues for mRNA analysis**

Total RNA was isolated from samples of minced, frozen scar tissue following a modification of the methods of Chomczynski and Sacchi (1987) and Reno *et al.* (1997). In brief, the scar tissue were homogenized in 2-3 mL of 4 M guanidine isothiocyanate solution containing 25 mM sodium citrate, 0.5% sodium lauryl sarcosinate and 0.1 M 2-mercaptoethanol using a Brinkmann Polytron PT 10/35 tissue homogenizer. The homogenate was centrifuged (11,000 rpm, 10 min,  $4\ ^\circ\text{C}$ ) and the resulting supernatant was mixed with an equal volume of aqueous saturated phenol (Cat #: P-4682, Sigma Chemical Co, St Louis, MO),  $1/10^{\text{th}}$  volume of 2 M sodium acetate (pH 4.0), and  $2/10^{\text{th}}$  volume of 49:1 (w/v) chloroform/isoamyl alcohol. Following centrifugation at 11,000 rpm for 10 min at  $4\ ^\circ\text{C}$ , the upper aqueous layer was carefully removed and then mixed with an equal volume of 70% ethanol. This aqueous ethanol mixture was then passed through a Qiagen RNeasy<sup>®</sup> Plus spin column. The column was washed and the RNA was eluted as per the manufacturer's instructions. To determine the quality of the isolated total RNA, an aliquot of each sample was subjected to denaturing gel electrophoresis, then stained with 1/1,000 dilution of Radiant Red<sup>®</sup> (BioRad, Cat # 170-3122) and examined under UV transillumination to visualize the 18S and 28S rRNA bands. Most RNA samples showed notable band smearing and streaks within the running lanes, suggesting the presence of residual DNA or protein impurities. To remove these impurities, the RNA samples were dissolved in a final volume of  $100\ \mu\text{L}$  RNase-free

water, then mixed with 300  $\mu\text{L}$  Trizol<sup>®</sup> LS (Cat #: 10296-010, Invitrogen, Carlsbad CA) and 80  $\mu\text{L}$  49:1 (w/v) chloroform/isoamyl alcohol. After centrifugation for 10 min at 11,000 rpm, 4°C, the upper aqueous layer was removed, combined with an equal volume of 70% ethanol, and then passed through a second RNeasy<sup>®</sup> Plus spin column (Cat #: 74134, Qiagen GmbH, Hilden). The total RNA yield from each sample was estimated by measuring the optical density (OD) at 260 nm using a SmartSpec<sup>™</sup>3000 spectrophotometer (Biorad, Hercules, CA) and the OD 260 nm/ 280 nm ratio was measured to assess RNA purity. Since the OD 260 nm readings for most samples were quite low and potentially unreliable, a more sensitive Ribogreen fluorometric RNA quantification assay was used to accurately quantify the relative amounts of total RNA in the various scar tissue samples.

### **3.1.8 RiboGreen RNA quantification assay.**

The relative total RNA contents of the scar tissue RNA samples after the clean up procedure were determined by the RiboGreen fluorescence assay (Molecular Probes) as per manufacturer's instructions. In brief, a 2  $\mu\text{L}$  aliquot of each RNA sample was combined with 18  $\mu\text{L}$  of deionized formamide and 500  $\mu\text{L}$  of TE buffer. A "1X RNA standard" was generated by pooling RNA aliquots from several scar tissue samples in a final volume of 200  $\mu\text{L}$  TE. A dilution series of this standard (1/2X, 1/4X, 1/8X, 1/16X, 1/32X) was prepared by successive 2-fold dilutions of the 1X standard with equal volumes of TE buffer containing 3.6% formamide. 100  $\mu\text{L}$  aliquots of each diluted RNA sample and each RNA standard were transferred to individual wells of a black 96-well microtiter plate, and then mixed with an equal volume of 1% RiboGreen reagent

dissolved in TE. The fluorescence intensity of each sample was measured using a Dynex Fluorolite 1000 fluometric plate reader set at 485 nm excitation and 530 nm emission wavelengths. A standard curve was obtained by plotting the fluorescence values of the RNA standard series against their relative RNA contents in arbitrary units (i.e. 1, 2, 4, 8, 16, 32 RNA units). The relative RNA content of each sample was then determined from the linear regression equation of this standard curve using InStat 2.01 software.

### **3.1.9 Analysis of gene-specific mRNA transcripts by RNA dot blot and Northern blot hybridization.**

#### **3.1.9.1 Primer design and generation of antisense cDNA probes to specific genes of interest using PCR cloning strategy.**

The cDNA sequences for rat Collagen type 1 ( $\alpha 2$ ), Collagen type 3 ( $\alpha 1$ ), Collagen type 4 ( $\alpha 1$ ), CD44, receptor hyaluronan mediated motility (RHAMM), hyaluronan synthases (HAS 1, HAS 3), heat shock protein-47, TGF- $\beta$ 1, TGF- $\beta$ 3 and GAPDH were obtained from GenBank<sup>®</sup> and used to design pairs of specific forward and reverse PCR primers. A degenerate PCR primer designed by Pearson et al (1996) was used for the isolation of rat hsp-47 cDNA in this study. All oligonucleotide primers were custom synthesized by Sigma Genosys, Canada or Integrated DNA Technologies. A complete list of the gene-specific PCR primers designed and the predicted size of their corresponding PCR amplicons is shown in **Table.4**.

Total RNA was isolated from the heads and torsos of 18 day rat embryos and reverse transcribed into cDNA using RevertAid<sup>™</sup> M-MuLV reverse transcriptase (Cat #: EP0441, Fermentas Life Sciences,) as per the manufacturer's procedure. In brief, 0.5  $\mu$ g of oligo(dT)18 primer was combined with 2  $\mu$ g rat embryo RNA in a final volume of 11

$\mu\text{L}$  nuclease free water, and incubated at  $70^{\circ}\text{C}$  for 5 min. Then 4  $\mu\text{L}$  5X reaction buffer, 2  $\mu\text{L}$  10 mM dNTP mix and 20 units of ribonuclease inhibitor (Promega) were added and the volume was adjusted to 19  $\mu\text{L}$  using nuclease free water. Following incubation for 5 min at  $37^{\circ}\text{C}$ , 200 units (1  $\mu\text{L}$ ) of RevertAid™ M-MuLV reverse transcriptase were added and the reaction mixture was incubated at  $42^{\circ}\text{C}$  for 60 min in a MJ Research thermocycler. The reaction was stopped by heating at  $70^{\circ}\text{C}$  for 10 min and then chilled on ice.

Aliquots of the above cDNA reaction mixture were used in combination with the gene-specific primer pairs listed in **Table 4** to amplify cDNA fragments corresponding to our various genes of interest. Amplifications were carried out in a 100  $\mu\text{L}$  reaction solution containing 2  $\mu\text{L}$  rat embryo cDNA template, 1 unit of Platinum Taq polymerase (Invitrogen™, Cat.no: 10966-018), 1X Taq buffer, 1.5-2.0 mM  $\text{MgCl}_2$ , 0.2 mM mixed dNTP, and 20 pmol of gene-specific forward primer and 20 pmol gene-specific reverse primer.

The amplification conditions were an initial “hotstart” of one min at  $94^{\circ}\text{C}$  followed by 30 cycles of  $95^{\circ}\text{C}$  denaturing for 30 sec,  $58^{\circ}\text{C}$  annealing for 30 sec, and  $72^{\circ}\text{C}$  primer extension for 45 sec in a MJ Research thermocycler. The PCR products obtained were separated on 1.5% agarose gels, stained with ethidium bromide (0.5  $\mu\text{g}/\text{mL}$ ) and examined by ultraviolet light in order to verify that the reactions amplified DNA fragments of the predicted size.

The resulting PCR products were then ligated into plasmid pBluescript (Stratagen) using a TA cloning strategy. First, 10  $\mu\text{g}$  of pBluescript vector was digested with EcoRV (Boehringer Mannheim). Then “T” overhangs were added by combining 10

µg digested vector with 10 X PCR buffer, 6 µL 25 µM MgCl<sub>2</sub>, 2 µL 10 mM dTTP and 10 Units of Taq polymerase (Invitrogen) into a total reaction volume of 100 µL. The reaction mixture was incubated for 2 h at 70°C after which the vector was purified by phenol:chloroform extraction and ethanol precipitation. Amplified cDNA fragments corresponding to our various genes of interest were ligated into the modified EcoRV site of the pBluescript vector. The ligation reaction mixture consisted of 0.5 µL or 1.5 µL of fresh RT-PCR products combined with 50 ng pBluescript plasmid and 4 units T4 DNA ligase (Invitrogen, 4 Units/µL) in 1X ligation buffer ( provided with ligase enzyme). The ligation reactions were incubated overnight at 14° C.

The ligated plasmids were transformed into chemically competent DH5α *E. coli* (Invitrogen) as per manufacturer's procedure. To a 50 µL aliquot of competent DH5α cells, 2 µL of ligation mixture was added and then incubated on ice for 30 min. The mixture was incubated at 37°C for exactly 20 sec, and chilled on ice for 2 min. Then 950 µL of room temperature SOC medium (2% Tryptone, 0.5% yeast extract, 10mM NaCl, 2.5mM KCl, 10mM MgCl<sub>2</sub>-6H<sub>2</sub>O, 20 mM Glucose) was added and the bacteria were then incubated in a shaking incubator at 37°C for 1 h. Approximately 100 µL of each transformation mixture was plated onto labeled LB agar plates (1.0% Tryptone, 0.5% yeast extract, 1.0% NaCl, 15 gm/L agar) containing 75 µg/mL ampicillin and 80 µg/mL X-gal (for blue/white color screening) and incubated overnight at 37°C.

**TABLE.4. Synthetic oligonucleotide PCR forward and reverse primer design.** Primer sequences were determined from the GenBank® accession numbers for rat specific genes and the rat specific primers for the genes of interest were designed and used for cDNA probe synthesis (*in vivo* studies – Northern and RNA dot blot hybridization) and RT-PCR (for *in vitro* studies)

	Primer sequences	NCBI Accession number	Corresponding nucleotide sequence	Amplified cDNA segment
<b>Collagen 1(<math>\alpha</math>2)</b>	FORWARD: 5'GGTCGCCCTGGAGAACCTG-3' REVERSE: 5'GGACCTCGGATTCCAATAGG-3'	NM_053356.1	1333-1850	518 bp
<b>Collagen 3(<math>\alpha</math>1)</b>	FORWARD: 5'-GAAGTCTCTGAAGCTGATGG-3' REVERSE: 5'-CGTCAACCAGTGAAAGTGAC-3'	AJ005395	1015-1637	623 bp
<b>Collagen 4(<math>\alpha</math>1)</b>	FORWARD: 5'-TTCCTTTGTGATGCACACCAGC-3' REVERSE: 5'-CGAGAACTCACAAGAAACC-3'	XM214400	4596 - 5191	596 bp
<b>CD-44</b>	FORWARD: 5'-CCAGGACTGAAGCAGCTGACC-3' REVERSE: 5'-GGATGACGCCTTCTTTATTGG -3'	NM012924	255-765	511 bp
<b>GAPDH</b>	FORWARD: 5'-CATTGACCTCAACTACATGG-3' REVERSE: 5'-CAGTGAGCTTCCC GTTCAGC-3'	M17701.1	135-712	578 bp
<b>hsp-47</b>	FORWARD: 5'- CGGGGCGGCCGCGAPGTNANARGAYGT-3' REVERSE: 5'- GCCCCGCGCCGCARRTG YTTTTCNARRTC-3'	(Degenerate sequence used)	-	~ 400 bp
<b>HAS-1</b>	FORWARD: 5'-CTATGAAGCCGTGGTTTCTG-3' REVERSE: 5'-AGCAGCAGTAGAGCCCAGAGTGC-3'	NM_172323	1263-1598	336 bp
<b>HAS-3</b>	FORWARD: 5'-TCTTGATGGCTGCTACTGG-3' REVERSE: 5'-TGAGCCTACAGAACCAGTGC-3'	NM_172319	1727-2014	288 bp
<b>RHAMM</b>	FORWARD: 5'-GGAGCATGATGGCTAAACAGG-3' REVERSE: 5'-CCACTGTGATTGCGCAAGAG-3'	AF133037	572-1351	780 bp
<b>TGF-<math>\beta</math>1</b>	FORWARD: 5'-CTGCAAGACCATCGACATGG-3' REVERSE: 5'-TGGTAGAGTTCTACGTGTTGC-3'	NM021578	508-926	419 bp
<b>TGF -<math>\beta</math>3</b>	FORWARD: 5'-CAGTTGTTACACATCCTCTGG-3' REVERSE: 5'-CCACATATGCCAGTGGTGATCAG-3'	AF153012	1615-2038	424 bp

Positive clones (white coloured colonies) on the LB agar plates were numbered, and using sterile toothpicks, cells from a portion of the positive clones were removed, and lysed in lysis buffer. The colony lysates were screened by PCR amplification using gene specific forward and reverse primers, and the products subsequently separated on a 1.5% agarose gel to verify that plasmids had successfully incorporated the desired cDNA inserts. The lysates were also subjected to PCR screening using M13 Forward and gene-specific reverse primers or M13 Reverse and gene specific forward primers to determine the orientation of the cDNA insert. The bacterial colonies containing the correct gene insert were identified and grown overnight in liquid LB medium containing 75 µg/mL ampicillin for plasmid isolation. The plasmid isolation was performed using a Qiagen MIDI prep kit according to manufacturer's detailed protocol. The isolated plasmid DNA pellets were dissolved in 50 µL of TE buffer (pH 8.0).

The resulting cloned cDNA plasmids were sequenced at the DNA sequencing core facility of the University of Calgary to confirm their identity with the Genbank sequences for rat Collagen type 1 ( $\alpha$  2) (GenBank accession #: NM\_053356.1), Collagen type 3 ( $\alpha$  1) (GenBank accession #: AJ005395), Collagen type 4 ( $\alpha$  1) (GenBank accession #: XM214400), GAPDH (GenBank accession #: M17701.1), TGF-  $\beta$ 1 (GenBank accession #: NM021578) and TGF-  $\beta$ 3 (GenBank accession #: AF153012). The cloned cDNA plasmids were used as templates to generate single stranded  $^{32}\text{P}$ -labelled antisense cDNA probes for use in Northern and RNA dot-blot hybridization analysis are described below (Kulyk *et al.*, 2000).

### 3.1.9.2 Generation of <sup>32</sup>P radio-labeled antisense cDNA probes using LPCR method

Single-stranded <sup>32</sup>P-labeled antisense cDNA probes were prepared by the “linear PCR” (LPCR) method of Konat (1996). Each LPCR reaction mixture consisted of 20 - 30 ng of double-stranded cDNA template for the gene of interest, 25 pmol of the corresponding gene-specific reverse oligonucleotide primer, 2 μL each of 0.5 mM dTTP, 0.5 mM dGTP and 0.5 mM dATP, 5 μL of 10 μM non-radioactive dCTP, 75 μCi of α-<sup>32</sup>P-dCTP (10 μCi/μl), 5 μL of 10X PCR buffer, 2 μL 50 mM MgCl<sub>2</sub>, and 1 μL (5 units) Taq polymerase in a final volume of 50 μL. Following 30 amplification cycles at 94 °C for 2 min; 55 °C for 2 min; and 72 °C for 5 min in an MJ Research thermocycler, the reaction mixture was passed through a Sephadex G-25 or Sephadex G-50 spin column packed in a Costar spin-X 0.2 μm micropore filtration unit in order to remove unincorporated label. The specificities of the resulting <sup>32</sup>P-labeled antisense cDNAs probes for target mRNAs of correct size were confirmed on preliminary Northern blots of total RNA isolated from heads and torsos of 18 day old rat embryos. Equal amounts (5-10 μg) of total RNA were separated by electrophoresis through 1.2% agarose gels containing 6% formaldehyde in 1X MOPS buffer running at 5 V/cm of gel. The RNA was transferred to nylon membranes by standard upward capillary transfer, pre-hybridized in Ultrahyb<sup>®</sup> solution (Cat #: 8669, Ambion, Austin, TX) and hybridized with <sup>32</sup>P-labeled antisense cDNAs probes as detailed in **Section 3.1.9.3**.

The cDNA probes hybridized to mRNA transcripts of appropriate lengths based on published reports (see **Figure 5**). The antisense cDNA probes for collagen type 1(α 2)

## FIGURE 5

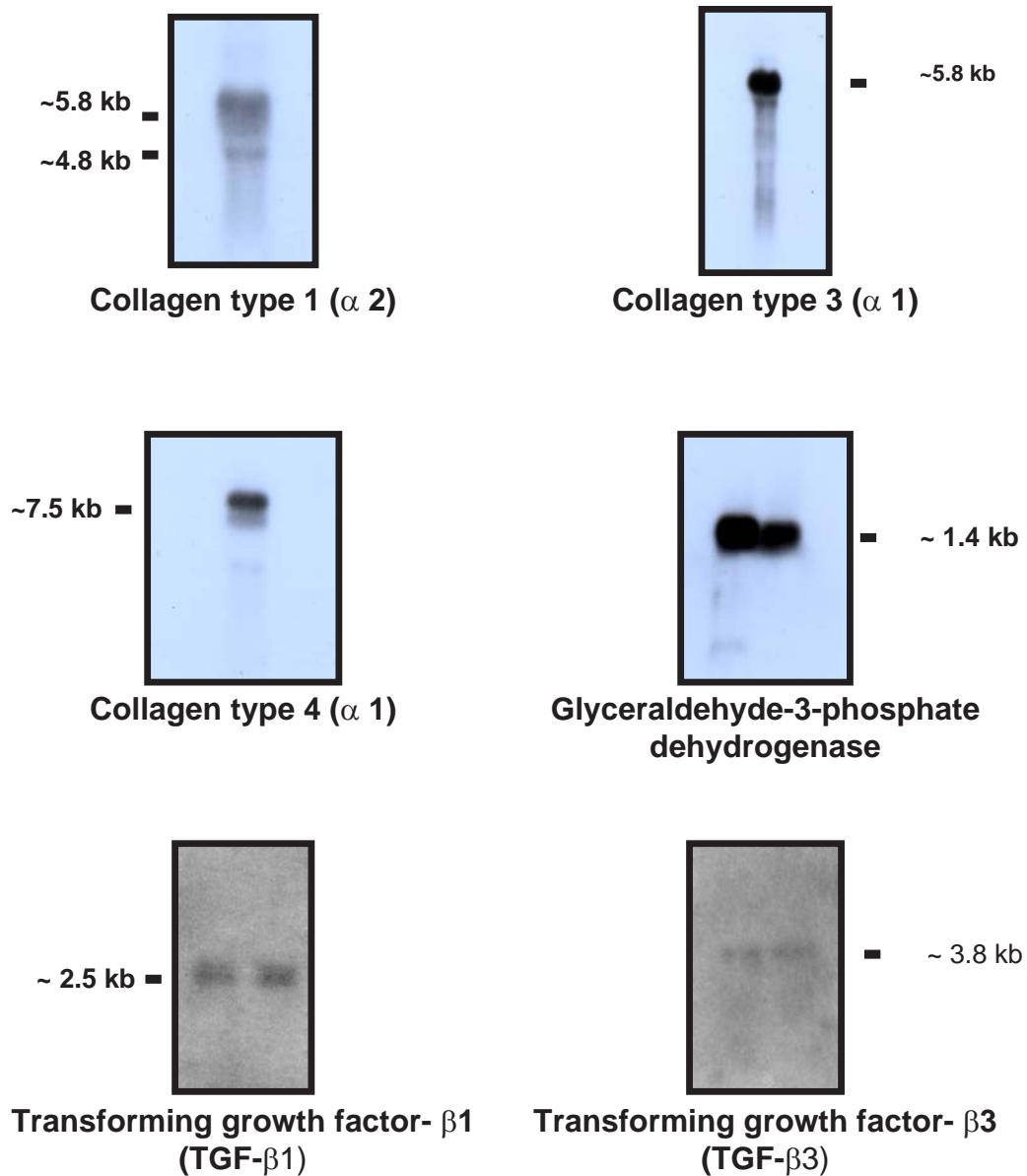


**Figure 5. Specificity of the cDNA probes developed.** Northern blot analysis using 18 day old rat embryo head and/or torso RNA shows specificity of anti-sense cDNA probes generated against rat collagen type 1 ( $\alpha$  2), collagen type 3 ( $\alpha$  1), collagen type 4 ( $\alpha$  1), glyceraldehyde-3-phosphate dehydrogenase (GAPDH), TGF- $\beta$ 1 and TGF- $\beta$ 3 transcripts. The antisense cDNA probes recognized mRNA transcript of appropriate lengths based on previously published reports.

hybridized to transcripts of 4.8 and 5.8 kb length, while collagen type 3 ( $\alpha$  1) cDNA hybridized to transcripts of 5.8 kb length (Annoni *et al.*, 1998; Stewart *et al.*, 1994). A single transcript of 7.5 kb was recognized by the collagen type 4 ( $\alpha$  1) cDNA probe (Olsen and Uitto, 1989). The GAPDH probe hybridized to a 1.4 kb mRNA transcript (Annoni *et al.*, 1998; Oikarinen *et al.*, 1991). The TGF- $\beta$ 1 cDNA probe recognized a 2.4 kb transcript (Annoni *et al.*, 1998; di Mola *et al.*, 2002) and a single faint band of 3.8 kb was recognized by the TGF- $\beta$ 3 probe (Annoni *et al.*, 1998; di Mola *et al.*, 2002; Wildi *et al.*, 2007).

### **3.1.9.3. Analysis of mRNA transcripts using RNA dot blot analysis.**

For RNA dot-blot analysis, equal aliquots of total RNA (as determined by the RiboGreen assay) were spotted onto MagnaGraph 0.45 micron nylon membrane (Osmonics Inc, MA) using a 96-well BioDot (Bio-Rad) vacuum filtration unit. Following transfer, all blots were baked in a vacuum oven for 1.5-2.0 hours at 80°C, then prehybridized overnight with Ultrahyb<sup>®</sup> solution (Cat #: 8669, Ambion, Austin, TX) at 42 °C. Next, the blots were hybridized at 55 °C overnight in Ultrahyb<sup>®</sup> solution containing <sup>32</sup>P labeled cDNA probes specific probes for Collagen Type 1 ( $\alpha$  2), Collagen Type 3 ( $\alpha$  1), Collagen Type 4 ( $\alpha$  1), TGF- $\beta$ 1, TGF- $\beta$ 3 or GAPDH. All the probes were labeled by the LPCR method (Konat, 1996) as described in **Section 3.1.9.2**. The blots were washed 4 times (5 min each) at 42-55 °C in 2X SSC (0.3 M NaCl and 0.03 M Sodium citrate) / 0.1% sodium dodecyl sulfate (SDS) (w/v), then 4 times (15 min each) at 42-55 °C in 0.1X SSC (0.015 M NaCl and 0.0015 M Sodium citrate) / 0.1% SDS (w/v), and exposed

to Kodak BioMax-AR film at -80 °C. Hybridization signals were quantified by densitometric measurements at 540 nm wavelength on the exposed autoradiographs using a Tecan SLT Spectra II spectrophotometric plate reader. To correct for any variations in sample loading, the hybridization signals for Collagen Type 1 ( $\alpha 2$ ), Collagen Type 3 ( $\alpha 1$ ), Collagen Type 4 ( $\alpha 1$ ), TGF- $\beta$ 1, and TGF- $\beta$ 3 mRNAs were normalized against signals for the constitutively expressed GAPDH transcript.

### **3.1.10 Analysis of proteins from scar tissue**

#### **3.1.10.1 Tissue preparation for protein analysis**

Minced tissues for protein analysis that had been stored frozen as described in **Section 3.1.4** were homogenized using a Polytron tissue homogenizer in Western lysis buffer consisting of 50 mM Tris, pH 7.4, 150 mM NaCl, 1% Nonidet P-40, 0.1% SDS, supplemented with protease and phosphatase inhibitors (Sigma). Homogenates were mixed with an equal volume of 2X SDS-Urea loading buffer (50 mM Tris, pH 7.5, 50 mg/mL SDS, 8M Urea, 0.4% bromophenol blue, 0.1% 2-mercaptoethanol) and then sonicated for 30 to 45 seconds using a VibraCell<sup>TM</sup> sonicator (Sonic & Materials Inc., Danbury, CT, USA). The homogenates were centrifuged to remove any insoluble material, and frozen at -20°C until needed for analysis.

#### **3.1.10.2 Total protein estimation using filter-paper dye binding assay**

The total protein content of the tissue homogenates was determined by the method of Minamide and Bamberg (1990). This filter paper-based adaptation of the Bradford protein dye-binding assay (Bradford, 1976) has much greater resistance to interference by

reagents commonly used in tissue lysis buffers such as SDS, Triton X-100, and urea. Protein samples dissolved in gel loading buffer were applied to a grid of 1.5 cm X 1.5 cm squares drawn on a sheet of Whatman filter paper, at volumes between 0.5 - 10  $\mu$ L per square. Each sample was applied in quadruplet. A series of protein standards in gel loading buffer (0 - 25  $\mu$ g per square) were applied in triplicate on the same piece of filter paper. Squares to which 1X SDS-Urea gel loading buffer alone were applied served as blanks. The spotted sheet of filter paper was dried then rinsed in methanol for 20 – 60 sec until the loading buffer dye was washed away. After air-drying, the sheet was stained for 30 min at room temperature in a solution of 0.5% Coomassie Brilliant Blue-G in 7% acetic acid. The filter paper was then destained in 7% acetic acid for about 90 min with gentle agitation until the background staining was adequately reduced. The sheet was air-dried overnight, then individual squares were cut out and placed in microfuge tubes containing 1 mL extraction buffer (66% methanol, 33% distilled water, 1% ammonium hydroxide). Tubes were vortexed until the bound dye was completely eluted into the extraction buffer, then 300  $\mu$ L aliquots of eluate were transferred to individual wells of a 96-well microtiter plate. The absorbance of each sample at 600 nm wavelength was determined using a Tecan Spectra II plate reader. A standard curve was obtained by plotting the absorbance values of the protein standard series against their protein content. The protein content for each scar tissue sample was determined from the linear regression equation of the standard curve using InStat <sup>®</sup> software.

Preliminary experiments were performed to determine a suitable protein standard for quantifying the relative protein contents of scar tissue homogenates as well as cultured rat cell homogenates. Bovine serum albumin (BSA),  $\gamma$ -globulin, and various

combinations of these two proteins were tested. A dilution series of each protein standard or protein standard mixture (0 - 25 µg content) were spotted in quadruplicate onto the filter paper grid. Aliquots of 1 - 8 µL of scar tissue homogenate and cultured rat cell homogenates were applied to the same sheet of filter paper. The filter paper was processed as described above and absorbance values at 600 nm were determined. The slopes for the tissue homogenates and for each series of protein standards were obtained by plotting individual absorbance values against their appropriate relative volume or protein content. The slope of the regression line for the 3 day scar tissue homogenate was 0.9999, while slopes of 0.9967 and 0.9999 were obtained for 21 day scar tissue homogenate and cultured rat cell homogenates respectively. A 1:3 mixture (w/w) of BSA and  $\gamma$ -globulin yielded a slope of 0.9998, corresponding well with both the scar tissue homogenates and cultured rat cell homogenates (**Figure 6**). Therefore, a 1:3 mixture of BSA: $\gamma$ -globulin mixture was used as the protein standard in all subsequent protein determinations.

### **3.1.10.3 SDS-PAGE gel preparation for Western blot analysis**

Proteins were separated by denaturing SDS-polyacrylamide gel electrophoresis following standard methods (Ausubel *et al.*, 1994) with the following modification. In order to simultaneously resolve high molecular weight proteins (100 - 300 kDa) and low molecular weight proteins (20 - 99 kDa ) within the gel, a dual concentration (5% / 12.5%, pH 8.8) SDS-polyacrylamide (PA) 'resolving' split gel was prepared in a Bio-Rad Protean III Minigel apparatus. Briefly, a 12.5% gel was poured into the lower 2.5 cm of the casting plates and allowed to solidify for 4 hours before pouring a 5% gel layer (~ 2.5

## FIGURE 6

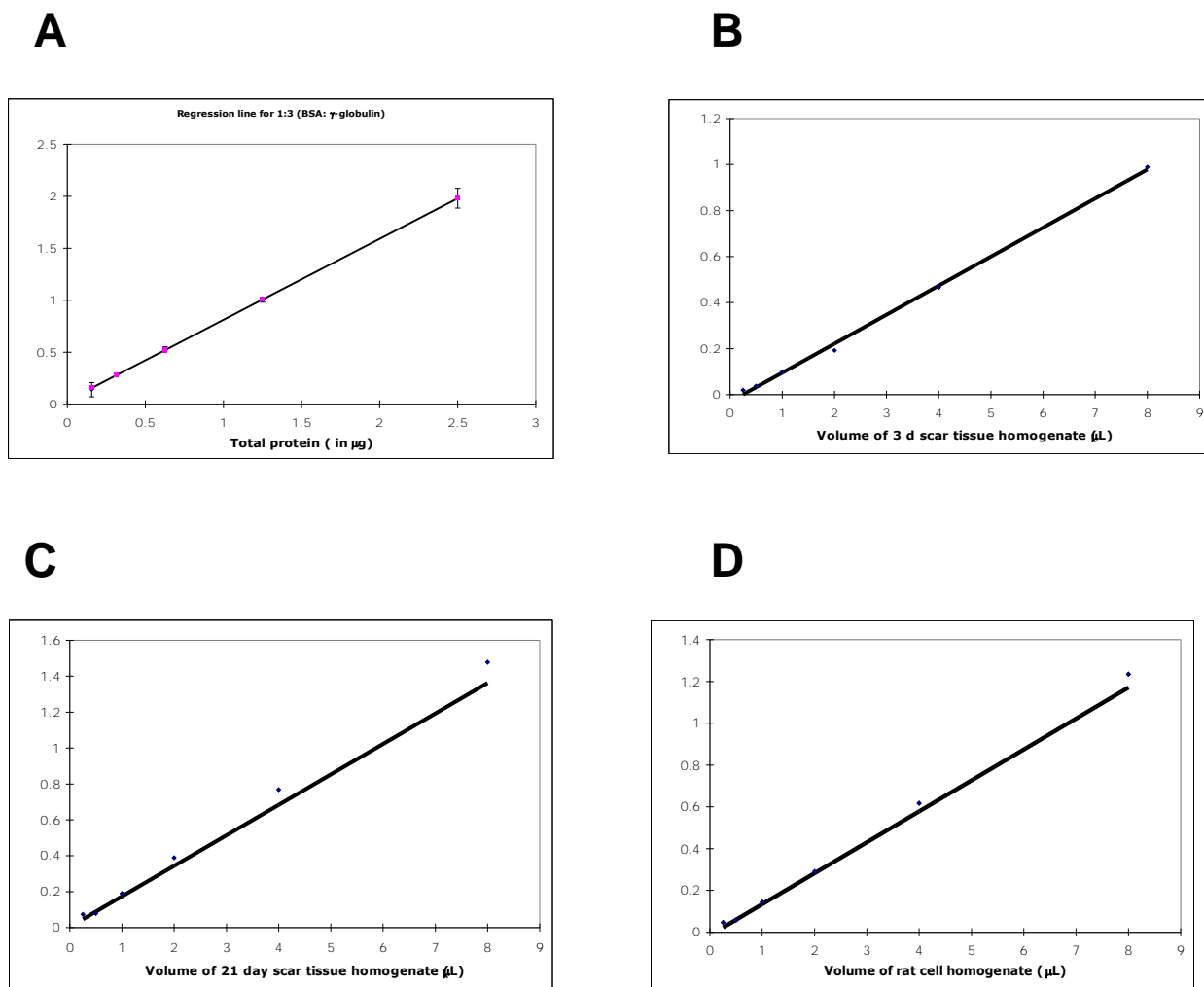


**Figure 6. Regression line analysis of rat tissue homogenates.** (A) shows that when BSA and  $\gamma$ -globulin were combined in a ratio of 1:3 (w/w) gave a slope of 0.9998 which corresponds well with 3 day peridural scar homogenate (B) with slope of 0.9999 and 21 day peridural scar homogenate (C) with slope of 0.9967 as well as cultured rat cell homogenates (D) with slope of 0.9999. In subsequent experiments where protein quantification is required the 1:3 (w/w) ratio of BSA and  $\gamma$ -globulin mixture was used as standard protein standard.

cm) above. The split gel was then allowed to solidify in presence of 0.1% SDS overlay overnight to allow pH equilibration. Then a 4 % 'stacking' gel (pH 6.8) was poured at the top of the casting plates and a 1.5 mm thick protein loading comb was inserted. The stacking gel was allowed to solidify for 45 min prior to sample loading. The rationale of this split gel method was to minimize procedural errors (such as sample loading, variability during protein resolution and transfer to nitrocellulose membranes) when performing repetitive western blotting for analyzing multiple proteins of varying molecular weight.

#### **3.1.10.4 Gel electrophoresis and immunoblotting**

Samples were loaded into SDS-PA gels at equivalent amounts of total protein (10-20 µg). Electrophoresis and subsequent protein transfer onto nitrocellulose was performed using a Bio-Rad Protean III Minigel apparatus according to a standard protocol. The nitrocellulose membrane was incubated for 1 h at room temperature in blocking solution (10 % w/v blotting grade nonfat dry skimmed milk [BioRad] in PBS/Tween-20 [PBST]) to prevent non-specific binding of antibodies to the membrane. Primary and secondary antibodies were diluted in 1% blotting grade nonfat dry milk in PBST. A variety of primary antibodies were used to detect the proteins of interest on the western blots, as tabulated in **Table 5**. A rabbit polyclonal antibody against the human type I procollagen was obtained from Dr. Larry Fisher (LF-67, NIDCR-NIH, Maryland, USA). This antibody was generated against a 26 amino acid synthetic C-terminal telopeptide of the human  $\alpha 1$  (I) procollagen chain (Fleischmajer *et al.*, 1990) and was shown to recognize rat type I collagen in tissue samples. Commercial polyclonal or

monoclonal primary antibodies were used to detect fibronectin, MyoD, myogenin, MyHC, hsp-47, VEGF, total ERK1/2, dual phosphorylated ERK1/2, dual phosphorylated p38 MAPK, total p38 MAPK, P4H and GAPDH in tissue homogenates as detailed in **Table 5**. The primary antibodies were detected using compatible horseradish peroxidase-conjugated secondary antibodies (BioRad) together with the Western Blot Chemiluminescence Reagent Plus detection system (Perkin-Elmer Life Sciences) as per the manufacturer's instructions. The specificities of the primary antibodies were confirmed by performing western blot analysis using tissue homogenate obtained from 18 day old rat embryos.

### **3.1.11 Statistical analysis**

Quantitative data pertaining to levels of picrosirius red stainable collagen, mRNA expression and relative protein abundance were analyzed using one-way analysis of variance (ANOVA) together with Kruskal-Wallis non-parametric test and Dunnett's multiple comparison post-tests (GraphPad Prism 4 software).

**Table 5. Primary antibodies used for western blot analysis (WB) and immunohistochemistry (IHC).**

<b>Antisera</b>	<b>Type and source of the antibody</b>	<b>Dilution used</b>	<b>Catalog number and Source</b>
<i>Anti-type I Collagen</i>	Rabbit polyclonal antibody raised against C-terminal telopeptide of human type I ( $\alpha 1$ ) collagen chain.	1:10,000 (WB) 1: 1000 (IHC)	LF 67, a gift by Dr Larry Fisher, NIH-NIDCR, MD, USA
<i>Anti-P4H</i>	Mouse monoclonal antibody raised against the beta subunit of rat prolyl-4-hydroxylase.	1:20,000 (WB)	AF-5150, Mediacorp Inc, Montreal, Canada
<i>Anti-hsp 47</i>	Mouse monoclonal antibody raised against rat Hsp-47.	1: 10,000 (WB)	M16.10A1; Stressgen, Ann Arbor MI, USA.
<i>Anti-fibronectin</i>	Rabbit polyclonal antibody raised against C-terminus of human fibronectin.	1:1000 (WB) 1: 100 (IHC)	sc-9068, Santa Cruz Biotech, CA, USA.
<i>Anti-MyoD</i>	Rabbit polyclonal antibody raised against mouse MyoD protein.	1:1000 (WB) 1: 250 (IHC)	sc-760, Santa Cruz Biotech, CA, USA.
<i>Anti-MyHC</i>	Mouse monoclonal antibody raised against human myosin heavy chain (MyHC).	1:1000 (WB) 1: 250 (IHC)	F1.652, Developmental Studies Hybridoma Bank, Iowa, USA
<i>Anti-myogenin</i>	Mouse monoclonal antibody raised against rat myogenin protein.	1: 500 (WB) 1:250 (IHC)	F5D, Developmental Studies Hybridoma Bank, Iowa, USA
<i>Anti-osteopontin</i>	Mouse monoclonal antibody raised against rat osteopontin.	1: 100 (WB) 1: 25 (IHC)	MPIIB10, Developmental Studies Hybridoma Bank, Iowa, USA

**Table 5. Primary antibodies used for western blot analysis (WB) and immunohistochemistry (IHC) (Contd...)**

<b>Antisera</b>	<b>Type and source of the antibody</b>	<b>Dilution used</b>	<b>Catalog number and Source</b>
<i>Anti-<math>\alpha</math>-sma</i>	Mouse monoclonal antibody raised against rat $\alpha$ -sma.	1: 1000 (WB) 1: 500 (IHC)	Gifted by Dr. Ronald Doucette, Dept of Anatomy and Cell Biology, University of Saskatchewan.
<i>Anti-<math>\beta</math> actin</i>	Mouse monoclonal antibody raised against chicken $\beta$ - $\square$ actin.	1: 1000 (WB) 1: 250 (IHC)	JLA 20, Developmental Studies hybridoma Bank, Iowa, USA.
<i>Anti-VEGF</i>	Mouse monoclonal antibody raised against human VEGF.	1: 1000 (WB)	sc-7269, Santa Cruz Biotech, CA, USA
<i>Anti-GAPDH</i>	Mouse monoclonal antibody raised against rabbit GAPDH	1: 10, 000 (WB)	MAB374, (Chemicon Intl) Cedarlane, ON, Canada.
<i>Anti-phospho ERK1/2</i>	Rabbit polyclonal antibody raised against synthetic KLH coupled Thr202/ Tyr 204 of human p44 MAP kinase	1: 1000 (WB) 1: 500 (IHC)	#9101, Cell Signaling Technology, MA, USA.
<i>Anti-total ERK2</i>	Rabbit polyclonal antibody raised against C-terminus of rat ERK 2	1: 1000 (WB) 1: 500 (IHC)	sc-154, Santa Cruz Biotech, CA, USA.
<i>Anti-phospho p38 MAPK</i>	Rabbit monoclonal antibody raised against KLH coupled Thr180/Tyr182 of human p38 MAPK	1: 1000 (WB) 1: 500 (IHC)	#4631, Cell Signaling Technology, MA, USA.
<i>Anti-total p38 MAPK</i>	Rabbit polyclonal antibody raised against C-terminus of mouse p38- $\square$ $\square$ protein.	1: 1000 (WB) 1: 500 (IHC)	sc-535, Santa Cruz Biotech, CA, USA.

### **3.2 *In vitro* studies using micromass co-culture technology**

The peridural scarring caused by lumbar spinal laminectomy in rats is likely to involve interactions of fibroblasts and injured muscle tissue at the wound region. Hence, the *in vitro* model system developed for our studies employed co-culturing fibroblasts (FR 3T3 fibroblasts) and myoblast cells (adult rat L8 myoblasts) at high cell density to generate a “micromass” tissue layer. These cell-lines were obtained from the American Type Cell Culture (ATCC) repository. All tissue culture reagents were obtained from Sigma-Aldrich, unless otherwise stated. Cell cultures were maintained aseptically at Biosafety level 1 and level 2 facilities at the Gene Expression Mapping using Synchrotron light (GEMS) laboratories maintained by the Department of Anatomy and Cell Biology, University of Saskatchewan and at Dr. Kulyk’s research laboratory.

#### **3.2.1 Cell culture propagation and maintenance.**

Rat L8 myoblasts (ATCC no. CRL-1769) were cultured at 37°C , 5% CO<sub>2</sub> in “L8 medium” consisting of Dulbecco’s modified Eagle’s medium-Nutrient mixture HAM F12 (Cat # D-8900, Sigma Aldrich) supplemented with 10% fetal bovine serum (FBS), 200 µg/mL kanamycin (Invitrogen), and 2% antibiotic-antimycotic (Invitrogen; 200 U/mL penicillin, 200 U/mL streptomycin, and 0.25 µg/mL amphotericin B). Rat FR fibroblast cells (ATCC no. CRL-1213) were cultured at 37°C, 5% CO<sub>2</sub> in “FR medium” consisting of Minimum Essential Medium (Cat #: 41500-034, Invitrogen) supplemented with 10% FBS, 1 mM Sodium pyruvate (Sigma Aldrich), 0.1 mM Non-essential amino acids (Sigma Aldrich), 200 µg/mL kanamycin (Invitrogen), and 2 % antibiotic-antimycotic (Invitrogen). The culture conditions and media that were used for initial propagation and

maintenance of the rat L8 myoblast and FR fibroblast cell-lines were based on the recommended protocols by the ATCC.

### **3.2.2 Preparation of micromass co-cultures**

High-density micromass co-cultures of rat L8 myoblast and rat FR fibroblast cells were established following a modification of the strategy of Ahrens *et al.*, (1977). In brief, rat L8 myoblast cells were grown in L8 medium in two separate sterile 75 cm<sup>2</sup> Falcon flasks (Cat#: 353136, BD Biosciences, Bedford, MA) and rat FR fibroblast cells were grown in FR media in three separate sterile Falcon flasks. All cells were grown to 80% confluence prior to trypsinization. Next the cells were detached by incubation for 5 min in a solution of 0.025 mg/mL trypsin, 10 mM EDTA and dissociated into a single cell suspension. The trypsin was neutralized by addition of FBS to final concentration of 5%. Cells of the same type were pooled together, then pelleted by centrifugation at 800 rpm for 10 min (Sorvall<sup>®</sup> LegendRT, Thermo Electron Corp, Germany).

The pelleted rat L8 myoblasts were resuspended in L8 media and adjusted to a final density of  $2 \times 10^7$  cells/mL using a hemocytometer. Similarly, the pelleted FR fibroblast cells were resuspended in FR medium at final density of  $2 \times 10^7$  cells/mL. The L8 myoblast and FR fibroblast cell suspensions were then mixed together in the following relative ratios: 1 volume of FR fibroblast cells + 1 volume of L8 myoblasts; 1 volume of FR fibroblasts + 2 volumes of L8 myoblasts; and 1 volume of FR fibroblasts + 3 volumes of L8 myoblasts. To establish micromass cultures, a single 10  $\mu$ l drop of cell suspension was spotted on to each 15 mm diameter well of sterile NUNC 4 well tissue culture dishes (Cat.no: 176740). After spotting, the dishes were pre-incubated for 4-6

hours at 37°C in 5% CO<sub>2</sub> incubator to permit cell attachment. Then each micromass culture was fed with 750 µL L8 media and incubated at 37°C, 5% CO<sub>2</sub> for a period of 1-2 days prior to the wound manipulation step.

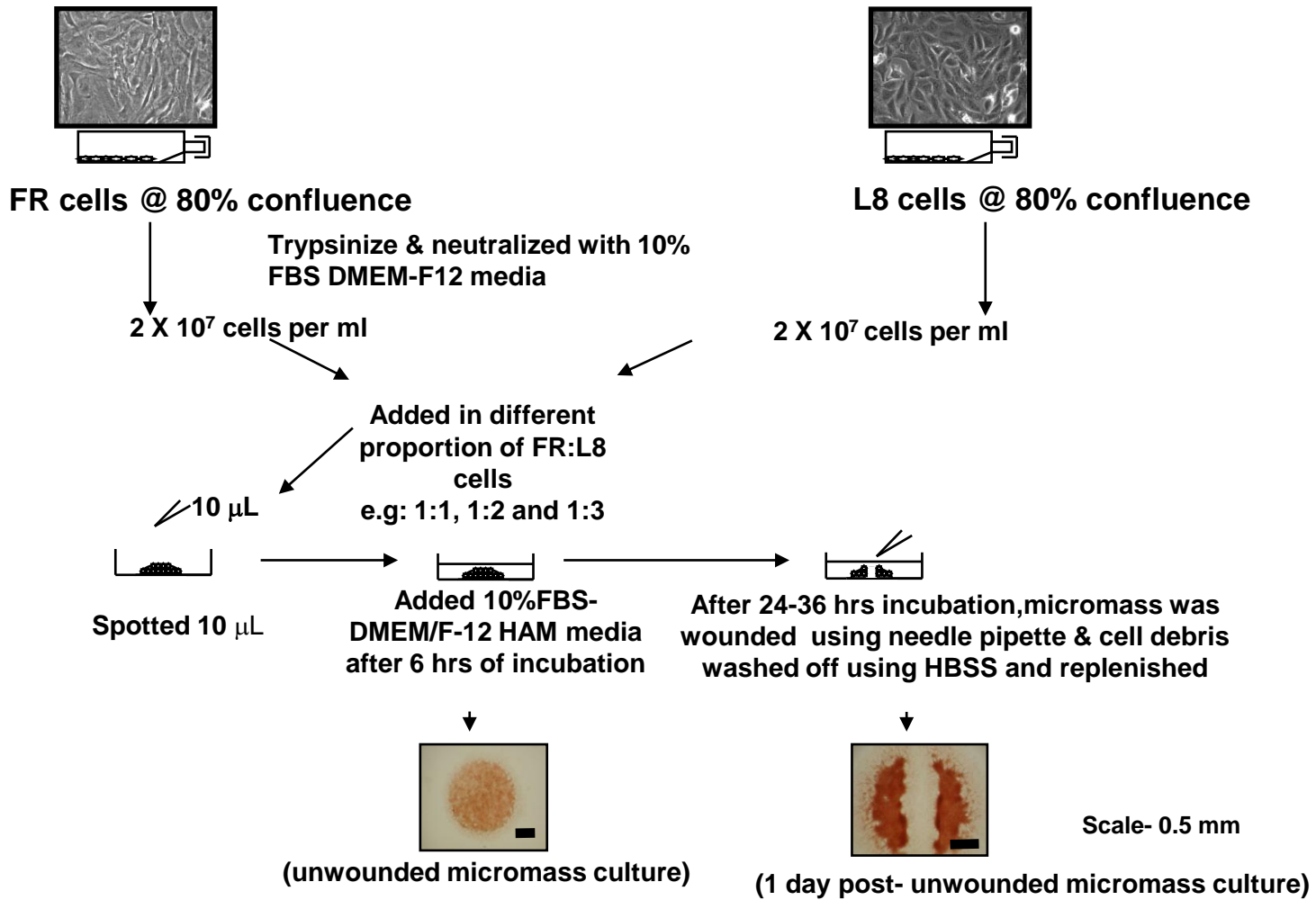
### **3.2.3 Wounding the micromass co-cultures**

After 1-2 days of incubation, a single scrape wound was inflicted across the diameter of the culture using a  $\sim 0.59 \pm 0.041$  mm diameter plastic microcapillary pipette tip (Cat #: 37001-270, VWR International). To eliminate cell debris, the original culture medium was removed, the wounded culture was washed with 37°C Hank's balance buffered salt solution, and the medium was replenished with 750 µL fresh L8 medium. The cultures were incubated at 37°C, 5% CO<sub>2</sub> for up to 8 days after wounding with a medium change at every third day (**Figure 7**).

### **3.2.4 MTT /Cell viability assay**

MTT assay is a standard colorimetric method to determine cell viability *in vitro*. A soluble yellow MTT substrate (3-(4,5-Dimethylthiazol-2-yl)-2,5-diphenyltetrazolium bromide) is reduced to insoluble purple formazan by a reductase enzyme present in living cells. Thus the level of MTT conversion provides a quantitative measure of cell viability. Our MTT assay was based on the method of Plumb *et al.*, 1989. In summary, the culture medium was replaced with L8 medium containing 5 µg/ml MTT and the cultures were incubated for a period of 4 hours. The MTT containing medium was removed, and the formazan crystals deposited on the cell layer were dissolved in 200 µl of DMSO. To the formazan-DMSO solution, 25 µl of Sorensen's glycine buffer (solution of 0.1M glycine

# FIGURE 7



69

**Figure 7. Illustration showing the setting up of micromass co-culture of FR 3T3 fibroblast and L8 myoblast cells based on the modification of Ahrens *et al.* (1977) method.** Initially the cultures were set up with different proportions of fibroblast and myoblast cells and the cultures were incubated for 24-36 hours prior to inflicting a single scrape wound across the diameter of the micromass co-culture.

and 0.1 M NaCl, adjusted to pH 10.5) was added and the absorbance was measured at 560 nm using 96-well format plate reader (SpectraMax 190, Molecular Devices).

### **3.2.5 Determination of total cellular DNA by fluorometric assay**

Total cellular DNA accumulation in micromass co-cultures was quantified using a fluorometric assay as described by Labarca and Paigen (1980). In brief, micromass cultures were collected in 400  $\mu$ L of Hanks buffered saline solution and homogenized by sonication. A 100  $\mu$ L aliquot of each cell homogenate or a chicken DNA standard (0  $\mu$ g, 0.25  $\mu$ g, 0.5  $\mu$ g, 1.0  $\mu$ g, 1.5  $\mu$ g, 2.0  $\mu$ g and 4.0  $\mu$ g) was combined with 200  $\mu$ L of 2X assay buffer (0.1 M sodium phosphate, 4M NaCl, pH 7.4) and 100  $\mu$ L of 4  $\mu$ g/mL Hoechst 33258 dye solution. Then, 200  $\mu$ L aliquots of each sample and standard were transferred to individual wells of a 96-well black microtitre plate and the relative fluorescence intensities were determined at an excitation wavelength of 365 nm and emission wavelength of 458 nm using a Dynex Fluorolite 1000 fluorometric plate reader. The  $\mu$ g DNA content of each sample was calculated from the linear regression equation of the standard curve using InStat software.

### **3.2.6. Histochemistry and Immunostaining**

#### **3.2.6.1 Picrosirius red staining and quantification of total collagen *in vitro***

To determine the total collagen levels in the micromass co-culture and to identify the collagen deposition at the wound site, we performed histochemical staining for with picrosirius red dye following a modification of the method of Marotta and Martino (1985). At representative time points of culture, the culture medium was removed and the

micromass cultures were washed with Hank's buffered salt solution. The cultures were incubated for 90 min at room temperature in a 300  $\mu$ L of picosirius red stain solution, and then washed several times with 0.5% glacial acetic acid. The stained micromass cultures were observed under a phase-contrast light microscope to visualize collagen fibril formation at the wound site and photographed using an attached CCD camera.

Total collagen deposition was quantified by eluting the bound picosirius red dye from the culture using 0.1 M NaOH and determining the absorbance of the eluate at 400 nm using a spectrophotometric plate reader (SpectraMax 190, Molecular Devices). A 1X dye-eluant standard was prepared by combining 50  $\mu$ L of the eluted dyes from each culture. A serial dilution series (1/2X, 1/4X, 1/8X, 1/16X and 1/32X) was prepared by diluting the 1X dye standard with 100  $\mu$ L of 0.1 M NaOH. The absorbance reading at 400 nm was normalized against total cellular DNA levels (in  $\mu$ g) to correct for differences in total cell number between treatment groups. The presence of glycosaminoglycans was determined by staining another set of unwounded and wounded cultures at pH 2.5 using Alcian blue (5 mg/mL Alcian blue in 3% acetic acid).

### **3.2.6.2 Immunostaining for dual phosphorylated p38, dual phosphorylated ERK1/2, type I collagen and fibronectin.**

*In situ* immunostaining was performed to examine the distribution of dual phosphorylated p38 MAP kinase, dual phosphorylated ERK1/2, fibronectin, and type I ( $\alpha$ 1) collagen protein in wounded and unwounded micromass co-cultures. After removing culture medium, the micromass cultures were washed with Hank's buffered salt solution supplemented with protease and phosphatase inhibitors, then fixed in 95% ethanol

containing 2% glacial acetic acid for 30 minutes. The fixed cultures were washed twice with 70% ethanol and stored in 70% ethanol. In preparation for immunostaining, the cultures were rehydrated through a graded ethanol series, and then post-fixed for 1 h in 4% paraformaldehyde. The fixed cultures were washed three times for 5 min in PBST and then incubated for 2 h in 5% sheep serum (Sigma)/PBST solution at room temperature. All primary and secondary antibodies were dissolved in 5% sheep serum/PBST solution.

The cultures were incubated for an hour with 1: 500 dilution of the rabbit monoclonal antibody against phosphorylated p38 MAP kinase (Cell Signaling Inc) and rabbit polyclonal antibody against phosphorylated ERK1/2 (Cell Signaling Inc). A 1: 100 dilution of rabbit polyclonal antibody against fibronectin (Santa Cruz Biotech) and 1: 1000 dilution of rabbit polyclonal antibody against type I ( $\alpha$  1) collagen were used to detect fibronectin and type I collagen protein distribution in the micromass culture.

The subsequent steps were performed as previously described (Bobick and Kulyk, 2004). In brief, the cultures were washed 4 times, 5 min each in PBST and the primary antibodies were detected by incubating for 1 h with compatible alkaline phosphatase-conjugated secondary antibodies. Next, the cultures were washed thrice, 10 min per wash in PBST containing 0.05% levamisole and twice, 15 min per wash in NTMT (100 mM Tris Hcl, pH 9.5, 50 mM MgCl<sub>2</sub>, 100 mM NaCl, 0.1% Triton X-100, 0.05% levamisole). Colour development was performed using nitroblue tetrazolium chloride (0.34 mg/mL) and 5-bromo-4-chloro-3-indolylphosphate (0.175 mg/mL) dissolved in NTMT. Colour development was stopped by three washes with PBST and the cultures were stored in

CMFET (0.137 M NaCl, 0.003 M KCl, 0.008 M Na<sub>2</sub>HPO<sub>4</sub>, 0.0015 M KH<sub>2</sub>PO<sub>4</sub>, 0.7 mM EDTA, 0.1% Tween-20) at 4°C for up to 2 weeks prior to photographing.

### **3.2.6.3 Actin filament and nuclear staining.**

The filamentous actin and nuclei of the cells within the micromass co-cultures were visualized using Oregon green 488-conjugated phalloidin and cell permeable Hoechst 33342 dye, respectively. The micromass cultures were fixed in 500 µL 3.7% formaldehyde dissolved in PBS overnight at 4 °C. The fixed cultures were rinsed three times with PBS then incubated overnight in 500 µL of 0.1% Triton X-100 in PBS. The cultures were rinsed thrice with PBS, then incubated at 4 °C overnight in 500 µL 1% BSA in PBS to reduce background fluorescence. The cultures were then incubated at 4 °C for 24 h in a solution of 200 Units/mL Oregon Green 488-conjugated phalloidin in PBS to stain filamentous actin. The stained cultures were washed thrice with PBS and incubated at 4 °C overnight in 20 µg/mL Hoechst 33342 dye to stain nuclei. Finally, the cultures were rinsed three times in PBS, about 10 drops of AquaPerm mounting medium (Immunon™, Shandon, Pittsburgh, PA) was added, and the cultures were visualized using a phase contrast fluorescent microscope.

### **3.2.6.4 Scanning electron microscopy (SEM)**

Micromass co-cultures used for electron microscopy were grown on 12 mm diameter glass cover slips (Cat #: 12-545-82, Fisher Scientific Co) within 4-well NUNC tissue culture dishes. The cover slips were sterilized by soaking for 15 minutes in 70% ethanol then air-dried for 1 h in a sterile biosafety cabinet, prior to spotting the cultures.

At representative time points, the cultures were fixed overnight at 4 °C in 3.7% formaldehyde in PBS, pH 7.5. After fixation the micromass co-cultures were washed thrice with PBST, the cover slips were removed from the 4-well NUNC culture plates and transferred to glass vials. The cells were dehydrated through a graded series of PBST: acetone mixtures (20%; 40%; 60% and 80% acetone) at 10 min per step. Then the cultures were washed twice with 100% acetone and stored at -20 °C in 100 % acetone. The dehydrated micromass cultures were critical point dried with liquid carbon dioxide using a Polaron Critical Point dryer and gold coated with Edwards S150B (BOC Edwards, Crawley, UK) sputter coater. The critical point drying and gold coating procedures were conducted with the assistance of Dr. Guosheng Liu (Department of Biology, University of Saskatchewan).

The processed samples were examined using a JEOL JSM 840A scanning electron microscope with the assistance of Dr. Thomas Bonli (Department of Geological sciences, University of Saskatchewan). The imaging of the samples was performed with an accelerator voltage set at 20 kV and an 8 mm working distance for image acquisitions. The images were captured digitally using Gellar Microanalytical dPICT software.

### **3.2.7 DiI and DiO labeling of cells.**

The fluorescent lipophilic tracer dyes, 1,1'-dioctadecyl-3,3,3',3'-tetramethylindocarbocyanine perchlorate (DiI) and 3,3'-dioctadecyloxacarbocyanine perchlorate (DiO) are commonly used in cell fate mapping because they are easily incorporated into the plasma membranes of live cells and exhibit distinct red and green fluorescence, respectively. DiI and DiO are highly fluorescent and photostable when

incorporated into membranes, and diffuse laterally within the plasma membrane, resulting in complete staining of the cells. The two dyes can be used in combination for multicolour imaging because dye transfer between intact membranes of DiI labeled cells and DiO labeled cells is negligible (Agmon *et al.*, 1995). Hence they are commonly used in long term tracer applications such as cell transplantation, migration, adhesion and fusion studies (Ledley *et al.*, 1992; Serbedzija *et al.*, 1989; Tajbakhsh *et al.*, 1994). In my studies, DiI and DiO were used to selectively label L8 myoblast and FR fibroblast cells in micromass co-cultures and to track the patterns of fibroblast and myoblast cell migration following wounding.

Rat L8 myoblast cells or rat fibroblast FR cells were grown to 80% confluence and then dissociated in 0.025 mg/mL trypsin, 10 mM EDTA solution. The dissociated cells were incubated for 1-2 hours at 37°C in culture medium containing either 25 ng/mL DiI or 25 ng/mL DiO tracker dyes. The labeled FR and L8 cells were washed 3 times in Hank's buffered salt solution to remove excess unbound dye, and then plated in micromass culture in varying ratios.

### **3.2.8. Treatment of micromass co-cultures with mitomycin, TGF- $\beta$ 1, Quercetin, L-2-oxothiazolidine-4-carboxylate (OTC), Anisomycin, SB202190 and PD 184352**

In some experiments, wounded micromass co-cultures were treated with either mitomycin (10  $\mu$ g/mL for 72 hours), TGF- $\beta$ 1 (final concentrations of 0, 0.1, 0.2, 0.4 and 0.8 ng/ml), quercetin (final concentrations of 0, 25 and 45  $\mu$ M), OTC (final concentrations of 0, 1 or 1.5 mM), anisomycin (final concentrations of 0, 100 or 200 ng/mL), SB202190 (final concentration of 0, 10, 15, 20  $\mu$ M) or PD 184352 (final

concentrations of 0, 2 or 4  $\mu\text{M}$ ) after wounding. An equivalent volume of medium was added to parallel control cultures. The medium for all cultures treated with TGF- $\beta$ 1, quercetin, anisomycin, SB202190 and PD184352 contained a final concentration of 0.1% DMSO (v/v). An equivalent amount of DMSO vehicle was administered to parallel control cultures.

### **3.2.9 Gene expression analysis of wounded and unwounded micromass cultures using RT-PCR**

#### **3.2.9.1 Isolation and purification of total RNA from micromass co-cultures**

Total RNA was isolated from wounded and unwounded micromass co-cultures using an RNeasy<sup>®</sup> Plus Mini kit (Qiagen, Cat. No: 74134) according to the manufacturer's procedure. The micromass co-cultures were solubilized in Buffer RLT (provided with the kit) and homogenized by centrifugation through QIAShredder columns. The homogenates were mixed with an equal volume of 70% ethanol and passed through RNeasy Plus columns to isolate total RNA, in accordance with the manufacturer's protocol. The total RNA yield for each sample was determined from the optical density (OD) measurement at 260 nm. The  $(\text{OD})_{260 \text{ nm}} / (\text{OD})_{280 \text{ nm}}$  ratios were between 1.6-1.9, consistent with high purity RNA.

Two micrograms total RNA from each sample was converted to cDNA using oligodT-18 and RevertAid<sup>™</sup> M-MuLV reverse transcriptase (Fermentas Life Sciences, Cat no: EP0441) as described in **Section 3.1.9.1**. The cDNA product was used to perform semi-quantitative RT-PCR analysis as described below.

### **3.2.9.2 RT-PCR analysis of gene transcript expression.**

Semi-quantitative RT-PCR analysis was used to examine the expression patterns of the gene transcripts for collagen type 1 ( $\alpha 2$ ), collagen type 3 ( $\alpha 1$ ) and collagen type 4 ( $\alpha 1$ ), hyaluronan synthase 1, hyaluronan synthase 3, receptor for hyaluronan-mediated motility (RHAMM), CD 44, TGF- $\beta$ 1, TGF- $\beta$ 3, hsp-47 and GAPDH in wounded and unwounded micromass co-cultures. PCR was performed in a 100  $\mu$ L reaction mixture containing 2  $\mu$ L of micromass co-culture cDNA as template, together with gene-specific forward and reverse primers listed previously in **Table 4**. The denaturing, annealing, and extension conditions for each amplification cycle were 94°C for 30 sec, 55°C for 30 sec, and 72°C for 45 sec respectively.

In order, to identify the exponential phase of the amplification reaction for each particular gene transcript being examined, a series of PCR experiments was performed using 2  $\mu$ g cDNA template (obtained from each micromass co-cultures) in a 100  $\mu$ L PCR reaction mixture. PCR was performed using the amplification conditions described in **Section 3.1.9.1** and the gene-specific primer pairs indicated in **Table 4**. However, the reaction was paused after every 5 cycles beginning at PCR cycle 10 and a 10  $\mu$ L aliquot was removed at each time-points. These aliquots were electrophoretically resolved in 1.5% agarose gels stained with EtBr, and photographed under UV transilluminator to visualize the relative amount of PCR product generated after 10, 15, 20, 25, 30, 40, 45, 50, 55, 60 and 65 amplification cycles.

The relative band intensities were quantified densitometrically using NIH Image J software and the values for each time-point were plotted to determine the exponential phase of PCR amplification for each specific gene of interest. The number of cycles that

was corresponded to be the exponential phase of PCR amplification for each gene was determined to be: 55 cycles for Collagen type 1 ( $\alpha$  2); 45 cycles for Collagen type 3 ( $\alpha$  1); 50 cycles for Collagen type 4 ( $\alpha$  1); 35 cycles for Hyaluronan synthase 1; 40 cycles for Hyaluronan synthase 3; 50 cycles for RHAMM; 35 cycles for CD 44; 45 cycles for TGF- $\beta$ 1; 35 cycles for TGF- $\beta$ 3; 30 cycles for heat shock protein 47 (hsp-47); 25 cycles for GAPDH.

Finally the PCR products obtained at these cycles were separated on 1.5% agarose gels and stained with EtBr and photographed under UV illumination. Densitometric measurements of relative band intensities were performed using NIH Image J software. The band intensities for the PCR products corresponding to the sequences of collagen type 1 ( $\alpha$  2), collagen type 3 ( $\alpha$  1), collagen type 4 ( $\alpha$ 1), Hyaluronan synthase 1, Hyaluronan synthase 3, RHAMM, CD 44, TGF- $\beta$ 1, TGF- $\beta$ 3, hsp-47 were normalized to that for GAPDH.

### **3.2.10 Western blot analysis of wounded and unwounded micromass co-cultures**

For determination of specific protein expression patterns, micromass co-cultures were collected in Western lysis buffer supplemented with protease and phosphatase inhibitors, as described in **Section 3.1.10.1** and homogenized by sonication for 45-60 sec using a VibraCell<sup>TM</sup> (Sonic & Materials Inc., Danbury, CT, USA). After sonication, the samples were mixed with equal volume of 2X SDS-Urea buffer and kept at -20 °C until use. For analysis of ERK1/2 and p38 MAPK expression, gel electrophoresis was performed on 8.5 % SDS-PA gels. For all other proteins of interest, electrophoresis was performed on resolving split gels as described in **Section 3.1.10.3**.

### **3.2.11 *In vitro* “micromass” co-culture wound closure assay**

To compare rates of wound closure in micromass cultures, we used an adaptation of a planimetric *in vitro* wound closure assay previously employed for monolayer culture systems (Gottrup *et al.*, 2000; Stojadinovic *et al.*, 2005; Tomic-Canic *et al.*, 2007). This method uses image analysis to quantify the progressive reduction in the open surface area (i.e. total cell free area) of the wounded region during the time course of *in vitro* wound closure. In brief, the micromass co-culture was inflicted with single scrape wound and the cell debris was removed as described in **Section 3.2.3**.

Each wounded culture was observed by phase contrast microscopy at various time points after wounding (0, 12 h, 1 d, 2 d, 3 d, 4 d, 5 d, 6 d, 7 d, 8 d, and 9 d) and photographs of the wound region including the wound edges were digitally captured at 10X magnification. The edges of the wound were manually traced using Image J 1.37G software's *Freehand selection* function. The traced wound areas were then calculated using the *Analyze particle* function in the Image J software and selecting the *Area* parameters. The changes in the wound surface area at each time point, and treatment conditions were thus quantified using the *Analyze particle* and *Measure* function. The progressive quantitative reduction in the open wound area was plotted as a graph using Microsoft Excel. The experiments were performed in quadruplicate for all treatment conditions.

### **3.2.12 Dual color fluorescent image analysis**

DiI and DiO labeled cells in micromass co-cultures were imaged in real-time using a close circuit digital camera attached to a fluorescent phase-contrast microscope.

Using Image J 1.37G software, the relative intensities of DiI labeled FR cells (red) and DiO labeled L8 myoblast (green) cells located at the wound site (including wound edges) and the outer periphery of the micromass co-culture were quantified at 1 day, 3 days and 8 days post-wounding to examine the patterns of fibroblast and myoblast migration. A total of twelve wounded micromass cultures were used for the migration studies. The cell migration pattern was determined by taking DiI and DiO fluorescence measurements at six different positions in the region of the wound site, which included the wound edges, and six defined positions in the peripheral region of the micromass culture as shown in **Figure 8**. The relative numbers of labeled cells in region were quantified using the procedures described for cell counting using NIH Image J software from the McMaster Biophotonics facility website (<http://www.macbiophotonics.ca/imagej/>). Plugins and automated macros for cell counting using NIH Image J were obtained from this website. In brief, the individual raw images obtained for red fluorescent DiI labeled cells and green fluorescent DiO labeled cells at each position within the wound site and the periphery of the micromass co-culture were converted to grayscale images using the *Image > Type > 8-bit* function of the Image J software. The threshold was automatically set for each grayscale images using *Image > Adjust > Threshold* functions. The threshold values were selected as “*auto*” and images were converted to a binary image by applying the *Process > Binary > Watershed* function. To define and count positive fluorescent cells, the images were deconvoluted by applying the *Plugin > Color function > Color deconvolution* function and selecting “vectors” from the *region of interest (ROI)* on the pop window. Finally, the fluorescent cells were counted using the program’s *Analyze particle* function after selecting “outline” option.

## FIGURE 8

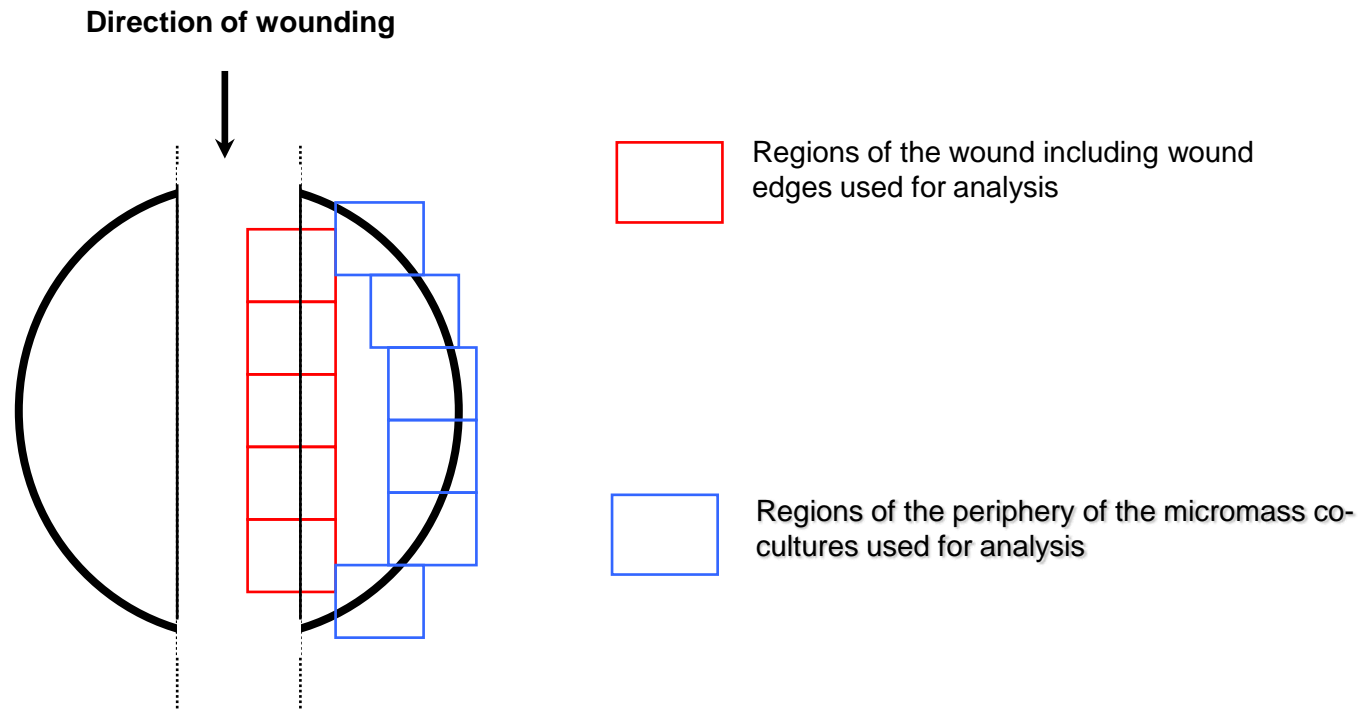


**Figure 8. Illustration of the regions of the wounded micromass co-culture imaged to determine cell migration pattern at the wound site (red) and the periphery (blue).** *In vitro* micromass wound assay was performed by taking a phase contrast images of the wound site including the wound edges to perform planimetry. DiI and DIO stained cells were determined by NIH Image J analysis by counting the red fluorescent cells (DiI-FR 3T3) and green fluorescent cells (DiO-L8).

### 3.2.13 Statistical Analysis

All quantitative data obtained from the *in vitro* experiments were analyzed using one-way analysis of variance (ANOVA) with either Dunnett or Tukey multiple comparison post-tests (GraphPad Prism 4 software). The graphs were prepared using Microsoft Excel software.

## CHAPTER 4. RESULTS

### 4.1 Effects of Quercetin and OTC on overall scar formation following experimental spinal laminectomy surgery in rats.

Based on their previously demonstrated anti-inflammatory properties, we hypothesized that both quercetin and OTC might have potential as anti-scarring agents. We performed the following qualitative comparisons to examine the effects of quercetin and OTC on the extent of cutaneous scar tissue formation in adult rats that were subjected to a spinal laminectomy surgery. The laminectomized rats were randomly administered i.p. injections of 0.025 mmol/ kg quercetin (*b.i.d* [twice daily] for 120 h), 1.0 mmol/ kg OTC (*b.i.d* for 72 h) or 3 mL saline solution (*b.i.d* for 120 h). At 21 days, 63 days and 7 months post-surgery, a cutaneous scar was visible along the length of the dorsal skin incision and the associated wound suture staples. The effects of OTC and quercetin on scar formation and the recovery of normal skin pigmentation at the cutaneous wound site were visually assessed. These qualitative observations were made in collaboration with Ms. Nicole Cox, a graduate student from Dr. B. Juurlink's laboratory (Anatomy and Cell Biology, University of Saskatchewan), who was investigating the anti-inflammatory actions of quercetin and OTC in the same group of animals. Her findings in regard to expression of inflammatory markers are detailed in her recent M.Sc thesis (Cox, 2008).

In animals observed at 3 day post-surgery, the skin incision wounds were not completely closed and the presence of suture staples at this time-point made qualitative evaluation of cutaneous scar formation difficult in all treatment groups. The suture staples were not removed till 7 days post-surgery. By 21 and 63 days post-surgery, the extent of scar formed in the vicinity of the dorsal skin incision and at the site of the former staple wounds was more readily visible. Our qualitative observations suggested that the animals from the quercetin and OTC treatment groups exhibited reduced cutaneous scarring as compared to control animals administered saline alone. Furthermore, when our collaborating laboratory observed the cutaneous scars at 7 months post-surgery, both quercetin and OTC treated animals showed improved recovery of skin pigmentation in and around the wound area as compared to saline treated animals (**Figure 9 B** and **9 C**). In the OTC treated rats it was comparatively difficult to visualize the original incision and staple wound sites as the dorsal skin wound appeared to be completely healed and the extent of dorsal skin pigmentation in that region was similar to that of the surrounding skin. In contrast, animals from the saline control group typically had raised dorsal skin scars with reduced skin pigmentation making the scar very obvious at the sites of incision and suture wounds (**Figure 9 A**) Some quercetin treated animals showed improved recovery of skin pigmentation as compared to saline treated control animals, however the dorsal incision and staple wound scars were still visible on close examination. The subjective grading of relative skin pigmentation can be represented as OTC treated rats > quercetin treated rats  $\geq$  saline treated control animals, while the relative visibility of dorsal skin incision and wound staple scars was OTC treated rats < quercetin treated rats  $\leq$  saline control animals. These qualitative observations suggested

## FIGURE 9

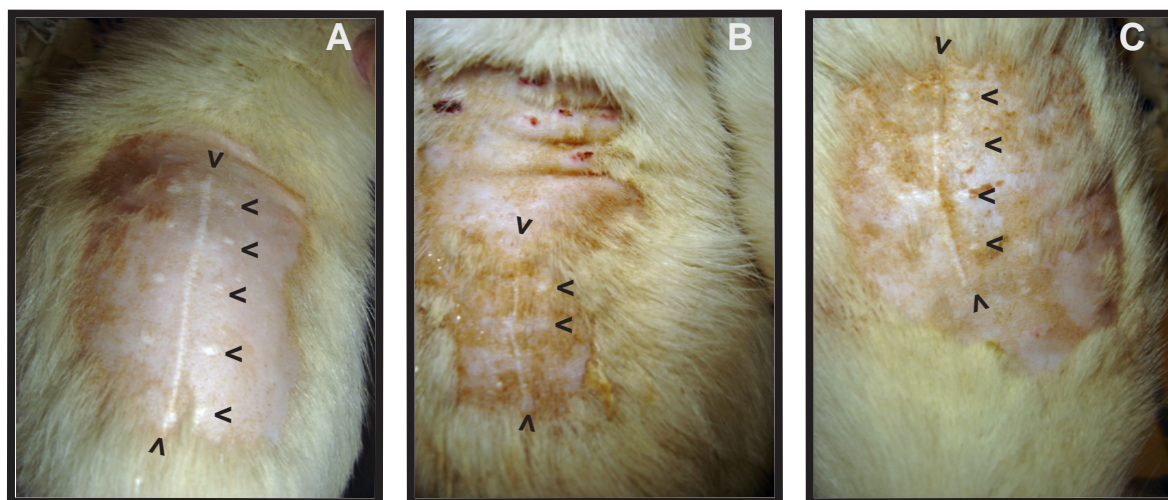


**Figure 9.** Images of cutaneous scar from (A) Saline, (B) OTC and (C) Quercetin treated laminectomized rats. The arrows show the location of incisional wound and suture wound on the dorsal skin. These images were taken from 7 month post-surgery rats by Nicole Cox for her experiments. The images were reproduced and adapted from Cox (2008).

the possibility that OTC might be able to reduce cutaneous scarring as compared to both saline treated and quercetin treated animals.

At 63 day post-surgery, when the laminectomized region of the sacrificed animals was dissected to excise the peridural scar tissue, it was observed that the amount of bone regrowth at the site of laminectomy appeared to be more extensive in OTC and quercetin treated animals as compared to saline treated rats (OTC  $\geq$  quercetin  $>$  saline control). When the peridural scar tissues were harvested for subsequent analysis, the bony tissue formed at the laminectomized region appeared to be denser in quercetin and OTC treated animals. Moreover, it was more difficult to separate the bony structures from the peridural scars of quercetin and OTC treated animals.

When the peridural scar tissues were excised for RNA and protein analysis, their total wet mass was measured. At 3 days post-laminectomy, the peridural scar tissue from quercetin treated animals had significantly higher wet mass in comparison to peridural scars isolated from either saline treated control animals or OTC treated animals (**Table 6**,  $p < 0.01$ ,  $n = 6$ ). At 21 day post-surgery, the peridural scar tissue harvested from both OTC and quercetin treated rats showed significantly lower mean wet mass as compared to saline treated controls (**Table 6**,  $p < 0.001$  for OTC and  $p < 0.01$  for quercetin,  $n = 5$ ). At 63 days, the peridural scar tissue wet mass for OTC treated animals remained significantly lower than compared to saline treated animals (**Table 6**,  $p < 0.001$ ,  $n = 6$ ), whereas the average peridural scar wet mass for quercetin treated rats was not significantly different than control.

**Table 6. Total wet weight, RNA yield, and protein yield of scar tissue samples harvested from Saline, OTC and quercetin treated animals.** The total wet mass of scar tissue harvested was determined by weighing the excised scar tissue. Total RNA was isolated from scar tissue samples and yield was determined by measuring the optical density at 260 nm. The protein concentration of scar tissue homogenates was determined by a Coomassie dye binding assay as described in **Section 3.1.9.2**. Values represent the Mean  $\pm$  SD for each treatment groups; n = 6 for 3 day and 63 post-surgical animal groups while n = 5 for 21 day post surgical animal groups. Asterisk indicate values that are significantly different than the corresponding saline control group p < 0.05 (\*), p < 0.01 (\*\*), or p < 0.001 (\*\*\*).

Quantitative parameter	Time after laminectomy surgery	Treatments		
		Saline	OTC	Quercetin
Total wet mass (in mg)	3 days	1192.53 $\pm$ 180.2	1239.7 $\pm$ 184.7	1699.92 $\pm$ 261.87**
	21 days	1331.68 $\pm$ 211.07	872.1 $\pm$ 108.71***	1082.18 $\pm$ 112.4**
	63 days	1307.95 $\pm$ 251.11	953.98 $\pm$ 139.93***	1496.53 $\pm$ 122.16
Total RNA yield (in $\mu$ g)	3 days	68.68 $\pm$ 24.1	63.75 $\pm$ 17.36	53.65 $\pm$ 19.4
	21 days	17.7 $\pm$ 4.5	24.65 $\pm$ 4.72*	31.02 $\pm$ 11.35*
	63 days	7.65 $\pm$ 2.02	11.45 $\pm$ 1.7**	13.55 $\pm$ 6.6
Total protein yield (in $\mu$ g)	3 days	830.1 $\pm$ 20.01	921.66 $\pm$ 22.3***	921.6 $\pm$ 26.87**
	21 days	1779.1 $\pm$ 285.1	1195.65 $\pm$ 441.41*	1115.98 $\pm$ 412.98**
	63 days	1648.85 $\pm$ 1057.21	1340.89 $\pm$ 1000.5	1445.56 $\pm$ 1011.85

When RNA was isolated from the peridural scar tissues of saline, OTC and quercetin treated animals, it was observed that the peridural scar tissues of 21 and 63 day animal groups yielded significantly lower amounts of total RNA than a similar amount of scar tissue excised from 3 day animal groups (**Table 6**,  $p < 0.05$ ,  $n = 18$ ). In contrast, 21 day and 63 day scar tissue samples yielded significantly higher amounts of total protein relative to 3 day scar tissue. These patterns might reflect an increased accumulation of collagens and other extracellular matrix proteins within the scar tissue, with a concurrent decrease in the relative density of cells containing rRNA and mRNAs (**Table 6**,  $p < 0.05$ ,  $n = 18$ ).

Indeed, reproducible tissue homogenization and protein solubilization proved to be problematic for 63-day scar tissue samples due to their highly fibrous nature. The solubilization of 63-day peridural scar tissues for western blot analysis was highly inconsistent as the homogenates formed precipitates even after addition of 2X SDS-urea buffer, and there was large variation in final protein yields from 63-day peridural scar tissue homogenates of saline, OTC and quercetin treated animals. In addition, total RNA yields were very low for 63-day scar tissues from all animal groups. The poor and inconsistent RNA and protein yields for 63 day scar tissues prompted us to use only samples collected at 3 and 21 days post-laminectomy for subsequent analysis of quercetin and OTC effects on the total collagen distribution, mRNA expression and specific protein levels (**Table 6**).

## **4.2. Effects of Quercetin and OTC on collagen distribution and biosynthesis in peridural scar tissue of laminectomized rats.**

### **4.2.1 Correlating Vibrational FTIR spectromicroscopy maps of scar tissue sections with picosirius red polarized light microscopy images of scar tissue to determine the orientation and distribution of collagen.**

Picosirius red histochemical staining was used to determine collagen fiber abundance and distribution in histological sections of peridural scar tissue from quercetin, OTC and saline treated rats. The picosirius-red stained tissue sections were visualized under a circularly polarized light microscope and the staining pattern was compared with FTIR spectral maps obtained from contiguous scar tissue sections using an advanced imaging technique known as synchrotron-based vibrational Fourier Transformed Infra Red (FTIR) microspectroscopy. When the picosirius red stained scar tissue sections were visualized using conventional bright field light microscopy, the entire area of the tissue was stained with the dye, although there was some regional difference in stain intensities. When the same stained tissue sections were visualized under circularly polarized light (**Figure 10**), bright orange to red birefringence was conspicuous within regions of high collagen fibril deposition, while regions with lower collagen deposition showed fainter green to yellow birefringence.

To verify the specificity of picosirius red polarization technique used in this study in determining the orientation and distribution of collagen fibrils in the scar tissue, contiguous histological sections of the scar were examined for total collagen deposition using the synchrotron FTIR spectromicroscopic tissue mapping technique by our collaborators at the University of Manitoba, Winnipeg (Wiens *et al.*, 2007).

## FIGURE 10

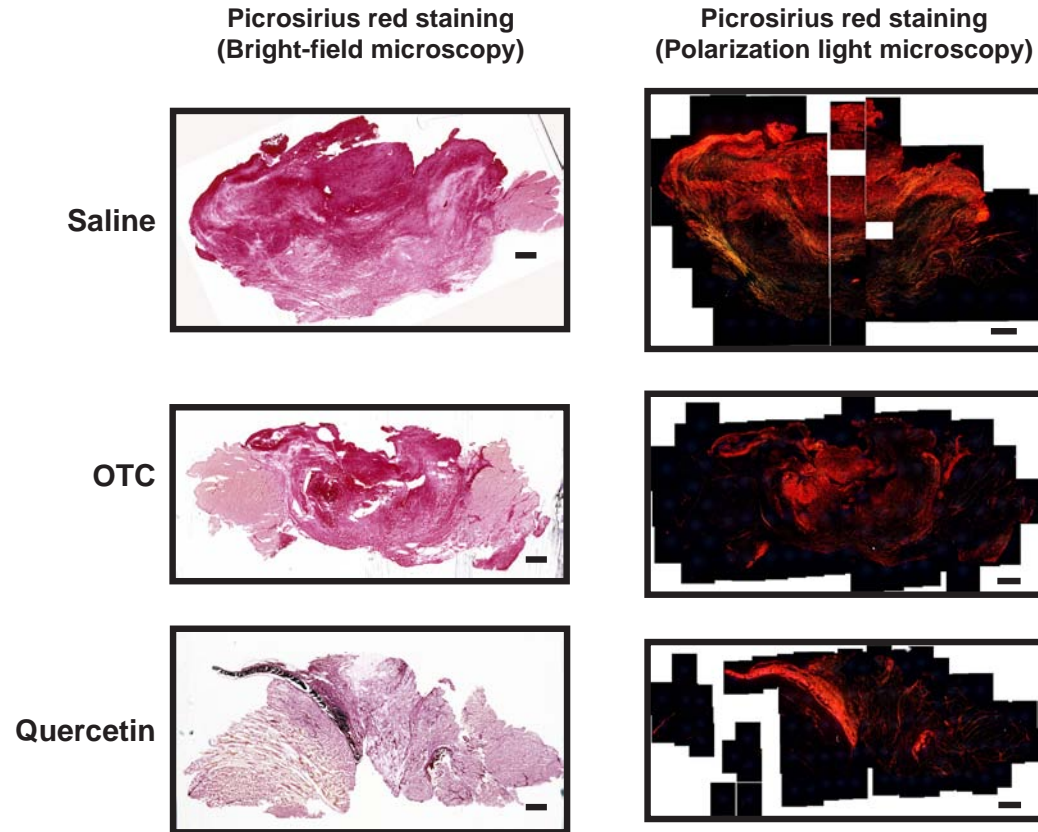
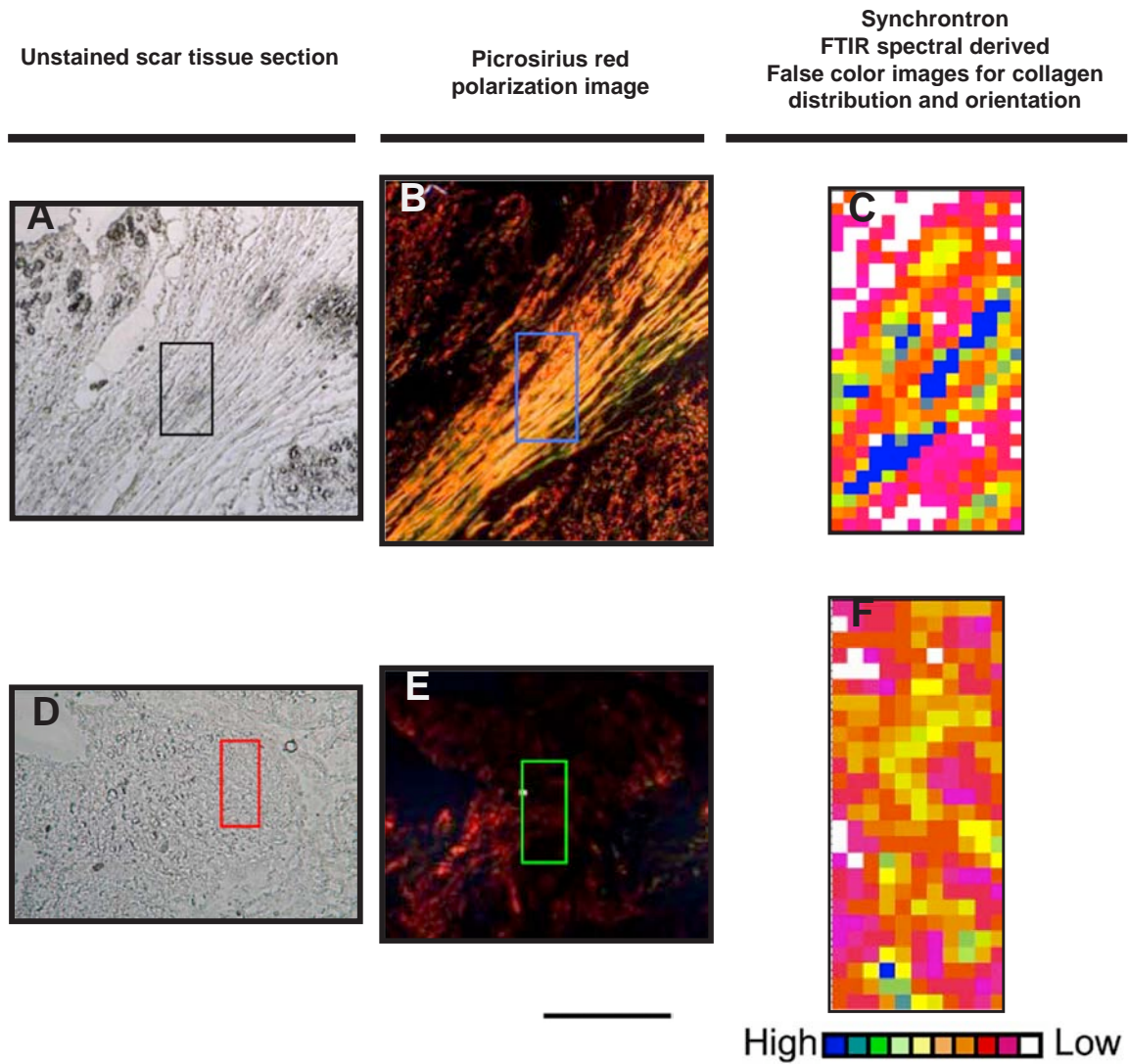


**Figure 10. Picrosirius red polarization method showing 21 day scar tissue sections of Saline, OTC and Quercetin treated animals.** The light microscopy images shows that picrosirius red non specifically stains both collagen rich regions of the scar tissue as well as musculatures. The photomontages of the picrosirius polarized images were prepared with Adobe Photoshop CS imaging software. These images show the specificity of the collagen staining as visualized under a circularly polarized light microscope. The polarization images generated for tissue sections obtained from individual animals for 3 and 21 day treatment groups were used for analyzing the total collagen levels following treatment with OTC and Quercetin. Scale corresponds to 100  $\mu\text{m}$ .

Regions of scar tissue used for FTIR mapping were selected based on a visual examination of the tissue section to ensure adequate representation of granulation tissue, wound healing matrix and the presence of fibrillar collagen in the area of analysis. Synchrotron FTIR maps were generated from contiguous histological sections using a Nicolet 860 FTIR instrument with a continuum microscope (National Synchrotron Light source, Brookhaven National laboratory, NY, USA) or Nicolet Magna 500 FTIR instrument with a Nic-Plan microscope (Synchrotron Radiation Center, Stoughton, WI, USA). All spectra were collected at  $4\text{ cm}^{-1}$  spectral resolution with a  $12\text{ X }12\text{ }\mu\text{m}$  aperture and  $10\text{ }\mu\text{m}$  step size. Nicolet OMNIC/Altus software was used for all data acquisition and map analyses. The maps were processed based on spectral markers for various tissue components (lipids, polysaccharides, nucleotides, collagens) using direct univariate analyses and the relative abundance of components of interest were displayed in a false color scale from red/white (for lowest level or absence of the components) to blue (highest level). The presence of collagen in tissues was determined by the spectral quartet band at  $1,204, 1,240, 1,284, 1,338\text{ cm}^{-1}$  and the sites of relative collagen signal intensity within the sections were mapped by integrating the area of  $1,204\text{ cm}^{-1}$  peak from  $1,198$  to  $1,211\text{ cm}^{-1}$  with a baseline from  $1,188$  to  $1,214\text{ cm}^{-1}$  and a display range of  $0.025$  to  $0.45$  (**Figure 11 C and 11 D**).

A comparison of the polarized light images of sirius red stained scar tissue sections with contiguous scar tissue sections subjected to FTIR mapping analysis demonstrates some correlation between the two techniques in determining the location and orientation of collagen fibres (**Figure 11**). Wiens *et al.* (2007) found that the orientation of the synchrotron light source relative to a tissue section's plane of axis plays a critical role in the ability of FTIR spectral mapping to detect aligned collagen fibrils. In

# FIGURE 11



Images reproduced and adapted from Wiens *et al.*, 2007

**Figure 11. Correlation of Picrosirius red polarization images with Vibrational FTIR spectro-microscopy maps for oriented collagen fibres in 21 day scar tissue regions.** Presence of collagen in scar tissue was determined by Fourier transformed infrared spectral mapping as described by Wiens *et.al.*,2007. The distribution of collagen in a contiguous scar tissue section and false color images corresponding to the levels of collagen fibril orientation were created using Nicolet Omnic/Atlas software. Panel A and D are photographs of two different unstained scar tissue sections. The rectangular black box in Panel A and red box in Panel D as well as rectangular blue box in Panel B and green box in Panel E denotes the position of FTIR map in the corresponding unstained and picrosirius red stained sections. (Panels C & F) shows the false color images processed at  $1204\text{ cm}^{-1}$  for FTIR mapping of collagen distribution in these scar tissue sections. Scale corresponds to  $100\text{ }\mu\text{m}$ .

contrast, our picosirius red polarization images demonstrates that this histochemical method was more effective at consistently detecting collagen fibrils within scar tissue sections and visualizing their orientation as compared to FTIR spectral maps (**Figure 11 B and 11 C**). One limitation of the picosirius red polarization method was its lower sensitivity in identifying sites of low collagen abundance in tissue sections as compared to FTIR spectral maps (**Figure 11 E and 11 F**).

Our results corroborate previous findings that have validated the picosirius red polarization technique as a routine, reliable histochemical method for detection of collagen fibril deposition within tissue sections.

#### **4.2.2 Effects of Quercetin and OTC on total collagen distribution in the histological sections of peridural scar tissue of laminectomized rats.**

Histological sections of peridural scar tissue from quercetin, OTC and saline treated animals were stained with picosirius red and photographed under circularly polarized light microscopy. Quantitative image analyses was performed on the captured digitalized images to determine whether quercetin and OTC treatments affected levels of total collagen accumulation in the histological sections of peridural scar tissue, obtained from animals at 3 and 21 days, after laminectomy surgery.

A visual inspection of the picosirius red polarization images of 3 day post-surgery peridural scar tissues from quercetin, OTC and saline treated rats suggested that there was a high degree of variation in the abundance of picosirius red stainable collagen fibrils between individual animals within each of the drug treatment groups including the saline control group (**Figure 12**). Quantitative analysis using NIH Image J software revealed no statistically significant effects of either OTC or quercetin treatment

## FIGURE 12

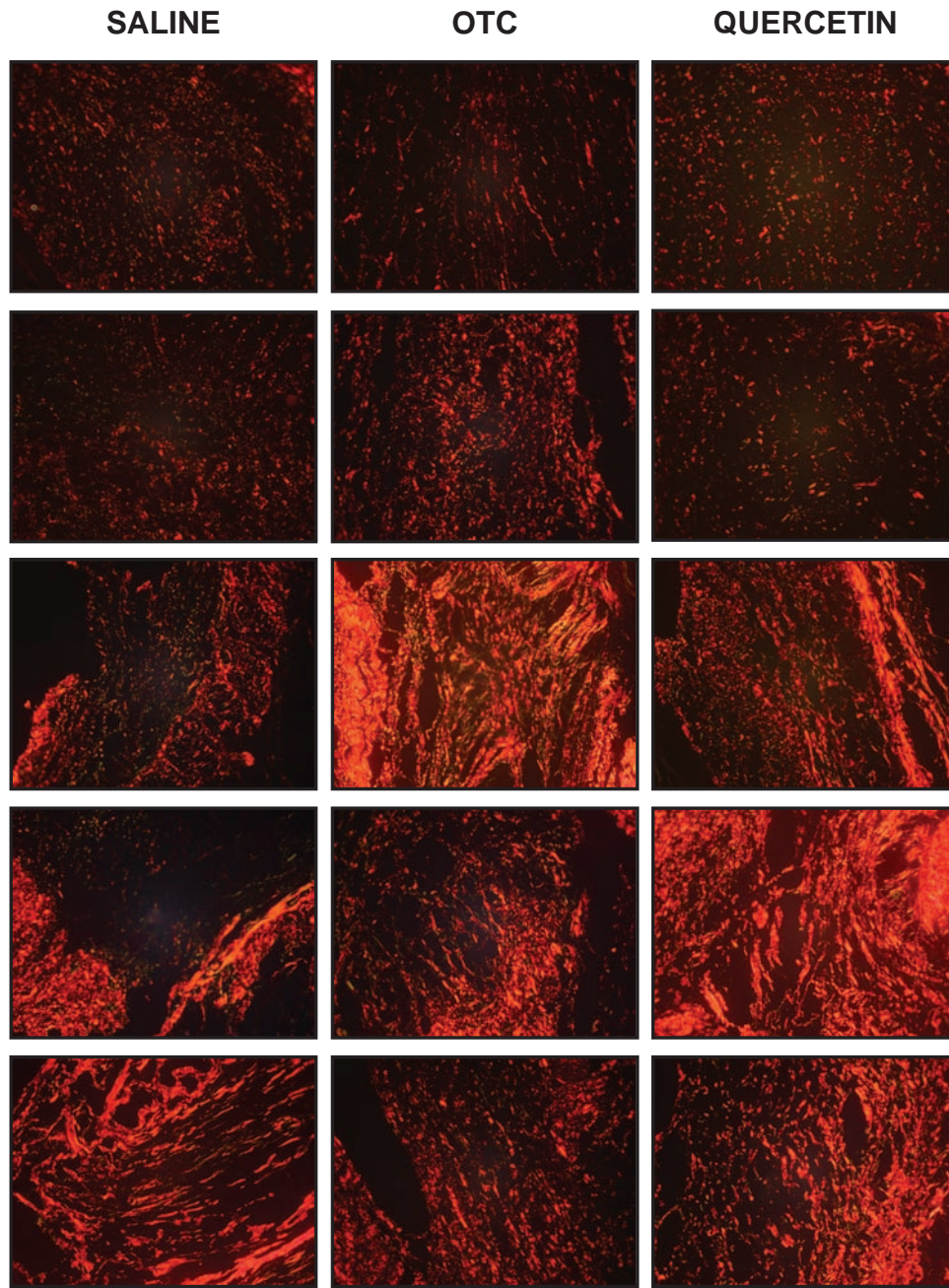


**Figure 12. Picrosirius red polarization images showing the corresponding 3 day scar tissue regions of Saline, OTC and Quercetin treated animals. The five images in each vertical column represent the field of view images from five different animals within each treatment groups. A majority of the 3 day treatment groups showed huge variation in total collagen staining with low to high intensity staining at the region of scar. All images were taken using circularly polarized light at 10X magnification. Scale represents 100  $\mu$ m**

**FIGURE 13**

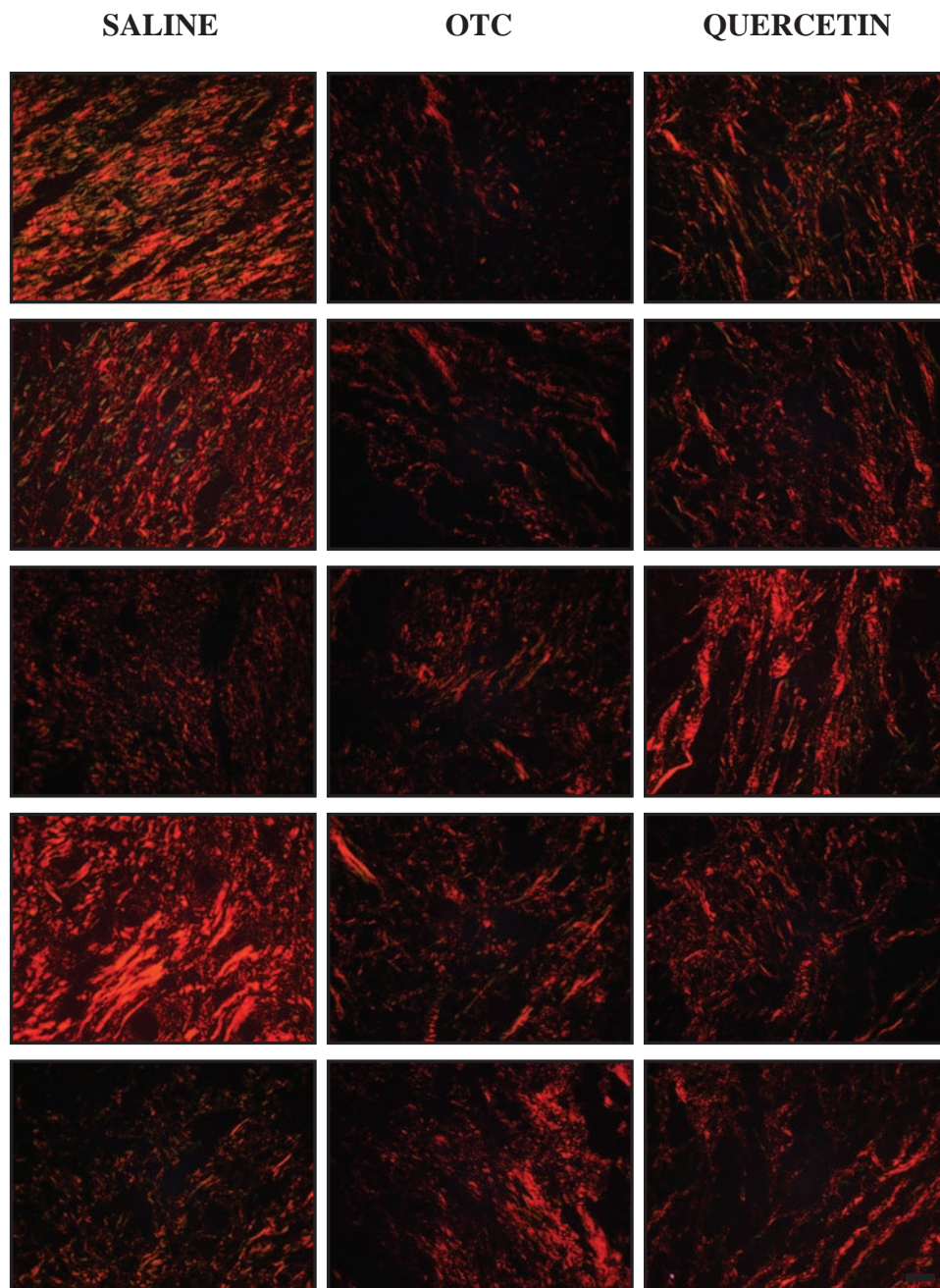


**Figure 13. Picrosirius polarization images showing the corresponding 21 day scar tissue regions of Saline, OTC and Quercetin treated animals. The five images in each vertical column represent the field of view images from 5 different animals within each treatment groups. Low intensity staining of the corresponding scar tissue region was observed in OTC treated groups. While both quercetin and saline treated animals showed huge variation in total collagen staining at the corresponding scar tissue region. All mages were taken using circularly polarized light at 10X magnification. Scale represent 100  $\mu\text{m}$ .**

## FIGURE 14

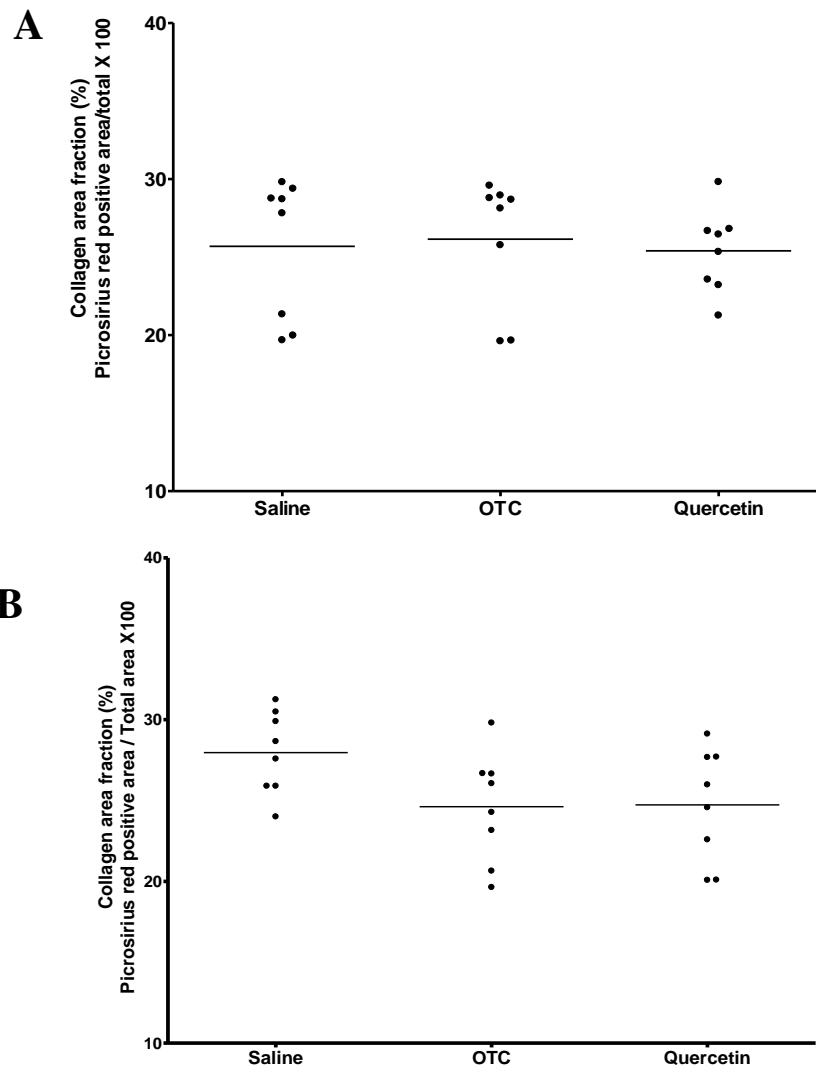


**Figure 14. Graph representing the collagen area fraction of the peridural scar tissue sections from saline, OTC and quercetin treated animals at 3 days (A) and 21 days (B) post laminectomy surgery.** The individual data points within the treatment groups represents the average collagen area fraction calculated from 9 separate fields of view within the picrosirius red stained tissue section obtained from each treated animals. (A) All 3 day treatment groups when compared with Saline control groups showed no statistical significant treatment effects ( $p > 0.05$ ,  $n = 8$ ). (B) While 21 day OTC and Quercetin treated animal showed a decrease in the mean total collagen stainable area as compared to the saline control group, the differences was not statistical significant (Mean  $\pm$  SD,  $p > 0.05$ ,  $n = 8$ ).

on the collagen area fraction (picosirius red positive area) relative to saline treated control animals (**Figure 14 A**,  $p > 0.05$ ,  $n = 8$ ).

Visual inspection of picosirius red polarized light images from 21-day peridural scar sections suggested that there might be a reduction in total collagen abundance in the scar tissue from OTC and quercetin treated as compared to saline treated animals (**Figure 13**). Quantitative image analysis of the polarized light images from 21-day scar tissue sections confirmed that the mean collagen area fraction for both OTC and quercetin treated animals was lower than for saline treated control animals. However, the reduction in picosirius red staining relative to control levels was not statistically significant for quercetin ( $p > 0.05$ ,  $n = 8$ ), or for OTC treatment (**Figure 14 B**,  $p > 0.05$ ,  $n = 8$ ). The 21-day peridural scar sections, like those of the 3-day time point, exhibited considerable variation in measured levels of picosirius red positive collagen (i.e. collagen area fraction) among the individual animals within each of the drug treatment groups.

#### **4.2.3 Effects of Quercetin and OTC on the expression of extracellular matrix proteins (type I collagen, fibronectin) and collagen biosynthesis markers, prolyl-4-hydroxylase (P4H) and heat shock protein- 47 (hsp-47).**

Since image analysis of picosirius red histochemical staining was unable to reveal differences in total collagen accumulation within the peridural scar tissues of OTC, quercetin and saline treated animals, I subsequently employed western blot analysis to assess the effects of these drugs on levels of type I collagen and fibronectin proteins and on the levels of two proteins involved in procollagen biosynthesis, P4H and hsp-47.

Specific antibodies for all four proteins were able to detect bands of the correct size on western blots of both 3 day and 21 day peridural scar tissue homogenates resolved by SDS-PAGE (**Figures 15 and 16**). The individual animals within each treatment group

showed a high degree of variation in their levels of the extracellular matrix proteins type I collagen and fibronectin as well as in their expression levels of hsp-47, a procollagen chaperone protein, and P4H, an enzyme involved in collagen biosynthesis (**Figure 15** and **16**). Densiometric analysis of the western blots revealed no significant effect of either OTC or quercetin on the mean levels of any of these proteins tested as compared to saline treated control animals in either 3 day or 21 day post-surgical animal groups (**Figure 17** and **18**,  $p > 0.05$ ,  $n = 6$ ).

Because of the large animal to animal variation seen in levels of protein expression, I employed RNA dot blot analysis to determine whether quercetin and OTC had any consistent effect on relative levels of the gene transcripts for collagen type 1 ( $\alpha 2$ ); collagen type 3 ( $\alpha 1$ ) and collagen type 4 ( $\alpha 1$ ). The expression level for each of the specific collagen mRNAs was normalized against the mRNA level of glyceraldehyde-3-phosphate dehydrogenase (GAPDH), a constitutively expressed gene transcript. Within the peridural scar tissue, the hybridization signals for the mRNA transcripts of the interstitial fibrillar collagens type 1 ( $\alpha 2$ ) and type 3 ( $\alpha 1$ ) were consistently higher than those of collagen type 4 ( $\alpha 1$ ), a predominantly basement membrane collagen (**Figure 19**). Detection of collagen type 4 ( $\alpha 1$ ) mRNA on autoradiographs required 6 times longer exposure as compared to detection of collagen type 1 ( $\alpha 2$ ) and collagen type 3 ( $\alpha 1$ ) mRNAs.

As seen with the previous protein analysis, the collagen mRNA levels also exhibited large animal to animal variation within each treatment group, including the saline controls. Densiometric quantification of RNA dot blot autoradiographs revealed no statistically significant effects of either quercetin or OTC treatments on type I, III or IV

**FIGURE 15**

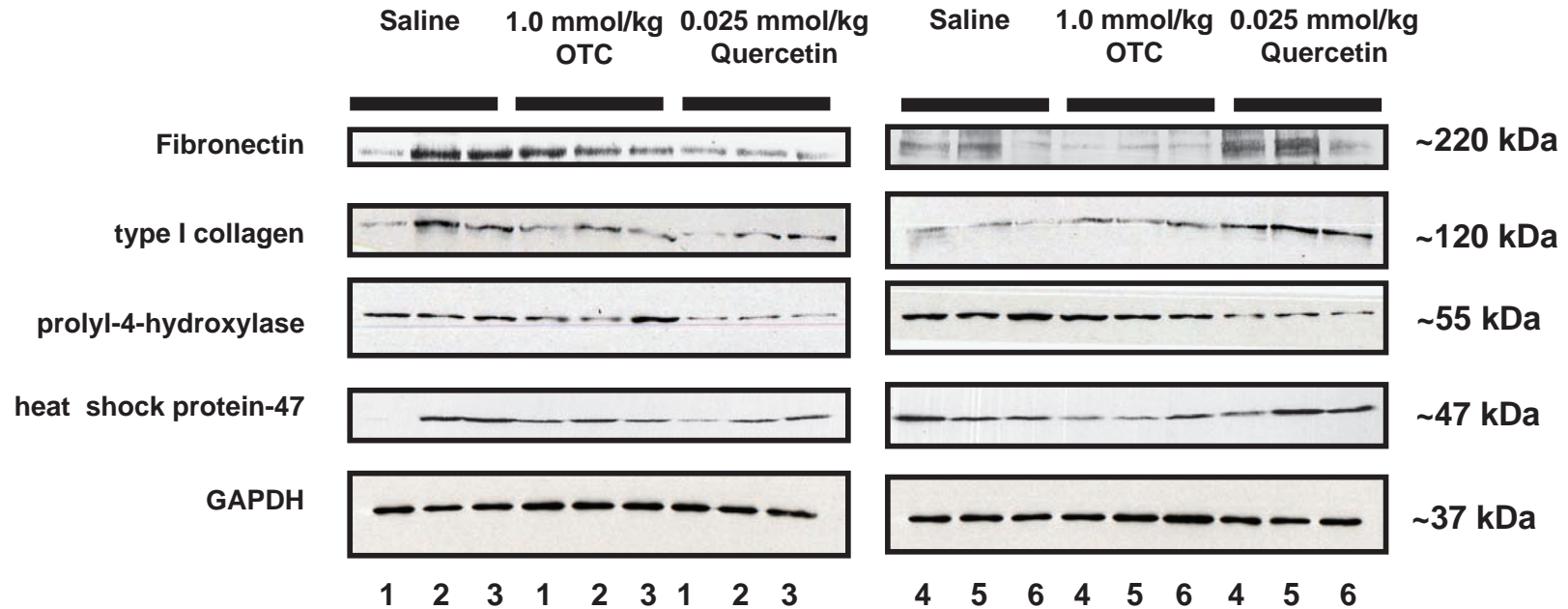


**Figure 15.** Western blot analysis of peridural scar tissue homogenates from 3 day post-surgical animals showing relative levels of Fibronectin, type I collagen, prolyl-4-hydroxylase, heat shock protein-47 and GAPDH following treatment with Saline, OTC and Quercetin. A total of six animals were used for the western blot analysis of the scar tissue homogenates obtained from 3 day post surgical animals, the left panel shows a set of western blots obtained from the first three animals (Animal # 1-3) for each of the treatment groups (Saline, OTC and Quercetin ) while the right panels shows the western blots from the rest of the animals (Animal # 4-6) for each treatment groups. There was a high amount of variability in fibronectin, type I collagen, P4H and hsp-47 expression in all treatment groups including saline treated control group. The GAPDH expression levels in each of the animal showed a high level of consistency as to the equal loading of proteins.

## FIGURE 16

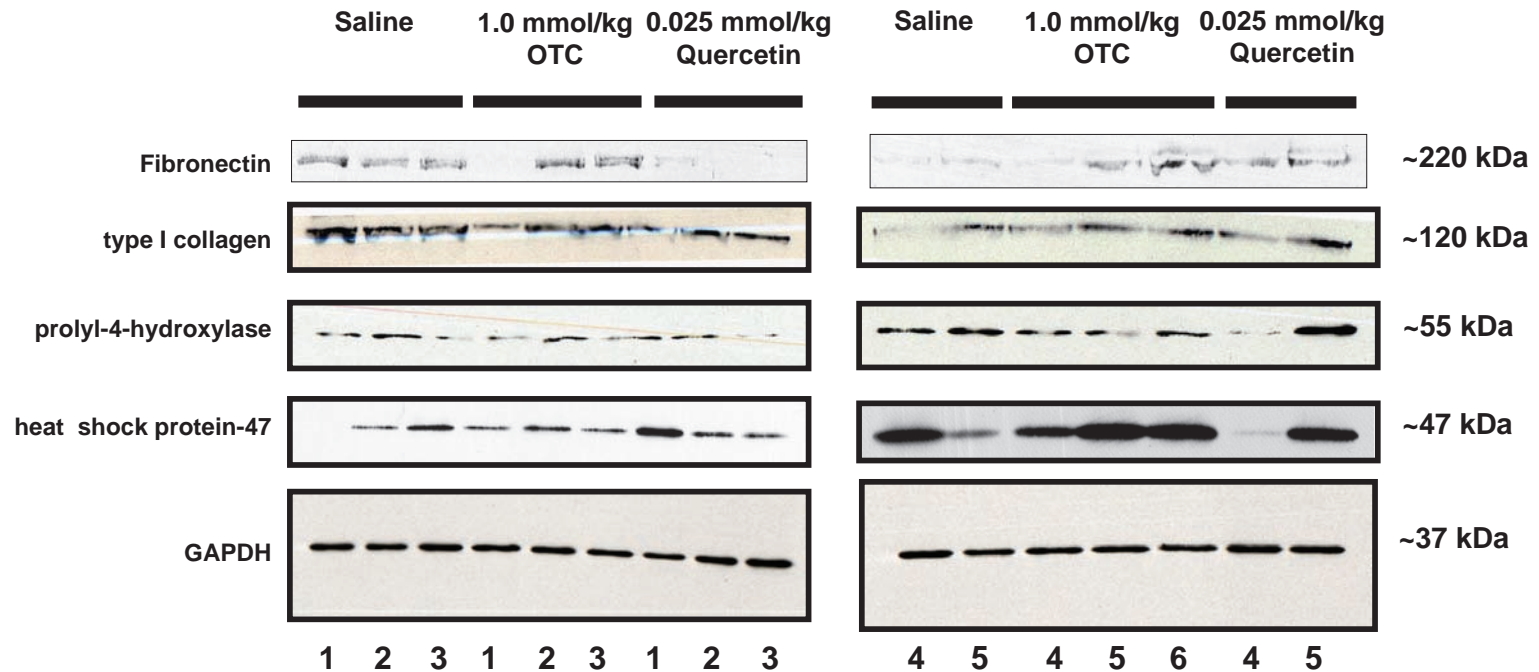


**Figure 16. Western blot analysis of peridural scar tissue homogenates from 21 day post-surgical animals showing relative levels of Fibronectin, type I collagen, prolyl-4-hydroxylase, heat shock protein-47 and GAPDH following treatment with Saline, OTC and Quercetin.** A total of five animals each were used for the western blot analysis of scar tissue homogenates obtained from 21 day Saline and Quercetin treated animals while six animals were used for the western blot analysis of scar tissue homogenates obtained from 21 day OTC treated animals, the left panel shows a set of western blots obtained from the first three animals (Animal # 1-3) for each of the treatment groups (Saline, OTC and Quercetin) while the right panels shows the western blots from the rest of the animals (Animal # 4-6 in case of OTC and Animal # 4 & 5 for Saline and Quercetin) for each the treatment groups. The GAPDH expression levels in each of the animal showed high level of consistency as to the equal loading of proteins. Variability in the levels of fibronectin, type I collagen, prolyl-4-hydroxylase and heat shock protein-47 expressions within each treatment group including saline treated control group.

# FIGURE 17

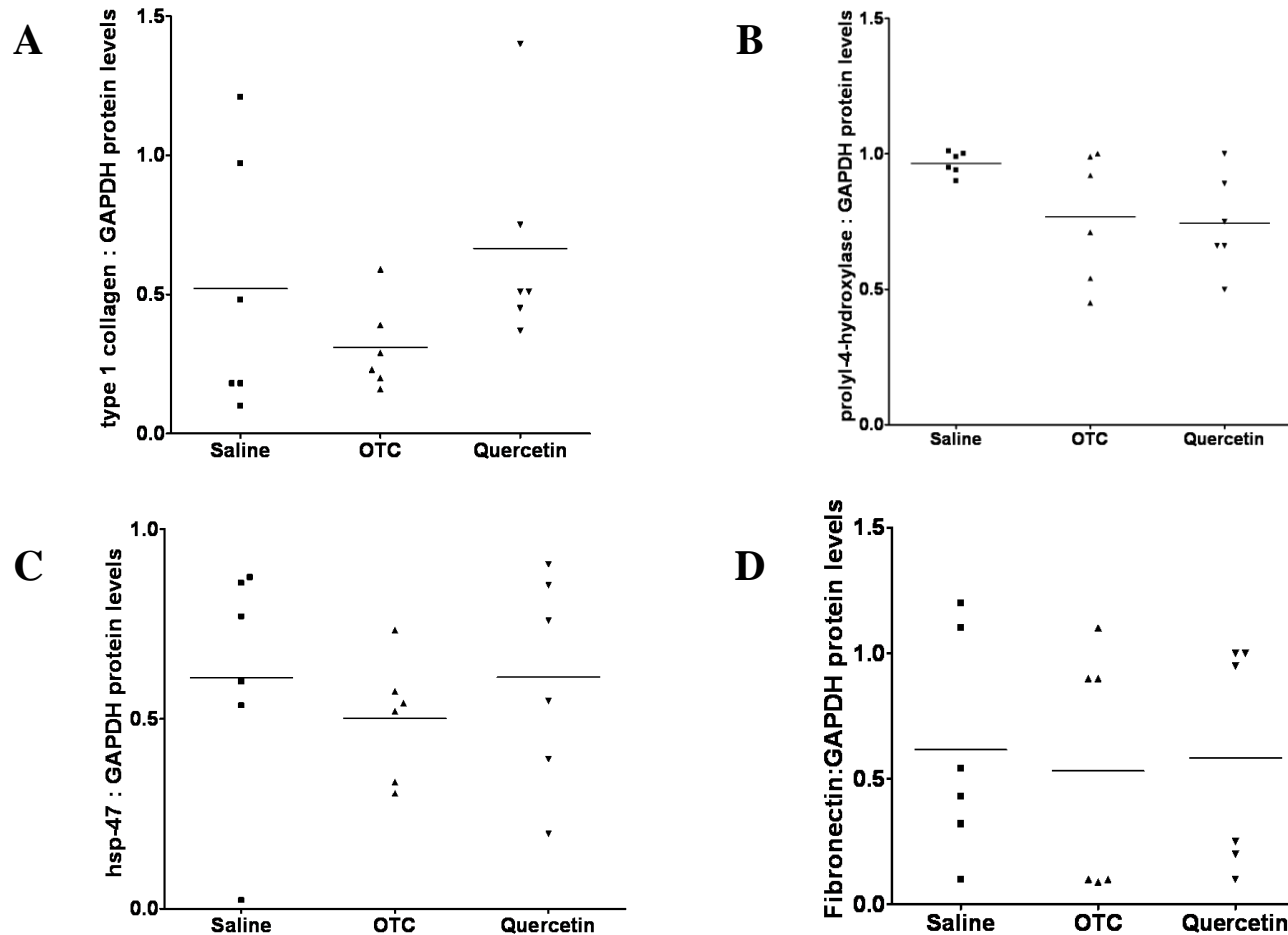


**Figure 17. Relative expression levels of type I collagen, prolyl-4-hydroxylase, heat shock protein-47 (hsp-47) and Fibronectin proteins in 3 day peridural scar tissue homogenate.** Densiometric analysis was performed on the western blots shown in Figure 15 using NIH Image J software. Relative protein expression levels were determined by normalizing the densitometric signal for the protein of interest against the GAPDH protein signal. One way ANOVA using Kruskal Wallis non-parametric test showed that there was no statistically significant treatment changes in expression of (A) type I collagen (B) prolyl-4-hydroxylase, (C) hsp-47 and (D) fibronectin proteins in 3 day animal groups treated with OTC and Quercetin as compared to Saline control groups.

# FIGURE 18

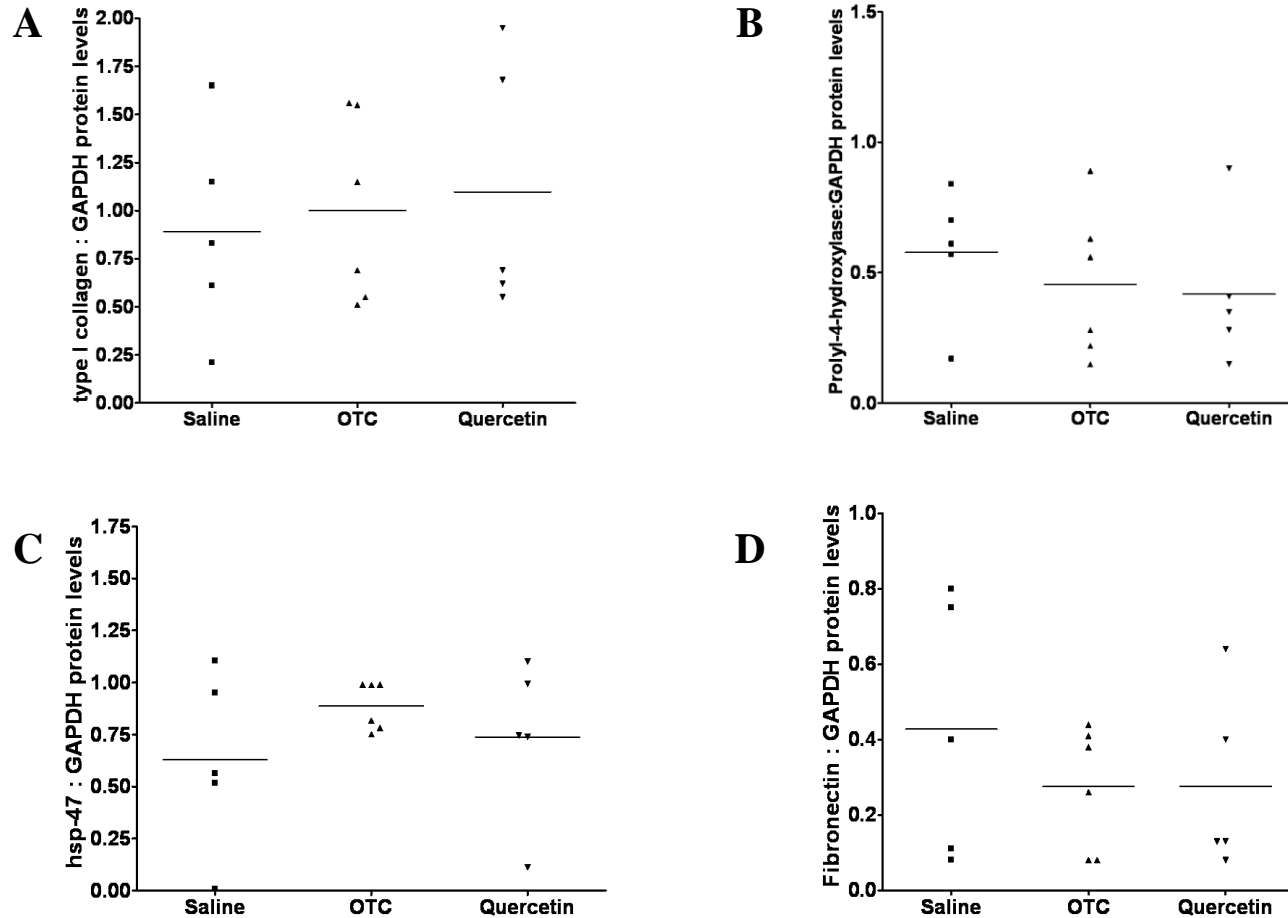


**Figure 18. Relative expression levels of type I collagen, prolyl-4-hydroxylase, heat shock protein-47 (hsp-47) and Fibronectin proteins in 21 day peridural scar tissue homogenate.** Densiometric analysis was performed on the western blots shown in Figure 16 using NIH Image J software. Relative protein expression levels were determined by normalizing the densitometric signal for the protein of interest against the GAPDH protein signal. One way ANOVA using Kruskal Wallis non-parametric test showed that there was no statistically significant treatment changes in expression of (A) type I collagen (B) prolyl-4-hydroxylase, (C) hsp-47 and (D) fibronectin proteins in 21 day animal groups treated with OTC and Quercetin as compared to Saline control groups.

**FIGURE 19**

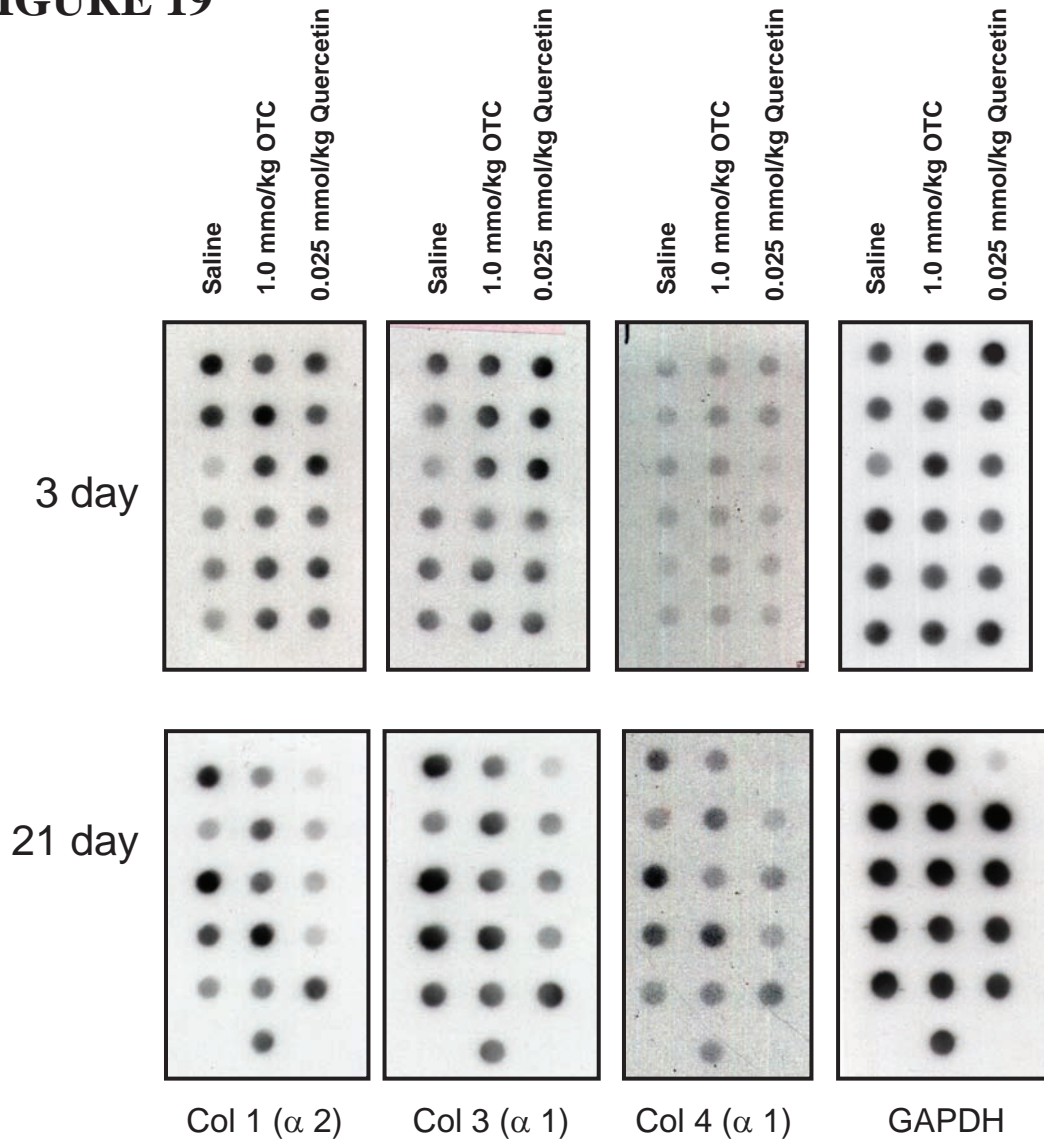


**Figure 19. Autoradiographs of RNA dot blots showing hybridization signals for Col 1( $\alpha$ 2), Col 3( $\alpha$ 1) and Col 4( $\alpha$ 1) with respect to GAPDH signals for peridural scar tissues isolated at 3 day and 21 days following spinal laminectomy surgery. As compared to Col 4 ( $\alpha$ 1) mRNA levels, both Col 1 ( $\alpha$ 2) and Col 3 ( $\alpha$ 1) mRNA levels were consistently expressed at higher levels in both 3 and 21 day animal groups. Autoradiographs for type IV collagen mRNA transcripts were exposed for 36 h, while it took only 6 h for type I and type III collagen mRNA transcripts to develop signals. The signal intensities for the individual animals within each of the Saline, OTC and quercetin treated groups showed considerable variability in the expression of type I, III and type IV collagen mRNA transcripts. Each dot represents expression of collagen mRNAs for individual animals within each treatment groups. For the mRNA analysis, all 3 day animal groups had a total of six animals within their treatment groups while 21 day animal groups had five animals for Saline and Quercetin group while six animals for OTC group were used for analysis.**

## FIGURE 20

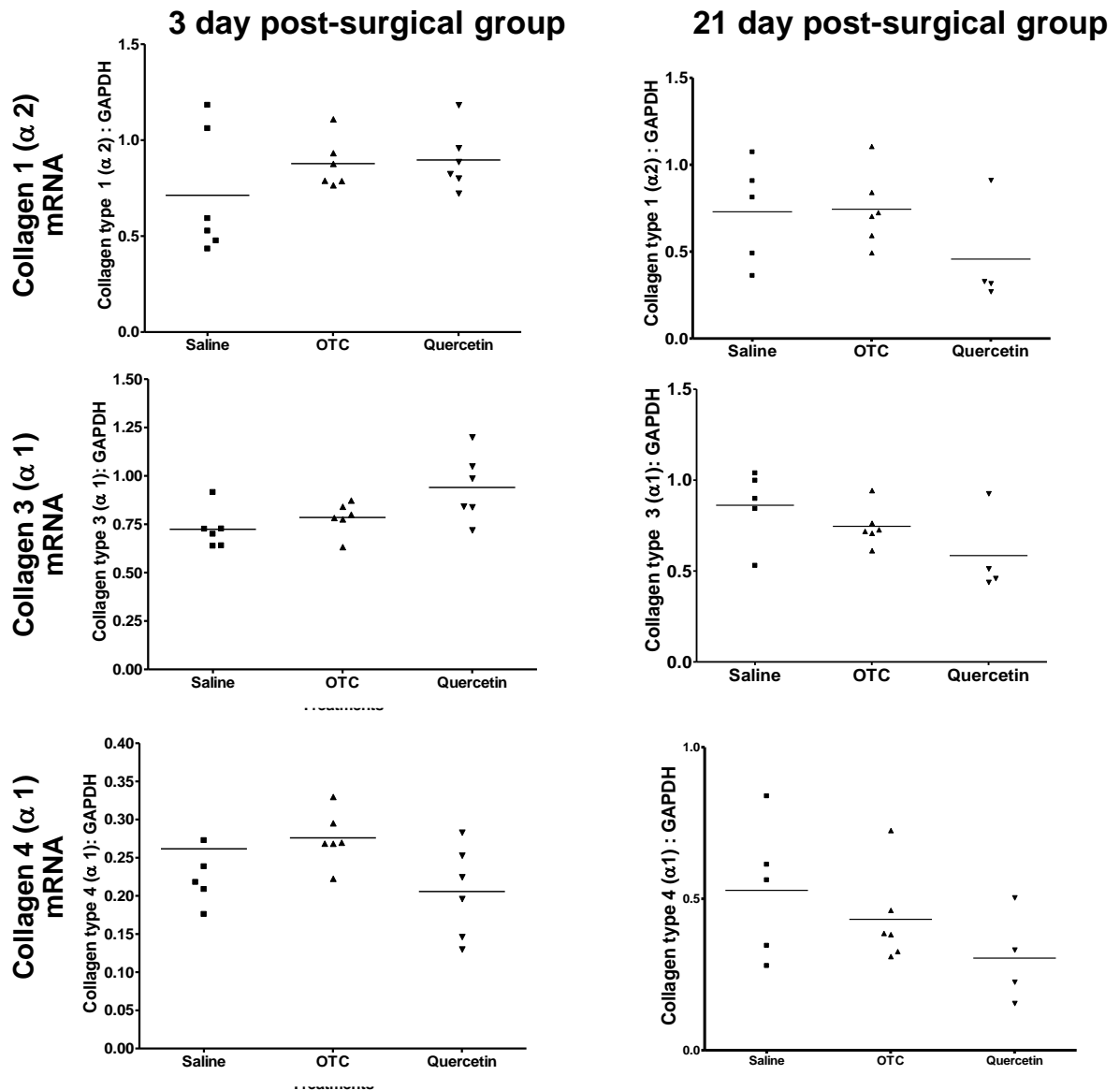


**Figure 20. Relative expression levels of Collagen 1 ( $\alpha 2$ ), Collagen 3 ( $\alpha 1$ ) mRNA and Collagen 4 ( $\alpha 1$ ) mRNA in 3 day and 21 day peridural scar tissue homogenates.** Densitometric analysis was performed on the RNA dot blots to determine the relative expression levels of the collagen mRNAs and the values obtained were normalized with GAPDH mRNA level values. Statistical analysis revealed no statistically significant differences in the expression of collagen mRNAs in peridural scars isolated from animals treated with OTC and Quercetin relative to Saline treated control animals ( $p > 0.05$ ,  $n = 6$ )

collagen mRNA levels relative to the saline control group in both 3 day and 21 day animal groups (**Figure 20**;  $p > 0.05$ ,  $n = 6$ ).

The scatter plots for each protein and mRNA assayed indicated large animal to animal variability within each treatment group. For each protein (or mRNA) some individual animals expressed at comparatively high levels while other expressed at relatively low levels. In order, to determine whether those individual animals that expressed high levels of a particular protein (e.g type I procollagen) also expressed high levels of functionally related proteins (e.g. hsp-47 or P4H) or vice versa. I performed Pearson Correlation Coefficient analyses using SPSS 17.0 statistical software on the western blot data for type I collagen, P4H, hsp-47 and fibronectin proteins. The results of this analysis are tabulated in **Appendix 1**. The analysis revealed that for 21 day OTC treated animals there was a significantly high correlation between levels of P4H and hsp-47 proteins. This indicates that those individual animals that expressed high levels of P4H protein also tended to express high levels of hsp-47 protein, while other animals expressed concurrently low levels of both proteins. Our findings suggest a potential ability of OTC to balance levels of proteins involved in collagen biosynthesis and post-translational modification.

Similarly, correlation coefficient analysis was performed on RNA dot blot data for type I, III and IV collagen mRNA transcripts (see **Appendix 2**). It was observed that the 3 day and 21 day saline treated animals showed strong correlation between type I and type III collagen mRNA transcript levels. This indicates that in saline treated animals when type I collagen mRNA transcript levels were high, the type III collagen mRNA transcript levels were also high, while others expressed concurrently low levels of both mRNAs. This finding correlates with the previous findings where both collagen type 1

( $\alpha 2$ ) and collagen type 3 ( $\alpha 1$ ) mRNA transcripts are been co-expressed at high levels in early healing tissues (Kinbara *et al.*, 2002) as well as in fibrotic tissues (Stewart *et al.*, 1994).

#### **4.3 Effects of Quercetin and OTC on the expression of potential regulatory molecules such as TGF- $\beta 1$ , TGF- $\beta 3$ , VEGF, ERK and p38 MAPK in the rat spinal laminectomy model.**

##### **4.3.1 Effects of Quercetin and OTC on TGF- $\beta 1$ and TGF- $\beta 3$ mRNA expression levels in 3 day and 21 day peridural scar tissues.**

Both the TGF- $\beta 1$  and TGF- $\beta 2$  growth factors have been implicated in promoting scarring (Adzick and Lorenz, 1994; Krummel *et al.*, 1988; Shah *et al.*, 1995). TGF- $\beta 1$  stimulates collagen synthesis, fibroblast proliferation and angiogenesis (Cannon and St Pierre, 1998; Massague, 1990) that are involved in scar formation. In contrast, TGF- $\beta 3$  has been shown to decrease scarring in a rat incisional wound model (Shah *et al.*, 1995).

Accordingly, I utilized RNA dot blot analysis to examine whether quercetin and OTC treatments would alter the relative levels of TGF- $\beta 1$  to TGF- $\beta 3$  mRNA expression during *in vivo* peridural wound healing in a manner consistent with scarless tissue repair. The hybridization signals for the TGF- $\beta$  mRNA were normalized against the GAPDH mRNA signal to correct for differences in sample loading. As seen in **Figure 21**, the hybridization signals for TGF- $\beta 1$  and TGF- $\beta 3$  were relatively low in RNA samples isolated from both 3 day and 21 day peridural scar tissue, requiring autoradiographic exposure times of  $\sim 2$  days for detection. This suggests that TGF- $\beta 1$  and TGF- $\beta 3$  mRNA levels were quite low in these tissues. Densitometric analysis of the signal intensities for TGF- $\beta 1$  and TGF- $\beta 3$  mRNA in scar tissue samples from 3-day and 21-day post-surgery

**FIGURE 21**

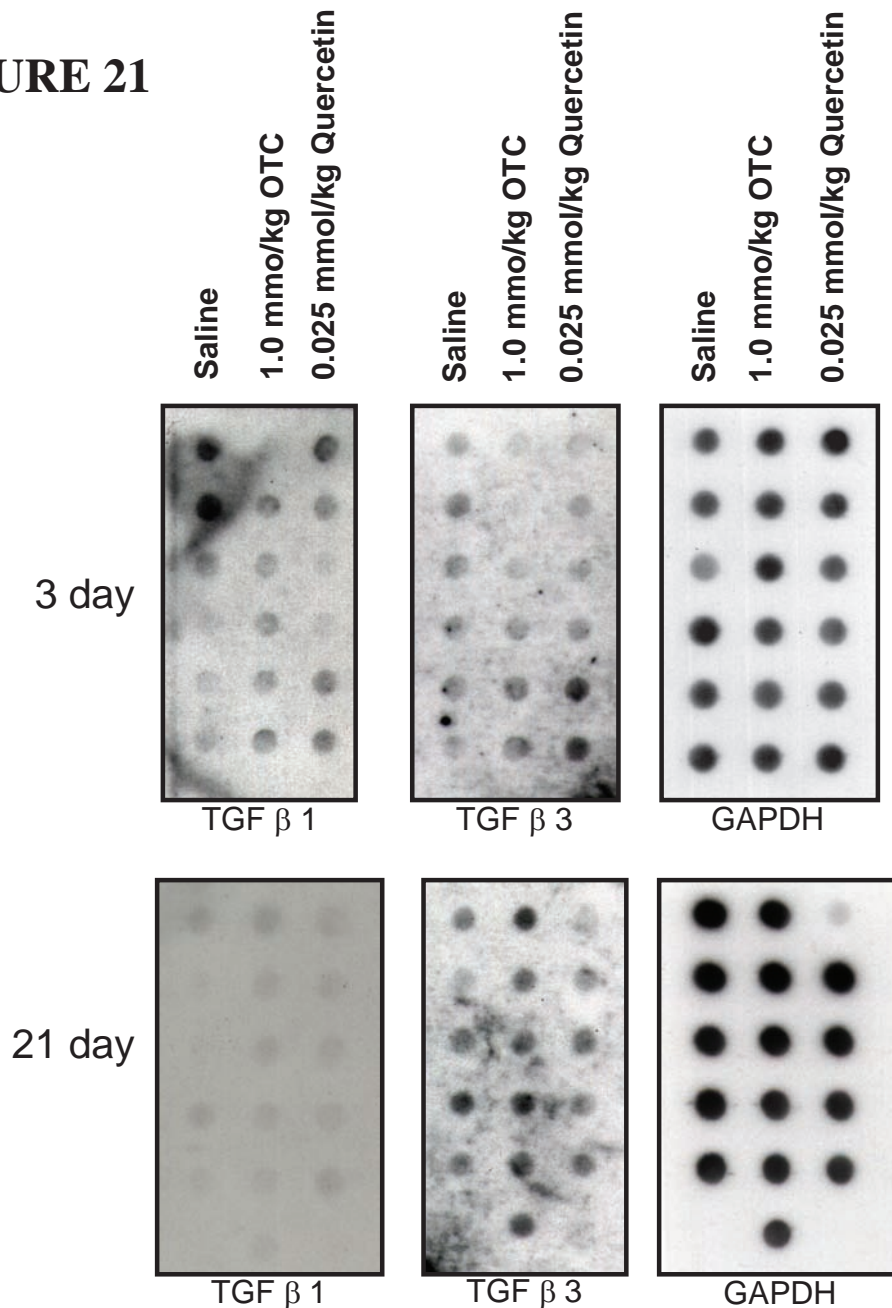


**Figure 21. RNA dot blot autoradiograph showing signal intensity for TGF- $\beta$ 1, TGF- $\beta$ 3 and GAPDH mRNAs for peridural scar tissues isolated at 3 day and 21 days following spinal laminectomy surgery.** The signal intensities for the individual animals within each of the Saline, OTC and Quercetin treated groups showed considerable variability in relative expression levels of TGF- $\beta$ 1 and TGF- $\beta$ 3. In 3 day treatment groups, TGF- $\beta$ 1 expression levels were higher as compared to 21 day treatment groups while TGF- $\beta$ 3 was consistently expressed at higher levels in both the treatment groups. Each dot represents expression of TGF- $\beta$  mRNAs for individual animals within each treatment groups. It took 48 hours for the autoradiograph to develop signals for both TGF- $\beta$ 1 and TGF $\beta$ 3 mRNA transcripts. For the mRNA analysis, all 3 day animal groups had a total of six animals within their treatment groups while 21 day animal groups had five animals for Saline and Quercetin group while six animals for OTC group were used for analysis.

**FIGURE 22**

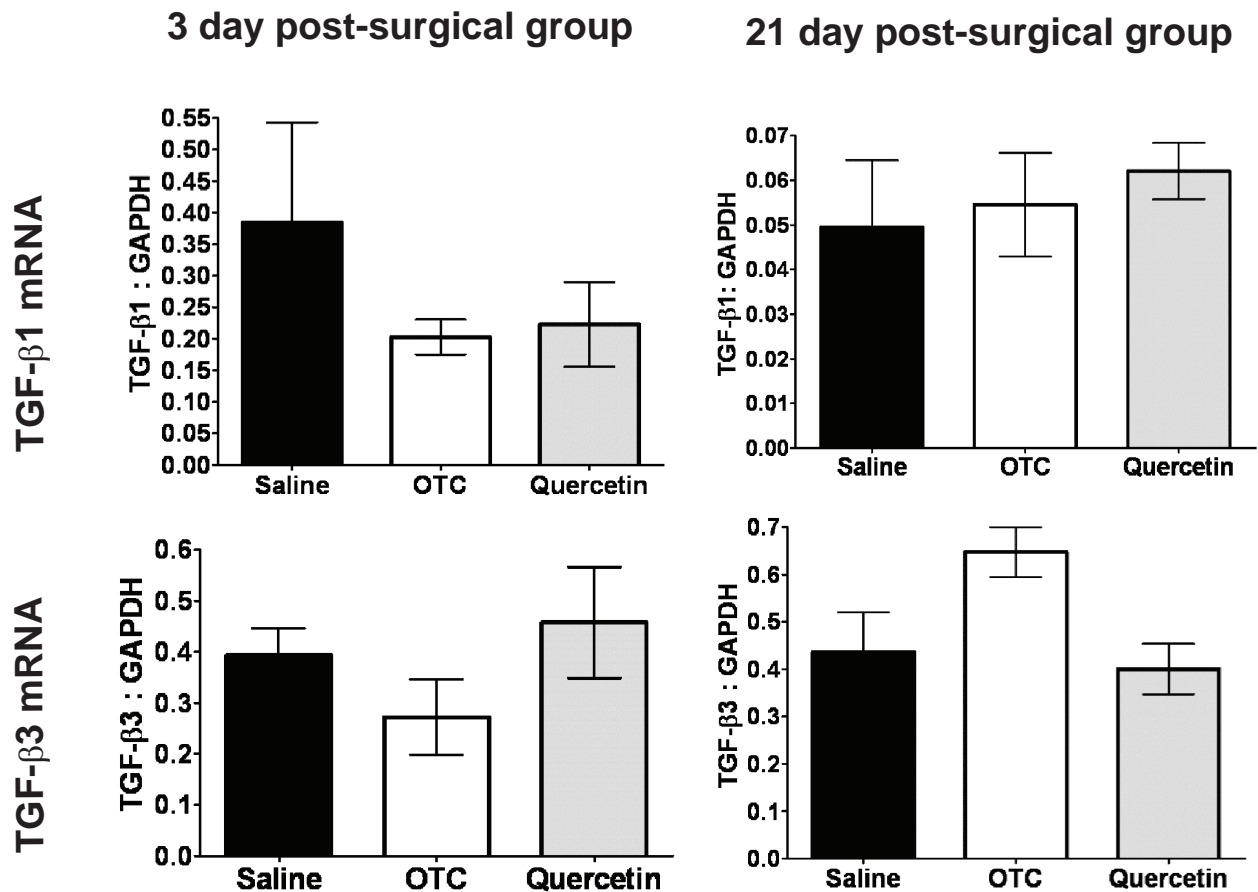


**Figure 22. Relative expression levels of TGF-β1 and TGF-β3 mRNA in 3 day and 21 day peridural scar tissue homogenates.** Densitometric analysis was performed on the RNA dot blots to determine the relative expression levels of the TGF-βs mRNA and the values obtained were normalized with GAPDH mRNA level values. Statistical analysis shows that there was no statistically significant changes in the expression of TGF-β mRNAs following treatment with OTC ( $p > 0.05$ ,  $n=6$ ) and Quercetin as compared to Saline control treatment (Mean  $\pm$  SD,  $p > 0.05$ ,  $n =6$ )

time points revealed no statistically significant effects of either quercetin and OTC treatment (**Figure 22**;  $p > 0.05$ ;  $n = 6$ ). However, in 21-day scar tissue samples from all drug treatment groups, there appeared to be a general trend for higher TGF- $\beta$ 3 expression relative to TGF- $\beta$ 1 (**Figure 21**).

Again, I performed Pearson Correlation coefficient analysis to determine whether any linear correlation exists between TGF- $\beta$ 1 and TGF- $\beta$ 3 or TGF  $\beta$ s and all collagen mRNA transcripts within the animals in the treatment groups. It was observed that no significant linear correlation existed between TGF- $\beta$ s and the majority of collagen mRNA transcripts tested in all treatment groups except for 3 day saline treated animal group (see **Appendix 2**). In 3 day saline treated animals it was observed that when TGF- $\beta$ 1 mRNA levels were high there was a linear increase in collagen 1 ( $\alpha$ 2) mRNA levels suggesting the potential fibrogenic role of TGF- $\beta$ 1. This finding directly correlates with previous findings that have shown increased TGF- $\beta$ 1 mRNA transcript levels may lead to increase in collagen 1 ( $\alpha$ 2) mRNA transcript levels (Kinbara *et al.*, 2002; Halper *et al.*, 2005).

Western blots of 3 and 21-day scar tissue homogenates that were probed with commercial antibodies (Santa Cruz Biotech) against TGF- $\beta$ 1, TGF- $\beta$ 2, and TGF- $\beta$ 3 proteins were unsuccessful in demonstrating detectable levels of any of these growth factors (data not shown). This was consistent with the low level of TGF- $\beta$ 1 and TGF- $\beta$ 3 transcript expression detected by standard RNA dot blot analysis. Due to the absence of detectable of TGF- $\beta$  protein expression and the weak, variable hybridization signals for TGF- $\beta$  mRNAs, we were unable to ascertain whether quercetin and OTC treatments were able to modulate TGF- $\beta$ 1 and TGF- $\beta$ 3 expression during peridural wound repair.

#### 4.3.2 Effects of Quercetin and OTC on the expression of VEGF protein and myogenic markers in 3 day and 21 day peridural scar tissue.

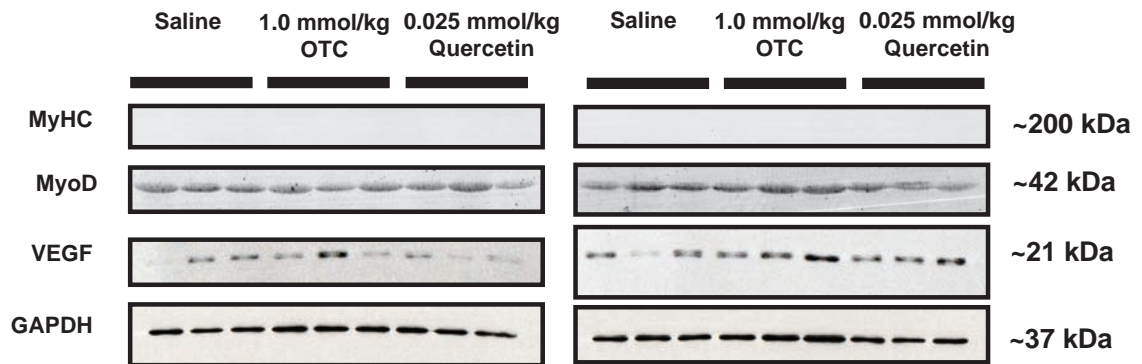
I also wished to determine whether quercetin and OTC had any effect on the expression of vascular endothelial growth factor (VEGF), an angiogenic factor that plays a key role in skeletal muscle repair. VEGF was shown to enhance myoblast migration *in vitro* and to prevent apoptosis of myoblasts in cell culture and in skeletal muscle following ischemia (Arsic *et al.*, 2004; Germani *et al.*, 2003). Moreover, delayed angiogenesis may lead to impaired skeletal muscle regeneration (Ochoa *et al.*, 2007). Western blot analysis of peridural scar tissue homogenates confirmed expression of VEGF proteins in both 3 day and 21-day post-surgical groups (**Figure 23**). Visual comparison of the blots 3 day and 21 day scar tissue homogenates suggests that the VEGF protein levels were usually higher in 21-day peridural scar tissue than in 3-day scar tissue (**Figure 23**). Nevertheless, VEGF protein levels exhibited substantial animal to animal variation within each treatment group at both post-surgical time points (**Figure 24**).

Densiometric analysis of the western blots obtained for 3 day peridural scars revealed that the mean VEGF protein levels were higher for both OTC and quercetin treated animals as compared to the saline control group (**Figure 24**), however these differences were not statistically significant ( $p > 0.05$ ,  $n = 6$ ). In 21 day peridural scar tissue, the mean levels of VEGF protein for OTC and quercetin treated animals were significant difference.

Western blot analysis demonstrated that peridural scar tissue isolated at 3 days and 21 days after laminectomy surgery expressed MyoD protein, a marker for immature myoblastic cells (**Figure 23**). In contrast, we did not detect expression of myosin heavy

## FIGURE 23

### 3 day post-surgical group



### 21 day post-surgical group

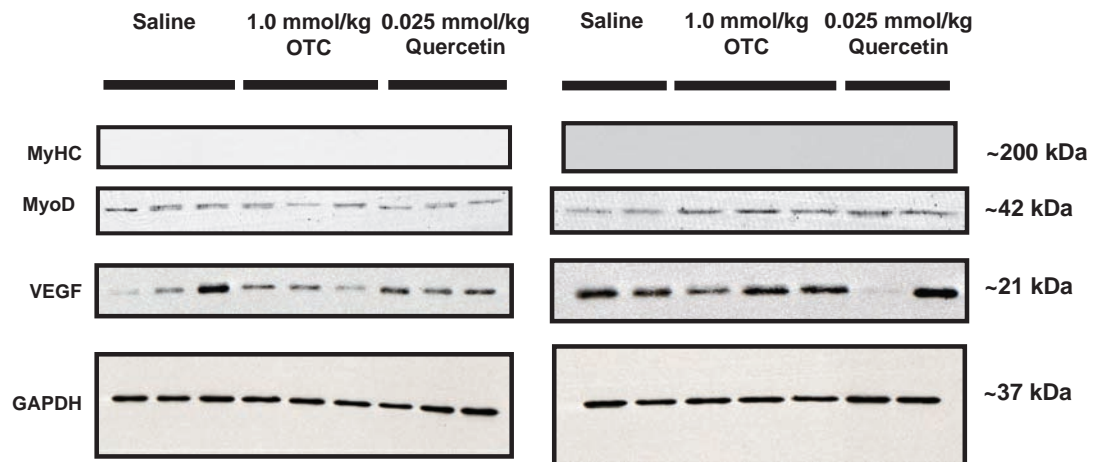


**Figure 23. Western blot analysis of peridural scar tissue homogenates from 3 day and 21 day post-surgical animals showing relative levels of MyHC, MyoD, VEGF and GAPDH following treatment with Saline, OTC and Quercetin.** Absence of MyHC protein in all treatment groups shows that peridural scar tissue homogenates did not have any differentiated muscle cells though presence of MyoD shows that the tissue homogenate did contain MyoD positive cells in the granulation tissue isolated for protein analysis. This is consistent with muscular healing process. The MyoD expression levels were higher in 3 day post-surgical groups as compared to 21 day post-surgical groups. The overall VEGF expression in 21 day post-surgical groups were higher than 3 day post-surgical groups. The variability in the expression of VEGF proteins was observed in all experimental treatment groups including saline control group in both 3 and 21 day post-surgical groups. Each lane shows protein level expression for individual animals within the treatment groups. For the protein analysis of the 3 day post-surgery groups, each treatment groups had six animals.

## FIGURE 24

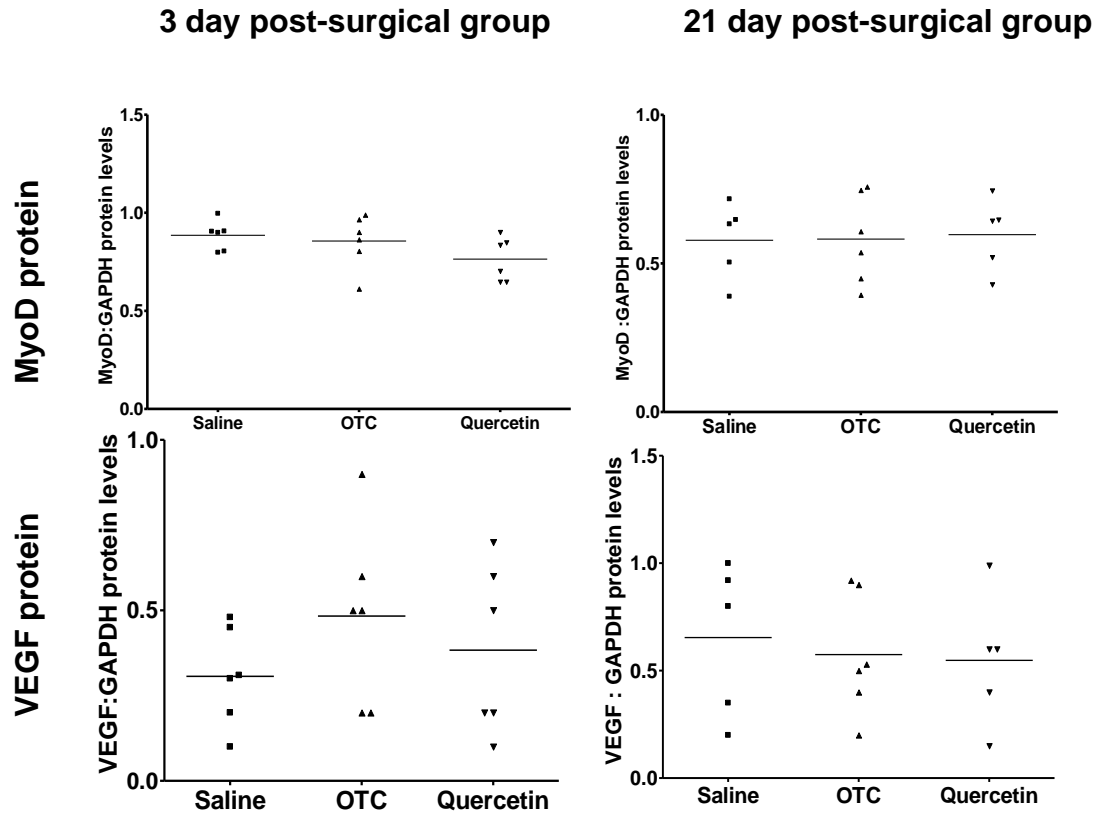


**Figure 24 Relative expression levels of VEGF and MyoD proteins in 3 day and 21 day peridural scar tissue homogenates.** The densitometric analysis was performed on western blots and the relative VEGF and MyoD protein expression levels were determined by normalizing the values with GAPDH protein expression levels. The overall mean VEGF protein expression were higher in 21 day post-surgical group as compared to 3 day post-surgical group, while overall mean MyoD protein expression were higher in 3 day post-surgical group as compared to 21 day post-surgical group. No statistical significant treatment effects of both OTC and quercetin was observed ( $p > 0.05$ ,  $n = 6$ ; One way ANOVA using Kruskal Wallis non-parametric test)

chain (MyHC), a marker for differentiated skeletal muscle fibres (**Figure 23**). These data suggest that both 3 day and 21 day peridural scar tissues contain immature myoblastic cells but few if any fully differentiated skeletal muscle fibres. Visual inspection suggests that expression of MyoD protein may be lower at 21-day post surgery than in 3-day peridural scar tissue. However, densitometric analysis revealed no statistically significant slightly lower than in saline treated animals but again statistical analysis revealed no effects of either OTC or quercetin treatment on MyoD protein levels (**Figure 23**,  $p > 0.05$ ,  $n = 6$ ).

Again, to determine whether there was any linear correlation that existed between VEGF and MyoD, or between VEGF/MyoD and type I collagen, P4H, hsp-47 and fibronectin proteins, within the animals in treatment groups. I performed Pearson Correlation analysis on the Western blot data and results are tabulated in **Appendix 1**. It was observed that in both 3 day and 21 day saline and quercetin treated animal groups there was no significant relationship between the ECM proteins, type I collagen and fibronectin, or P4H and hsp-47, with the VEGF or MyoD proteins which may suggest no correlation between these proteins. However, when the analysis was performed on the 21 day OTC treated animals; it showed strong linear correlation between hsp-47 levels and MyoD protein levels. The animals that expressed high levels of VEGF expressed high levels of MyoD proteins while animals that expressed low levels of VEGF also expressed low levels of MyoD protein. Similarly, 21 day OTC treated animals also showed strong linear correlation between P4H and VEGF proteins. These findings may suggest that OTC could promote fibroblast cells to produce VEGF protein (Takamiya *et al.*, 2002) and also help in the migration of myoblast cells that aid in muscle regeneration (Higuchi *et al.*, 2007).

### **4.3.3 Effects of Quercetin and OTC on ERK and p38 MAP kinase expression in 3 and 21 day peridural scar tissue.**

Activation of both p38 and ERK1/2 MAPK is necessary for resolution of keloid scar through stimulation of keloid fibroblast apoptosis (Kuo *et al.*, 2005). In skeletal muscle repair, p38  $\alpha/\beta$  MAPK activation is necessary to activate quiescent satellite cells and promote their proliferation and eventual differentiation into muscle fibres (Chen *et al.*, 2007). In corneal wound healing, ERK 1 and ERK 2 activation has been implicated in the initiation of cell migration and proliferation during early repair phases (Imayasu and Shimada, 2003). The prominent involvement of MAPK signaling in wound healing processes prompted us to examine whether OTC and quercetin treatments altered the levels of ERK and p38 MAPK expression and phosphorylation in peridural scar tissues following laminectomy surgery.

#### **4.3.3.1 Effects of Quercetin and OTC on p38 MAPK expression in peridural scar tissue.**

Western blot analysis of peridural scar tissue homogenates demonstrated the presence of both total p38 MAPK and phosphorylated p38 MAPK in all post-surgical animals groups (**Figure 25 A** and **25 B**). At 3 day post-surgery, the blots showed very low levels of dual-phosphorylated (active) p38 MAPK protein relative to total p38 MAPK proteins for animals from all drug treatment groups (**Figure 25 A**). Densitometric analysis of the 3-day peridural scar samples revealed no statistically significant effects of either quercetin or OTC on levels of p38 MAPK activation as compared to saline treated control animals (**Figure 25 C**).

Western blots of 21-day peridural scar tissue showed expression of both total and dual phosphorylated p38 MAPK protein (**Figure 25 B**). Dual phosphorylated (active) p38

# FIGURE 25

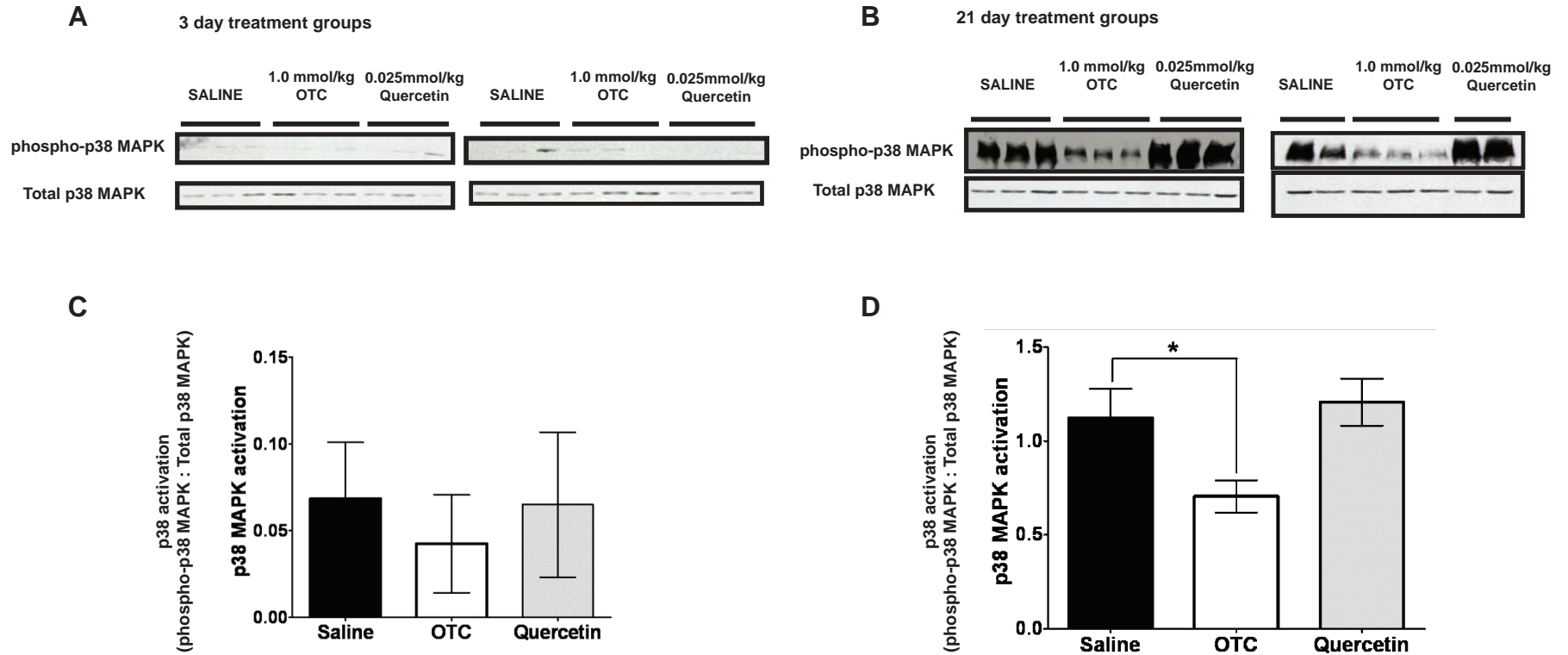


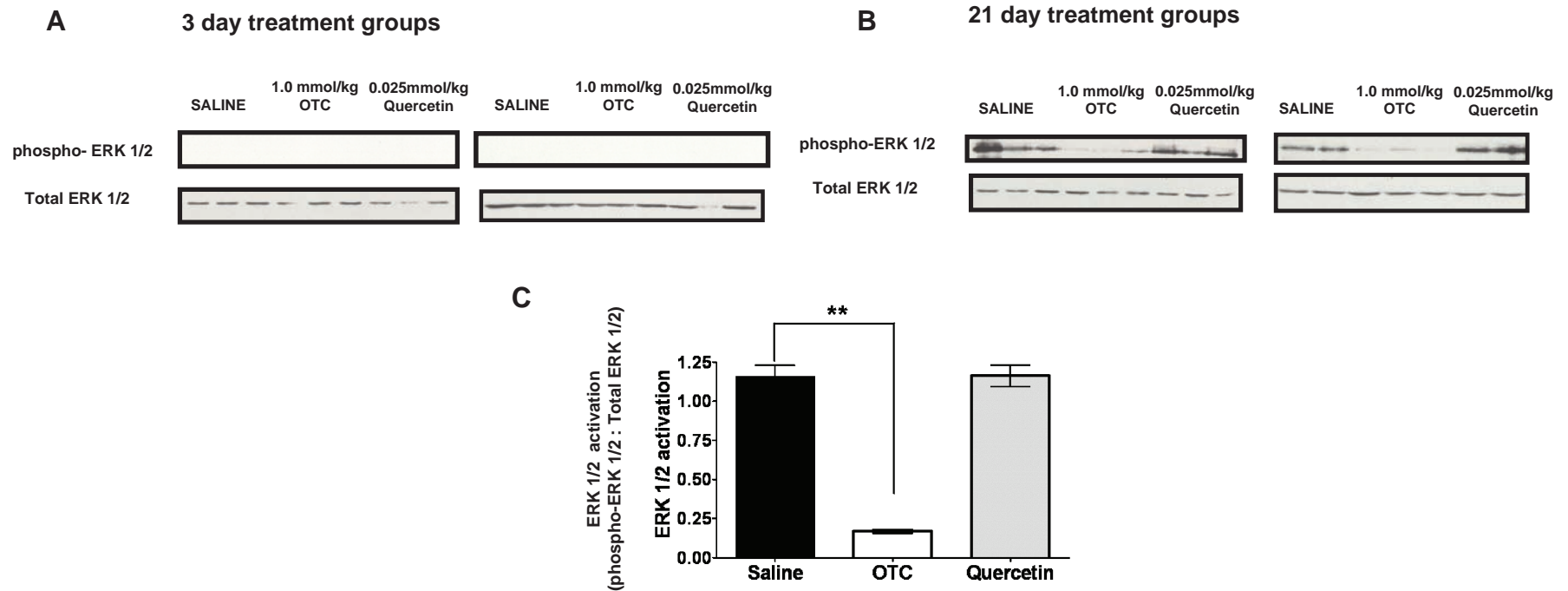
**Figure 25. Western blot analysis for dual phosphorylated p38 mitogen activated protein kinases (MAPK) and total p38 MAPK in 3 day and 21 day post-surgical scar tissue homogenates obtained from Saline, OTC and Quercetin treated animals.** For both dual phosphorylated (active) and total p38 MAPK expression analysis, 12.5 % SDS-acrylamide gels were used to resolve the proteins. Each blot represents a set of animals with saline, OTC and quercetin treatment groups. Six animals per drug treatment group (including saline control) were used for 3 day treatment groups, while 5 animals were used for 21 day animals treated with quercetin and saline control. (A) It was observed that in 3 day treatment groups, dual phosphorylated p38 MAPK were expressed at very low levels as compared to 21 day treatment groups, (B) while total p38 MAPK proteins were present in both 3 day and 21 day treatment groups. Densitometric analysis was performed on the western blots shown in Figure 25 a and 25 b using NIH image J software. p38 activation levels were determined by normalizing the densitometric signal for dual phosphorylated p38 MAPK against corresponding total p38 MAPK protein signal. It was observed 21 day post-surgical scar tissue from OTC treated animals exhibited significantly lower p38 activation as compared to saline treated control animals. ( Mean  $\pm$  SD, \* indicates significance at  $p < 0.05$ ; Kruskal Wallis non-parametric one way ANOVA)

MAPK was relatively abundant in 21-day scar samples from all three-treatment groups as compared to 3-day scar tissues (**Figure 25 B**). Densitometric analysis of the 21-day peridural scar samples was performed to determine the relative p38 MAPK activation levels between the drug treatment and saline control groups (**Figure 25 D**). At 21-day post surgery, peridural scar tissue from OTC treated animals exhibited significantly lower p38 MAPK activation levels as compared to saline treated control animals (**Figure 25 D**;  $p < 0.05$ ;  $n = 6$ ). In contrast, the level of p38 MAPK activation in peridural scar tissue from quercetin treated animals was not statistically different than that of saline treated control animals (**Figure 25 D**;  $p > 0.05$ ;  $n = 5$ ).

#### **4.3.3.2. Effects of Quercetin and OTC on ERK expression in peridural scar tissues**

We also examined the effects of quercetin and OTC treatments on levels of total ERK1/2 protein and dual phosphorylated (active) ERK1/2. Western blot analysis of peridural scar tissues collected at 3 days after laminectomy surgery revealed expression of total ERK1/2 protein for all drug treatment groups, but dual phosphorylated ERK1/2 was undetectable (**Figure 26 A**). In contrast, 21-day peridural scar tissue samples expressed dual phosphorylated ERK1/2 as well as total ERK1/2 proteins (**Figure 26 B**). Densitometric analysis of the 21-day peridural scar samples was performed to determine the relative ERK1/2 activation levels between the drug treatment and saline control groups (**Figure 26 C**). At 21-day post-surgery, the levels of ERK1/2 phosphorylation/activation was significantly lower in peridural scar tissue from OTC treated animals as compared to saline treated control animals (**Figure 26 C**,  $p < 0.05$ ,  $n = 6$ ). In contrast, ERK activation levels for the 21-day scar tissue from the quercetin treatment group were equivalent to saline controls.

# FIGURE 26



146

**Figure 26. Western blot analysis for dual phosphorylated ERK 1/2 and total ERK 1/2 in 3 day and 21 day post-surgical scar tissue homogenates obtained from Saline, OTC and Quercetin treated animals.** For the ERK 1/2 expression analysis, 12.5 % SDS-acrylamide gels were used to resolve the proteins. Six animals per drug treatment group (including saline control) were used for 3 day post-surgical groups while 5 animals were used for 21 day animals treated with quercetin and saline control. (A) The expression of total ERK 1/2 were present in all 3 day and 21 day treatment groups, while dual phosphorylated ERK 1/2 was undetected in 3 day treatment groups (B). Densitometric analysis was performed on the western blots shown in Figure 26 b using NIH Image J software (C). ERK1/2 activation levels were determined by normalizing the densitometric signal for dual phosphorylated ERK1/2 against corresponding total ERK1/2 protein signal. It was observed that 21 day OTC treated animal showed statistically significant lower levels of ERK1/2 activation as compared to Saline treated animals while ERK 1/2 activation was similar for both 21 day saline and quercetin treated animals ( Mean ± SD, \*\* indicate significance at  $p < 0.01$ ;  $n = 5$ . Kruskal Wallis non parametric one way ANOVA).

Our findings suggest that OTC treatment consistently reduced both ERK and p38 MAPK signaling in our spinal laminectomy model of peridural wound repair.

#### **4.4 Development of a novel *in vitro* co-culture model to study the wound-healing process: Method development and validation**

##### **4.4.1 Introduction**

Large animal to animal variation was a persistent problem for most of our assay parameters in the rat spinal laminectomy model. Variability was observed for the expression levels of a variety of mRNAs and proteins implicated in fibrosis and tissue repair including collagens, fibronectin, P4H, hsp-47, VEGF, TGF- $\beta$ 1 and TGF- $\beta$ 3. As such we could not clearly establish whether OTC or quercetin exerted anti-fibrotic effects on peridural scarring *in vivo*. Hence, the focus of my thesis research was shifted toward developing an improved *in vitro* wound repair model for use in drug development studies, with specific emphasis on evaluating the effects of quercetin and OTC. Accordingly, my experimental strategy was to develop a more consistent and economical *in vitro* model that would mimic characteristics of *in vivo* peridural scar tissue, and to employ this model to examine effects of OTC and quercetin on collagen biosynthesis and other parameters of tissue fibrosis.

In establishing my *in vitro* wound repair model, I employed “micromass” co-cultures of an adult rat myoblast cell line and a rat fetal skin fibroblast cell line to permit the interaction of these distinct cell types in a 3-D tissue like context that would simulate *in vivo* peridural muscle tissue repair.

#### **4.4.1.1 Method development: Characterization of “micromass” co-culture based technology as a 3-D scaffold free *in vitro* wound repair model.**

##### **4.4.1.1.1** Determination of the relative proportions of L8 myoblast cells and FR 3T3 fibroblast cells that promote micromass adhesion and withstand wounding manipulation.

In my initial experiments, I determined the optimum combination of rat L8 skeletal myoblast cells and rat FR fibroblast cells that would promote adhesion of micromass tissue layer to the culture dish and also withstand a scrape wound laceration injury. L8 myoblast and FR fibroblast cells were grown separately to 80% confluence and trypsinized. High-density cell suspensions of FR cells and L8 cells were mixed in varying relative proportions (1:1; 1:2 and 1:3 respectively), then 10  $\mu\text{L}$  droplets of cell suspension ( $2 \times 10^5$  cells / 10  $\mu\text{L}$ ) were plated onto culture dishes to establish micromass cultures. Micromass cultures composed either of FR fibroblast or L8 myoblast cells alone were also prepared. In order to distinguish the two cell types in micromass co-culture, in some experiments the FR fibroblast and L8 myoblast cells were differentially labeled with DiI and DiO lipophilic tracking dyes and examined by fluorescence microscopy with rhodamine and FITC filters. The specificity of the DiI (red) and DiO (green) labeling is shown in **Figure 27**, which demonstrates that the rhodamine filter eliminated signals from DiO labeled L8 myoblast cells while the FITC filter blocked fluorescence from DiI labeled FR fibroblast cells.

The FR fibroblast: L8 myoblast cell mixtures tested were able to form micromass spot cultures that adhered to the culture dish, as were cultures comprised of L8 myoblast cells alone (**Figure 28 A**). However the various cultures differed in their ability to remain firmly attached to the culture dish following infliction of a single linear scrape wound (see **Figure 28 B**). When micromass of FR fibroblast cells alone were wounded, they

## FIGURE 27

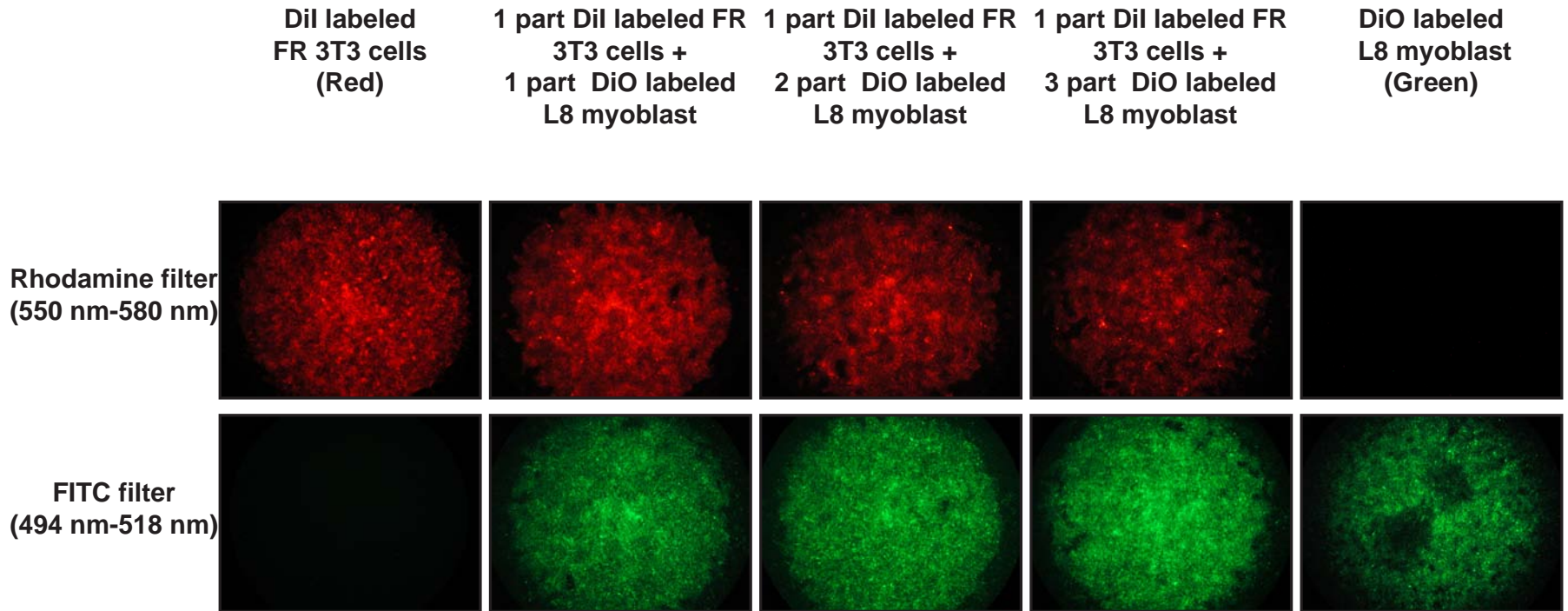


**Figure 27. Micromass and micromass co-culture of FR 3T3 fibroblast cells and L8 myoblast cells.** Images shown here of 1 day micromass spot cultures, with FR 3T3 fibroblast cells (Red) and L8 myoblast cells (Green) labeled with DiI and DiO lipophilic tracer dyes respectively. The DiI labeled FR 3T3 cells were detected using standard Rhodamine optical filter (550 nm-580 nm) while DiO labeled L8 cells were detected using Fluorescein optical filter (494 nm-518 nm) separately. Rhodamine filter was highly specific in detecting DiI labeled cells while FITC filter was highly specific in detecting DiO labeled cells.

## FIGURE 28

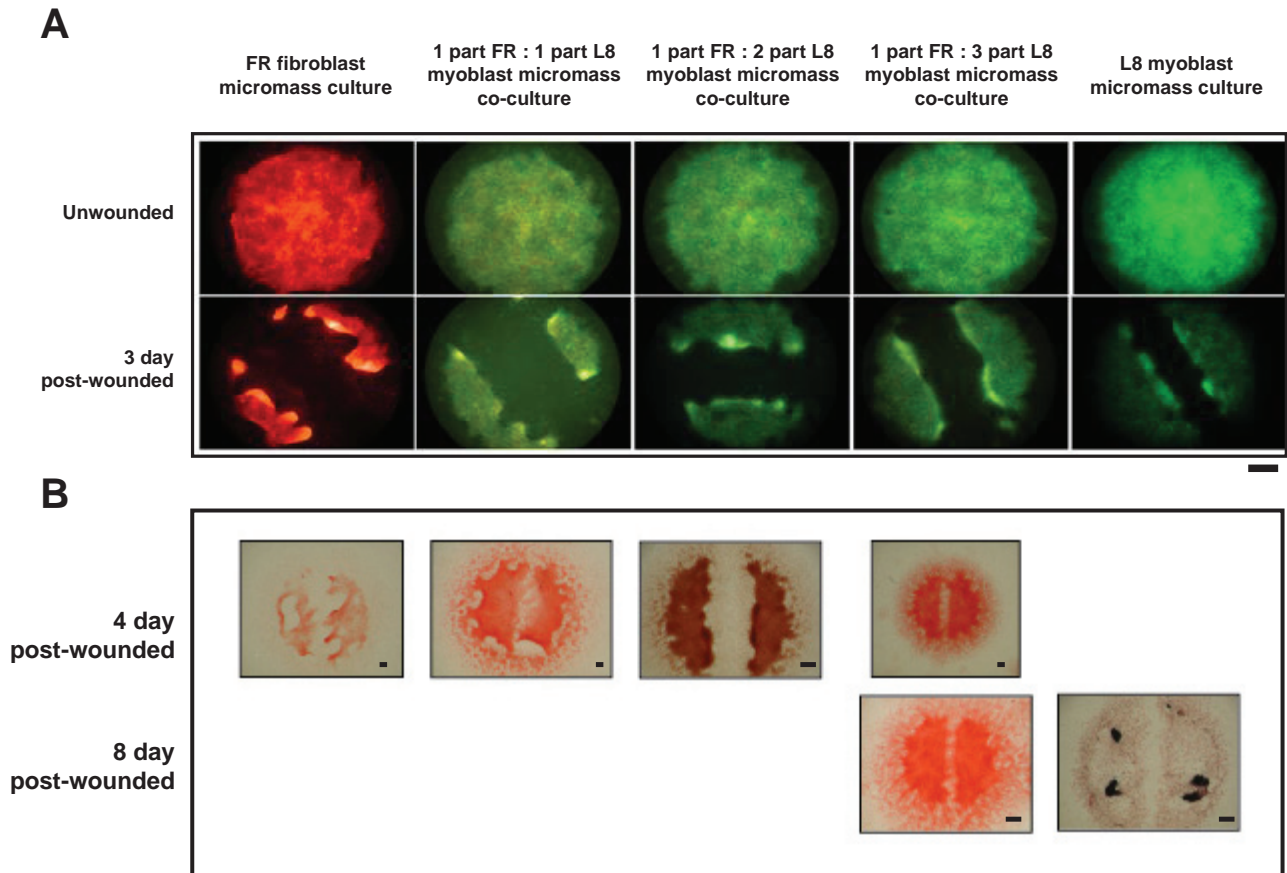


**Figure 28. Determination of the relative seeding ratio of FR 3T3 fibroblast and L8 myoblast cells that could best withstand a scrape wound manipulation.** (A) Shows fluorescence microscopy images taken from 3 day post-wounded micromass cultures and corresponding un-wounded micromass cultures. The FR fibroblast cells were labelled with DiI (red) fluorescent tracer dye, and L8 myoblasts were labelled with DiO (green). The FR and L8 cells were then combined in varying relative proportions (1:0, 1:1, 1:2, 1:3, 0:1). Micromass cultures seeded at a 1:3 ratio of FR fibroblast: L8 myoblasts best withstood a laceration or scrape wound injury without detaching from the culture dish. (B) Micromass cultures at 4 day and 8 day post wounding were stained with picosirius red to show the overall morphology after prolonged culture. The 1FR:3L8 micromass co-cultures seem to better withstand wound manipulation and can be used for prolonged analysis of the wound site as compared to 1FR:1L8, 1FR:2L8, FR and L8 micromass cultures alone. The 8 day post wounded L8 micromass culture appeared to curl up into two halves and eventually detach from culture plates, while the 8 day post wounded FR micromass culture disintegrated and detached from the culture plates completely. Scale represents 500  $\mu\text{m}$ .

began to detach from the plate within 2 days post-wounding, with each half of the culture usually curling up into a ball-like mass by 4 days post-wounding (**Figure 28 A and 28 B**). When micromass cultures of L8 myoblast cells alone were wounded, they remained attached during the initial 3 days post wounding. However, by 8-days post wounding the two halves of the L8 myoblast micromass culture would contract and then detach from the culture dish (**Figure 28 B**).

Micromass co-cultures prepared from 1:1 and 1:2 ratios of FR: L8 cells also exhibited significant contraction of the two halves of the wounded micromass tissue layer. By 3 days post-wounding, the 1:1 and 1:2 micromass co-cultures had developed jagged wound edges (**Figure 28 A and 28 B**) and after prolonged incubation beyond 4 days, they too tended to curl up and detach from the culture dishes. In contrast, micromass cultures prepared from a 1:3 ratio of FR fibroblast relative to L8 myoblast cells were able to withstand the wound manipulation without detachment of the tissue layer from the culture dish even after prolonged culture beyond 8 days post wounding (**Figure 28 A and 28 B**). There was clear demarcation of the wound edges, permitting more uniform control of the wound width, which was important for subsequent analysis of the wound healing process (**Figure 28 B**).

#### **4.4.1.1.2** Microtissue formation and the 3-D nature of the micromass co-culture of 1 part rat FR fibroblast cells and 3 part L8 myoblast cells.

Scanning electron micrography (SEM) was performed on both intact and wounded micromass co-cultures (1: 3 ratio of FR fibroblast and L8 myoblast cells) to reveal the general morphology and topographic organization of the resulting microtissue (**Figures 29 and 30**). SEM images of the surface of an intact micromass co-culture taken

at 500X magnification suggest the integration of both FR and L8 cells into a microtissue-like structure *in vitro* (**Figure 29 B**). It is difficult to distinguish individual cell boundaries because of the intermingling and close contacts of the cells comprising the microtissue, though some rounded presumably dividing cells were visible on the surface. A transverse section of the intact micromass co-culture revealed the multilayer three-dimensional organization of the microtissue *in vitro* (**Figure 29 C**).

SEM images of 1:3 micromass co-cultures at 5 min post wounding confirm the 3-D morphology of the microtissue and the absence of cell debris at the wound site (**Figure 30 A, 30 B**). At higher magnification (200X- 500X), the wound edges revealed several rounded cells suggesting changes in cell morphology following wounding (**Figure 30 B and 30 C**). SEM image from the 8 day post-wounded micromass culture that was transversely cut across the closed wound gap suggests that the wound site is comprised of compacted cells and extracellular matrix components (**Figure 30 F**).

Histochemical staining with picosirius red and alcian blue (pH 2.5) revealed the presence of extracellular matrix collagens and polysaccharides respectively, in the unwounded and wounded micromass co-cultures. Unwounded micromass co-cultures of 1 part FR fibroblast and 3 parts L8 myoblast cells revealed more intense staining for picosirius red positive collagen fibrils as compared to Alcian blue (pH 2.5) stainable polysaccharides (**Figure 31 A, 31 B**). These findings suggest that the micromass tissue structure is formed in its natural biomatrix, which comprise of collagen and extracellular matrix polysaccharides. Micromass co-cultures (1:3 FR to L8 cells) at 4 days post wounding also showed the deposition of picosirius red stainable collagen fibrils within the wound and wound edges of the injury site (**Figure 31 C, 31 E**), while less intense staining for Alcian blue (pH 2.5) positive polysaccharide at the wound region (**Figure 31**

**FIGURE 29**

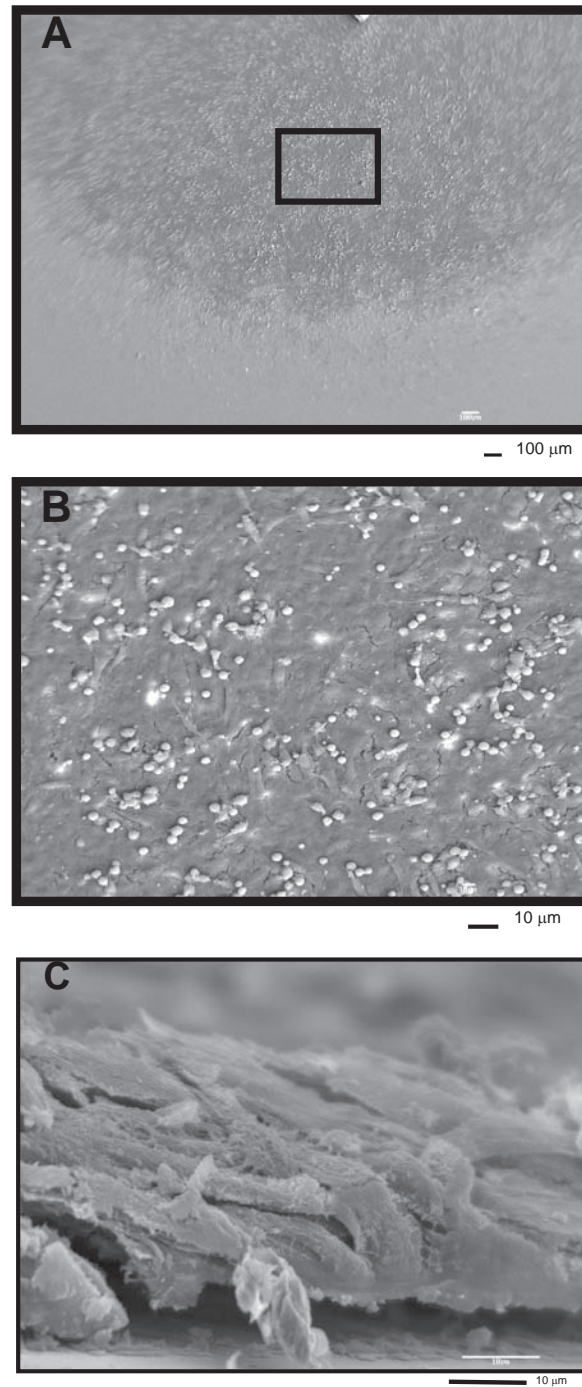


**Figure 29. Scanning electron micrographs of an intact micromass co-culture seeded at a 1:3 ratio of FR fibroblast to L8 myoblast cells.** All images were taken from 2 day unwounded micromass cultures. **(A)** An image photographed at 60X magnification shows the outline of an unwounded micromass co-culture in the culture plate. **(B)** shows a higher magnification image (500 X) of the region marked with a rectangle in Panel A. The topography of the upper surface of the micromass tissue layer is apparent. **(C)** the transverse section of the micromass as observed at 1000 X magnification confirms that the micromass co-culture system developed is indeed a multilayer three dimensional model system.

## FIGURE 30

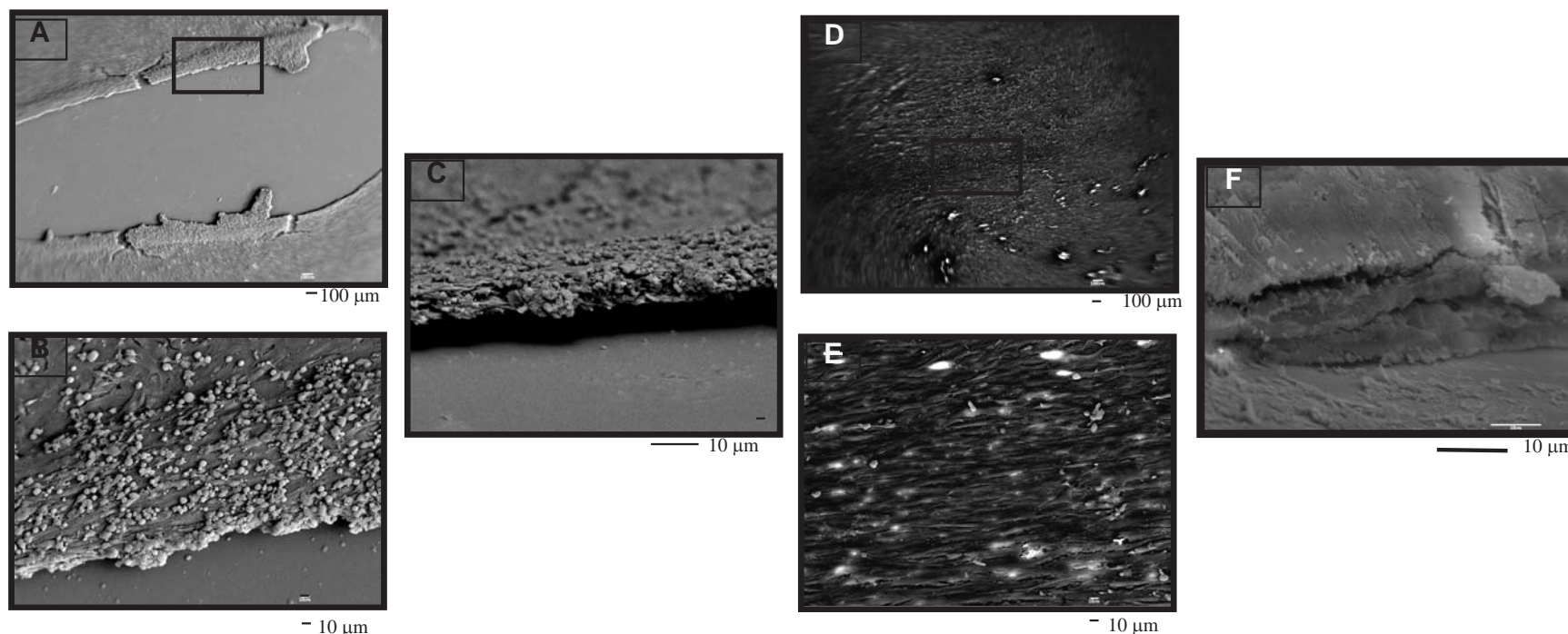


**Figure 30. Scanning electron micrographs (SEM) of micromass co-cultures ( 1FR: 3L8) at 5 minutes and 8 days after infliction of a scrape wound.** (A) shows the image of a micromass cultures at 5 min post-wounding. The two wound edges are clearly visible at 60X magnification. The region indicated by the rectangular insert is shown at higher magnification (500 X) in Panel B below. (B) As seen in the micrographs, a high number of rounded cells were visible at the wound edges following wounding. (C) A SEM of the wound edge in a 5 min post wounded culture taken at 500 X magnification and at 75 degree angle clearly showing the 3-D nature of the micromass culture. (D) A SEM image of an 8 day post wounded micromass co-culture taken at 60X magnification showing the region of wound closure in the micromass cultures. The area indicated by the rectangular insert is shown at higher magnification (500 X) in Panel E below. (F) a transverse section made perpendicular across the wounded region of the 8 day post wounded culture, taken at 1000 X magnification, and at 75 degree angle shows compaction of the cells within extracellular matrix components.

## FIGURE 31

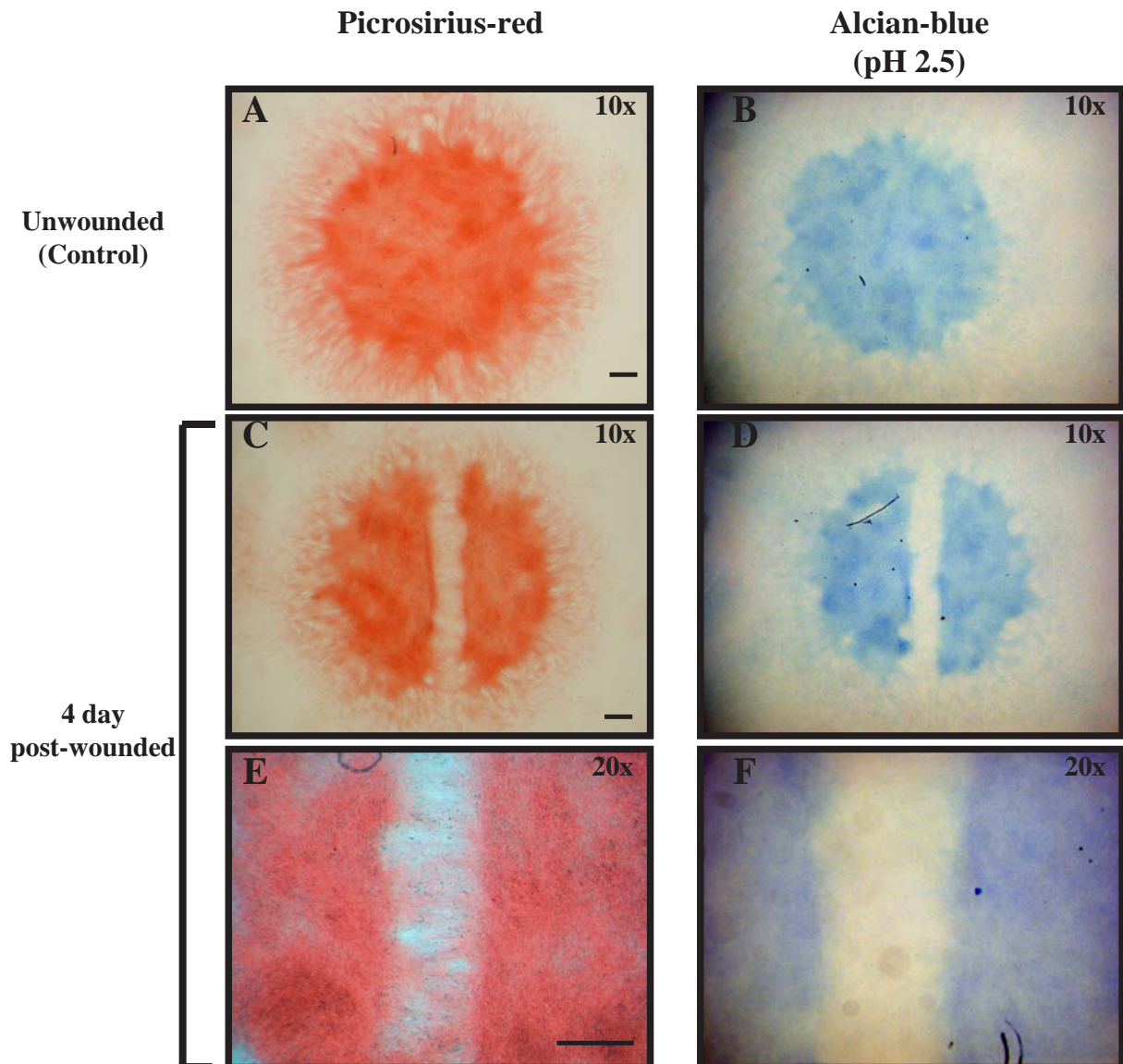


**Figure 31. Picrosirius red and Alcian blue (pH 2.5) staining of 4 day wounded and unwounded micromass co-cultures of 1 part FR 3T3 and 3 part L8 myoblast cells. (A, C, E) shows picrosirius red stainable collagen fibrils while (B, D, F) shows acidic alcian blue (pH 2.5) stainable polysaccharides in the micromass co-cultures. Higher magnification images of 4 day post-wounded cultures shows strong sirius red stainable collagen fibrils at the wound site and intense staining of alcian blue (pH 2.5) stainable extracellular matrix at the wound edges and weak staining at the wound site. Scale represents 500 microns.**

**D and 31 F).** *In situ* immunostaining was performed to examine the localization of two extracellular matrix proteins, type I collagen and fibronectin, in the (1:3) FR: L8 cell micromass co-cultures (**Figure 32**). Intense violet purple staining of type I collagen was observed throughout the wounded micromass culture and there was a progressive increase in type I collagen accumulation within the wound gap between 2 and 8 days post wounding.

Similarly, immunostaining of fibronectin protein confirmed its presence throughout the wounded micromass cultures. Progressive accumulation of fibronectin with the wound gap seemed to correlate with that of type I collagen at 2, 4, and 8 days post-wounding (**Figure 32**). However, immunostaining for fibronectin was considerably weaker than for type I collagen (see **Figure 32** legend), which suggests that fibronectin was expressed at lower levels relative to type I collagen.

Total DNA accumulation in micromass co-cultures over an 8-day period of incubation was determined by a fluorometric Hoechst assay. The rise in total cellular DNA levels serves as an indirect measure of cell proliferation in the micromass cultures. Both unwounded and wounded cultures showed a progressive increase in total DNA levels between 1 h and 4 days of culture. The rise in total DNA was most steep between 1 day and 4 days, suggesting that there is a rapid cell proliferation at these time points (**Figure 33**). Wounded micromass cultures exhibited significantly lower total DNA levels as compared to the corresponding unwounded cultures at 5 min, 1 hr, 1 day and 3 days post wounding. The lower total DNA level in the wounded cultures is likely due to the initial loss of cells from the wound infliction. However by 4-8 days post wounding, the total DNA levels had reached a plateau and were not significantly different in wounded

## FIGURE 32

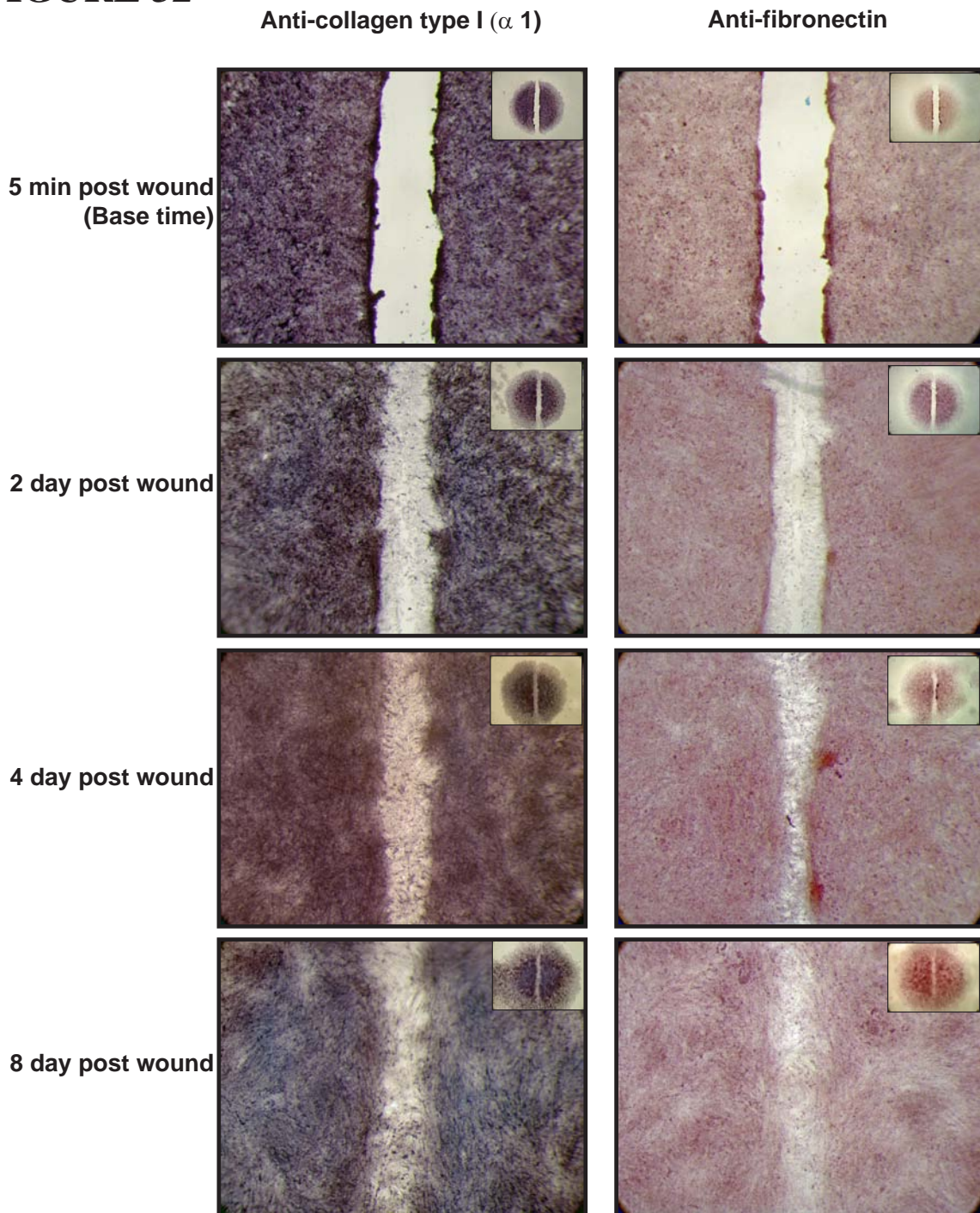


**Figure 32. Localization pattern of type I collagen and fibronectin in the wounded micromass co-culture of 1 part FR 3T3 fibroblast cells and 3 part L8 myoblast cells.** Using AP-conjugated immunostaining, the localized expression pattern of type I collagen and fibronectin was detected. type I collagen was expressed throughout the micromass cultures, collagen fibres were visible at the wound site after 2 day post wounding with gradual increase in collagen fibres visible after 4 day and 8 day post wounding. Fibronectin was expressed at lower levels than type I collagen with localized expression at the wound site visible after 2 day post wounding. The time taken for the colour reaction for type I collagen staining was 20-25 minutes as compared to 3 hours for fibronectin staining. Fibronectin localization seem to correlate with type I collagen proteins in the wounded micromass cultures

and unwounded cultures (**Figure 33**). This suggests that the micromass co-cultures had no further net increase in cell proliferation occurring beyond the 4-day time point.

In order to determine the metabolic activity of both wounded and unwounded micromass co-cultures, an MTT assay was performed on the micromass cultures at different time points (**Figure 34**). The MTT assay measures the mitochondrial activity of the cells by determining their ability of the cells to convert soluble MTT into reduced formazan precipitate, which can be quantified by absorbance readings at 560 nm. It was observed that unwounded micromass co-cultures remained metabolically active even beyond 8 days of incubation (**Figure 34**).

The reduced MTT values for wounded cultures were significantly lower at 5 min, 1 day and 2 days post wounding than the corresponding unwounded cultures. This could be attributed to the disruption of the microtissue structure immediately after wounding and the initial loss of cells from the site of scrape wound infliction. However by 3-8 day time points, the reduced MTT values for wounded cultures had recovered to a level approximately equivalent to that of unwounded cultures. Thus the wounded micromass co-cultures remained metabolically active even after 8 day post wounding.

#### **4.4.1.1.3** Optimization of the tissue culture media for high-density micromass co-culture of 1 part FR 3T3 cells and 3 part L8 myoblast cells.

To determine the best culture medium for growing 1: 3 micromass co-cultures of FR fibroblast: L8 myoblast cells, unwounded cultures were grown in either “L8 medium” consisting of Dulbecco’s modified Eagle’s medium-Nutrient mixture/ HAM F12 supplemented with 10% FBS and antibiotics or “FR medium” consisting of Minimum Essential Medium supplemented with 10% FBS, 1 mM sodium pyruvate, 0.1 mM non-

## FIGURE 33

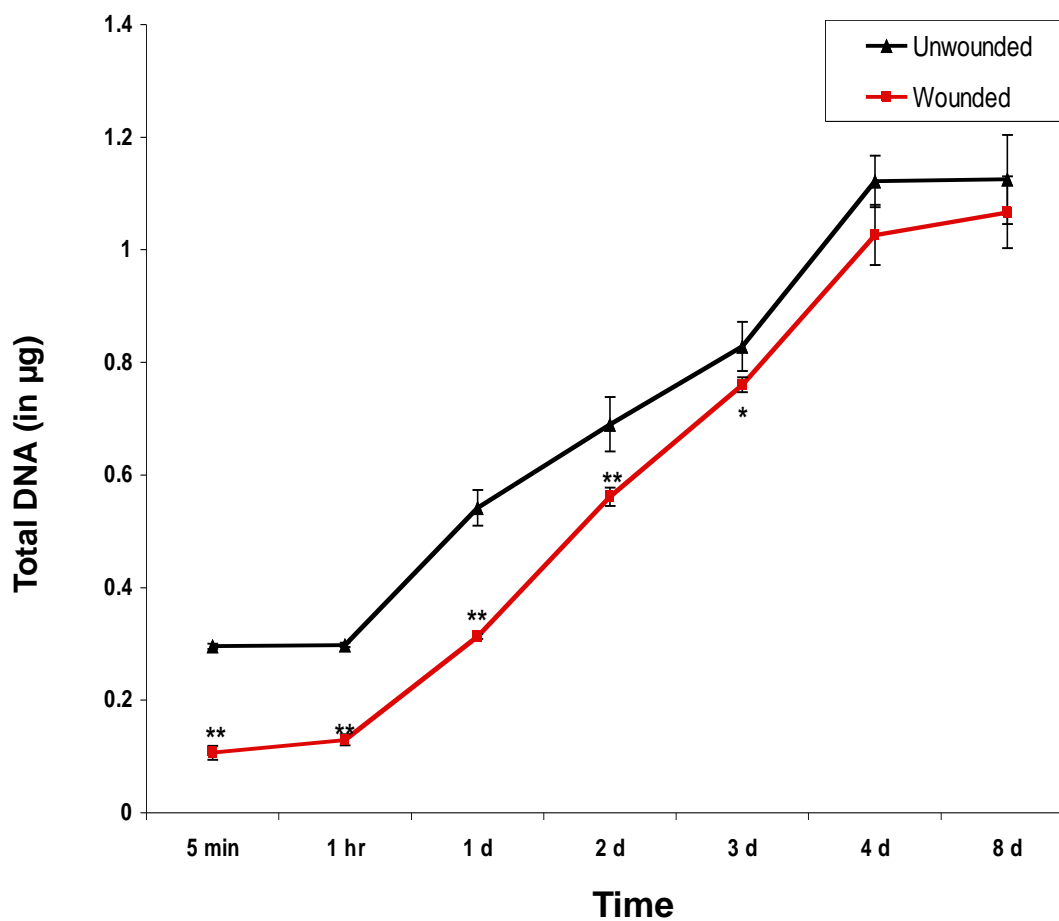


**Figure 33. Total DNA levels of wounded and corresponding unwounded micromass co-cultures of 1 part FR 3T3 fibroblast and 3 part L8 myoblast cells.** Using DNA Hoechst assay, the total DNA levels were determined for both wounded and corresponding unwounded micromass co-cultures at each time point. The data points represent Mean  $\pm$  SD (n =6). \* indicates value significantly different as compared to control at  $p < 0.05$  while \*\* indicates p value is  $< 0.01$ .

## FIGURE 34

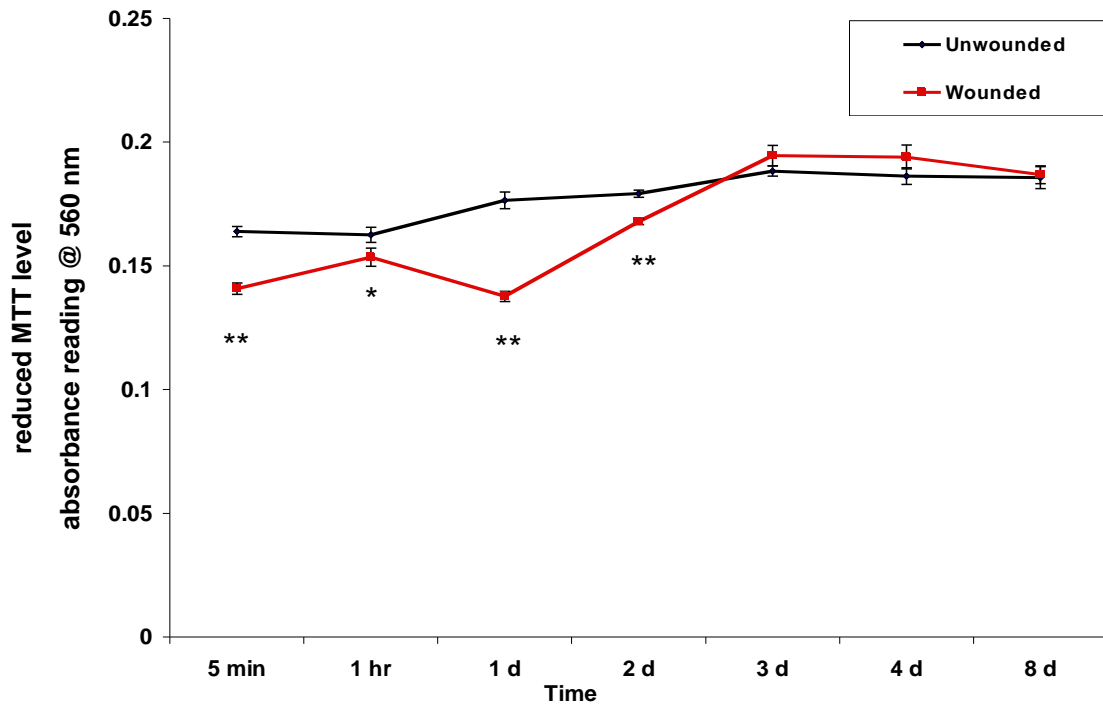


**Figure 34. Metabolic activity of wounded and corresponding unwounded micromass co-cultures of 1 part FR 3T3 fibroblast and 3 part L8 myoblast cells.** Using the MTT assay, the metabolic activity was determined by taking the absorbance reading of the reduced MTT levels in both wounded and corresponding unwounded micromass co-cultures at each time point. It was observed that both unwounded and wounded cultures were metabolically active. The data points represent Mean  $\pm$  SD (n =6). \* indicates value significantly different as compared to control at  $p < 0.05$  while \*\* indicates  $p$  value is  $< 0.01$ .

essential amino acids and antibiotics. In addition, the effects of medium supplementation with ascorbate (100 ng/mL) were tested. Ascorbic acid is known to stimulate collagen synthesis and cell proliferation in fibroblast cells, although for certain other cell types ascorbate supplementation may be toxic. The effects of medium composition on cell viability and metabolic activity of unwounded micromass co-cultures were assessed using MTT and Hoechst DNA assays, after growing all cultures for 4 days. For the sake of comparison, these experiments were also performed on micromass cultures composed of either FR 3T3 fibroblast or L8 myoblast cells alone.

Micromass cultures composed of L8 myoblast cells alone, FR 3T3 fibroblast cells alone, and micromass co-cultures of 1 part FR 3T3 and 3 parts L8 myoblast cells were propagated in either L8 or FR medium in the presence or absence of 100 ng/mL ascorbate. Micromass cultures composed of FR 3T3 fibroblasts alone were observed to have highest total cellular DNA accumulation and metabolic activity when cultured in either FR or L8 medium. Addition of 100 ng/mL ascorbate to these medium resulted in reduced cell viability and MTT values (**Figure 35 A and 35 B**,  $p < 0.01$  considered significant,  $n = 4$ ).

Similarly, L8 myoblast micromass cultures grown in L8 medium were observed to have significantly higher DNA values and metabolic activity, as compared to L8 myoblast micromass cultures grown in media supplemented with 100 ng/mL ascorbate (**Figure 35 A and 35 B**,  $p < 0.01$  considered significant,  $n = 4$ ).

Micromass co-cultures seeded at 1: 3 ratio of FR fibroblast: L8 myoblast cells exhibited significantly higher metabolic activity when grown in L8 medium alone as compared FR medium alone (**Figure 35 A and 35 B**,  $p < 0.01$  considered significant,  $n = 4$ ). Ascorbate supplementation had no positive or negative effect on either total cellular

**FIGURE 35**

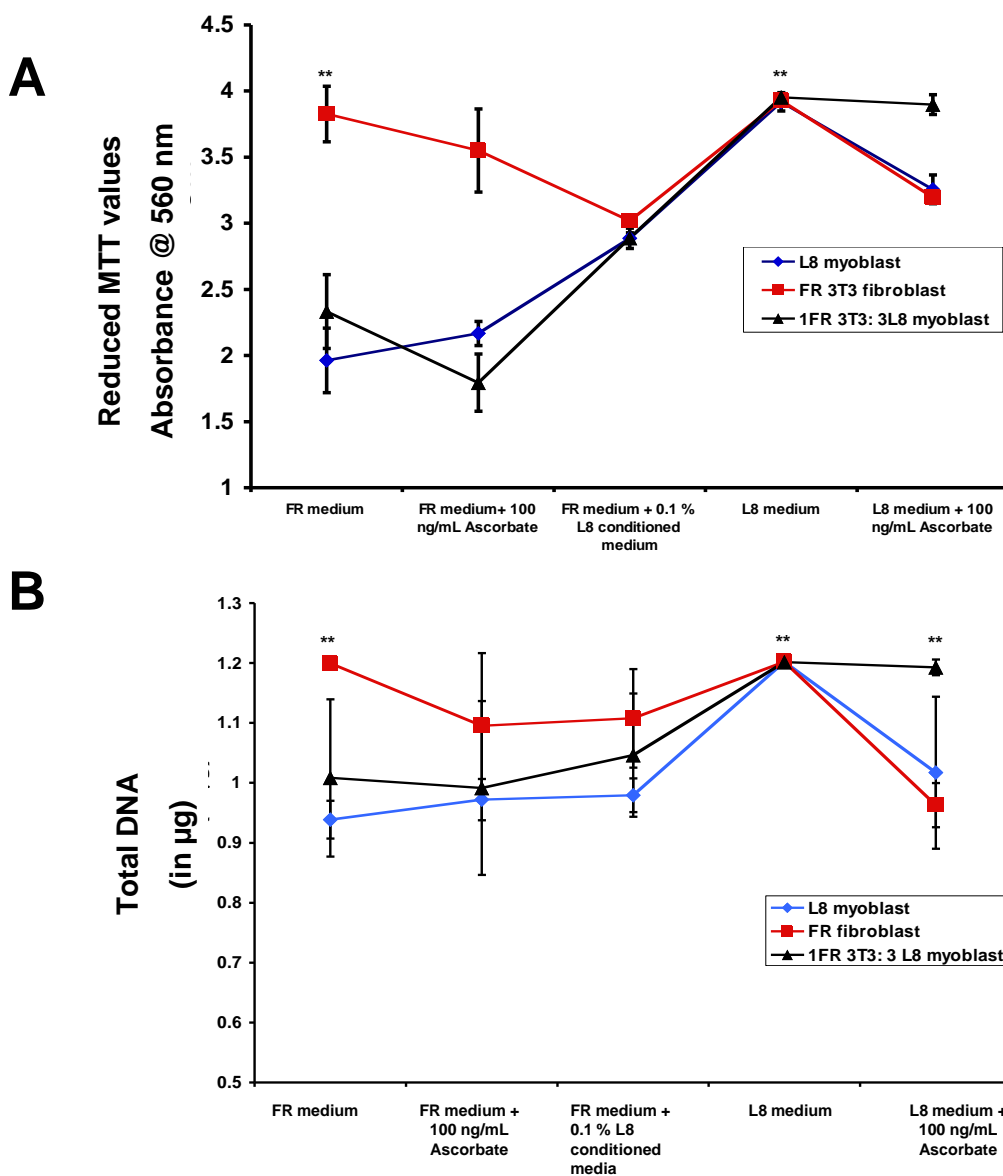


**Figure 35. Optimization of the propagation media that were used for all cell culture experiments involving micromass cultures.** (A) MTT assay was performed on the cultures to show the metabolic activity of the different micromass cultures grown in different media for a period of 4 days. The absorbance reading of reduced MTT at 550 nm represent relative metabolic activity (B) shows cell viability of the different micromass cultures grown for 4 days in different media as represented by the total DNA levels determined by DNA Hoechst assay. Based on the observations made, the reduced MTT values (metabolic activity) and total DNA levels (cell viability) suggest that L8 medium to be preferred medium for culturing 1FR 3T3 fibroblast : 3 L8 myoblast micromass cultures ( Mean  $\pm$  SD, \*\* suggest statistical significance at p value < 0.05 compared to corresponding cultures grown in FR medium along. Kruskal Wallis non-parametric One way ANOVA, n =4).

DNA accumulation or MTT values. It was also observed that ascorbate supplementation did not alter levels of collagen accumulation in these cultures as determined by picrosirius red staining (data not shown).

To test soluble factors released by L8 myoblast cells into the medium might promote better cell proliferation of fibroblast cells within 1:3 micromass co-cultures, the cultures were grown in FR medium supplemented with 0.1 % L8 cell conditioned medium. The L8 cell conditioned medium was prepared by growing L8 myoblast cells in L8 medium for a period of 2 days to condition the medium, after which the conditioned medium was removed and sterile filtered.

Micromass co-cultures that were grown in FR medium supplemented with 0.1% L8 cell conditioned medium showed no improvement in DNA accumulation or MTT values as compared to cultures grown in standard FR medium or L8 medium (**Figure 35 A, 35 B**). When micromass cultures of FR fibroblast cells alone were grown in FR medium supplemented with 0.1% L8 cell conditioned medium, no change in DNA accumulation or MTT values was observed as compared to cultures grown in standard FR medium or L8 medium (**Figure 35 A, 35 B**). The wounded micromass co-cultures grown in either L8 or FR media, also resulted in similar culture growth profile as was observed in unwounded micromass co-culture. Overall, these findings suggested that L8 medium alone provided optimum growth conditions for the 1:3 FR fibroblast and L8 myoblast micromass co-cultures. Hence, L8 medium was used for propagating micromass co-cultures in all the subsequent *in vitro* “micromass” wound-healing experiments.

#### 4.4.1.1.4 Muscle specific protein expression pattern in unwounded and wounded 1:3 fibroblast and L8 myoblast micromass co-cultures.

Western blot analysis was performed to determine how micromass co-culture conditions affected the expression patterns of several myogenic and non-myogenic proteins by the FR fibroblast and L8 myoblast cells. We examined the expression of the myogenic transcription factors, MyoD and myogenin, which are early stage myoblast markers, as well as expression of MyHC and tropomyosin, which are markers of differentiated skeletal muscle fibers. We also analyzed expression of  $\alpha$ -smooth muscle actin ( $\alpha$ -sma), a biomarker expressed by fibroblast cells and the extracellular matrix protein, osteopontin (OPN). Both  $\alpha$ -sma and OPN play critical roles in tissue remodeling, and initiating myogenic differentiation during later stages of skeletal muscle repair (Uaesoontrachoon *et al.*, 2008).

Western blot analysis was performed on lysates prepared from 3 day micromass cultures composed of either L8 myoblast cells or FR fibroblast cells alone, as well as lysates from 1:3 micromass co-cultures of FR fibroblasts and L8 myoblasts. Micromass cultures composed of FR fibroblast cells alone expressed only  $\alpha$ -sma (**Figure 36**). Micromass cultures composed of L8 myoblast cells alone expressed low levels of the early myoblast marker, MyoD, along with high levels of MyHC, and faintly detectable levels of tropomyosin (**Figure 36**). These cultures also expressed OPN but not  $\alpha$ -sma. This expression pattern indicates that L8 myoblast cells cultured alone under micromass conditions express markers of differentiated skeletal muscle fibres.

In contrast, when the L8 myoblast cells were co-cultured together with FR fibroblast cells under micromass conditions only MyoD and  $\alpha$ -sma expression were detectable (**Figure 36**). Accordingly, the presence of fibroblast cells suppresses the

## FIGURE 36

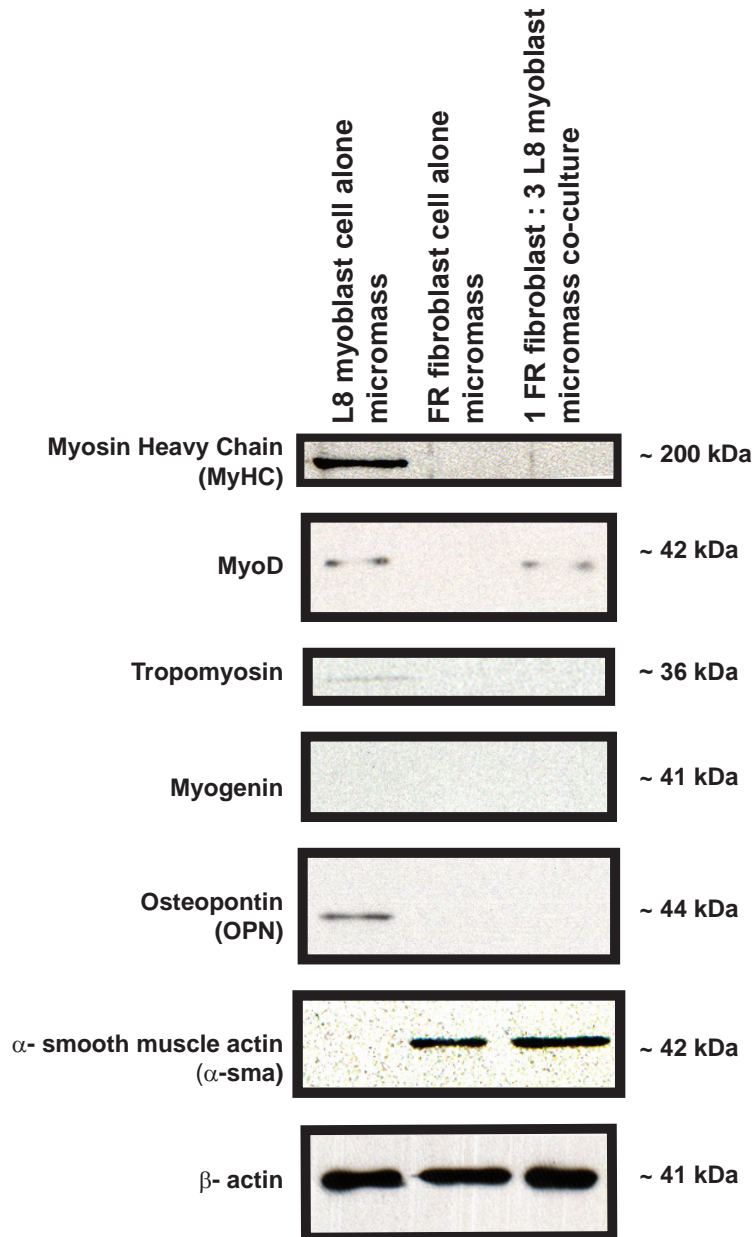


**Figure 36. Expression pattern of muscle specific proteins and fibroblast specific protein ( $\alpha$ -smooth muscle actin) in 1:3 ratio of FR fibroblast and L8 myoblast cells.** All the micromass cultures were grown for a period of 3 days before homogenizing the cultures and the equal protein concentration were used for western blotting. It was observed that L8 myoblast micromass culture homogenates expressed all muscle specific proteins except myogenin while FR fibroblast micromass culture expressed only  $\alpha$ -sma. The 1:3 ratio of fibroblast and L8 myoblast cell micromass co-culture showed bands for MyoD and  $\alpha$ -sma proteins.

## FIGURE 37

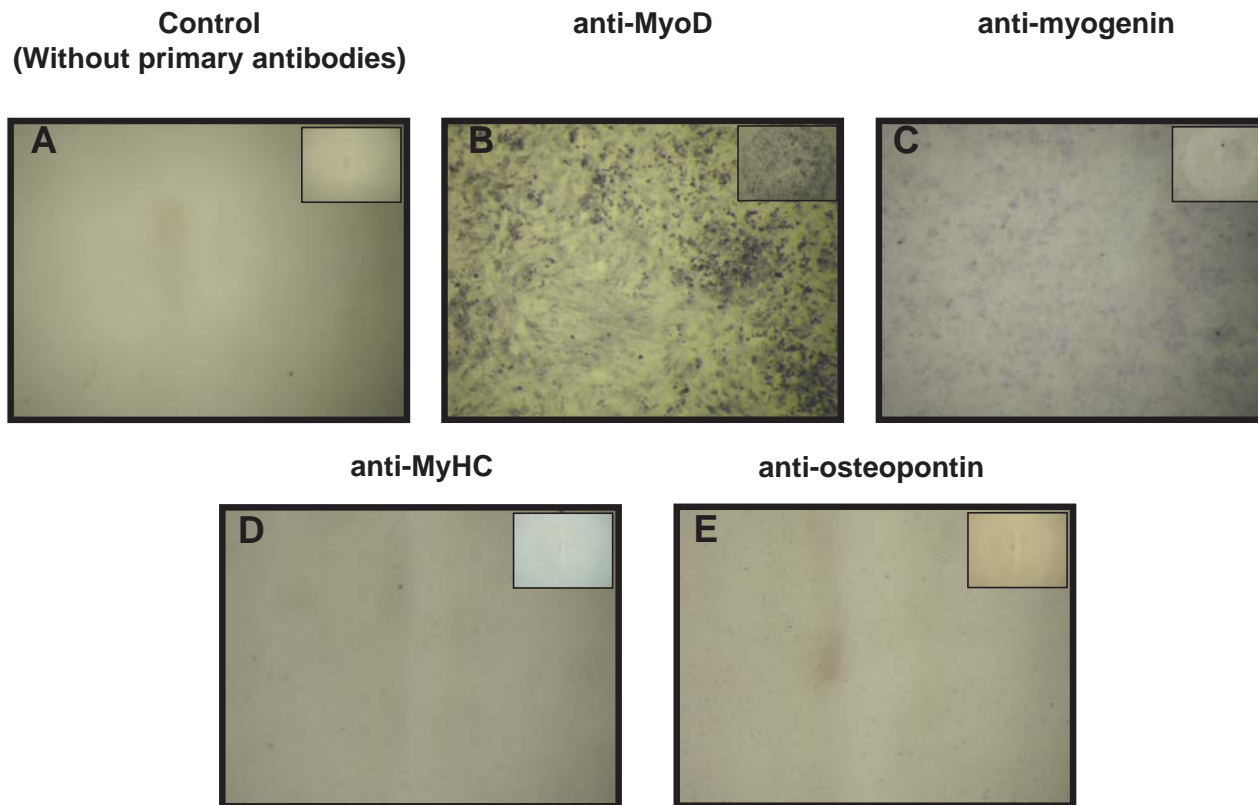


**Figure 37. Determination of the effect of wounding on the expression of muscle specific proteins and osteopontin in the wounded 1:3 ratio of fibroblast and myoblast micromass co-culture.** Using AP conjugated immunostaining, expression of (B) MyoD, (C) myogenin, (D) MyHC and (E) osteopontin was determined for 8 day post wounded micromass co-cultures. It was observed that MyoD protein was expressed within the micromass cultures and it was localized throughout the micromass while myogenin protein were expressed at very low levels as compared to MyoD proteins. No expression of Osteopontin and MyHC was observed in the wounded micromass cultures. The time taken for the colour reaction for MyoD staining was 1 h as compared to 24 h for the myogenin staining.

expression of MyHC and tropomyosin proteins by L8 myoblast cells in micromass culture, and it also suppressed OPN expression. Collectively, these results suggest that L8 myoblast cell interaction with fibroblasts in micromass co-culture encourage the myoblast to retain an early stage myogenic phenotype and their differentiation into skeletal muscle fibres is suppressed.

In order to examine whether the expression of myogenic proteins might change following wounding of the micromass co-culture, I performed *in situ* immunostaining on FR fibroblast: L8 myoblast micromass co-cultures at 8 days post-wounding. MyoD expression was detectable by immunostaining (**Figure 37**), which was consistent with western blots of 8 day post wounded cultures (data not shown). Immunostaining also showed very low levels of myogenin protein in FR: L8 micromass co-cultures (**Figure 37**), although myogenin was not detected by western blotting (data not shown). Myosin heavy chain (MyHC) and osteopontin were absent in the wounded culture (**Figure 37**), suggesting that wounding did not induce differentiation of myoblast cells into myofibres *in vitro*.

#### **4.4.1.1.5** Specific gene expression profiling in both unwounded and wounded micromass co-cultures of 1 part FR 3T3 fibroblast cells and 3 part L8 myoblast cells.

Semi-quantitative RT-PCR was used to examine the gene expression profiles of Collagen type 1( $\alpha$ 2), Collagen type 3 ( $\alpha$ 1), Collagen type 4 ( $\alpha$ 1), TGF- $\beta$ 1, TGF- $\beta$ 3, hyaluronan receptors RHAMM and CD 44, hyaluronan synthases 1 and 3 (HAS 1, HAS 3), hsp-47 and Glyceraldehyde-3-phosphate dehydrogenase (GAPDH), as these genes have been implicated in wound repair and scarring processes.

Preliminary experiments established the appropriate number of amplification cycles for each specific gene transcript to ensure that reactions were terminated during the exponential phase of PCR (see **Section 3.2.9.2** and **Figure 38** legend). Based on amplicon bands, GAPDH, HAS 1, hsp-47, CD 44, TGF- $\beta$ 3, HAS 3 transcripts required lesser number of cycles and hence their transcript levels were abundant in both wounded and unwounded micromass co-cultures as compared to TGF- $\beta$ 1, Collagen type 3 ( $\alpha$ 1), Collagen type 4 ( $\alpha$ 1), RHAMM and Collagen type 1 ( $\alpha$ 2), transcripts (**Figure 38**). Using NIH Image J software, the relative expression levels of Collagen type 1 ( $\alpha$ 2), Collagen type 3 ( $\alpha$ 1), Collagen type 4 ( $\alpha$ 1), TGF- $\beta$ 1, TGF- $\beta$ 3, RHAMM, CD 44, HAS 1, HAS 3, hsp-47 at all time points for the unwounded micromass co-cultures was determined by densitometric measurement of the band intensities for these gene of interests and normalized against the corresponding GAPDH band intensity at that same time point (**Figure 39 A**). It was observed that the overall relative expression of TGF- $\beta$ 3, HAS 1, hsp-47 and collagen type 1( $\alpha$  2) gene transcripts in unwounded cultures were higher as compared to TGF- $\beta$ 1, RHAMM, CD 44, collagen type 4 ( $\alpha$ 1) and collagen type 3 ( $\alpha$ 1). The expression of TGF- $\beta$ 3, TGF- $\beta$ 1, CD 44, HAS 3, hsp-47, collagen type 4 ( $\alpha$ 1), collagen type 3 ( $\alpha$ 1) and collagen type 1 ( $\alpha$ 2) were highest in unwounded cultures at 4 day time points as compared to other time points (1d, 2 d and 8d) (**Figure 39 A**).

To examine changes in the gene transcript levels following wounding, I compared the relative expression levels of collagen type 1 ( $\alpha$  2), collagen type 3 ( $\alpha$ 1), collagen type 4 ( $\alpha$ 1), TGF- $\beta$ 1, TGF- $\beta$ 3, RHAMM, CD 44, HAS 1, HAS 3, hsp-47 in wounded cultures (**Figure 39 B**) with corresponding unwounded micromass cultures (**Figure 39 A**). It was observed that the expression of TGF- $\beta$ 1, TGF- $\beta$ 3, HAS 1 and hsp-47 were significantly

## FIGURE 38

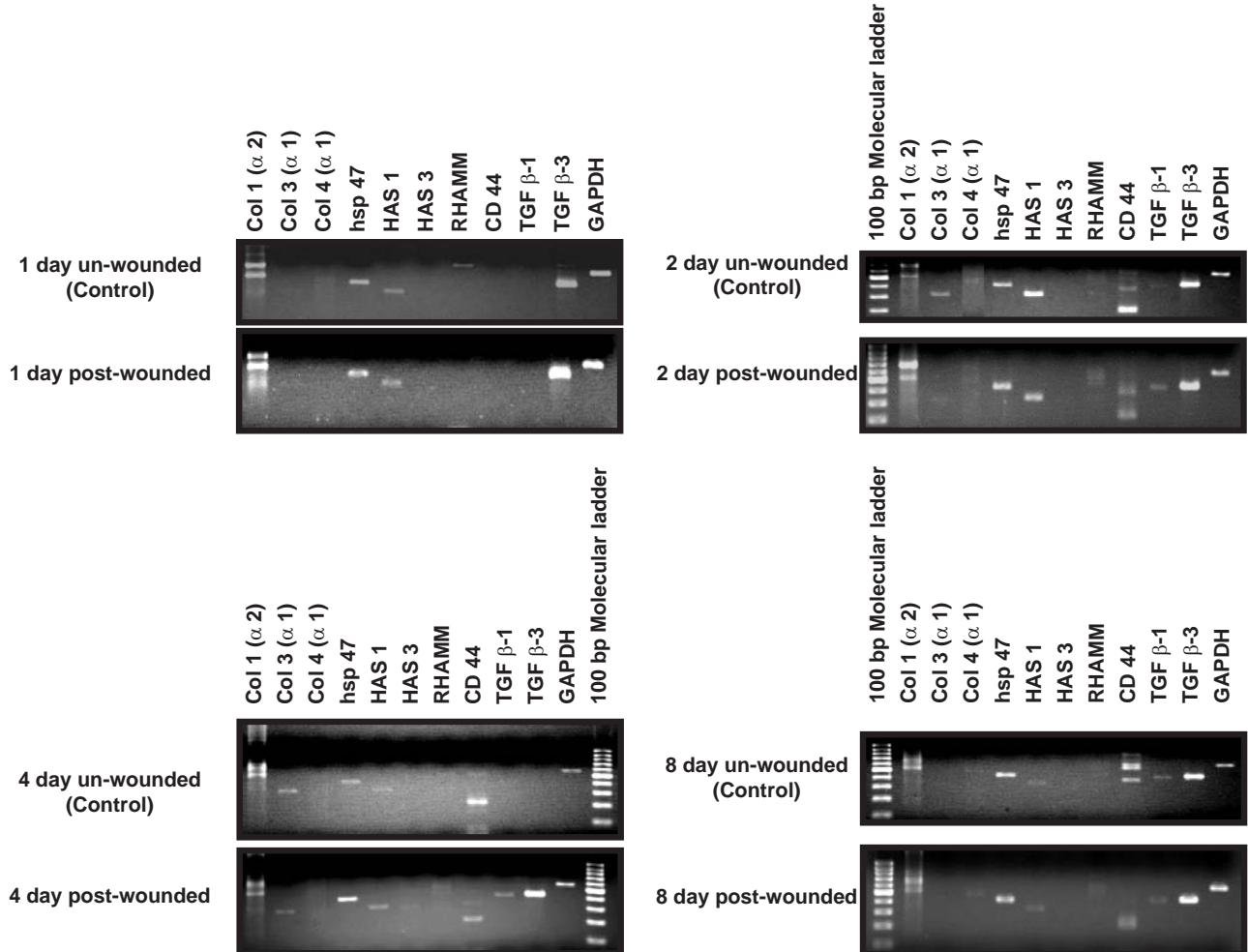


**Figure 38.** RT-PCR DNA gels showing relative band intensities for Collagen type 1( $\alpha 2$ ), Collagen type 3( $\alpha 1$ ) and Collagen type 4( $\alpha 1$ ) Hyaluronan synthase 1, Hyaluronan synthase 2, Hyaluronan synthase 3, Receptor for hyaluronan-mediated motility (RHAMM), CD 44, Transforming growth factor  $\beta$ -1, Transforming growth factor  $\beta$ -3, heat shock protein 47 (hsp-47) and Glyceraldehyde –3-phosphate dehydrogenase (GAPDH). cDNA obtained from 1 day, 2 day, 4 day and 8 day post-wounded cultures and their corresponding unwounded cultures were used to run PCR. The Primer sequences used for the specific genes of interests and the number of cycles chosen to be the exponential phase of PCR amplification for each of the genes of interest were determined to be 23 cycles for GAPDH, 32 cycles for HAS-1, hsp47, CD44; 35 cycles for TGF- $\beta$ 3; 40 cycles for HAS-3, 45 cycles for TGF- $\beta$  1 and Collagen type 3( $\alpha 1$ ); 50 cycles for RHAMM and Collagen type 4( $\alpha 1$ );.55 cycles for Collagen type 1( $\alpha 2$ ). The PCR products obtained were seperated on 1.5% agarose gel and stained with ethidium bromide and photographed under UV illumination.

## FIGURE 39

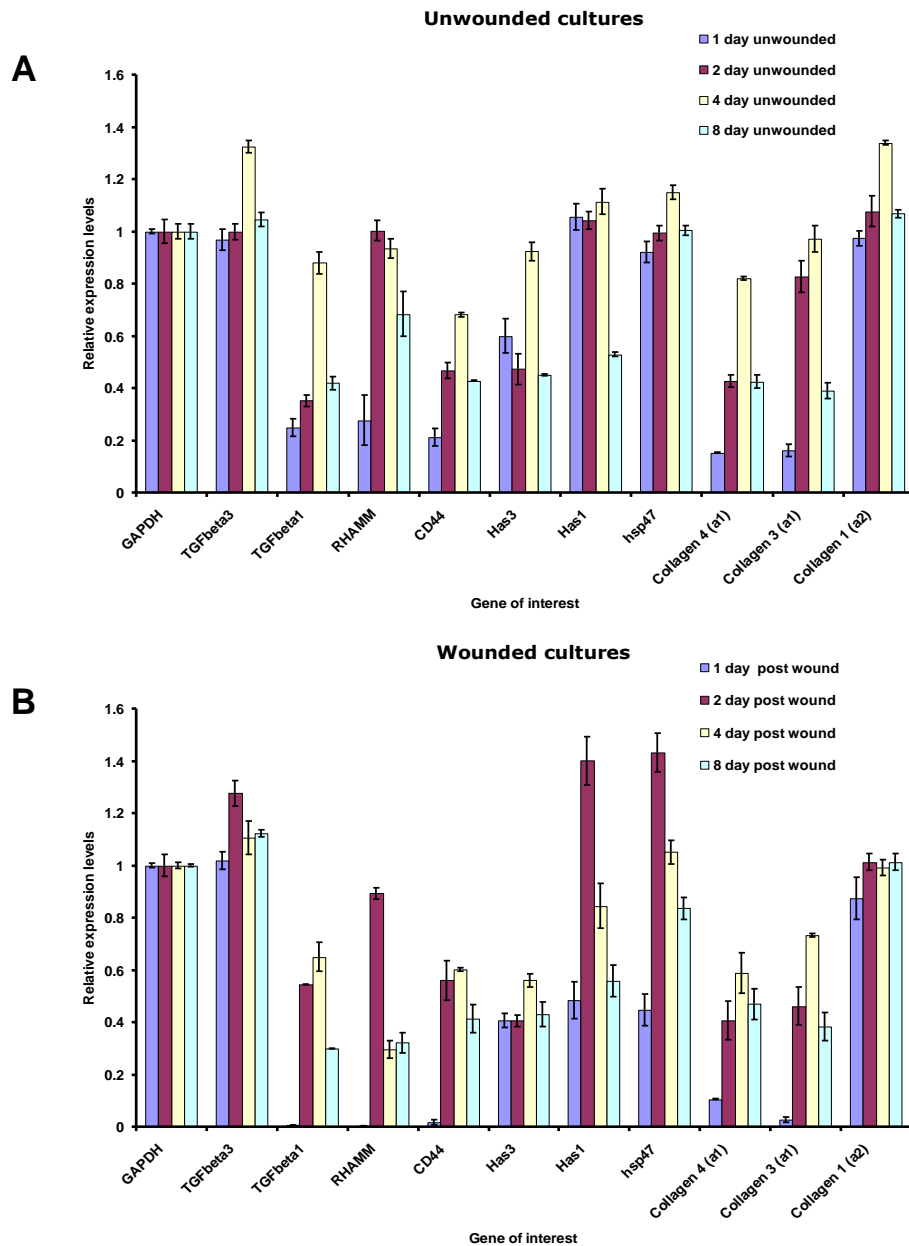


**Figure 39. Gene expression profile of various genes implicated in tissue repair and regeneration.** The bar graph represents densitometric measurements of the relative band intensities obtained from the DNA gel shown in previous figure using NIH Image J software. The band intensities for the genes of interest were normalized with Glyceraldehyde-3-phosphate dehydrogenase (GAPDH). **(A)** Shows the relative expression levels of the genes of interest in the intact micromass co-cultures of 1 part FR 3T3 and 3 part L8 myoblast cells. **(B)** shows the relative expression levels of the genes of interest in the wounded micromass co-cultures. All values are expressed in Mean  $\pm$  SD and n = 4.

higher in 2 day post-wounded cultures as compared to corresponding unwounded cultures (**Figure 39 A and 39 B**,  $p < 0.001$ ,  $n = 4$ ). In 2 day post wounded cultures, the expression levels of collagen type 3 ( $\alpha 1$ ) were lower as compared to corresponding unwounded cultures (**Figure 39 A and 39 B**,  $p < 0.001$ ,  $n = 4$ ). There was no change in the relative expression of RHAMM, CD 44, HAS 3, collagen type 4 ( $\alpha 1$ ) and collagen type 1 ( $\alpha 2$ ) at the 2-day time point. In contrast, the relative expression levels of RHAMM, CD 44, HAS 3, HAS 1 levels were significantly lower in 4 day and 8 day post wounded cultures (**Figure 39 B**,  $p < 0.001$ ,  $n = 4$ ) as compared to corresponding unwounded cultures (**Figure 39 B**,  $p < 0.0001$ ,  $n = 4$ ). TGF- $\beta 3$  showed no increase or decrease in gene transcript levels at 4 day and 8 day time-points for wounded versus unwounded cultures.

Based on the overall gene expression profiles of RHAMM, CD 44, HAS 1, HAS 3, hsp-47, collagen type 1 ( $\alpha 2$ ), collagen type 3 ( $\alpha 1$ ), and collagen type 4 ( $\alpha 1$ ) it appears that a majority of changes in gene transcript levels occurred between the 2 d and 4 d time points, when a large percentage of the wound gap in the wounded micromass co-culture is repopulated by cells and the integrity of the micromass co-culture is partially restored (see **Figure 40**). Hence, these time points were chosen for subsequent RT-PCR analyses, which examined the effects of OTC, and quercetin treatments on the expression of these gene transcripts during micromass tissue repair.

#### **4.4.1.1.6** Determination of the rate of wound closure in the micromass co-culture model and the effect of cell proliferation on *in vitro* wound repair.

Experiments were performed to determine the rate of wound closure in 1:3 micromass co-cultures of FR fibroblasts and L8 myoblasts. Following a scrape wound injury, observations were made at the wound region using phase contrast microscopy in

real time. When the micromass co-cultures were grown over a period of 8 days following wounding, there was a progressive increase in the number of cells occupying the wound region (**Figure 40**). The cells gradually started infiltrating the wound region from 1 day post-wounding.

By 8 days after wounding, cells covered almost the entire region of the wound although a few cell-free areas were occasionally visible at the wound site (**Figure 40**). The progression of wound closure in the micromass co-culture was quantified as described in Section 3.2.11, by measuring the reduction in the surface area of the wound that was unoccupied by cells over time (**Figure 41**).

I wished to determine whether wound closure in the micromass co-culture was primarily dependent on cell proliferation or cell migration. To inhibit cell proliferation, micromass co-cultures were pretreated with 10  $\mu\text{g}/\text{mL}$  mitomycin for 1 hour, then a scrape wound was inflicted and mitomycin treatment was continued for an additional 72 hours after wounding. Phase contrast images of the same culture were captured over an 8-day period. When cell proliferation was inhibited by mitomycin treatment, there was a striking reduction in the number of cells that entered the wound site as compared to parallel untreated control cultures (**Figure 40**). Quantitative planimetry analysis confirmed that there was a significant inhibition of wound closure in mitomycin treated cultures relative to controls (**Figure 41**,  $p < 0.01$ ,  $n = 6$ ). Indeed, even after 9 days of culture there was only a slight decrease in total surface area of the wound region. Our findings suggest that a wound closure assay based on planimetric image analysis could be reliably used to quantify the effects of wound modulating molecules, in this newly

**FIGURE 40**

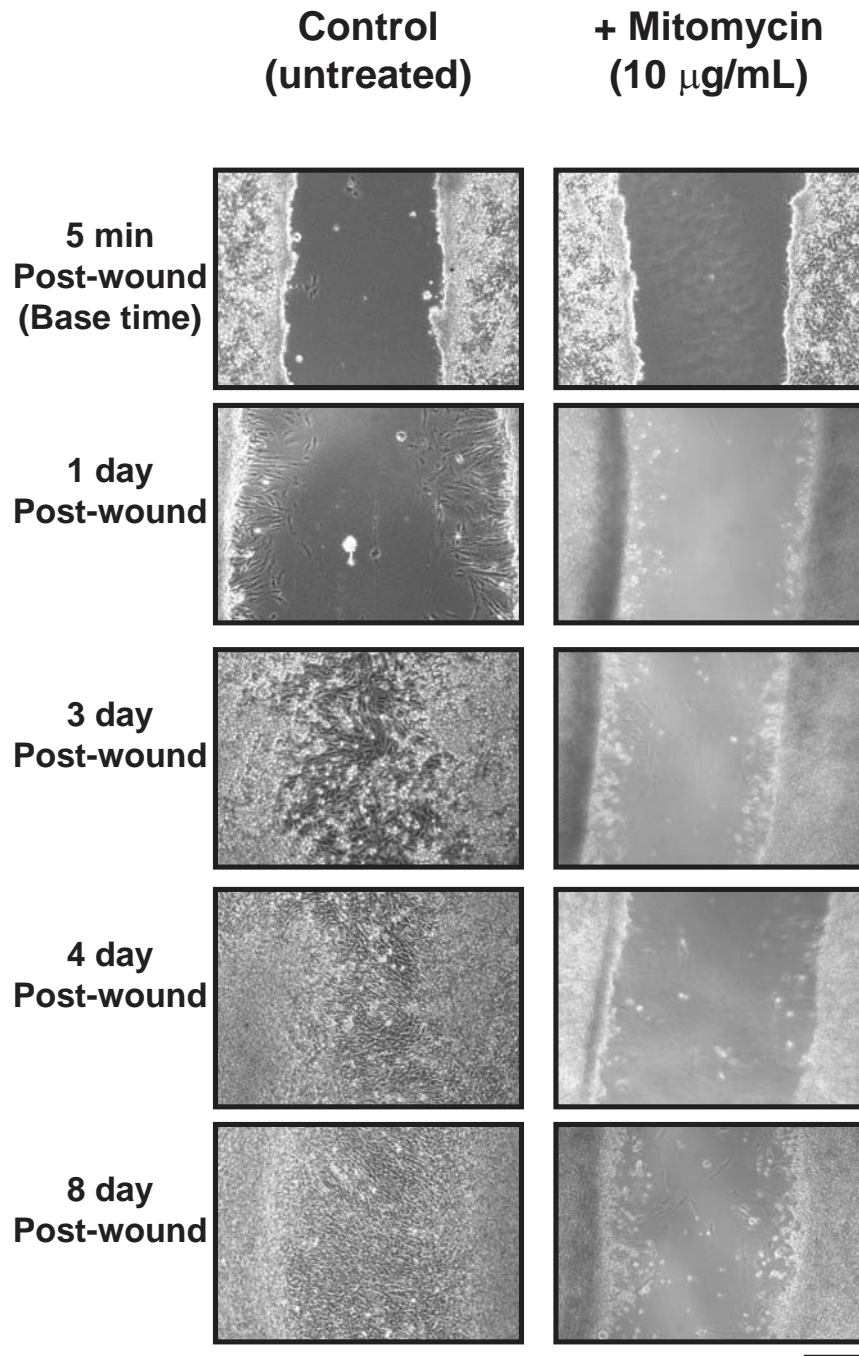


**Figure 40. Wound closure as function of time in micromass co-culture of 1 part FR fibroblast cells and 3 part L8 myoblast cells.** Micromass cultures were subjected to scrape wound injury and then cultured in presence and absence of 10  $\mu\text{g}/\text{mL}$  mitomycin, an inhibitor of cell proliferation. The five photographs in each vertical rows are phase contrast images of the same culture at successive time point after wounding. Using the phase contrast light microscopy, the time taken for wound closure was determined. As seen from the phase contrast images, the wound site seem to be covered by cells within 4 days after wounding. When the wounded micromass cultures were treated with 10  $\mu\text{g}/\text{mL}$  mitomycin, the wound closure was considerably delayed and the wound was not covered by the cell even after 8 day post wounding. Scale represents 500 microns

# FIGURE 41

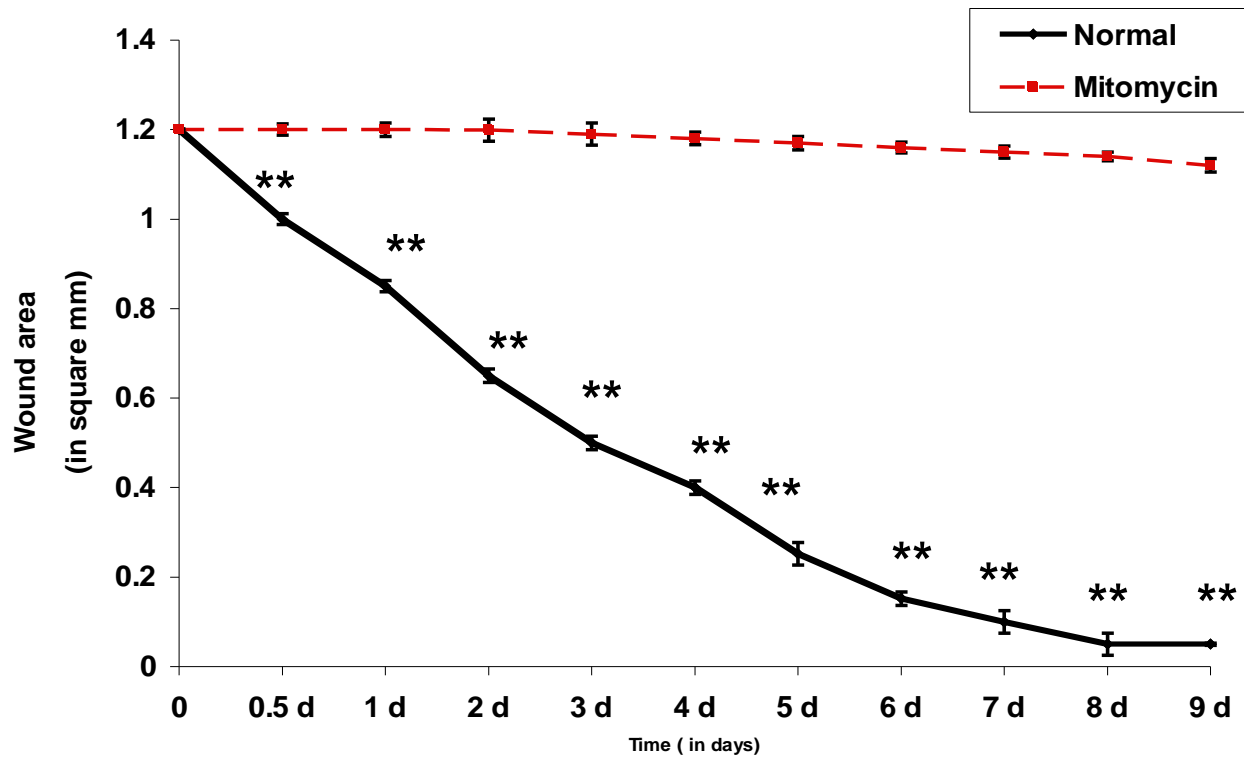


**Figure 41. Effect of cell proliferation on the wound closure in the wounded micromass co-culture of 1 part FR 3T3 fibroblast and 3 part L8 myoblast cells.** Using phase contrast microscopy, the total wound area unoccupied by cells as function of time was determined using planimetric image analysis method. The rate of *in vitro* wound closure was compared in the presence and absence of mitomycin, an inhibitor of cell proliferation and thus delay wound closure. It was observed that cell proliferation is essential for proper wound closure and integrity of the wounded micromass cultures. A total of 6 replicate cultures were tested and all cultures were grown continuously and the wound closure in each culture was analyzed on real time using phase contrast microscopy ( Mean  $\pm$  SD, \*\* indicates significant difference at p value  $<$  0.01 using Kruskal Wallis non parametric One way ANOVA).

developed *in vitro* wound repair model. Hence, in subsequent experiments this assay was employed to determine the effects of drugs on wound closure as function of time.

#### **4.4.1.1.7** Studies on the migratory pattern of rat skeletal L8 myoblast cells and rat fibroblast FR cells in wounded micromass co-cultures.

To examine the migratory patterns of the myoblast cells and fibroblast cells in wounded micromass co-cultures, in some experiments the FR cells and L8 cells were differentially labeled with fluorescent lipophilic tracer dyes DiI and DiO just prior to plating the micromass layer. The distribution of tracer dye labeled fibroblast and myoblast cells was examined in 3 day post wounded cultures and parallel unwounded cultures by fluorescence microscopy at 5X magnification. Both fibroblast and myoblast cells appeared to be uniformly distributed through the tissue layer in unwounded micromass cultures (**Figure 42 A, 42 B, 42 E and 42 F**). Wounded cultures showed the greatest concentrations of labeled fibroblast cells at the wound edges (**Figure 42 D and 42 H**), whereas labeled myoblast cells appeared to be more evenly distributed throughout the micromass tissue layer (**Figure 42 C and 42 G**). These findings suggest the possibility of preferential migration of fibroblast cells to the micromass wound edges.

To further confirm this finding, image analysis was performed to measure the relative fluorescence intensities of DiI labeled FR fibroblast cells (red) and DiO labeled L8 myoblast cells (green) present at the wound site (including the wound edges and a part of the wound gap) as compared to the periphery of the micromass co-culture (as shown in **Figure 8**). The DiI and DiO positive cells were identified using the deconvolution function of the NIH Image J software and quantitative image analysis was performed at 1 day, 3 days and 8 days post-wounding. At the wound site, there was a progressive time dependent increase in the fluorescence intensity of DiI labeled FR fibroblast cells

between 1 and 8 days after wounding, while DiO labeled L8 myoblast cells showed a more modest increase in fluorescence intensity (**Figure 43 A**). Accordingly, the fluorescence intensity of DiI labeled FR fibroblast cells was significantly higher than the fluorescence intensity of DiO labeled L8 myoblast cells at the wound site at 3 and 8 days after wounding (**Figure 43 A**,  $p < 0.01$ ,  $n = 4$ ). These observations are consistent with a preferential migration of FR fibroblast cells to the wound edges and possibly to the wound gap.

To examine the presence of labeled cells within the wound gap itself, both 3 day and 4 day post-wounded micromass cultures were examined at higher magnification (20X), under phase contrast and fluorescence illumination. The fluorescence images were captured using a CCD camera with extended shutter exposure times (**Figure 44**).

Although phase contrast images confirmed that the wound gap was filled with cells by 3 – 4 days post wounding, there were surprisingly few DiO labeled (green) L8 myoblast cells and DiI labeled (red) fibroblast cells visible within the wound gap (**Figure 44**). The low number of DiI and DiO positive cells detectable within the wound gap is likely due to the ongoing proliferation of cells that migrate into this region, which would progressively dilute the concentration of the tracer dye within individual daughter cells. Despite the limitations of conventional fluorescence microscopy in determining fluorescent labeled cells within a 3-D micromass tissue layer, this study suggests a novel approach for using lipophilic dyes and fluorescence microscopy to track the distribution pattern of two different cell types within a 3-D *in vitro* co-culture system.

## FIGURE 42

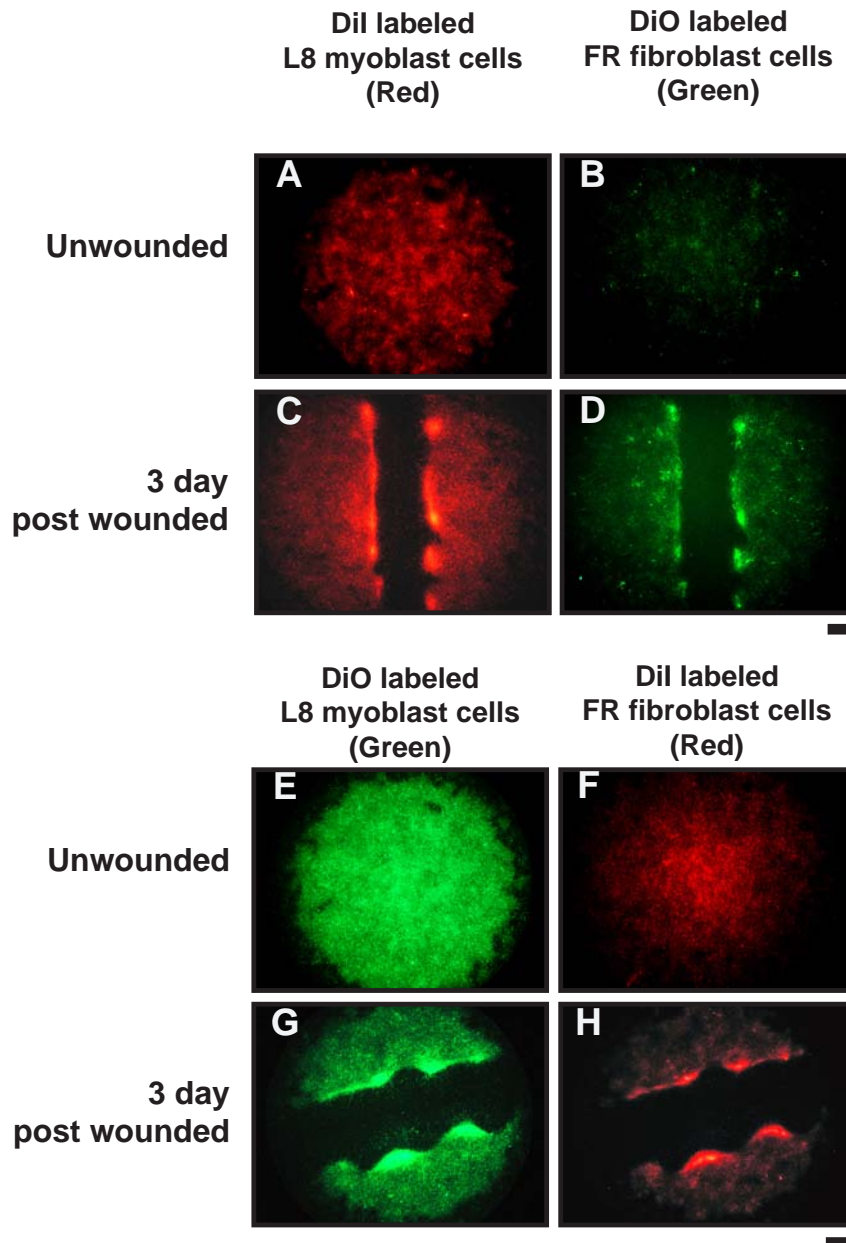


**Figure 42. Distribution and localization of FR fibroblast and L8 myoblast cells in the 3 day post-wounded 1: 3 ratio of FR fibroblast and L8 myoblast cell micromass co-cultures and corresponding unwounded cultures. (A, B, C, D) shows images that were taken at 5 X magnification showing the distribution of DiI labeled L8 myoblast cells and DiO labeled FR fibroblast in both unwounded and wounded micromass co-cultures, while (E, F, G, H) shows images taken at low magnification for DiO labeled L8 myoblast cells and DiI labeled FR fibroblast cells. Localization and distribution pattern of both DiI and DiO- labeled FR fibroblast cells (D, H) in the 3 day post wounded micromass cultures at the wound edges suggest possible preferential migration of the fibroblast cells towards the wound site. Scale represent 100  $\mu$ m.**

# FIGURE 43

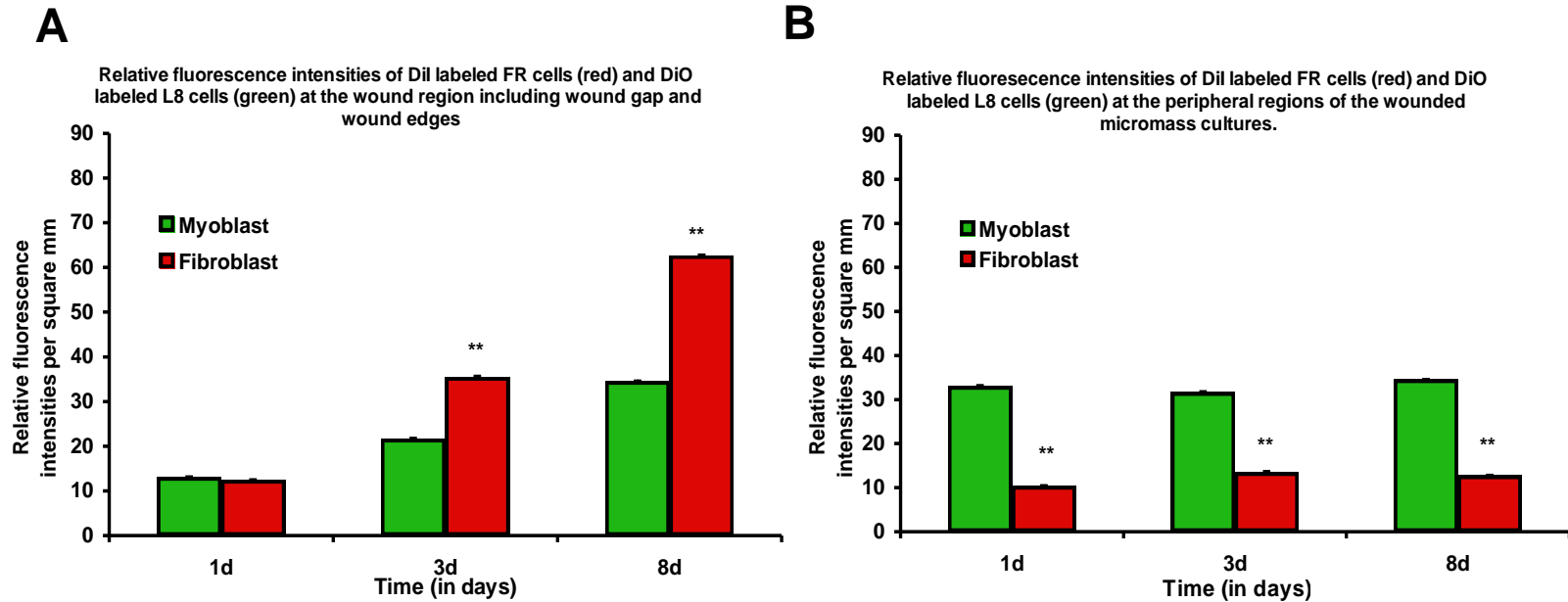
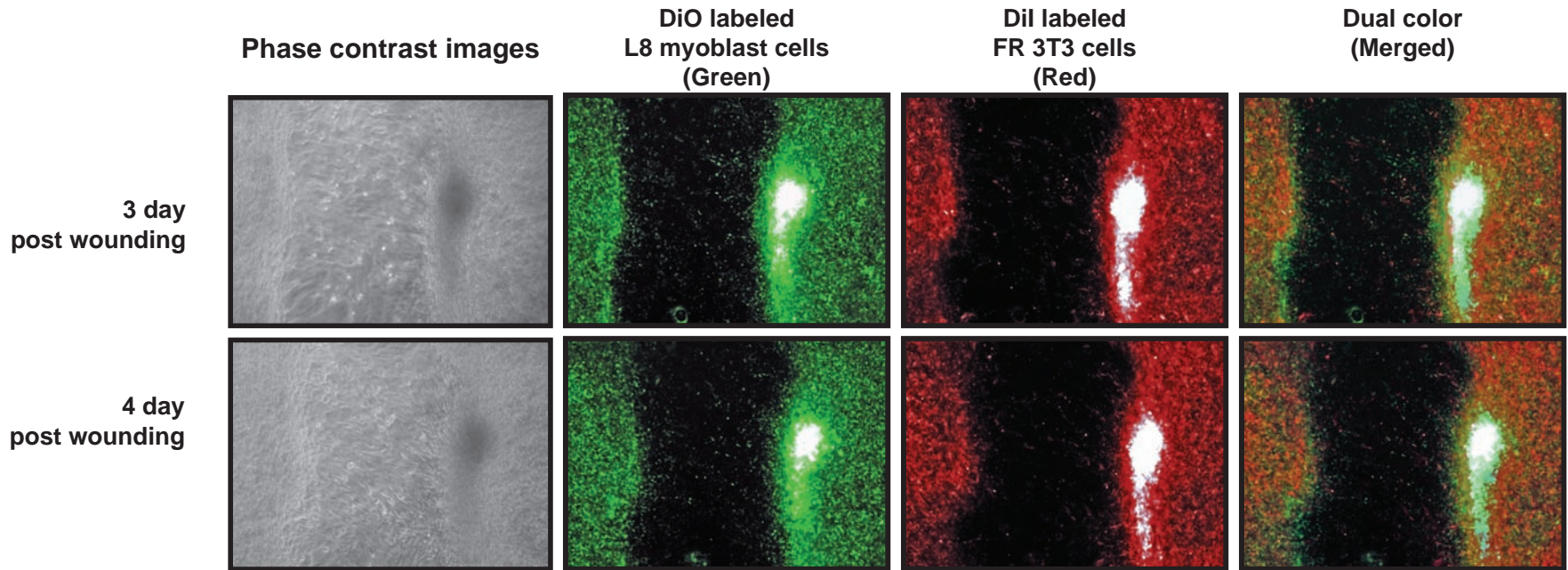


**Figure 43. Quantitative analysis of fluorescence intensities of DiI labeled FR fibroblast cell and DiO labeled L8 myoblast cells at wounded region and peripheral regions of micromass co-culture.** The relative fluorescence intensities of DiI labeled FR 3T3 cells (red) and DiO labeled L8 myoblast cells (green) at the wound and peripheral regions of the 1 day, 3 day and 8 day post wounded micromass co-cultures were determined. **(A)** shows relative fluorescence intensities of DiI labeled FR cells (red) were found to be significantly higher at the wound region wound sites as compared to the DiO labeled L8 myoblast cells, while **(B)** suggests that the relative fluorescence intensities of DiO labeled L8 myoblast cells were found to be at significantly higher at the periphery of the micromass cultures as compared to DiI labeled FR cells. (Mean  $\pm$  SD, \*\* indicates significant difference at  $p < 0.05$ ,  $n = 4$ ).

# FIGURE 44



179

**Figure 44. Presence of DiI labeled FR 3T3 fibroblast cells and DiO labeled L8 myoblast cells at the wound gap and wound edges.** Images of the wound site (wound gap and wound edges) were taken at 20 X magnification for both 3 day and 4 day post wounded micromass co-cultures, Phase contrast images shows that the wound gap was completely filled with cells. When the same wound region was visualized under fluorescent microscopy using FITC and Rhodamine filters, a few DiO labeled L8 myoblast cells (Green) and DiI labeled FR 3T3 fibroblast cells (Red) were visible at the wound gap.

**4.4.1.1.7.1** *Effects of exogenous TGF- $\beta$ 1 treatment on skeletal myoblast cells and fibroblast cells in wounded micromass co-cultures of 1:3 FR fibroblast and L8 myoblast cells*

TGF- $\beta$ 1 is a pro-fibrotic cytokine that promotes the synthesis and deposition of collagens and other extracellular matrix proteins that are important for wound closure. TGF- $\beta$ 1 treatment also promotes fibroblast proliferation both *in vivo* and *in vitro*. In myogenic cells, exogenous TGF- $\beta$ 1 has been shown to inhibit myoblast fusion, differentiation, and expression of muscle-specific proteins.

I wished to determine whether TGF- $\beta$ 1 treatment could affect cell proliferation and collagen biosynthesis within micromass co-cultures of 1:3 FR fibroblast and L8 myoblast cells. The cultures were incubated in the presence of TGF- $\beta$ 1 (0.1-0.8 ng/mL final concentration) for a period of 2 days. Total collagen deposition in the micromass co-cultures was determined by picosirius red staining as described in **Section 3.2.6.1**, while total cellular DNA was determined by fluometric Hoechst assay (**Section 3.2.5**). As shown in **Figure 45 A**, TGF- $\beta$ 1 treatment resulted in a dose dependent decrease in both picosirius red stainable collagen and total DNA accumulation in the micromass co-cultures. These declines were statistically significant even at the lowest TGF- $\beta$ 1 dose tested (0.1 ng/mL) (**Figure 45 A**,  $p < 0.01$ ,  $n = 16$ ). When the collagen values were normalized against total DNA levels to correct for differences in cell number between the various treatment groups, I observed a decrease in total collagen accumulation per microgram DNA at all TGF- $\beta$ 1 doses. However, the values were not significantly different from those of untreated control cultures (0 ng/mL). This indicates that the primary effect of TGF- $\beta$ 1 treatment in fibroblast:myoblast co-cultures was to reduce cell proliferation and or cell viability rather than to affect average levels of collagen synthesis

per cell. It was also observed that exogenous TGF- $\beta$ 1 concentrations of 0.2 ng/mL and higher caused the micromass co-cultures to curl up and detach from the culture plate after 2 days of incubation (data not shown).

To determine whether exogenous TGF- $\beta$ 1 treatment had differential effects on fibroblasts and myoblast cells under micromass conditions, I treated cultures composed of FR fibroblast cells alone or L8 myoblasts alone with varying concentration of TGF- $\beta$ 1 (0- 0.8 ng/mL) for a period of 2 days. In micromass cultures of FR fibroblast cells alone, TGF- $\beta$ 1 treatment caused a dose dependent increase in picosirius red stainable collagen deposition and total DNA accumulation (**Figure 46 A and 46 B**). In addition, collagen accumulation per microgram DNA was modestly elevated in fibroblast cultures at concentrations of 0.4 - 0.8 ng/mL TGF- $\beta$ 1. In contrast, when micromass cultures composed of L8 myoblasts alone were subjected to TGF- $\beta$ 1 treatment there was a significant reduction in levels of total DNA and picosirius stainable collagen at doses of 0.2 ng/ml TGF- $\beta$ 1 and higher (**Figure 47 A and 47 B**). Collagen accumulation per microgram DNA was also significantly reduced. These findings suggest that in FR fibroblast: L8 myoblast co-cultures, exogenous TGF- $\beta$ 1 treatment may promote FR fibroblast cell proliferation but inhibit the proliferation of myoblasts. The fact that L8 myoblast cells represent the more abundant cell type in 1:3 fibroblast: myoblast co-cultures is likely to account for the net reduction in total DNA when cultures are exposed to TGF- $\beta$ 1. I also examined whether exogenous TGF- $\beta$ 1 treatment affected the rate of wound closure in the micromass co-cultures of 1:3 FR fibroblast and L8 myoblast cells. The wounded micromass co-cultures were treated with 0.1 ng/mL TGF- $\beta$ 1, because higher doses caused contraction and eventual detachment of the micromass layer as

mentioned previously. Phase contrast images demonstrated a progressive migration of cells into the wound gap starting from 1 to 8 days post-wounding in both TGF- $\beta$ 1 treated and untreated control cultures and by 8 days the wound gap was almost completely filled with cells (**Figure 48**). Quantification of the wound closure rates by the planimetry method revealed that the presence of 0.1 ng/mL TGF- $\beta$ 1 stimulated a statistically significant increase in the rate of wound closure at 1 day and 2 days post wounding as compared to wounded control cultures (**Figure 49**;  $p < 0.05$ ,  $n = 16$ ). However the final extent of wound closure in TGF- $\beta$ 1 treated cultures was equivalent to wounded cultures at later time points (3 to 8 days post wounding) (**Figure 49**).

In another experiment, FR fibroblasts and L8 myoblast cells were labeled with DiI and DiO lipophilic dyes respectively to determine whether TGF- $\beta$ 1 treatment affected cell migration at the wound site in fibroblast:myoblast co-cultures. The cultures were imaged by fluorescence microscopy at time points of 1, 3 and 8 days post wounding (**Figure 50**), then NIH image analysis software was used to quantify changes in the fluorescence intensity of DiI labeled (red) FR fibroblast cells at the wound gap and wound edges as compared to DiO labeled (green) L8 myoblast cells.

As shown in **Figure 51 A**, both TGF- $\beta$ 1 treated cultures and untreated control cultures exhibited a progressive increase in the levels of DiI labeled fibroblast cells at the wound gap and wound edges between 1 day and 8 day after wounding. At 1 day post-wounding, the level of DiI labeled fibroblasts in the wound region was significantly higher for TGF- $\beta$ 1 treated cultures than parallel control cultures (**Figure 51 A**,  $p < 0.05$  considered significant,  $n = 16$ ). In contrast, TGF- $\beta$ 1 treated cultures exhibited a decrease in DiO labeled myoblasts (red) at the wound edges relative to control cultures (**Figure 51**

## FIGURE 45

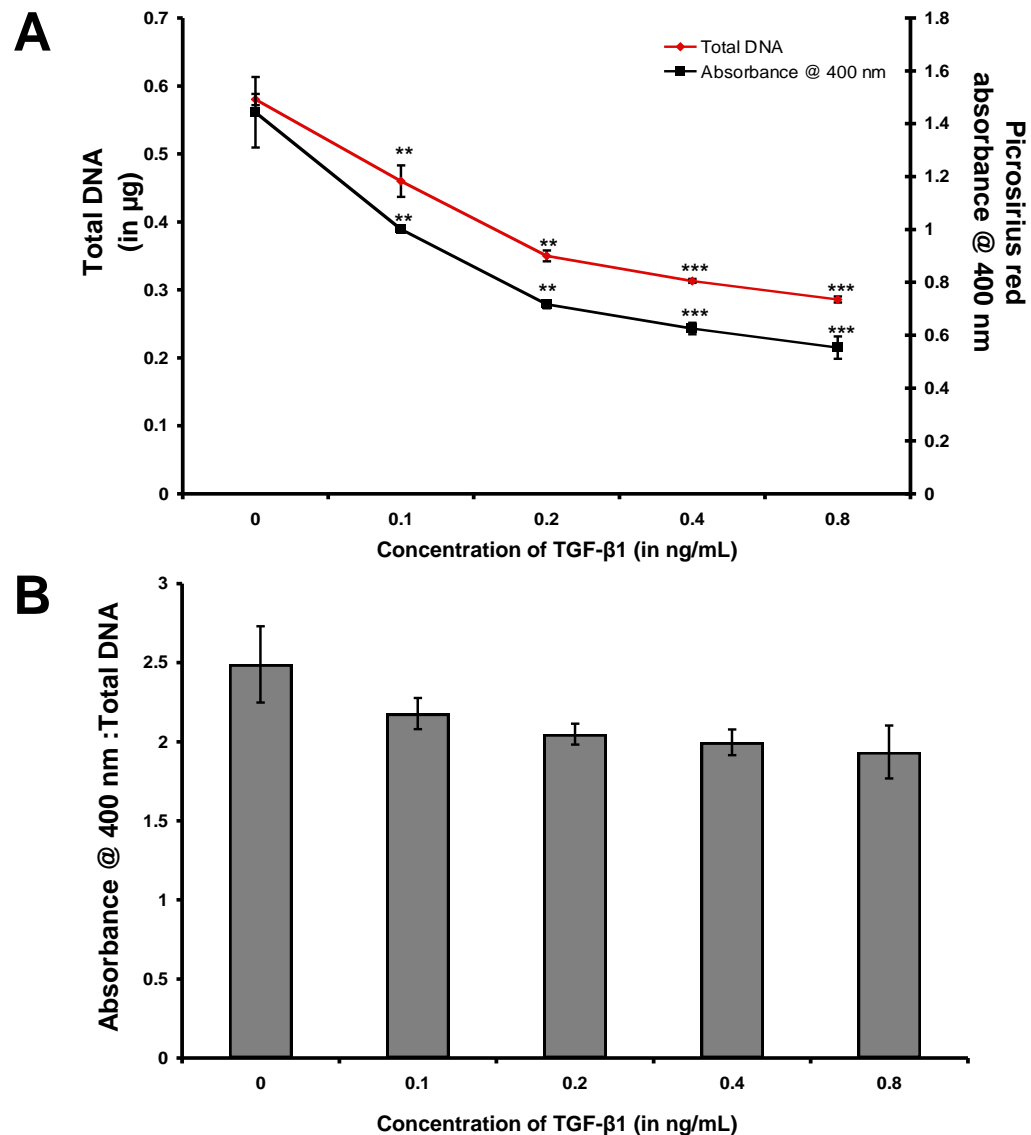


**Figure 45. Dose response effects of Transforming growth factor-  $\beta$  1 (TGF-  $\beta$  1) on the micromass co-culture of 1 part FR 3T3 fibroblast and 3 part L8 myoblast cells. (A) Total collagen levels as determined by the absorbance reading @ 400 nm of the Picrosirius red stain eluant and total DNA levels were determined by DNA Hoechst assay. Its been observed that there was a dose dependent decrease in the absorbance reading and total DNA levels. (B) The relative levels of collagen was determined by normalizing the absorbance reading to that of total DNA levels, There seems to be a decrease in total collagen synthesis in a dose-dependent manner following treatment with TGF- $\beta$ 1, though the treatment effects were not statistically significant. (Mean  $\pm$  SD, \*\*\* indicates significant difference at  $p < 0.001$ ,\*\* indicates significant difference at  $p < 0.01$ , \* indicates significant difference at  $p < 0.05$ ,  $n = 16$ )**

## FIGURE 46

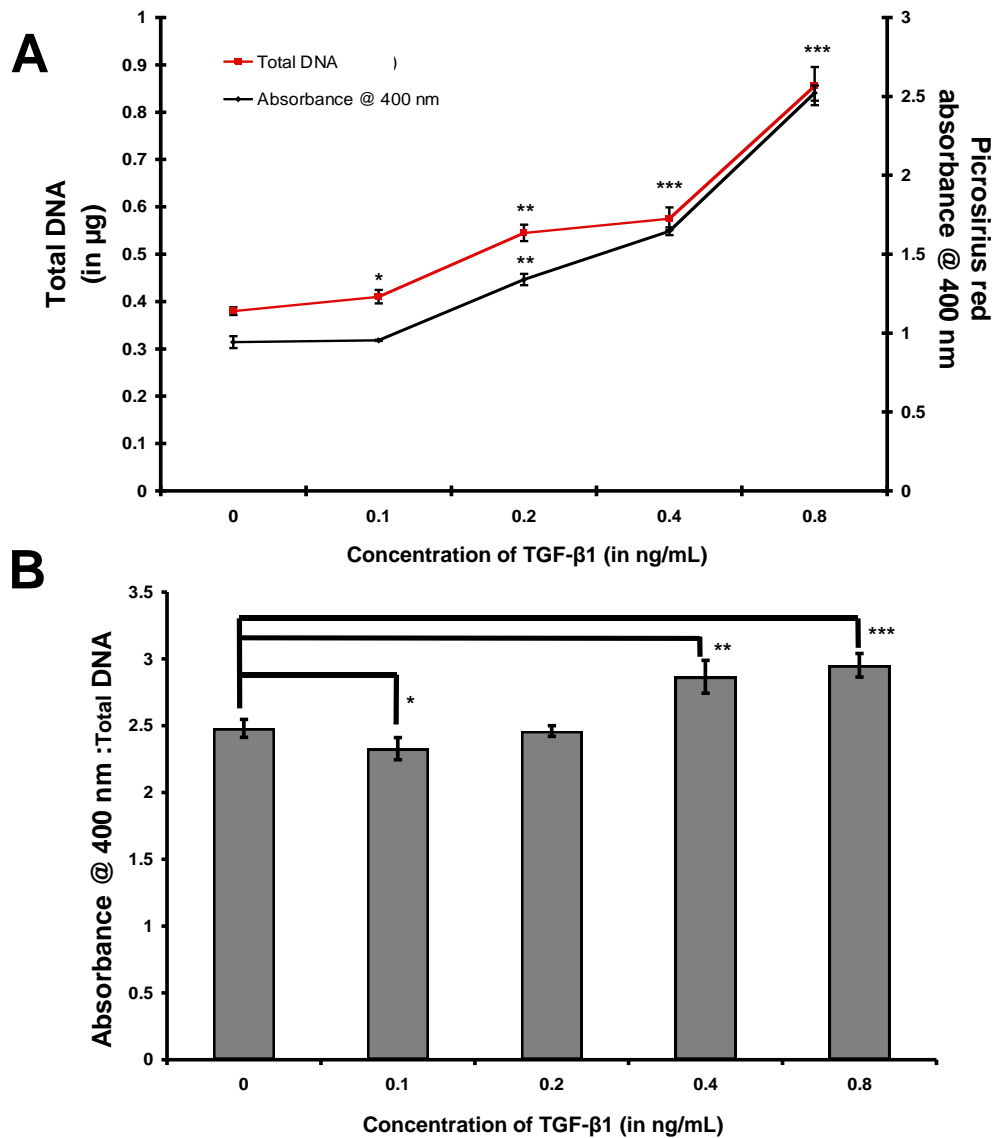


**Figure 46. Dose response effects of Transforming growth factor-β1 (TGF- β 1) on FR 3T3 fibroblast micromass cultures.** (A) Total collagen levels was determined by taking the absorbance reading @ 400 nm for the picrosirius red stain eluant, while total DNA levels was determined by DNA Hoechst assay. It is been observed that there was a dose dependent increase in the absorbance reading and total DNA levels. (B) The relative levels of collagen was determined by normalizing the absorbance reading to that of total DNA levels, There was a significant increase in total collagen synthesis in a dose-dependent manner following treatment with TGF-β1. (\*\*\*) indicates significant difference at  $p < 0.001$ , \*\* indicates significant difference at  $p < 0.01$ , \* indicates significance at  $p < 0.05$ ,  $n = 16$ )

## FIGURE 47

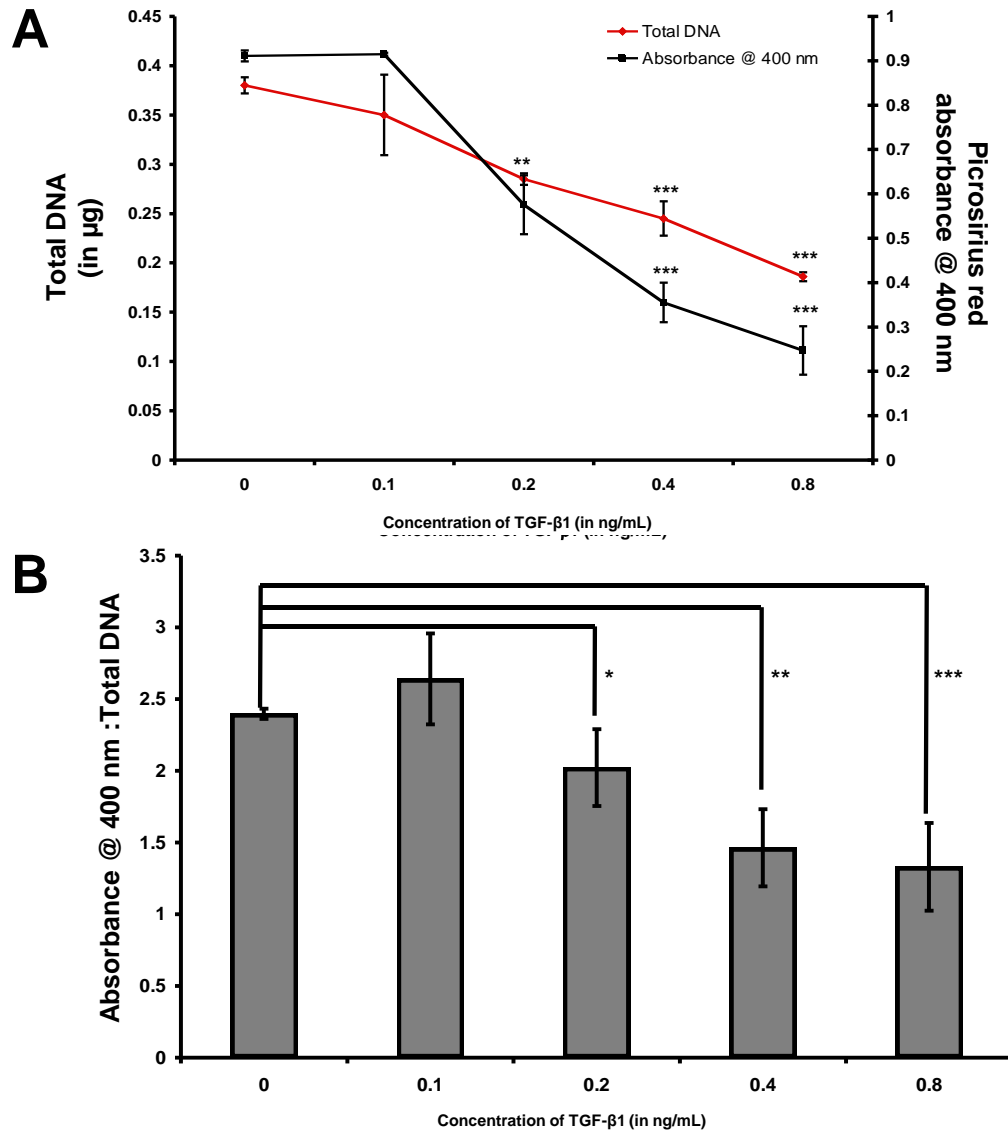


**Figure 47. Dose response effects of Transforming growth factor-  $\beta$  1 (TGF- $\beta$  1) on L8 myoblast micromass cultures.** (A) Total collagen levels was determined by taking the absorbance reading @ 400 nm of the picosirius red stain eluant while total DNA levels was determined by DNA Hoechst assay. Its been observed that there was a dose dependent decrease in the absorbance reading and total DNA levels. (B) The relative levels of collagen was determined by normalizing the absorbance reading to that of total DNA levels, There was a significant decrease in total collagen synthesis in a dose-dependent manner following treatment with TGF- $\beta$ 1. (Mean  $\pm$  SD,\*\*\* indicates significant difference compared to control at  $p < 0.001$ , \*\* indicates significant difference compared to control at  $p < 0.01$  while \* indicates significant difference compared to control at  $p < 0.05$ ,  $n = 16$ )

**FIGURE 48**

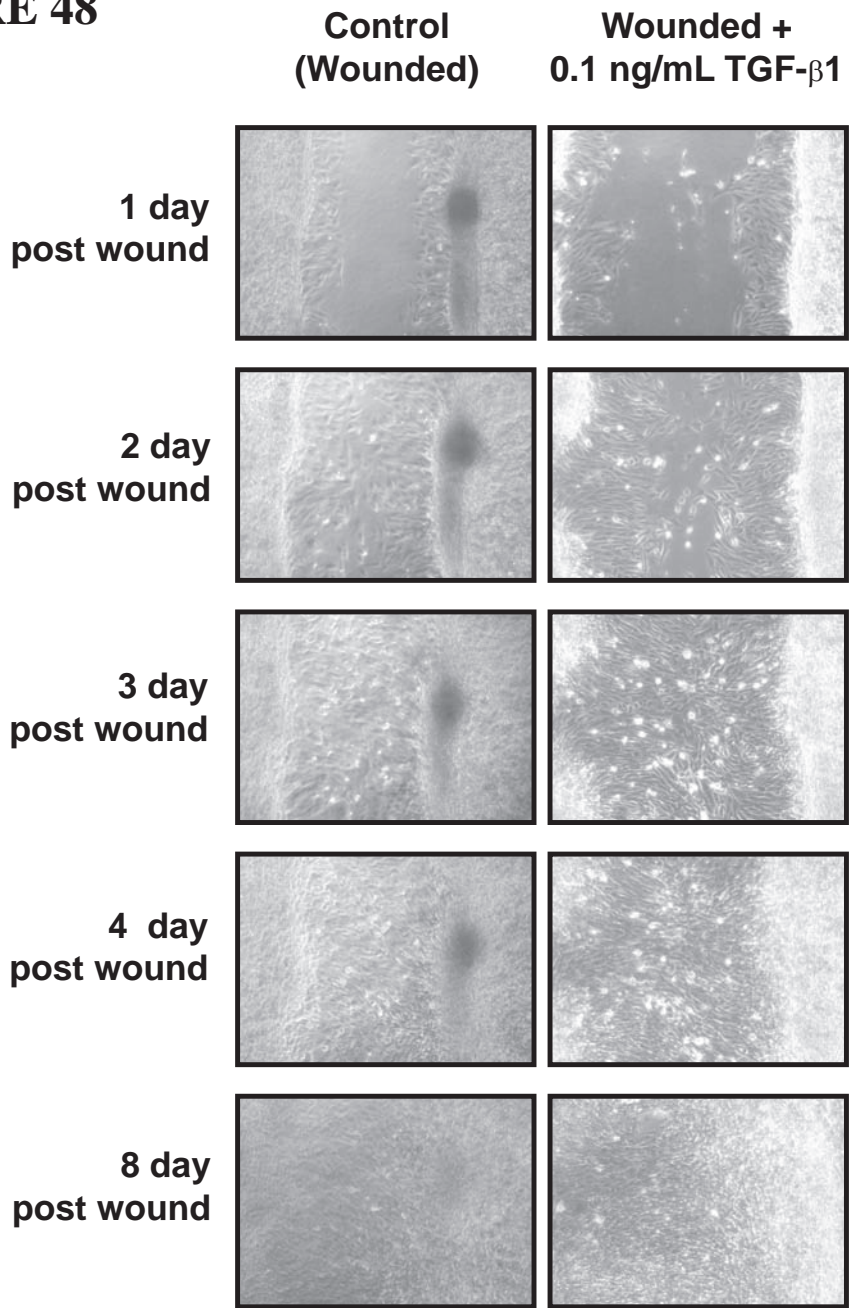


**Figure 48. Effect of TGF- $\beta$ 1 on wound closure in the wounded micromass co-culture of 1 part FR 3T3 and 3 part L8 myoblast cells.** The five photographs in each vertical rows are phase contrast images of the same culture at successive time point after wounding. Using phase contrast light microscopy, the time taken for wound closure in 0.1 ng/mL TGF- $\beta$ 1 treated and untreated control cultures. As seen from the phase contrast images the wounded micromass cultures treated with both 0.1 ng/mL TGF- $\beta$ 1 and untreated control cultures were repopulated with cells within 3 days after wounding. The TGF- $\beta$ 1 treated cultures appeared to show improved wound closure as compared to Control (untreated) cultures. Scale corresponds to 100 microns.

**FIGURE 49**

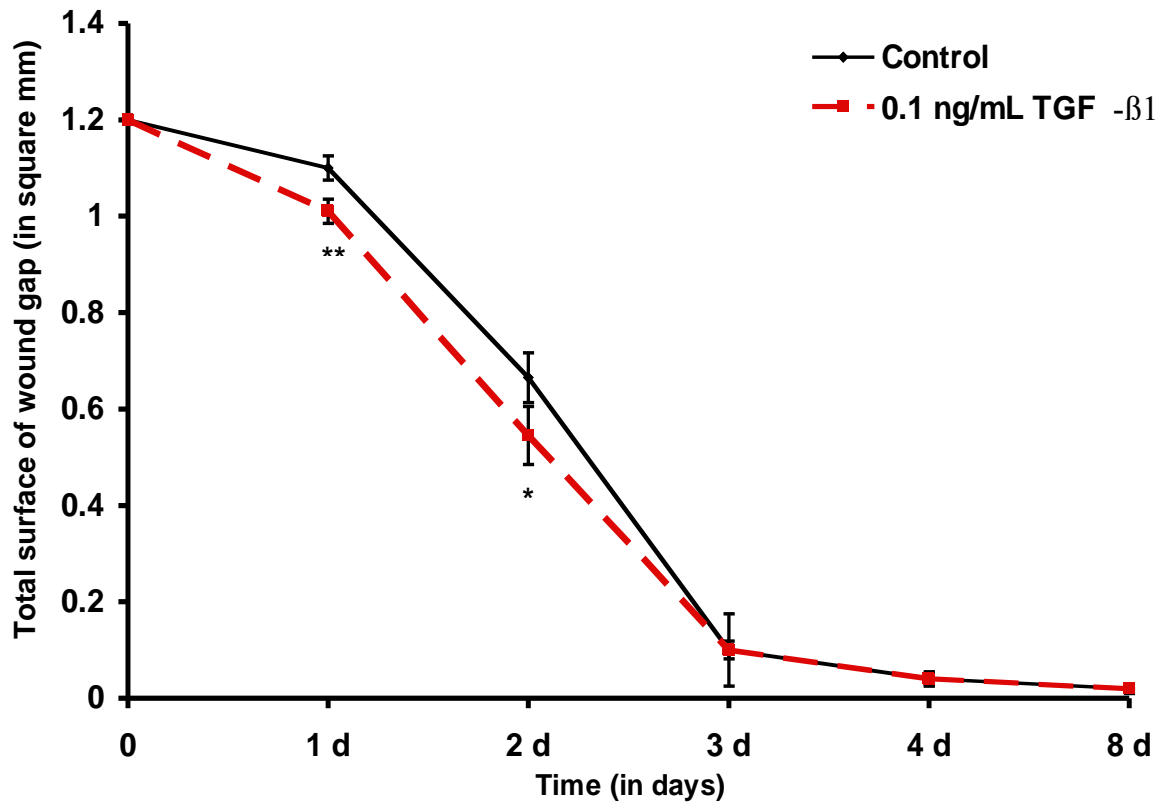
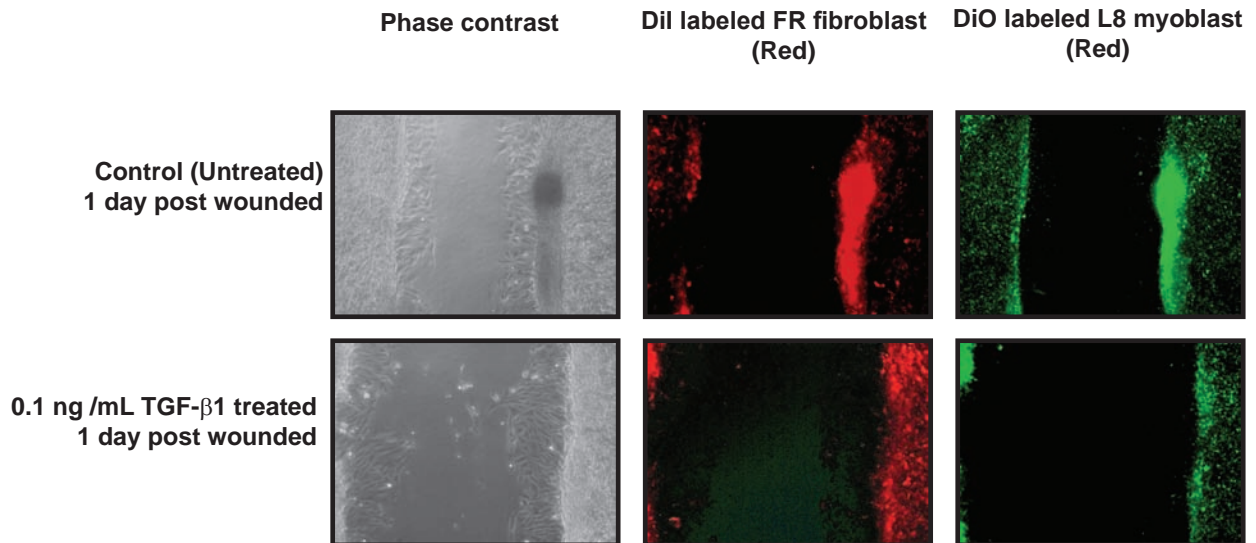


**Figure 49. Effect of Transforming growth factor-β1 (TGF-β1) on wound migration pattern.** *In vitro* micromass co-culture wound assay was performed to quantify the wound closure pattern as function of time. It was observed that there was increased cell migration at the wound site in TGF-β1 treated wounded cultures as compared to control treated wounded cultures. In comparison to control treated wounded cultures, the TGF-β1 treated wounded cultures had the rate of wound closure that was significantly higher between 1 day and 2 day post wounding but by 3 day post-wounding, the wound closure recovered to that of control treated cultures. (Mean  $\pm$  SD, \*\* indicates significant difference compared to control at  $p < 0.01$ , while \* indicates significant difference compared to control at  $p < 0.05$ ,  $n = 16$ )

## FIGURE 50

### Panel 1



### Panel 2

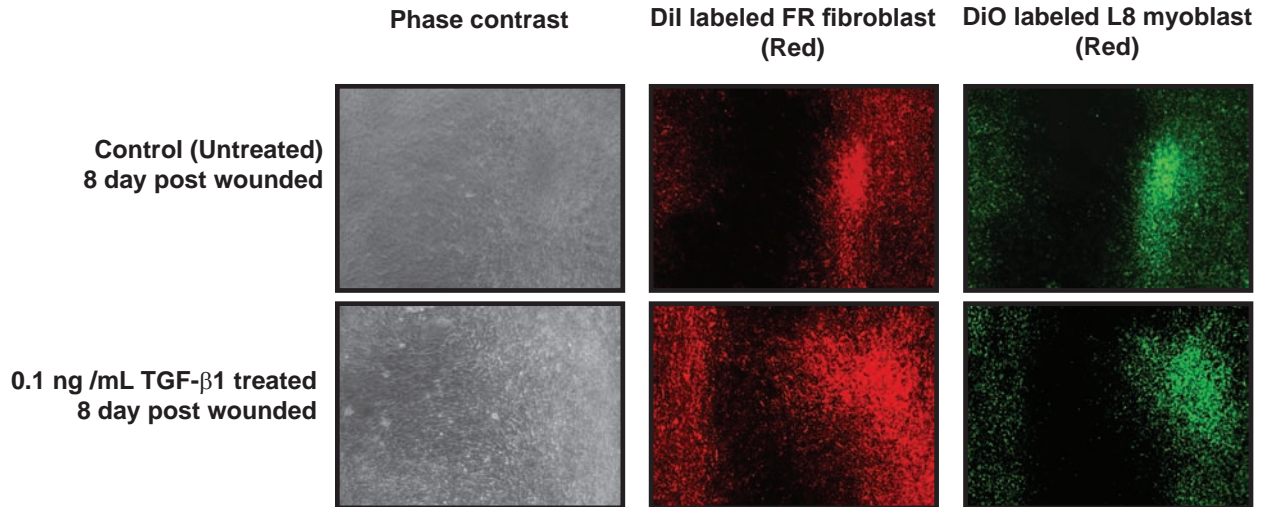


**Figure 50. Migratory pattern of FR fibroblast and L8 myoblast cells to the wound gap and wound edges following treatment with 0.1 ng/mL TGF-β1.** (Panel 1) shows relative levels of DiI labeled FR fibroblast and DiO labeled L8 myoblast at the wound site in the 1 day post wounded cultures treated with 0.1 ng/mL TGF-β1 and their corresponding untreated control wounded cultures. (Panel 2) shows relative levels of DiI labeled FR fibroblast and DiO labeled L8 myoblast at the wound site in the 8 day post wounded cultures that were treated with 0.1 ng/mL TGF-β1 and corresponding untreated control wounded cultures. Notice the gradual increase in relative levels of DiI labeled FR fibroblast cells (red) in the 3 day and 8 day post wounded cultures treated with 0.1 ng/mL TGF-β1.

**B**,  $p < 0.05$ , considered significant,  $n = 16$ ). This experiment suggests that TGF- $\beta$ 1 treatment may improve fibroblast cell migration and inhibit myoblast migration to the wound site in micromass co-cultures of 1:3 FR fibroblast and L8 myoblast cells.

#### **4.4.1.1.8 Expression of p38 and ERK1/2 mitogen-activated protein kinases in wounded and unwounded micromass co-cultures of 1 part FR 3T3 fibroblast and 3 parts L8 myoblast cells.**

As described in **Sections 4.3.3.2 and 4.3.3.3**, our *in vivo* studies on the rat spinal laminectomy model had demonstrated increased ERK1/2 and p38 MAPK activation during the peridural scarring process and that these signaling pathways were attenuated by OTC treatment. Moreover, previous studies have implicated ERK1/2 and p38 MAPKs in both epithelial and muscular wound healing (Li *et al.*, 2001; Lluís *et al.*, 2006; Sharma *et al.*, 2003; Tolg *et al.*, 2006; Zetser *et al.*, 1999). Hence, I wished to determine whether activation of ERK1/2 and p38 MAPK was also a feature of our micromass co-culture wound repair model.

Micromass co-cultures were subjected to single scrape wound at approximately 36 h after initial plating. The cell debris was removed by rinsing with warm saline and the culture medium was replaced. Parallel-unwounded control cultures were subjected to the saline rinse and medium replacement only. The cultures were harvested at representative time points over an 8 day period, and western blot analysis was performed to determine the expression of total ERK1/2 protein and active dual phosphorylated ERK1/2 in wounded and unwounded cultures. Neither wounding nor the time in culture caused any obvious change in the level of total ERK1 (p44) or ERK2 (p42) proteins in the micromass co-cultures (**Figure 52**). The levels of dual phosphorylated (active) ERK1 and ERK2 exhibited a rapid and transient expression pattern in wounded culture as

# FIGURE 51

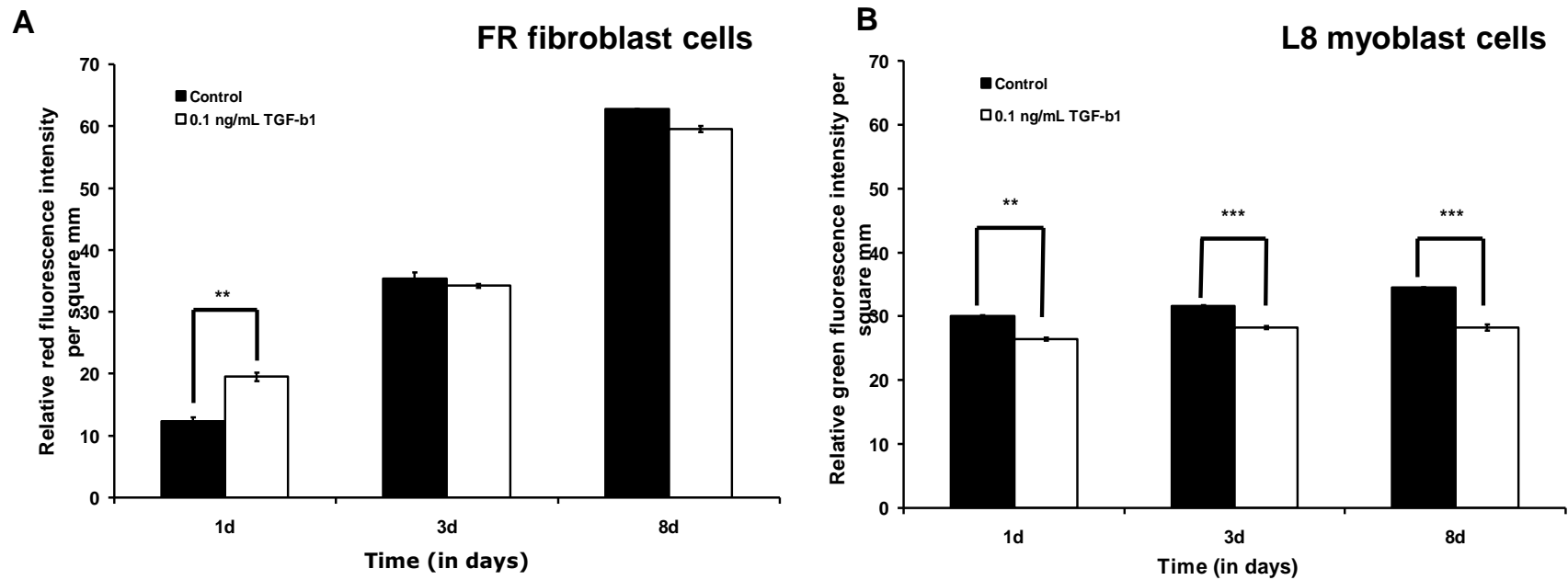


**Figure 51. Effect of Transforming growth factor-β1 (TGF- β1) on the migratory pattern of myoblast cells and fibroblast cells at the wound site.** The fibroblast and L8 myoblast cells were labeled with DiI and DiO lipophilic dyes and visualized through a fluorescent microscope at 1 day, 3 day and 8 day post wounding. The relative pixel intensities of DiI labeled FR fibroblast (red) and DiO labeled L8 myoblast (green) were quantified using NIH image J software. **(A)** shows the relative intensity of DiI labeled FR 3T3 fibroblast cells that were present at the wound site including wound edges, it seems to suggest that at 1 day post wounding 0,1 ng/mL TGF-β1 treated wound cultures had significantly higher levels of DiI labeled FR cells at the wound site as compared to untreated wounded cultures. **(B)** shows the relative intensity of DiO labeled L8 myoblast cells that were present at the wound site including wound edges. The observations suggest that the DiO labeled L8 myoblast cells were significantly lower at the wound site in the 0.1 ng/mL TGF- β1 treated wounded cultures as compared to untreated cultures at all time points. This also suggest that as compared to untreated wounded cultures, the TGF- β1 treatment could potentially inhibit L8 myoblast cell migration. (Mean ± SD, \*\*\* indicates significance at p value < 0.001 and \*\* indicates significance at p value < 0.01, n = 16)

## FIGURE 52

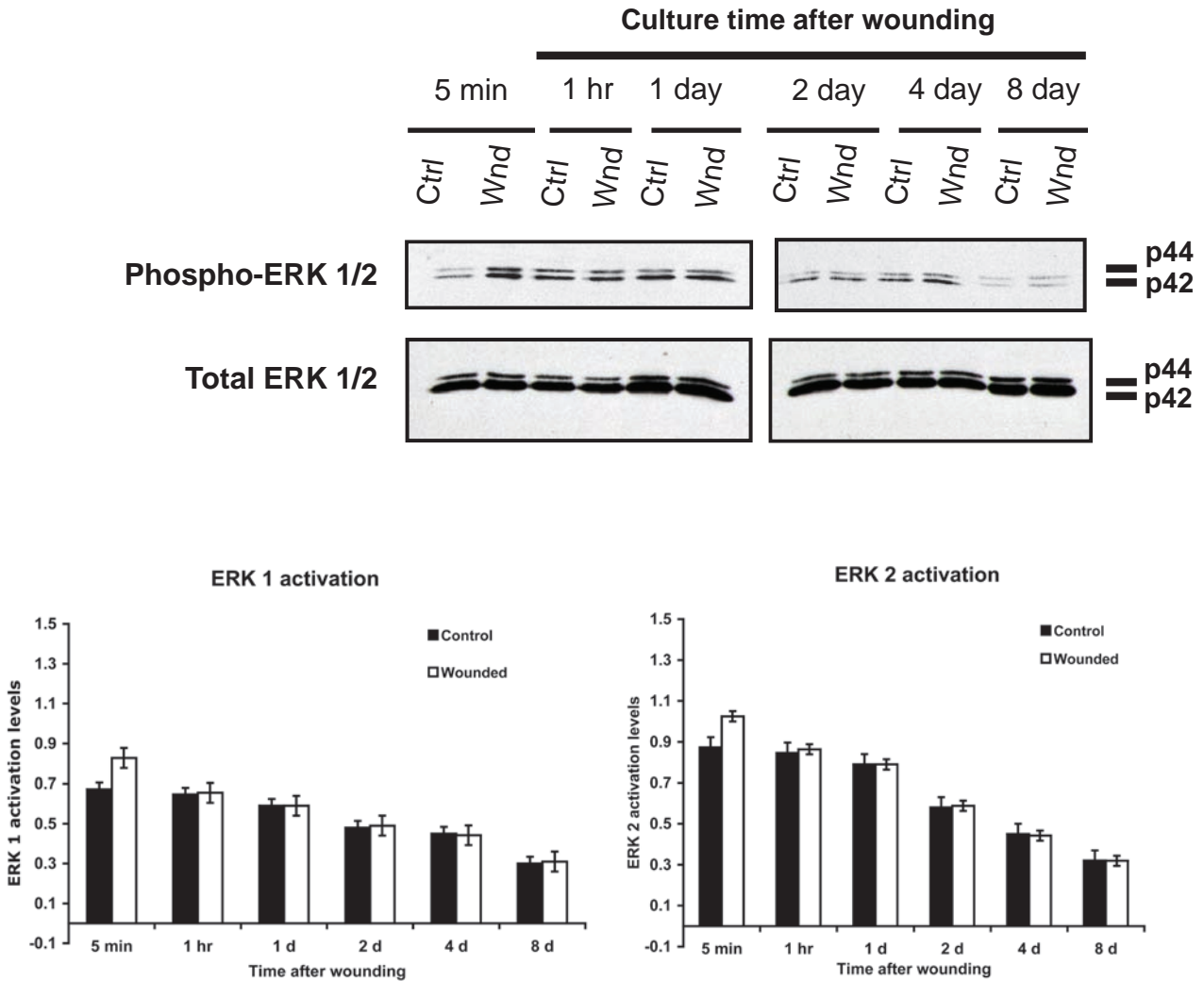


**Figure 52. Expression of dual phosphorylated ERK1/2 mitogen activated protein kinases in wounded micromass co-culture of 1 part FR fibroblast cells and 3 part L8 myoblast cells.** Cultures were collected at representative time points following wounding, and expression of total ERK1/2 and dual phosphorylated ERK1/2 were determined by Western blotting. Both total ERK1/2 and dual phosphorylated ERK1/2 were present in all culture homogenates at all time points. Homogenates that were obtained from 5 min post-wounded cultures seem to show relatively higher expression of dual phosphorylated ERK1/2 as compared to the corresponding unwounded cultures. However, the ERK activation levels suggest a time-dependent decrease in expression of dual phosphorylated ERK1/2. Densitometric analysis of western blots were performed on samples from two replicate cultures, and ERK1 and ERK2 activation was determined by normalizing the dual active phosphorylated ERK1 and ERK2 protein levels with total ERK1 and ERK2 protein levels. The ERK1 and ERK2 activation values are expressed in Mean  $\pm$  Range.

compared to corresponding unwounded culture (**Figure 52**). In unwounded control cultures, phosphorylated ERK1 and ERK2 protein levels were highest at 1 hr and 1 day of culture then declined to faintly detectable levels by 8 days of culture (**Figure 52**). In comparison to the control cultures, the wounded micromass cultures demonstrated a rapid transient increase in ERK1 and ERK2 phosphorylation at 5 min post-wounding (**Figure 52**). However, at all subsequent time points tested (1 h, 1 d, 2 d, 4 d and 8 d), the levels of ERK1/2 phosphorylation in wounded and unwounded control cultures were virtually equivalent.

I also performed *in situ* immunostaining for active dual phosphorylated ERK1/2 on the wounded micromass co-cultures. Highest levels of ERK phosphorylation were observed within cells located at the wound edges at 5 min and 1 day time points after wounding (**Figure 53**). Total ERK1/2 protein was more uniformly expressed throughout the micromass culture. This preferential distribution of phosphorylated ERK1/2 within the cells at the wound edges suggests that ERK1/2 activation is a localized response to microtissue injury in the micromass co-culture model. Western blot analysis was also performed to examine activation of the p38 MAPK signaling pathway in wounded and unwounded micromass co-cultures. Total p38 MAPK protein was expressed at similar levels in both wounded and unwounded cultures at all time points (**Figure 54**). In contrast, dual phosphorylated (active) p38 MAPK was not detectable at any time point in unwounded cultures. Wounded cultures exhibited a faint band for phosphorylated p38 MAPK at five minute post-wounding, however phosphorylated p38 was not detectable at any subsequent time point (1 h, 1 d, 2 d, 4 d or 8 d post wounding) (**Figure 54**). These data suggest p38 MAPK activation is a rapid transient response to tissue injury in FR fibroblast: L8 myoblast micromass co-cultures.

## FIGURE 53

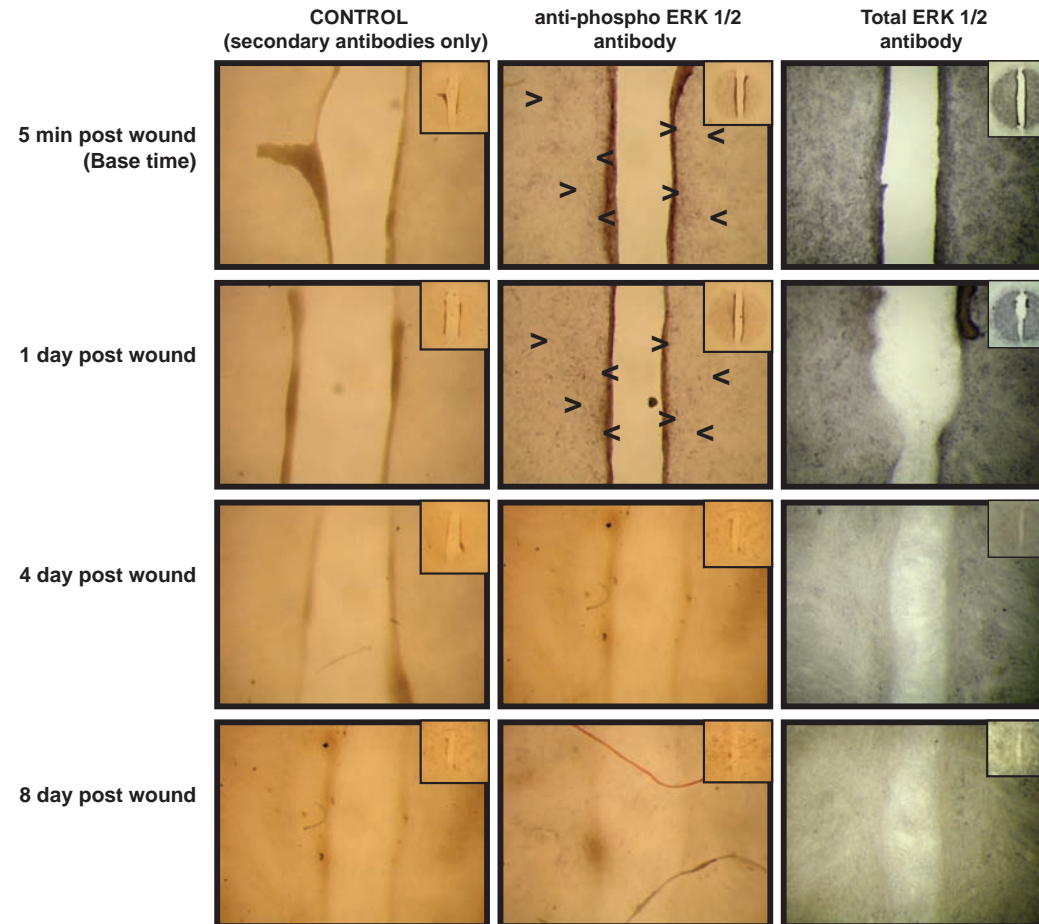


**Figure 53. Localization of dual phosphorylated and total ERK1/2 mitogen activated protein kinases in wounded micro-mass co-culture.** Alkaline phosphatase conjugated immunostaining shows the expression of dual phosphorylated ERK1/2 (dark brown and black) at the wound edges of the micromass cultures in 5 min post-wounded and 1 day post-wounded cultures, respectively. The arrowheads show the staining where expression of phosphorylated ERK1/2 in the wounded micromass co-culture was prominent as compared to control unstained cultures. In contrast, staining for dual phosphorylated ERK1/2 was observed to be lower in 4 day and 8 day post-wounded cultures than in 5 min and 1 day post wounded cultures. The staining for total ERK1/2 was observed throughout the wounded micromass at all time points with low distribution of total ERK1/2 in 8 day post wounded

**FIGURE 54**

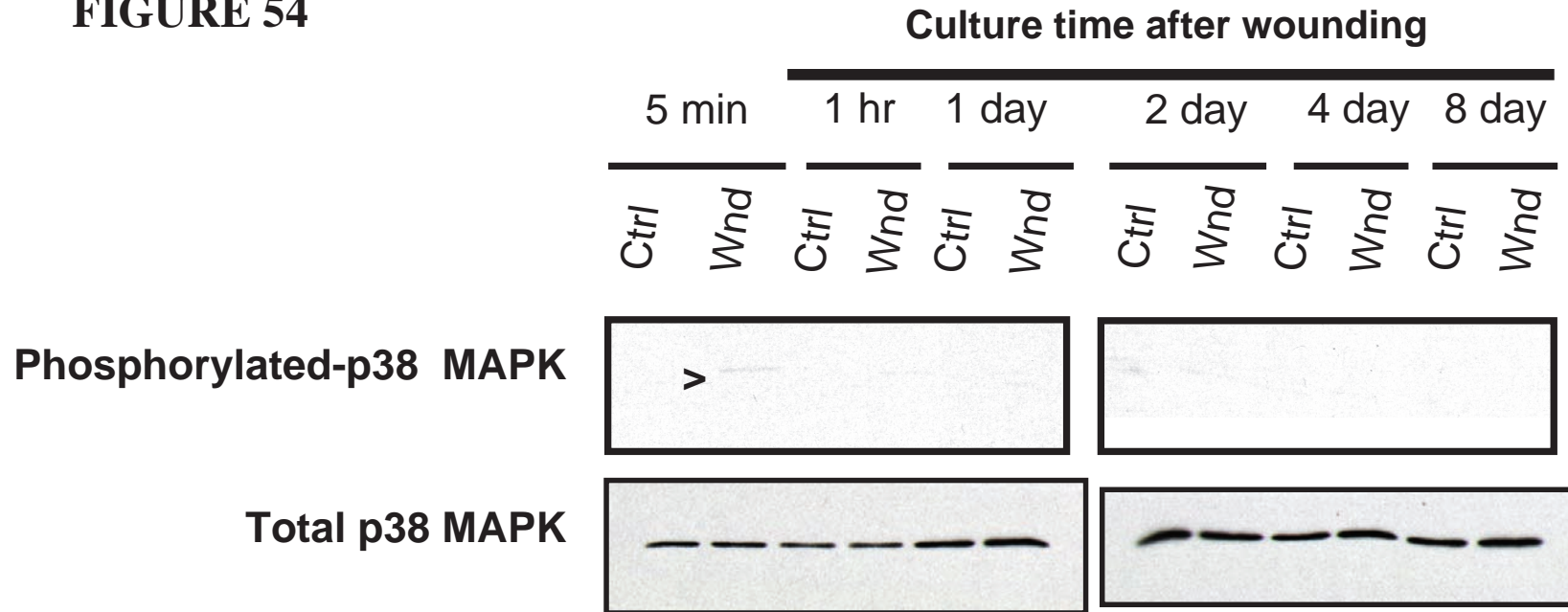


**Figure 54. Expression of dual phosphorylated p38 mitogen activated protein kinases (p38 MAPK) in wounded micromass co-culture and corresponding unwounded micromass co-cultures of 1 part FR fibroblast and 3 parts L8 myoblast cells.** Western blot analysis was performed on homogenates of wounded micromass co cultures and corresponding unwounded control cultures. Total p38 MAPK was expressed in both wounded and unwounded cultures at all time points. In contrast, dual phosphorylated (active) p38 MAPK was not detectable in unwounded control cultures, and was faintly expressed at 5 min post injury in wounded micromass cultures. The experiments was performed in quadruplicate cultures with equivalent results.

*In situ* immunostaining was performed to determine the localization of phosphorylated p38 MAPK within the wounded micromass co-cultures (**Figure 55**). Expression of active dual phosphorylated p38 MAPK appeared to be highest in cells at the wound edges (**Figure 55**) at 5 min and 1 day after wounding. Levels of phosphorylated p38 MAPK declined at the wound edges by 4 d and 8 d post-wounding. Total p38 MAPK protein was present throughout the micromass culture, but was expressed at highest levels at 5 min post wounding at the wound edges (**Figure 55**). In contrast to phosphorylated p38 MAPK, total p38 protein levels remained quite high throughout the micromass cultures at 1 day through 8 days post wounding.

#### **4.4.1.1.8.1** *Effect of ERK inhibitor, PD184352, on wound closure in micromass co-cultures of 1:3 FR fibroblast and L8 myoblast cells.*

In order to investigate the role of ERK1/2 signaling in wound closure within micromass co-cultures of 1:3 FR fibroblast and L8 myoblast cells, the wounded micromass co-culture were treated with PD184352, a potent and specific pharmacological inhibitor of the MEK1/2 enzyme that phosphorylates /activates ERK1/2. Western blot analysis confirmed that treatment with 2  $\mu$ M PD184352 was effective in blocking ERK1/2 phosphorylation in wounded micromass FR fibroblast: L8 myoblast micromass co-cultures (**Figure 56**). Phase contrast images suggested that when wounded micromass co-cultures were treated with 2  $\mu$ M PD184352, there was a noticeable delay in the movement of cells into the wound gaps, which resulted in a comparatively lower cell density in the wound gap at 3 days and 8 days post-wounding relative to untreated control cultures (**Figure 57**). The quantitative *in vitro* wound closure assay confirmed

## FIGURE 55

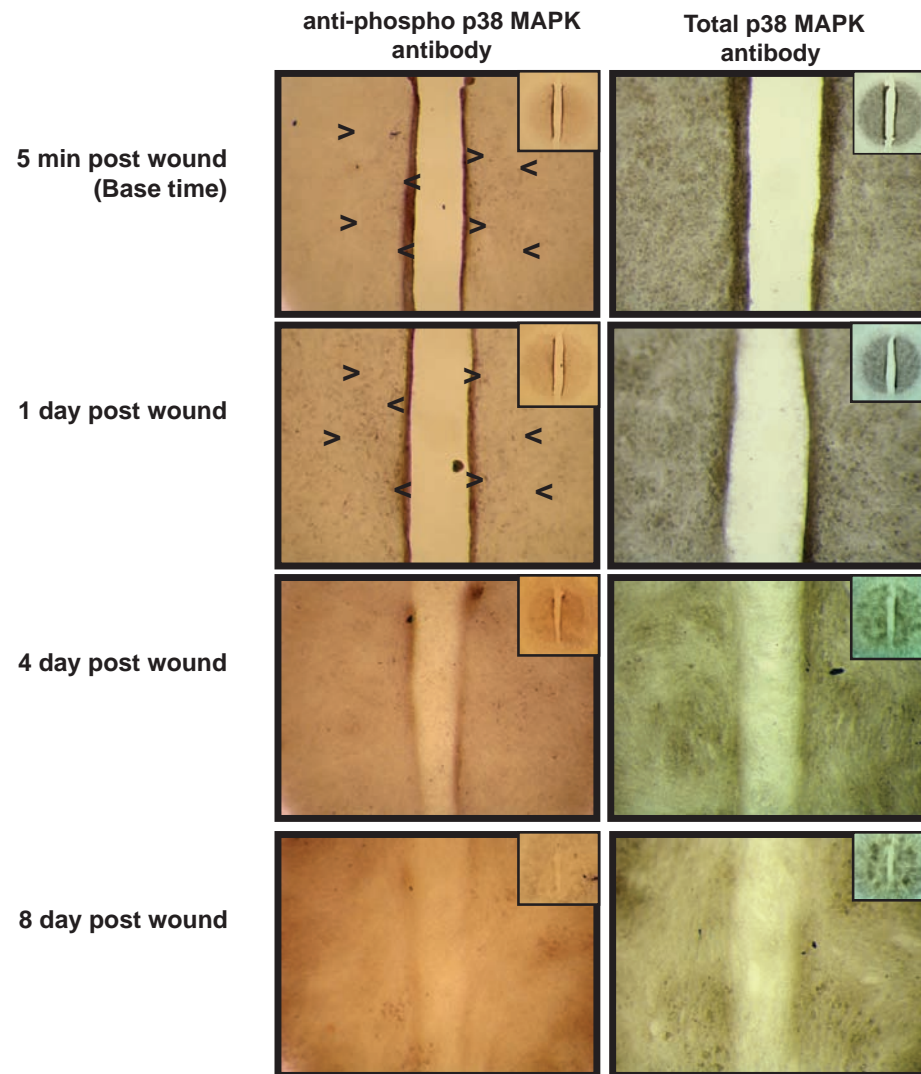


**Figure 55. Localization and distribution of phosphorylated and total p38 mitogen activated protein kinases (p38 MAPK) in wounded micromass co-culture.** Alkaline phosphatase conjugated immunostaining shows the expression of dual phosphorylated p38 MAPK (dark brown and black) at the wound edges of the cells at the wound site in 5 min post-wounded and 1 day post-wounded cultures, respectively. The arrowheads show the staining where expression of phosphorylated p38 MAPK in the wounded micromass co-culture was prominent. In contrast, staining for phosphorylated p38 MAPK was observed to be lower in 4 day and 8 day post-wounded cultures than in 5 min and 1 day post wounded cultures. The staining for total p38 MAPK was observed throughout the micromass in all wounded cultures.

## FIGURE 56

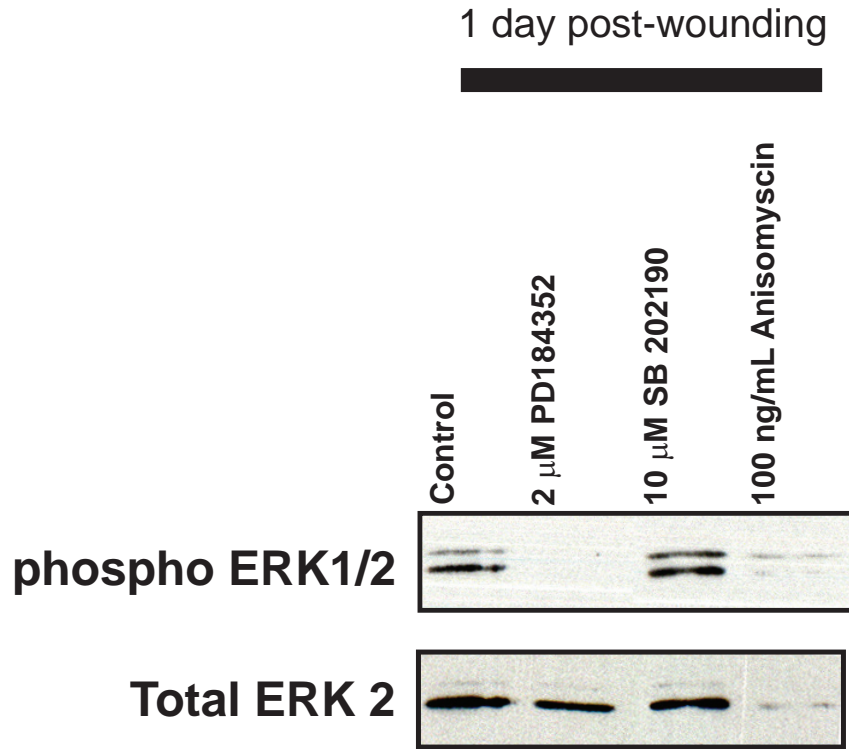


**Figure 56.** Western blot analysis to detect total ERK2 and dual phosphorylated ERK1/2 in the wounded micromass co-culture of 1 part FR 3T3 fibroblast cells and 3 part L8 myoblast cells treated with 2  $\mu$ M PD 184352, 10  $\mu$ M SB 202190 and 100 ng/mL Anisomycin. The cultures were incubated in PD184352, SB202190 and anisomycin for 1 day after the infliction of scrape wound. The 1 day post wounded culture were lysed and lysates subjected to western blot analysis. Treatment with ERK pathway inhibitor PD184352 was effective in suppressing phosphorylation of ERK1 and ERK 2, relative to cultures treated with 0.1% DMSO vehicle alone (control). Treatment with p38 inhibitor compound SB202190 had no effect on ERK1/2 phosphorylation or total ERK1/2 protein levels. Treatment with anisomycin, a protein synthesis inhibitor, reduced both total ERK 2 protein expression as well as levels of phosphorylated ERK1/2.

## FIGURE 57

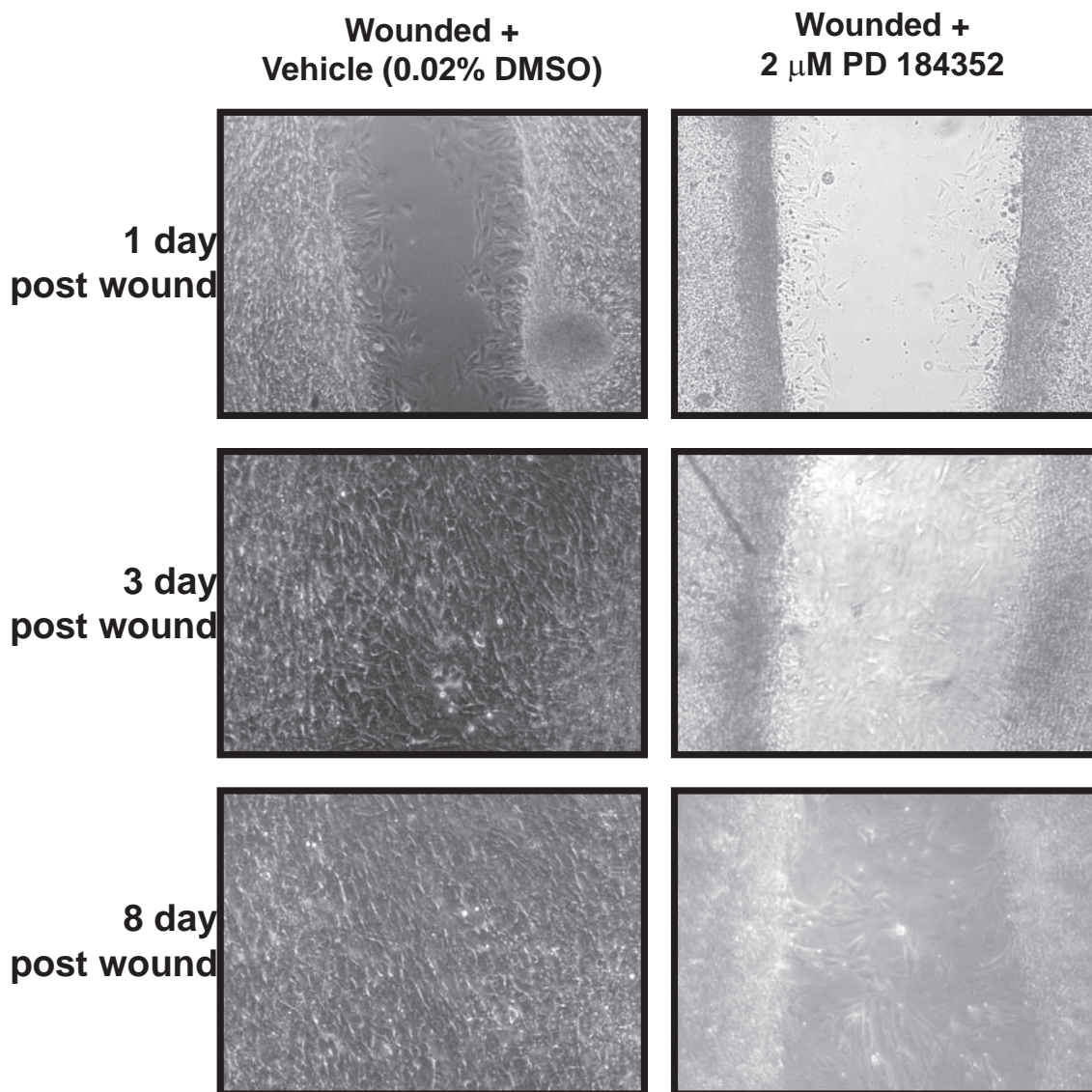


**Figure 57. Effect of PD 184352 on wound closure pattern in the wounded micromass co-culture of 1 part FR fibroblast and 3 part L8 myoblast cells.** Phase contrast images shows wounded micromass co-culture treated with 2  $\mu$ M PD 184352 and corresponding wounded control cultures treated with 0.02 % DMSO (Vehicle control). The three photographs in each vertical rows are phase contrast images of the same culture at successive time point after wounding. The 3 day and 8 day post wounded cultures treated with 2  $\mu$ M PD 184352 showed a delay in wound closure, with lower cell density at the wound edges and wound gap.

that treatment with 2  $\mu$ M PD184352 resulted in a significant delay in the rate of wound closure as compared to untreated control cultures (**Figure 58**,  $p < 0.01$ ,  $n = 16$ ). This experiment suggests that ERK1/2 activation is involved in facilitating optimum rates of wound closure in 1:3 fibroblast:myoblast micromass co-culture model.

#### **4.4.1.1.8.2** *Effect of p38 MAPK inhibitor, SB202190, on wound closure in micromass co-culture of 1:3 FR fibroblast and L8 myoblast cells.*

In order to determine whether p38 MAPK signaling affects wound closure in micromass co-cultures of 1:3 FR fibroblast and L8 myoblast cells, the wounded micromass co-cultures were treated with SB202190, a potent and selective inhibitor of p38 MAPK that does not affect the JNK or ERK1/2 MAPK signaling pathways. Western blot analysis performed on micromass co-cultures confirmed that treatment with 10  $\mu$ M SB202190 was effective in blocking the transient increase in p38 phosphorylation that normally occurred at 5 min post wounding (**Figure 59**). Because p38 activation after wounding was a transient response, phosphorylated p38 MAPK was undetectable at subsequent time points (1 to 8 days post wounding) in both the presence and the absence (control) of SB202190 (**Figure 59**). To verify that our primary antibody was indeed capable of detecting phosphorylated p38 on western blots, some micromass cultures were treated with anisomycin, a protein synthesis inhibitor that is known to elevate p38 phosphorylation in cells. As seen in **Figure 59**, treatment with 100 ng/mL anisomycin resulted in expression of phosphorylated p38 MAPK even at 1 days post wounding.

**FIGURE 58**

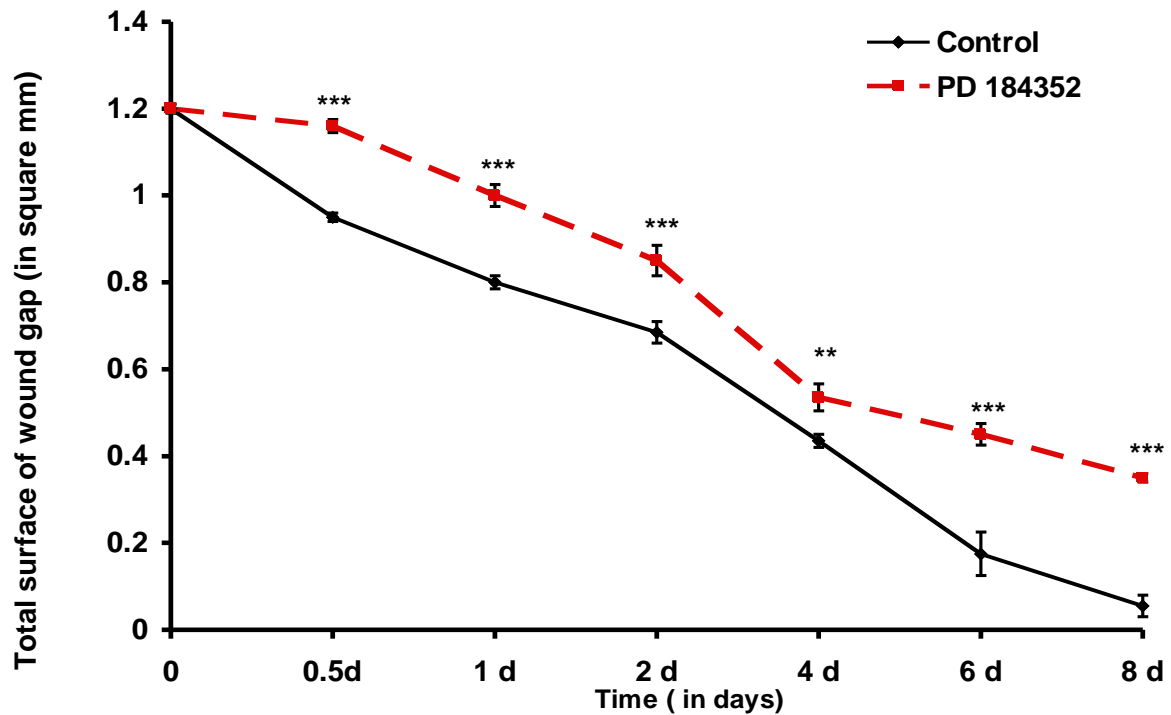


**Figure 58. Effect of PD 184352 treatment on the rate of wound closure in the micromass co-culture of 1 part FR 3T3 fibroblast and 3 part L8 myoblast cells.** *In vitro* micromass co-culture wound assay was performed to determine the effect of 2  $\mu$ M PD 184352 treatment on wound closure pattern. It was observed that there was significant delay in the total wound area being covered by cells following treatment with PD 184352 ( Mean  $\pm$  SD, \*\*\* indicates significant difference compared to control at  $p < 0.001$ , \*\* indicates significant difference to control at  $p < 0.01$ ,  $n = 16$ ).

## FIGURE 59

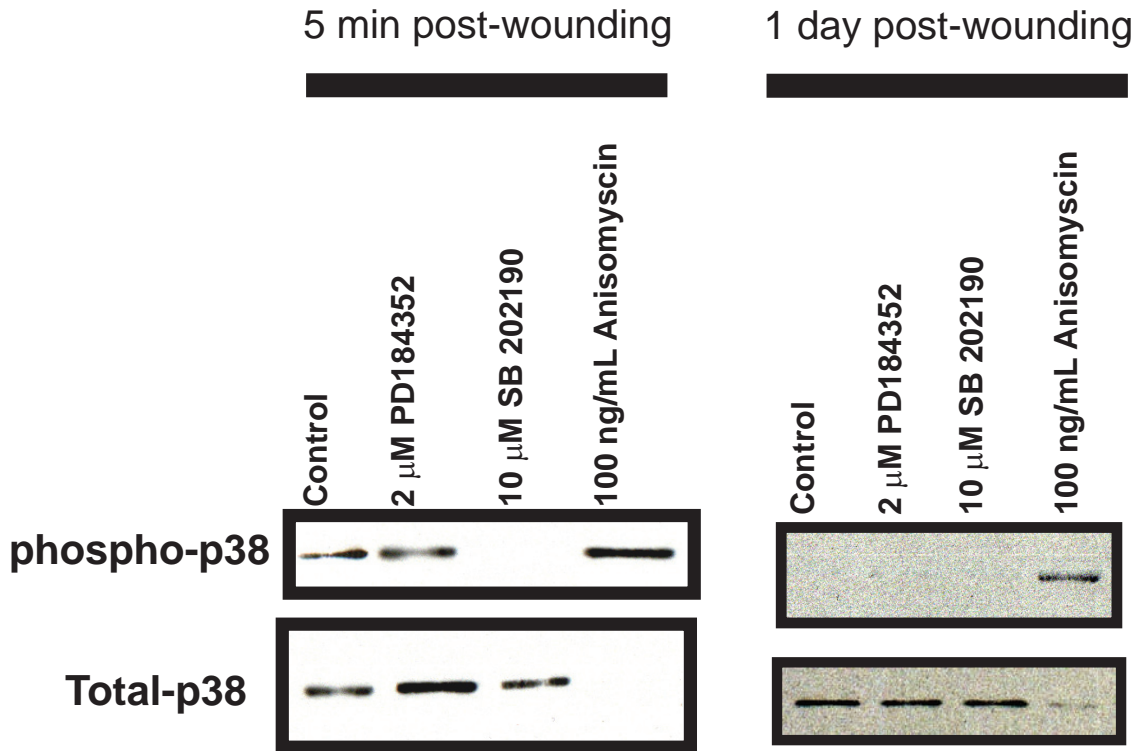


**Figure 59.** Western blot analysis to detect total and dual phosphorylated p 38 MAPK in the wounded micromass co-culture of 1 part FR 3T3 fibroblast cells and 3 part L8 myoblast cells treated with 2 μM PD 184352, 10 mM SB 202190 and 100 ng/mL Anisomycin. In 5 min post wounded cultures, the dual phosphorylated p38 MAPK expression was present in 2 μM PD 184352 and 100 ng/mL Anisomycin treated wounded cultures, while the dual phosphorylated p38 MAPK expression was absent in 10 μM SB 202190 treated cultures. In 1 day post wounded cultures, phosphorylated p38 MAPK expression was absent in untreated control wounded cultures, SB 202190 and PD 184352 treated cultures. However anisomycin treated culture showed presence of dual phosphorylated p38 MAPK proteins. The total p38 protein levels were observed in both 5 min and 1 day post wounded control (untreated), PD 184352 and SB 202190 treated cultures. The total p38 protein levels were not detectable in anisomycin treated cultures at 5 min post wounding. Faint band for total p38 protein was observed in 1 day post wounded cultures treated with anisomycin.

**FIGURE 60**

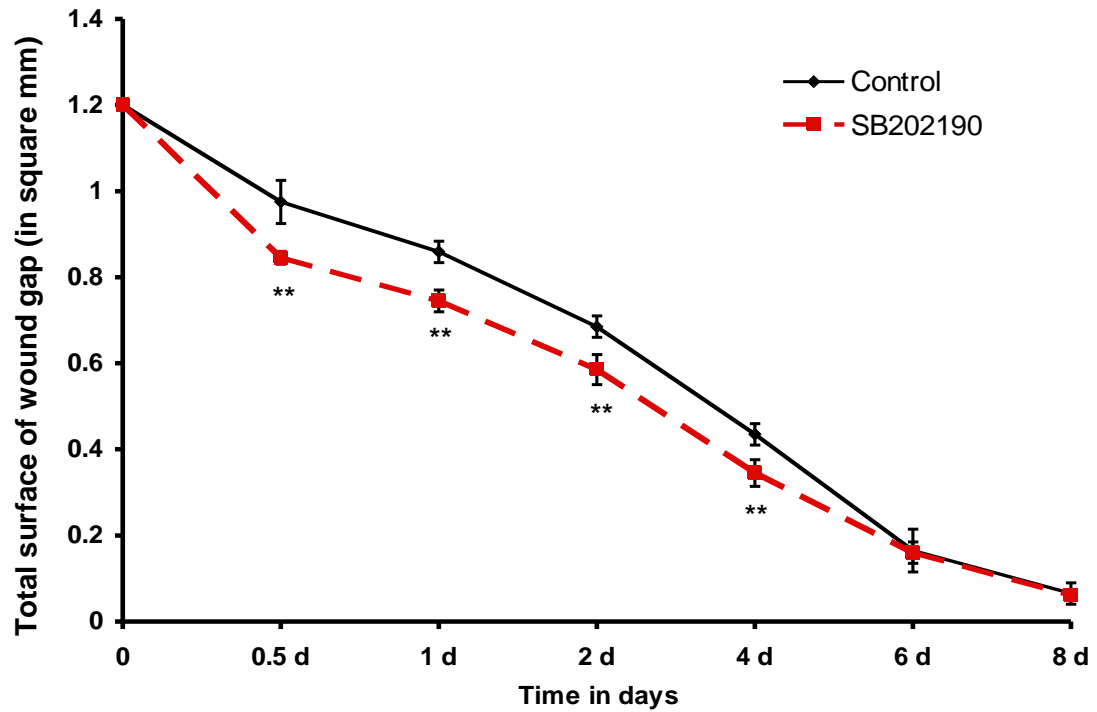


**Figure 60. Effect of SB 202190 treatment on the rate of wound closure in the micromass co-culture of 1 part FR 3T3 fibroblast and 3 part L8 myoblast cells.** *In vitro* micromass co-culture wound assay was performed to determine the effect of 10  $\mu$ M SB 202190 treatment on wound closure pattern. It was observed that there was significant acceleration in the total wound being covered following treatment with SB 202190 ( Mean  $\pm$  SD, \*\* indicates significant difference at p value < 0.01, n =16).

Treatment of wounded micromass co-cultures with p38 inhibitor, SB202190 resulted in acceleration of wound closure rate as compared to parallel control cultures that were administered with 0.1 % DMSO vehicle alone (**Figure 60**). Wound closure in SB202190 treated cultures was significantly higher than control cultures at 0.5, 1, 2 and 4-day time points after wounding (**Figure 60**,  $p < 0.01$ ,  $n = 16$ ). However by 6 days post wounding the extent of wound closure in control and SB 202190 treated cultures was equivalent.

#### **4.4.2. Effects of OTC and Quercetin on unwounded and wounded micromass co-cultures of 1 part FR fibroblast and 3 part L8 myoblast cells.**

The final objective of my thesis project was to test the utility of the newly developed micromass co-culture based wound repair model in preclinical drug development studies. OTC and quercetin are anti-inflammatory compounds that were used in our initial live animal studies to investigate their potential in ameliorating peridural scarring associated with spinal lumbar laminectomy surgery. As a follow up to our *in vivo* experiments, I examined the effects of OTC and quercetin on *in vitro* wound healing in our micromass co-culture model.

##### **4.4.2.1. Effect of OTC on collagen biosynthesis and DNA accumulation in the unwounded FR fibroblast : L8 myoblast micromass co-culture.**

Initial experiments examined the effects of OTC and quercetin on total collagen production and DNA accumulation in unwounded micromass co-cultures of 1part FR fibroblast and 3 parts L8 myoblast cells. The cultures were treated with varying doses of OTC (0, 0.25, 0.5, 1.0, 1.5 and 2.0 mM) or quercetin (0, 5, 10, 20, 40, 80  $\mu\text{M}$ ) and analyzed by fluorometric Hoechst DNA assay and picosirius red histochemical staining.

As shown in **Figure 61 A**, the micromass co-cultures that were treated with OTC at concentrations of 1.5 - 2.0 mM exhibited a dose dependent decrease in levels of both picosirius red stainable collagen and total DNA relative to untreated control cultures. ( $p < 0.01$ ,  $n = 16$ ). OTC concentrations of 0.25 –1.0 mM had no significant effect on either total collagen or DNA accumulation. When the levels of total collagen accumulation were normalized against total cellular DNA values there was a significant decrease in total collagen per microgram DNA at 1.5 mM and 2.0 mM OTC treatment doses relative to parallel control cultures (**Figure 61 B**,  $p < 0.05$ ,  $n = 16$ ).

To determine which of the two cell types (FR fibroblasts versus L8 myoblasts) within the micromass co-culture are most sensitive to OTC treatment, micromass cultures composed of FR fibroblast cells alone or L8 cells alone were also treated with different concentrations of OTC. In cultures of FR fibroblast cells alone, OTC treatment caused a dose dependent decrease in picosirius red stainable collagen levels at concentrations as low as 0.25 mM OTC (**Figure 62 A**,  $p < 0.05$ ,  $n = 16$ ), whereas total DNA levels decreased in a dose dependent manner starting at 0.5 mM OTC (**Figure 62 A**,  $p < 0.05$ ,  $n = 16$ ). Normalization of the collagen levels against total cellular DNA (**Figure 62 B**) revealed that there was a significant decrease in collagen accumulation per microgram DNA at all OTC doses from 0.25 - 2.0 mM, suggesting that OTC reduces collagen synthesis by FR fibroblast cells. In contrast, low concentrations of OTC (0.25 - 1.0 mM) had no significant effect on either total collagen or total DNA accumulation in micromass cultures composed of L8 myoblast cells alone (**Figure 63 B**). Only higher doses of OTC (1.5 - 2.0 mM) caused significant decreases in total DNA levels and collagen accumulation per microgram DNA (**Figures 63 A and 63 B**,  $p < 0.05$ ,  $n = 16$ ).

## FIGURE 61

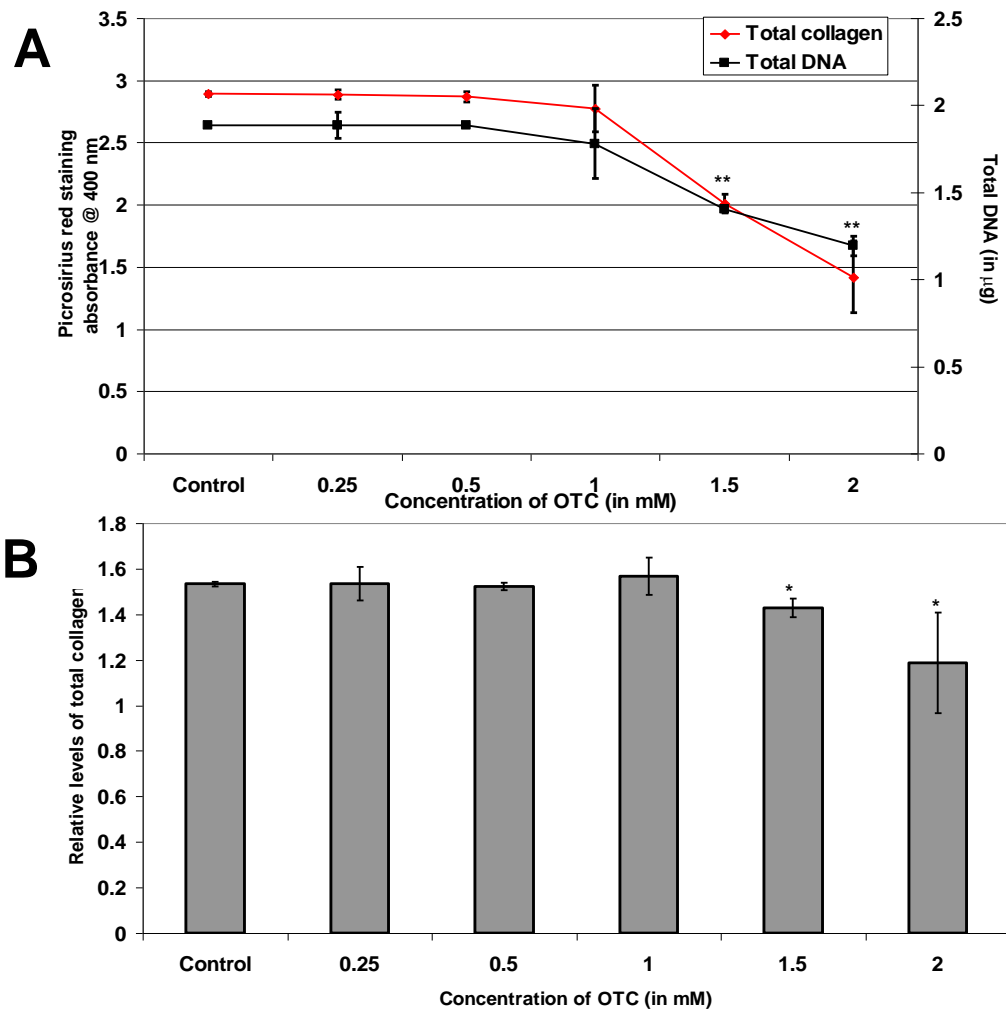


**Figure 61. Dose dependent effects of OTC on micromass co-cultures of 1 part FR 3T3 fibroblast and 3 part L8 myoblast cells.** Cultures were administered OTC at doses of 0.25-2.0 mM, parallel control cultures were maintained in standard medium (0 mM OTC). **(A)** shows total DNA and total collagen levels as determined by DNA Hoechst assay and picrosirius red staining, there is was a significant decrease in total DNA and absorbance reading for total collagen levels in both 1.5 mM and 2.0 mM OTC treated cultures. **(B)** shows the relative total collagen levels determined by normalizing with total DNA levels. It seems to suggest that there was a significant dose-dependent decrease in total collagen synthesis in both 1.5 mM and 2.0 mM OTC treated cultures. (Error bars represent Mean  $\pm$  SD, \* indicates significance at p value < 0.05 as compared to control and \*\* indicates significance at p value < 0.01, n =16).

**FIGURE 62**

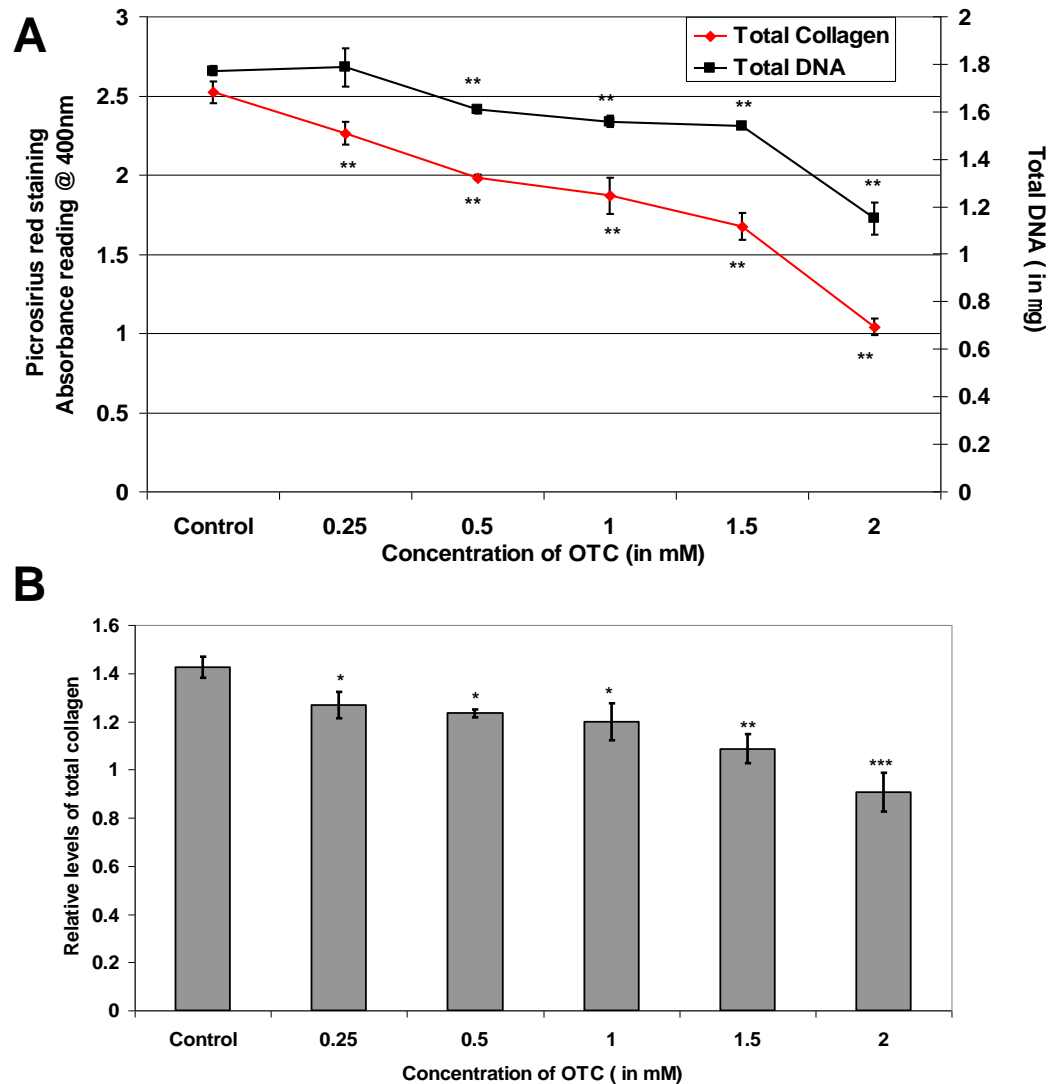


**Figure 62. Effect of OTC on FR 3T3 fibroblast micromass cultures.** Cultures were administered OTC at doses of 0.25-2.0 mM, parallel control cultures were maintained in standard medium (0 mM OTC). (A) shows total DNA and total collagen levels as determined by DNA Hoechst assay and picrosirius red staining, there is a dose dependent decrease in total DNA and absorbance reading for total collagen levels. (B) shows the relative total collagen levels determined by normalizing with total DNA levels. It seems to suggest that there was a significant dose-dependent decrease in total collagen synthesis. (Error bars represent Mean  $\pm$  SD, \* indicates significance at p value < 0.05 as compared to control and \*\* indicates significance at p value < 0.01, n =16).

## FIGURE 63

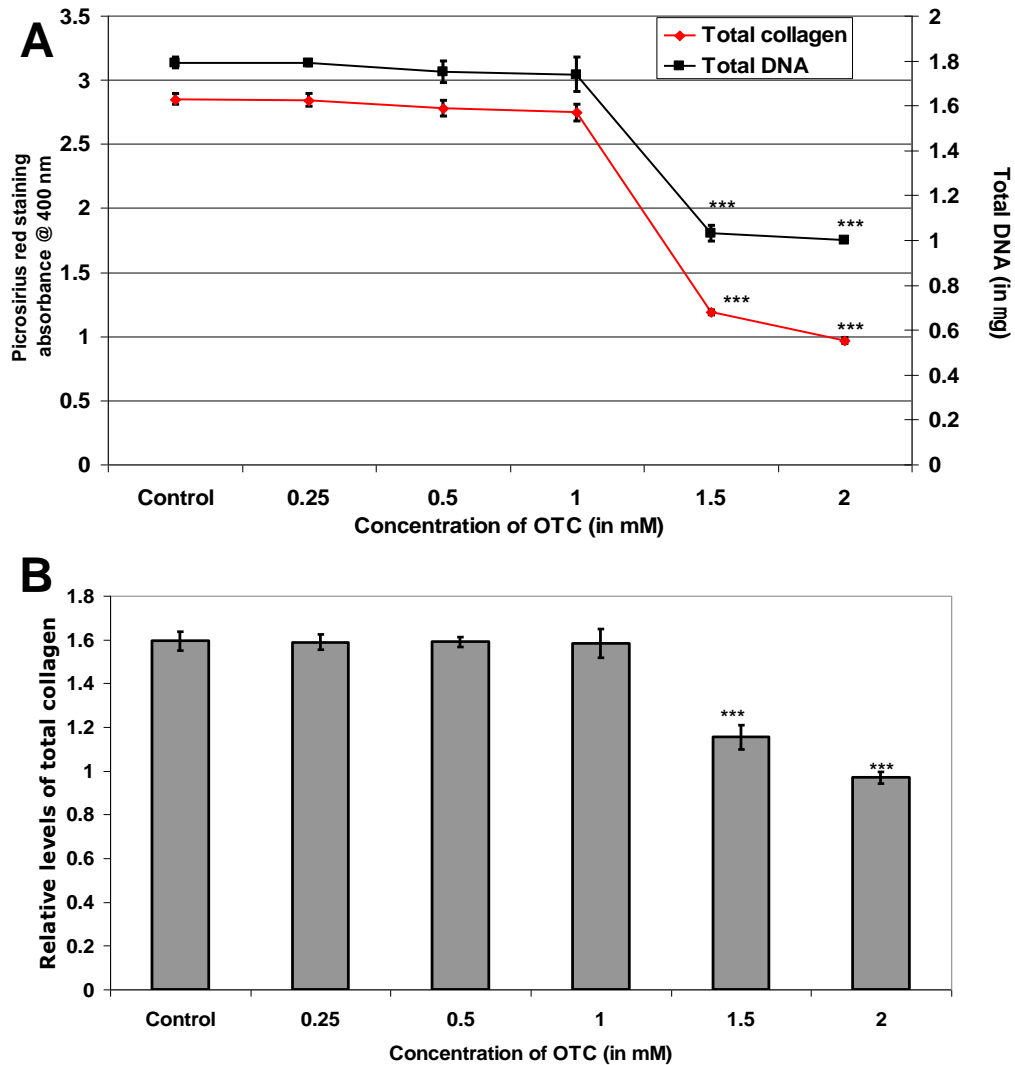


**Figure 63. Effect of OTC on L8 myoblast micromass cultures.** Cultures were administered OTC at doses of 0.25-2.0 mM, parallel control cultures were maintained in standard medium (0 mM OTC). (A) shows total DNA and total collagen levels as determined by DNA Hoechst assay and picrosirius red staining, there is was a significant decrease in total DNA and absorbance reading for total collagen levels in both 1.5 mM and 2.0 mM OTC treated cultures. (B) shows the relative total collagen levels determined by normalizing with total DNA levels. It seems to suggest that there was a significant dose-dependent decrease in total collagen synthesis in both 1.5 mM and 2.0 mM OTC treated cultures. (Mean  $\pm$  SD, \*\*\* indicates significance at p value  $<$  0.001, n =16).

The greater sensitivity of FR fibroblast cells to low doses of OTC in comparison to L8 myoblast cells is striking. The relatively high proportion of L8 myoblast cells in our 1:3 FR fibroblast: L8 myoblast co-cultures would account for the observation that OTC doses of 1.5 - 2.0 mM were required to significantly reduce collagen and DNA accumulation in these co-cultures.

#### **4.4.2.2. Effects of Quercetin on collagen biosynthesis and DNA accumulation in unwounded 1:3 FR fibroblast and L8 myoblast micromass co-cultures.**

When micromass co-cultures of 1:3 ratio FR fibroblast and L8 myoblast cells were treated with various doses of quercetin, it was observed that the total DNA levels as well as levels of picosirius red stainable collagen were significantly decreased in cultures treated with 40  $\mu$ M and 80  $\mu$ M quercetin as compared to control untreated cultures (**Figure 64 A**,  $p < 0.05$ ,  $n = 16$ ). Normalized collagen accumulation per microgram DNA was also significantly decreased by treatment with 40  $\mu$ M and 80  $\mu$ M quercetin (**Figure 64 B**,  $p < 0.01$ ,  $n = 16$ ), while quercetin doses below 20  $\mu$ M had no significant effect on either collagen or total DNA accumulation.

To determine whether quercetin had differential effects on DNA accumulation and collagen synthesis by the two cell types comprising the micromass co-cultures, we also tested cultures composed of either FR fibroblasts or L8 myoblasts alone. In micromass cultures of FR fibroblasts alone, there was a dose dependent decrease in the levels for picosirius red stainable collagen beginning at a quercetin doses of 5  $\mu$ M, while there was a dose dependent decrease in total DNA at quercetin doses of 10  $\mu$ M and above (**Figures 65 A and 65 B**,  $p < 0.05$ ,  $n = 16$ ).

## FIGURE 64

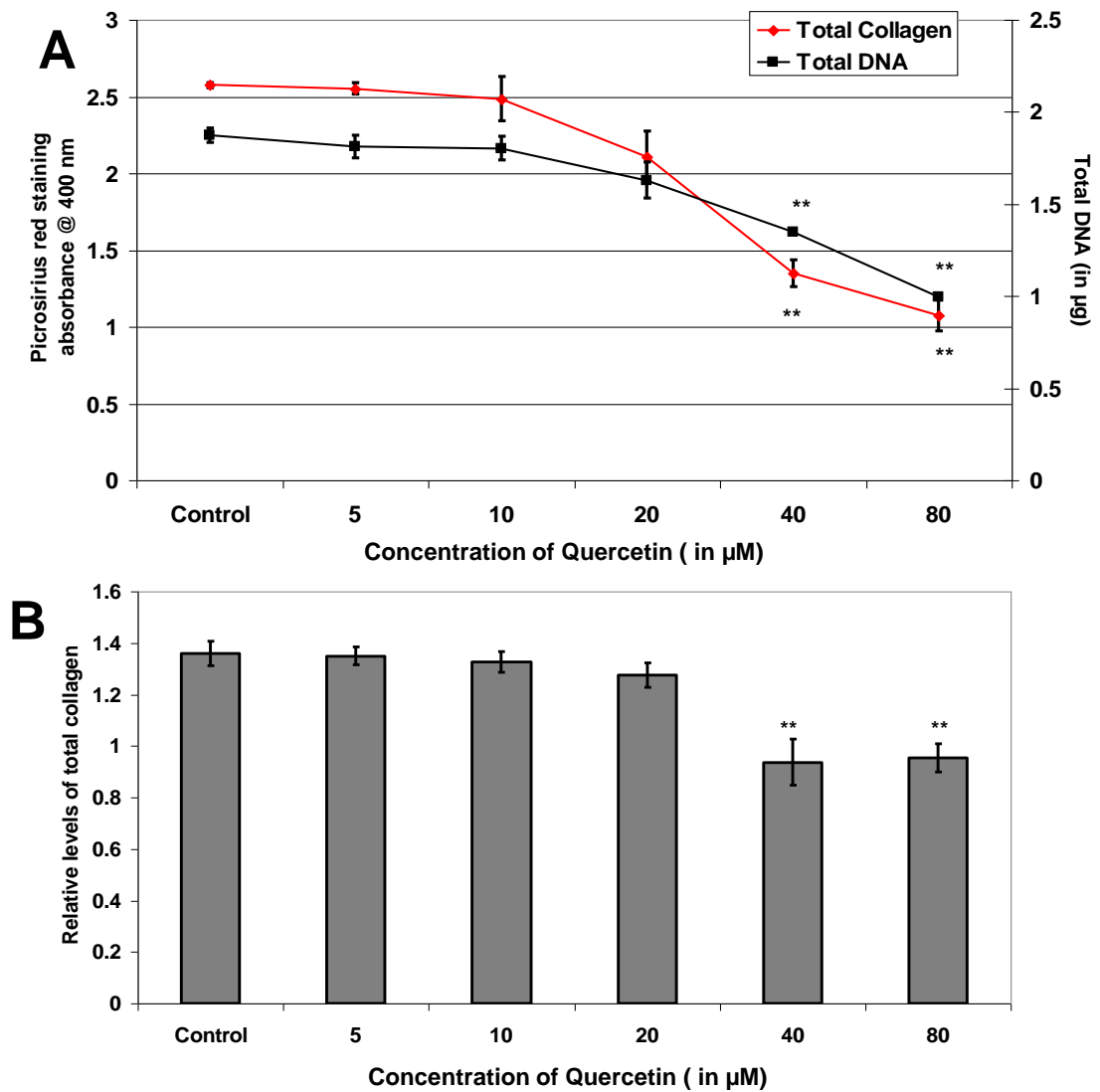


**Figure 64. Effect of Quercetin on the micromass co-culture of 1 part FR 3T3 fibroblast and 3 part L8 myoblast cells.** (A) shows total DNA and total collagen levels as determined by DNA Hoechst assay and picrosirius red staining, there is was a significant decrease in total DNA and absorbance reading for total collagen levels in both 40  $\mu\text{M}$  and 80  $\mu\text{M}$ . Quercetin treated cultures. (B) shows the relative total collagen levels determined by normalizing with total DNA levels. It seems to suggest that there was a significant dose-dependent decrease in total collagen synthesis in both 40  $\mu\text{M}$  and 80  $\mu\text{M}$  Quercetin treated cultures. ( Mean  $\pm$  SD, \*\* indicates significance at p value  $<$  0.01, n =16).

## FIGURE 65

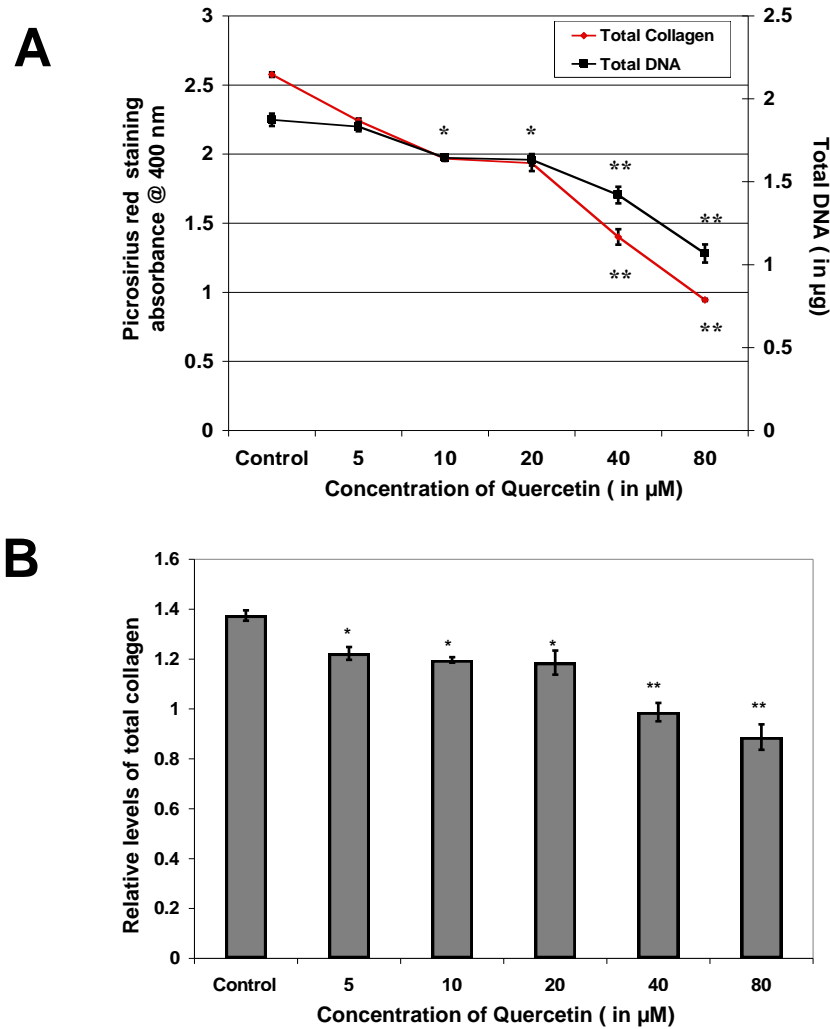


**Figure 65. Effect of Quercetin on FR 3T3 fibroblast micromass cultures.** (A) shows total DNA and total collagen levels as determined by DNA Hoechst assay and picrosirius red staining, there is was a significant dose dependent decrease in total DNA and absorbance reading for total collagen levels. (B) shows the relative total collagen levels determined by normalizing with total DNA levels. It seems to suggest that there was a significant dose-dependent decrease in total collagen synthesis. (Mean  $\pm$  SD, \*\* indicates significance at p value  $< 0.01$ , \* indicates significance at p value  $< 0.05$ , n = 16).

## FIGURE 66

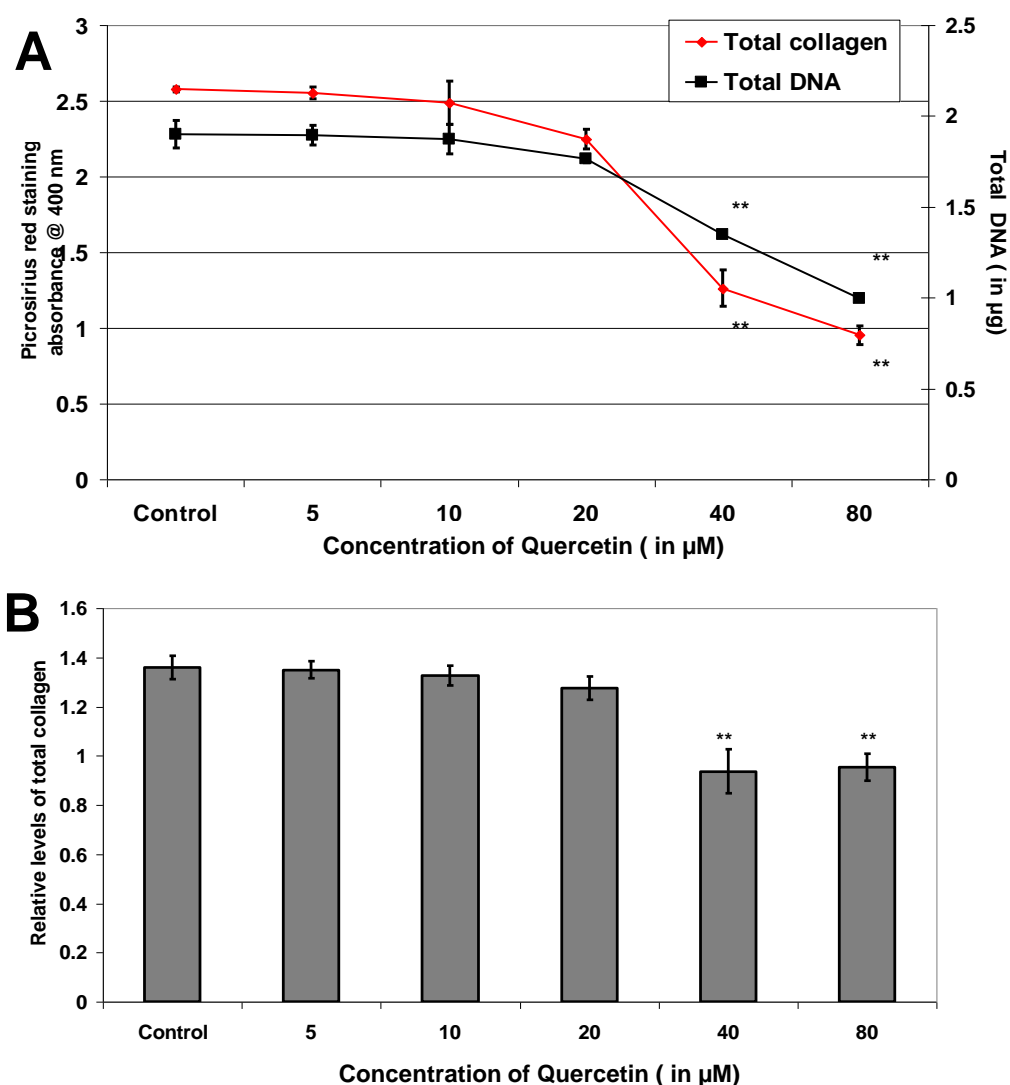


**Figure 66. Effect of Quercetin on L8 myoblast micromass cultures.** (A) shows total DNA and total collagen levels as determined by DNA Hoechst assay and picrosirius red staining, there is was a significant decrease in total DNA and absorbance reading for total collagen levels in both 40  $\mu\text{M}$  and 80  $\mu\text{M}$  Quercetin treated cultures. (B) shows the relative total collagen levels determined by normalizing with total DNA levels. It seems to suggest that there was a significant dose-dependent decrease in total collagen synthesis in both 40  $\mu\text{M}$  and 80  $\mu\text{M}$  Quercetin treated cultures. (Mean  $\pm$  SD,  $p < 0.05$  considered significant,  $n = 16$ ).

In contrast, higher doses of 40  $\mu\text{M}$  - 80  $\mu\text{M}$  quercetin were required to inhibit total collagen and DNA accumulation in micromass cultures composed of L8 myoblast cell alone (**Figure 66 A**,  $p < 0.05$   $n = 16$ ). Normalized collagen accumulation per microgram DNA showed a dose-dependent decrease in relative total collagen levels starting from 40  $\mu\text{M}$  concentration of quercetin (**Figure 66 B**,  $p < 0.01$ ,  $n = 16$ ).

Accordingly, quercetin doses between 5  $\mu\text{M}$  - 20  $\mu\text{M}$  were sufficient to reduce collagen synthesis in FR fibroblast cells, while higher quercetin doses (40  $\mu\text{M}$  and above) was required to reduce collagen synthesis in the L8 myoblast cells. Again, the relatively high proportion of L8 myoblast cells in our 1:3 FR fibroblast: L8 myoblast co-cultures would account for the observation that quercetin doses of 40  $\mu\text{M}$  and above were required to significantly reduce collagen and DNA accumulation in the co-culture model.

#### **4.4.2.3 Effects of OTC and Quercetin on wound closure in the wounded micromass co-culture of 1 part FR fibroblast cells and 3 part L8 myoblast cells.**

Experiments were performed to determine whether OTC and quercetin treatment affected the rate of wound closure in micromass co-cultures of 1:3 ratio FR fibroblast and L8 myoblast cells. Phase contrast microscopy and a quantitative wound closure assay were performed to examine the extent of wound closure as a function of time in wounded micromass cultures treated with 1.5 mM OTC, 40  $\mu\text{M}$  quercetin and a combination of 1.5 mM OTC and 40 mM quercetin. These doses were chosen based on our previous finding that concentrations of 1.5 mM OTC and 40  $\mu\text{M}$  quercetin were effective in reducing total accumulation and collagen deposition in micromass co-cultures. Phase contrast images of OTC treated cultures and control cultures treated with vehicle alone showed generally

## FIGURE 67

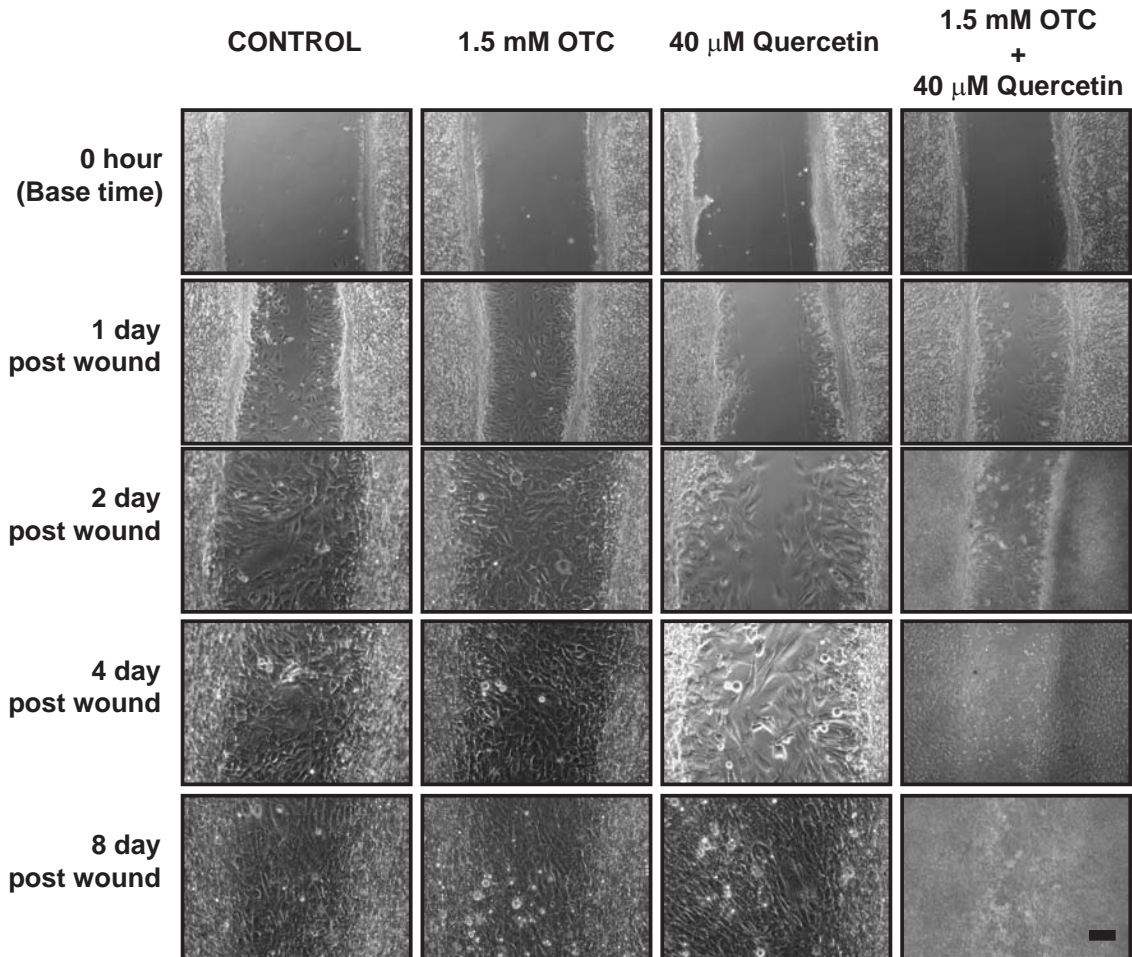


**Figure 67. Effect of OTC and Quercetin on wound closure in the wounded micromass co-culture of 1 part FR 3T3 and 3 part L8 myoblast cells.** Phase contrast images were taken from the same wounded cultures at different time points to show time-scale changes to the wound closure pattern for the wounded micromass cultures were treated with either 1.5 mM OTC or 40  $\mu$ M Quercetin or a mixture of 1.5 mM OTC and 40  $\mu$ M Quercetin. The Quercetin treated cultures showed a delay in the wound closure as compared to Control (untreated), while OTC treated cultures shows similar wound closure as compared to Control (untreated) cultures. Quercetin treated cultures showed some contraction at the edges and this was consistent in almost all cultures treated with Quercetin. However, the cultures treated with mixture of OTC and Quercetin showed initial delay in closure of wound without any wound contraction as seen with Quercetin treated cultures until 2 day post-wounding after which the cultures seem to recover to wound closure pattern as that of control untreated cultures. Scale corresponds to 100 microns.

## FIGURE 68

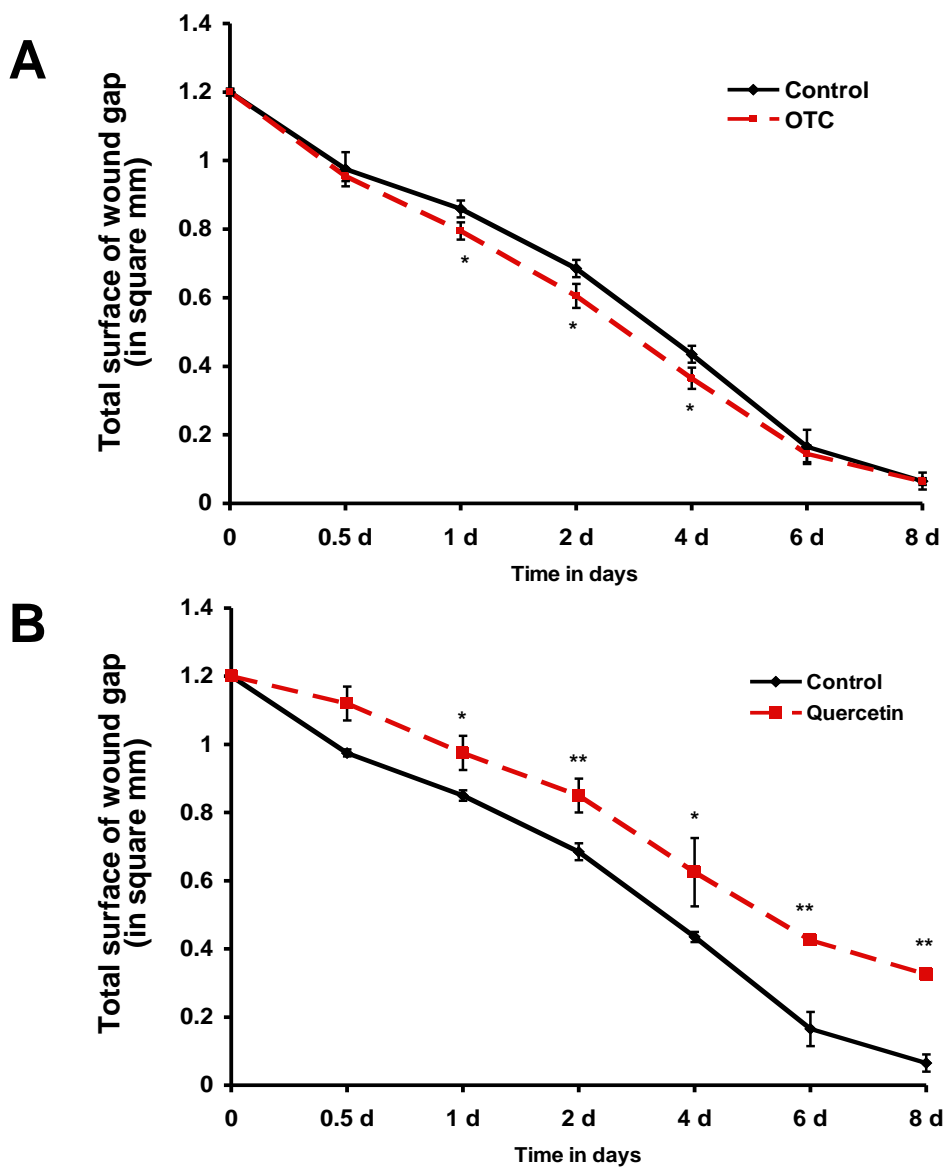


**Figure 68. Effect of OTC and Quercetin on wound closure pattern (A)** the wounded micromass cultures were treated with 40  $\mu$ M Quercetin, show a delay in the wound closure as compared to control untreated wounded cultures (**B**) when the wounded micromass cultures were treated with 1.5 mM OTC, there was significant acceleration in the wound closure as compared to control untreated wounded cultures. (Mean  $\pm$  SD, \*\* indicates significance at p value < 0.01, while \* indicates significance at p value < 0.05, n = 4)

**FIGURE 69**

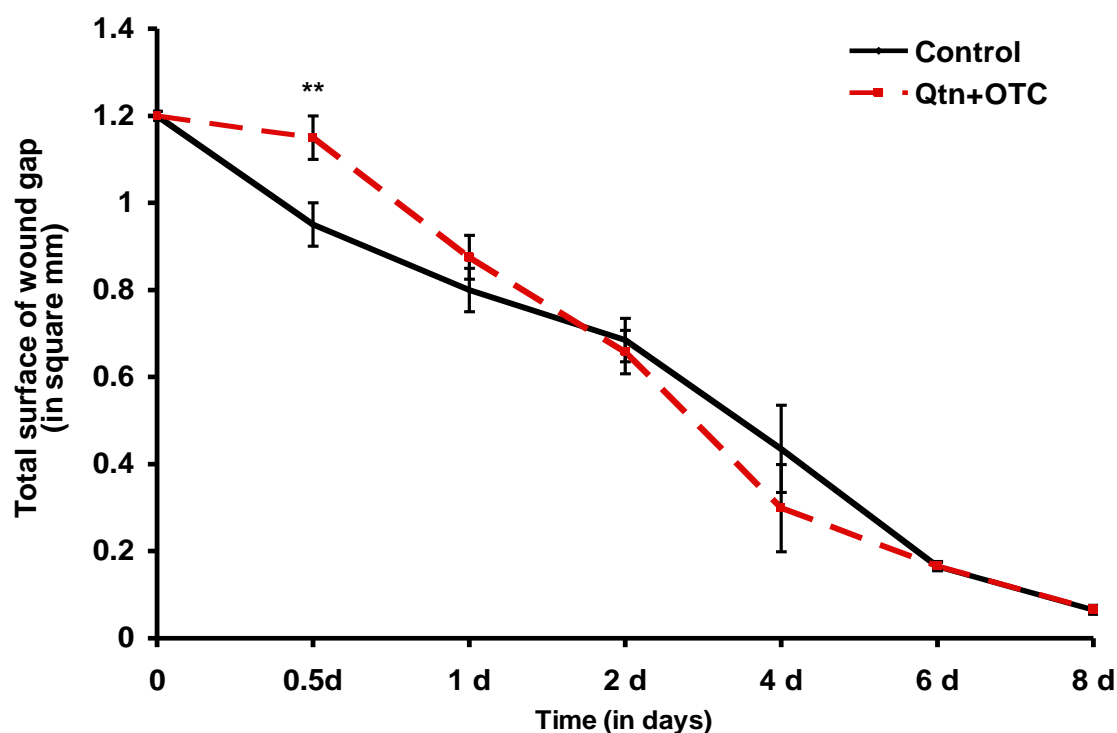


**Figure 69. Effect of the mixture of Quercetin and OTC on wounded micromass co-culture of 1 part FR 3T3 fibroblast and 3 part L8 myoblast cells.** When the wounded cultures were treated with a mixture of 40  $\mu$ M Quercetin and 1.5 mM OTC, I observed an initial delay in the wound closure pattern as compared to control untreated wounded cultures after which the wound closure pattern recovered to that of control untreated wounded cultures. (Mean  $\pm$  SD, \*\* indicates significance at p value < 0.01, n =6).

similar trends in cell movement into the wound gap over the time (**Figure 67**). However quantitative image analysis revealed a slight acceleration in the rate of wound closure in micromass co-cultures treated with 1.5 mM OTC as compared to control cultures administered vehicle alone (**Figure 68 A**,  $p < 0.05$ ,  $n = 4$ ).

Phase contrast observations suggested that 40  $\mu\text{M}$  quercetin treatment of wounded micromass cultures delayed movement of cells into the wound gap at 1-2 days post-wounding as compared to control cultures (**Figure 67**). The quantitative wound closure assay confirmed that there were significant delays in wound closure in cultures treated with 40  $\mu\text{M}$  quercetin treated wounded cultures as compared to control vehicle treated wounded cultures relative to controls (**Figure 68 B**,  $p < 0.05$  considered significant,  $n = 4$ ). When wounded micromass co-cultures were treated with a combination of 1.5 mM OTC and 40  $\mu\text{M}$  quercetin, there were slight delays in wound closure at the 0.5 day time-point, however the extent of wound closure recovered to that of untreated control cultures (**Figure 67 and 69**). The initial delay in wound closure might be due to quercetin exerting its effects during the initial wound healing process, whereas the recovery of wound closure at later time points might reflect the counteracting effects of OTC.

#### **4.4.2.4. Effects of OTC and Quercetin on p38 MAPK and ERK 1/2 activation in wounded micromass co-cultures of 1 part FR fibroblast cells and 3 parts L8 myoblast cells.**

In our live animal studies, OTC treatment reduced both p38 MAPK and ERK1/2 activation in peridural scar tissue, while quercetin had no effect on either p38MAPK or ERK1/2 activation within peridural scar tissue. Therefore, experiments were performed to determine whether OTC and quercetin treatment would influence MAPK activation in the

micromass co-culture wound model. The wounded cultures were treated with 40  $\mu\text{M}$  quercetin or 1.5 mM OTC and western blotting was performed to determine the levels of phosphorylated ERK1/2 and p38 MAPK proteins. As seen in **Figure 70**, micromass co-cultures treated with 1.5 mM OTC exhibited significantly lower expression of active dual phosphorylated p38 MAPK at 5 minutes post wounding in comparison to parallel control cultures ( $p < 0.05$ ,  $n = 8$ ).

In contrast, 40  $\mu\text{M}$  quercetin had no effect on the expression level of active dual phosphorylated p38 MAPK relative to wounded control cultures at 5 min post wounding (**Figure 70**). Phosphorylated p38 MAPK was undetectable at 1 h, 1 d, 2 d, 4 d and 8-day time points after wounding in control, OTC and quercetin treated cultures although total p38 protein was present (data not shown).

Western blot analysis indicated that levels of dual phosphorylated ERK1/2 expression were significantly reduced at 5 min post wounding in OTC treated cultures relative to wounded cultures (**Figure 71**,  $p < 0.05$ ,  $n = 8$ ). Cultures treated with quercetin also showed significantly decreased levels of active dual phosphorylated ERK1/2 at 5 min post wounding in comparison to wounded control cultures, however ERK1/2 expression was lower than that of control cultures at subsequent time points (**Figure 71**). This experiment suggests that OTC administration depresses both the ERK and p38 MAPK signaling pathways while quercetin inhibits ERK1/2 signaling alone.

## FIGURE 70

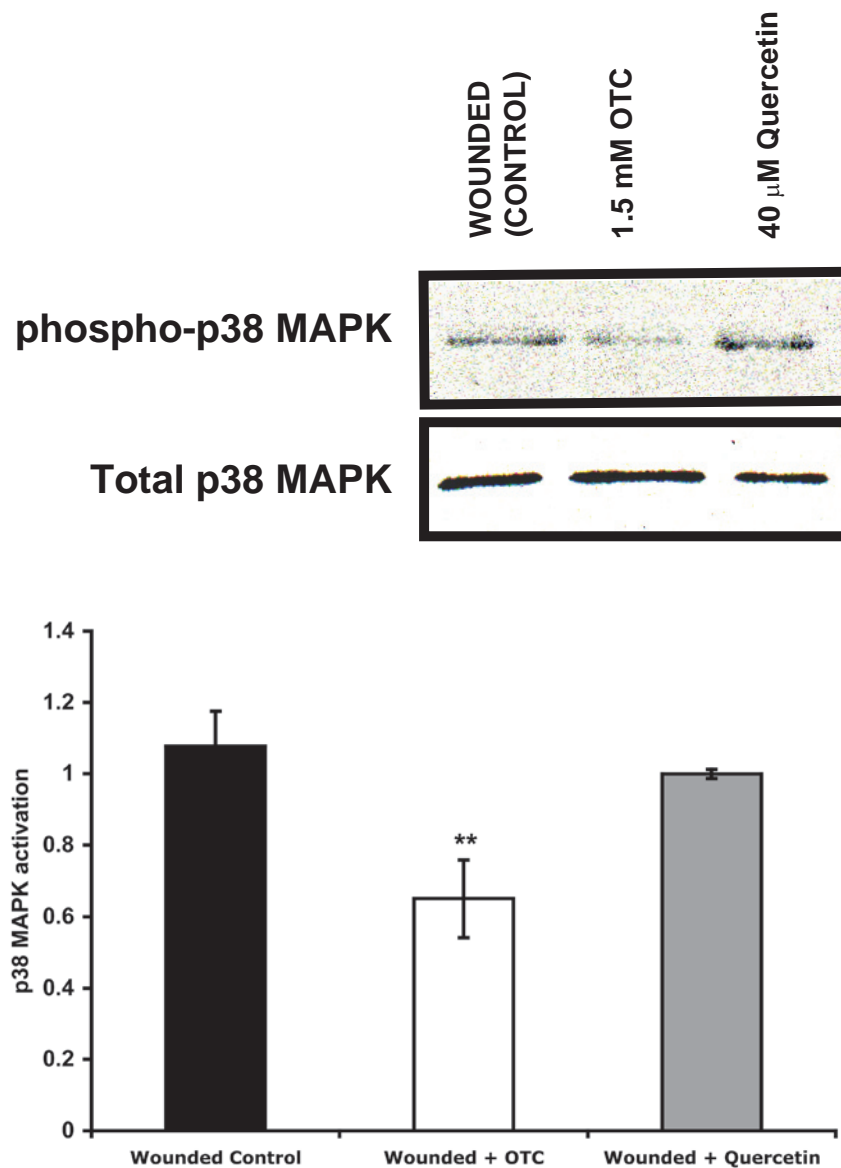


**Figure 70. Effect of OTC and Quercetin on the expression of dual phosphorylated p38 MAPK in the 5 minute post-wounded micromass co-cultures of 1 part FR 3T3 and 3 part L8 myoblast cells.** Dual phosphorylated p38 MAPK was expressed in both quercetin and OTC treated wounded cultures with OTC treated wounded cultures showing lower levels of p38 MAPK expression as compared to untreated control wounded cultures. However expression of total p38 MAPK protein was equivalent in all treated cultures. On densitometric analysis using NIH Image J software, the OTC treated wounded cultures showed significantly lower p38 MAPK activation as compared to untreated control cultures. However p38 MAPK activation was similar in both quercetin treated and untreated control wounded cultures ( Mean  $\pm$  SD, \*\* indicates significance at p value < 0.01, n =8)

# FIGURE 71

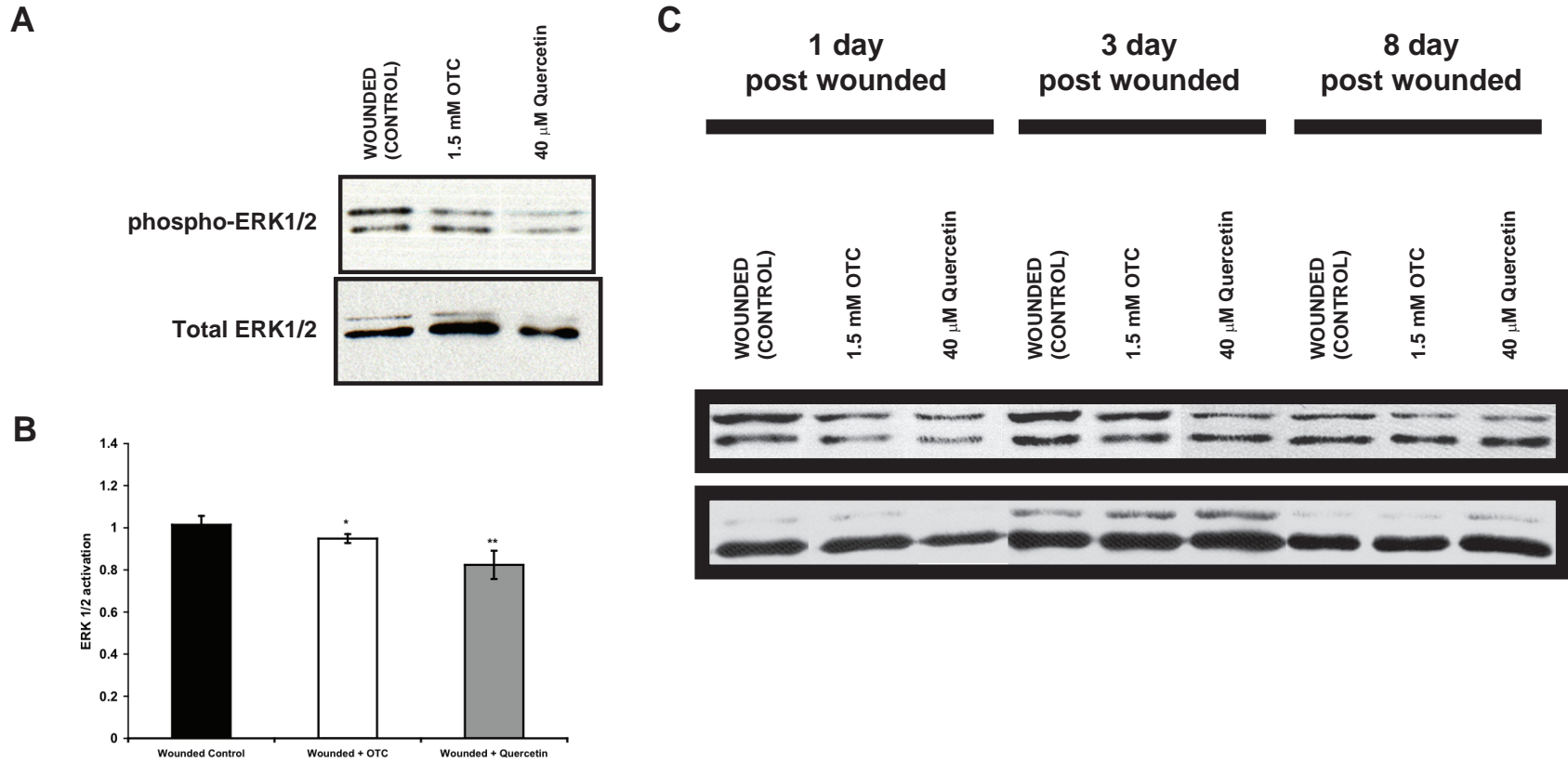


**Figure 71. Effect of OTC and Quercetin on the expression of dual phosphorylated ERK1/2 in the 5 minute, 1 day, 3 day and 8 day post-wounded micromass co-cultures of 1 part FR 3T3 and 3 part L8 myoblast cells. (A)** The quercetin treated cultures at 5 min post wounding showed significantly lower levels of dual phosphorylated ERK1/2 as compared to control untreated wounded cultures however **(B)** When densitometric analysis was performed using NIH Image J software to determine the ERK1/2 activation levels, both quercetin and OTC treated cultures at 5 min post wounding showed significant decrease in ERK1/2 activation as compared to untreated control cultures **(C)** Total p44/42 MAPK (ERK1/2) was expressed in all treatment groups at all time points, while no change in expression of dual phosphorylated ERK1/2 was observed in 1 day, 3 day, and 8 day post wounded OTC or quercetin treated wounded cultures (Mean  $\pm$  SD, \*\* indicates significance at p value < 0.01, while \* indicates significance at p value < 0.05, n = 8).

#### **4.4.2.5. Effect of OTC and Quercetin on the genes involved in tissue repair and regeneration within wounded micromass co-cultures of 1 part FR fibroblast and 3 parts L8 myoblast cells.**

Our wound closure assay data suggested that at 2 d to 4 day post injury there are major changes occurring in the rate of wound closure in the micromass co-culture model. Moreover, RT-PCR data on wounded micromass co-cultures suggested that gene transcript levels for RHAMM, HAS 1, HAS 3, hsp-47, collagen 1 ( $\alpha 2$ ), collagen 3 ( $\alpha 1$ ) and collagen 4( $\alpha 1$ ) were increased at the 2 – 4 day time points. Hence, I wished to determine whether OTC and quercetin treatments altered levels of expression of the gene transcripts for TGF- $\beta 3$ , TGF- $\beta 1$ , RHAMM, CD 44, HAS 1, HAS 3, hsp-47, collagen 4 ( $\alpha 1$ ), collagen 3 ( $\alpha 1$ ) and collagen 1 ( $\alpha 2$ ) genes in patterns that might account for their opposing effects on wound closure in the micromass co-culture model.

Semiquantitative RT-PCR was performed as described in Section 3.2.9 to analyze levels of TGF- $\beta 3$ , TGF- $\beta 1$ , RHAMM, CD 44, HAS 1, HAS 3, hsp-47, collagen 4 ( $\alpha 1$ ), collagen 3 ( $\alpha 1$ ) and collagen 1 ( $\alpha 2$ ) gene transcripts in wounded micromass co-cultures treated for 2 or 4 days with 1.5 mM OTC or 40  $\mu$ M quercetin (**Figure 72**). The amplified collagen 1 ( $\alpha 2$ ), collagen 3 ( $\alpha 1$ ), collagen 4 ( $\alpha 1$ ), hsp-47, HAS 1, HAS 3, RHAMM, CD 44, TGF- $\beta 1$ , TGF- $\beta 3$  and GAPDH sequences were separated on agarose gels (**Figure 72**) and the relative band intensities for each gene were quantified densitometrically using NIH Image J software and normalized against the intensity of the corresponding GAPDH band (**Figure 73**). The appropriate number of PCR cycles for each gene of interest was determined in earlier experiments (see **Section 4.4.1.1.5**). It was observed that the wounded cultures treated with OTC showed changes in the expression of RHAMM, HAS 3, CD 44, HAS 1 and Collagen 3 ( $\alpha 1$ ) gene transcripts between 2 day and 4 day post

wounded cultures (**Figure 73 A** and **Figure 73 B**). The wounded cultures treated with quercetin showed changes in the expression of CD 44, HAS 1 and Collagen 3 ( $\alpha 1$ ) gene transcripts between 2 day and 4 day post wounded cultures (**Figure 73 A** and **Figure 73 B**). The changes in the gene transcript levels of collagen 1 ( $\alpha 2$ ), collagen 3 ( $\alpha 1$ ), collagen 4 ( $\alpha 1$ ), hsp-47, HAS 1, HAS 3, RHAMM, CD 44, TGF- $\beta 1$ , TGF- $\beta 3$  in 2 day and 4 day post wounded cultures treated with OTC and quercetin are summarized in **Table 7**.

The 2 day post wounded cultures treated with 1.5 mM OTC showed significantly lower levels of TGF- $\beta 1$ , CD-44, HAS-1, collagen type 4 ( $\alpha 1$ ), collagen type 3 ( $\alpha 1$ ), collagen type 1 ( $\alpha 2$ ) as compared to untreated wounded control cultures (**Figure 73 A**,  $p < 0.01$ , **Table 7**), while significantly higher levels of RHAMM, HAS-3 and hsp-47 was observed in OTC treated cultures as compared to controls. TGF- $\beta 3$  gene transcript levels were similar in OTC treated and control cultures at 2 days post wounding.

The 4 day post wounded cultures treated with 1.5 mM OTC showed significantly lower levels of RHAMM, HAS 3, collagen type 4 ( $\alpha 1$ ) and collagen type 1 ( $\alpha 2$ ) (**Figure 73 B**,  $p < 0.01$  and **Table 7**) relative to untreated control cultures, while TGF- $\beta 1$ , CD 44, HAS 1 and collagen type 3 ( $\alpha 1$ ) transcript levels were higher. TGF- $\beta 3$  and hsp-47 levels were unchanged in OTC treated cultures at 4 days post wounding.

The 2 day post wounded cultures treated with 40  $\mu$ M quercetin showed significantly lower levels of TGF- $\beta 1$ , HAS 1, collagen type 3 ( $\alpha 1$ ) and collagen type 1 ( $\alpha 2$ ) as compared to control untreated wounded cultures (**Figure 73 A**,  $p < 0.01$  and **Table 7**) while higher levels of RHAMM, CD 44, HAS 3 and hsp-47 were observed in quercetin post wounded cultures treated with 40  $\mu$ M quercetin showed significantly lower levels of CD44 (**Figure 73 B**,  $p < 0.01$  and **Table 7**) though RHAMM, HAS 1, collagen

## FIGURE 72

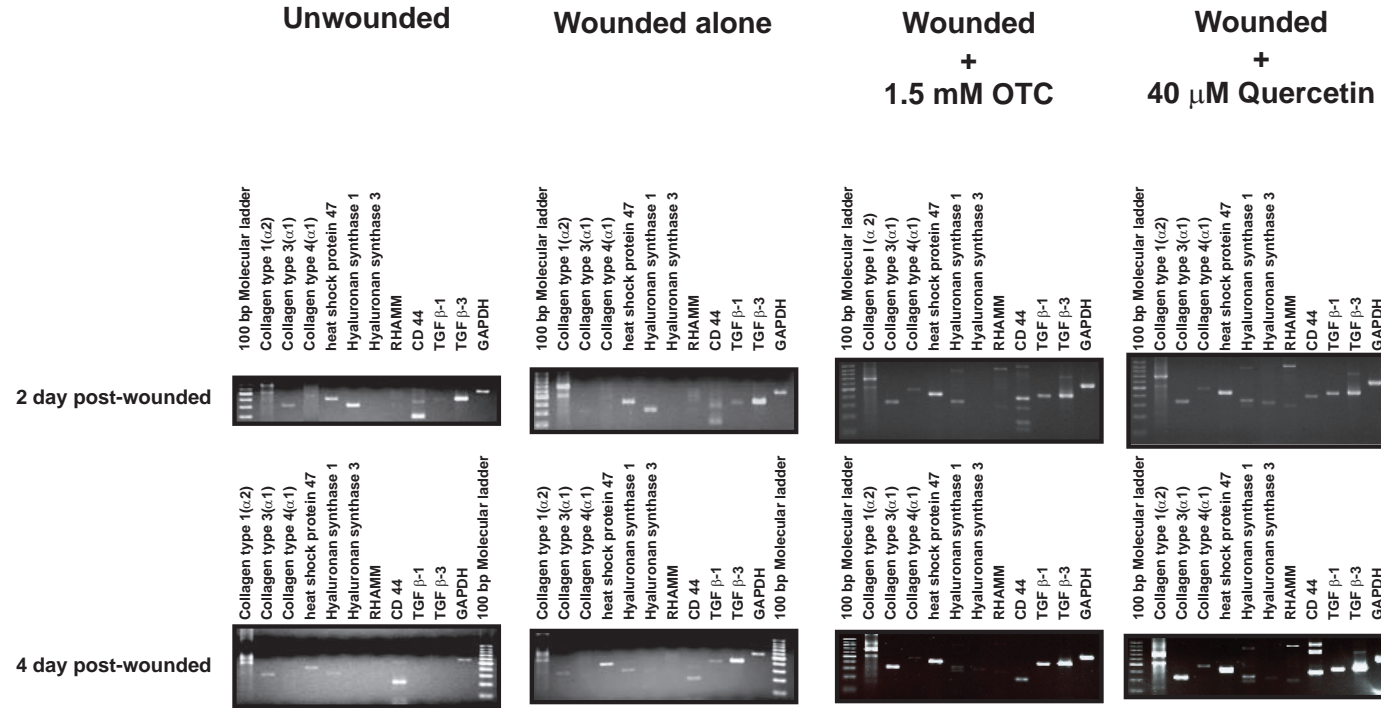
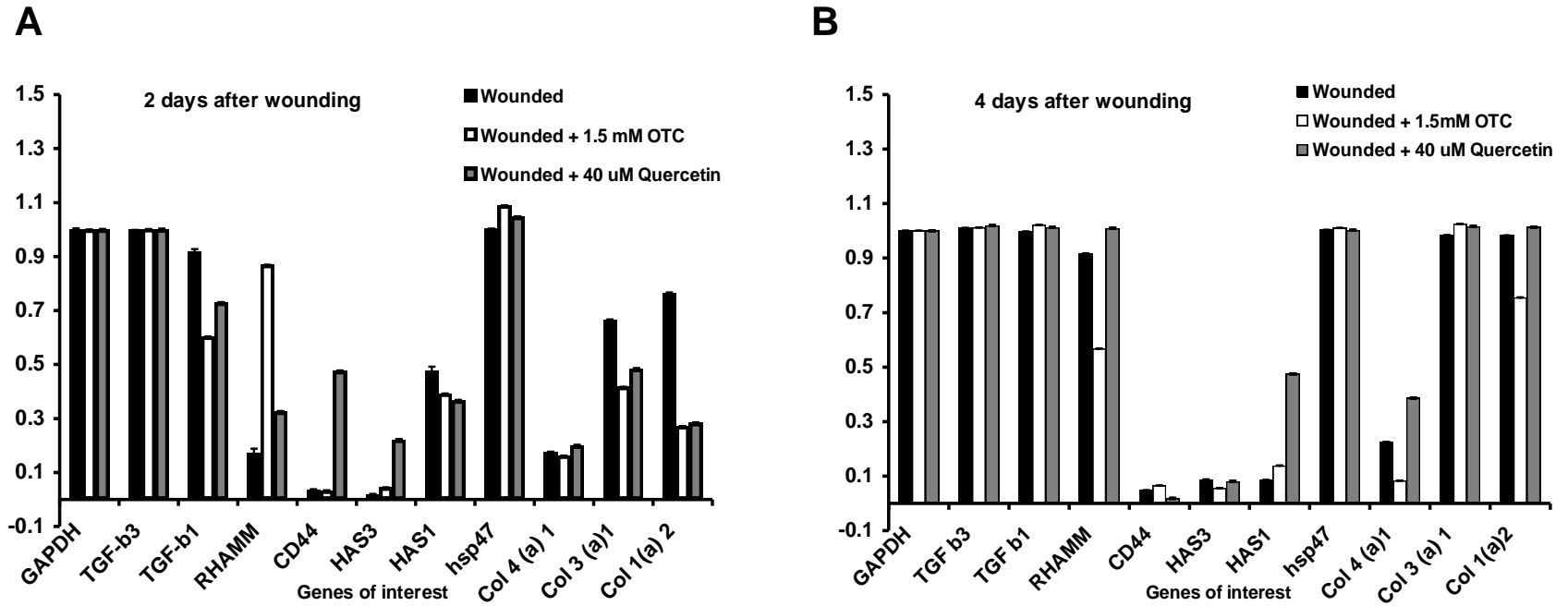


Figure 72. RT-PCR DNA Agarose gels showing relative band intensities for Collagen type 1( $\alpha$ 2), Collagen type 3( $\alpha$ 1) and Collagen type 4( $\alpha$ 1) Hyaluronan synthase 1, Hyaluronan synthase 2, Hyaluronan synthase 3, Receptor for hyaluronan-mediated motility (RHAMM), CD 44, Transforming growth factor  $\beta$ -1, Transforming growth factor  $\beta$ -3, heat shock protein 47 (hsp-47) and Glyceraldehyde-3-phosphate dehydrogenase (GAPDH) in unwounded and wounded micromass cultures treated with and without 1.5 mM OTC and 40  $\mu$ M Quercetin.

# FIGURE 73

223



**Figure 73. Effect of Quercetin and OTC on the genes involved in tissue repair and regeneration in the wounded micromass co-culture of 1 part FR fibroblast and 3 part L8 myoblast cells.** Expression profile of GAPDH, TGF β3 and β1, RHAMM, CD 44, HAS 3, HAS 1, hsp 47, Collagen type 4(α1)[Col 4 (a) 1], Collagen type 3(α1) [Col 3 (a) 1], and Collagen type 1(α2) [Col 1 (a) 2], were determined using semiquantitative RT-PCR. **A.)** Shows the relative expression levels of the genes of interest in the 2 day post-wounded cultures. Both OTC and Quercetin treated cultures showed decreased Collagen type 4(α1), Collagen type 3(α1) and Collagen type 1(α2) expression levels with respect to wounded and unwounded cultures while Quercetin treated cultures showed increased CD44 expression as compared to unwounded, wounded and OTC treated wounded cultures.**B.)** shows the relative expression levels of the genes of interest in the 4 day post wounded micromass co-cultures. Quercetin treated cultures showed increased RHAMM expression as compared to OTC treated cultures and untreated wounded culture. (Kruskal Wallis non parametric One way ANOVA; Mean ± SD, p < 0.01, considered significant, n=4)

**TABLE. 7. Effect of OTC and quercetin treatment on the relative gene transcript levels in the wounded micromass co-culture.** The gene transcript levels of TGF- $\beta$ 3, TGF- $\beta$ 1, RHAMM, CD 44, HAS 1, HAS 3, hsp-47, Collagen 4( $\alpha$ 1), Collagen 3( $\alpha$ 1) and Collagen 1( $\alpha$ 2) were determined using semi-quantitative RT-PCR and the relative gene transcript levels were compared with vehicle (control) treated wounded micromass co-culture for 2 day and 4 day post wounding.

Treatments	Time of culture (after wounding)	Relative gene transcript levels		
		Increased gene transcript levels	Decreased gene transcript levels	Unaffected gene transcripts
1.5 mM OTC	2 day	RHAMM HAS 3 Hsp-47	TGF- $\beta$ 1 CD 44 HAS 1 Collagen 3( $\alpha$ 1) Collagen 4( $\alpha$ 1) Collagen 1( $\alpha$ 2)	TGF- $\beta$ 3
	4 day	TGF- $\beta$ 1 CD 44 HAS 1 Collagen 3( $\alpha$ 1)	RHAMM HAS 3 Collagen 4( $\alpha$ 1) Collagen 1( $\alpha$ 2)	TGF- $\beta$ 3 Hsp-47
40 $\mu$ M Quercetin	2 day	RHAMM CD 44 HAS 3 Hsp-47	TGF- $\beta$ 1 HAS 1 Collagen 3( $\alpha$ 1) Collagen 1( $\alpha$ 2)	TGF- $\beta$ 3, Collagen 4 ( $\alpha$ 1)
	4 day	RHAMM HAS 1 Collagen 4( $\alpha$ 1) Collagen 3( $\alpha$ 1)	CD 44	TGF- $\beta$ 3 TGF- $\beta$ 1 HAS 3 Hsp-47 Collagen 1 ( $\alpha$ 1)

type 4 ( $\alpha$ 1) and collagen type 3 ( $\alpha$ 1) transcript levels were significantly higher than in corresponding control cultures. TGF- $\beta$ 1, TGF- $\beta$ 3, HAS 3, hsp-47 and collagen type 1 ( $\alpha$ 2) transcript levels were unaffected by quercetin treatment at the 4 day time point.

## CHAPTER 5. DISCUSSION

### 5.1 Outcome of the *in vivo* studies using rat spinal laminectomy model

The first objective of this project was to determine the effects of quercetin and L-2-oxothiazolidine-4-carboxylate (OTC) on collagen distribution and biosynthesis within an *in vivo* model of peridural scar formation, the rat spinal laminectomy model. The changes in potential regulatory molecules (e.g. TGF- $\beta$ s, ERK1/2 and p38 MAP kinases) involved in the tissue repair were also examined in this animal model. The outcomes of these live animal studies are discussed below.

#### 5.1.1 Characterization of the peridural scar tissue indicates the presence of myoblastic cells, VEGF protein, hsp-47, P4H and expression of types I and III collagen

The peridural scar tissue homogenates obtained from both 3 day and 21 day post-surgery animal from all three groups showed expression of a single ~ 42 kDa band for MyoD protein and the absence of any detectable myosin heavy chain (MyHC) protein (see **Figure 23**). This suggests that the peridural scar tissue contained immature skeletal muscle progenitor cells (myoblasts) and few, if any, differentiated muscle fibre cells. The MyoD band intensities in 21-day post-surgery scar tissue homogenates were significantly lower than those in 3-day post-surgery scar tissue. This finding suggests that progressive

maturation of the peridural scar tissue is accompanied by a decline in the relative abundance of MyoD positive cells. It is possible that at later stages of peridural scarring, some myoblastic cells might have matured to a stage when the cells no longer express MyoD but are not yet expressing MyHC.

In contrast, the mean relative level of VEGF protein was higher in the peridural scar tissue obtained from 21 day post-surgery animals when compared to 3 day post-surgery animals (see **Figure 24**) suggesting its potential involvement in the later stages of peridural wound repair. Moreover, it was observed that p38 MAPK levels were higher in 21 day post-surgery animals (see **Figure 25**) which correlates with the expression of VEGF protein at that time-point. This finding correlates with a previous study where p38 MAPK has been shown to induce VEGF synthesis in aortic smooth muscle cells (Yamamoto *et al.*, 2001). VEGF is a potent inducer of endothelial cell proliferation and angiogenesis (Bates and Jones, 2003).

Both VEGF and angiogenesis have been shown to play diverse roles in wound healing. In a study of a fetal skin wound model, it was observed that exogenous VEGF administration stimulated proliferation of both endothelial cells and dermal fibroblasts resulting in an increase in scar formation (Wilgus *et al.*, 2008). In contrast, angiogenesis has been associated with scarless wound healing in oral mucosa (Szpaderska *et al.*, 2005), while a reduction in angiogenesis had little effect on the outcome of wound healing in a mouse model of full-thickness excisional dermal wound repair (Bloch *et al.*, 2000).

Previous studies have suggested that delayed angiogenesis may lead to impaired skeletal muscle regeneration (Ochoa *et al.*, 2007) because VEGF is required for myoblast migration and regeneration of muscle fibres following injury (Arsic *et al.*, 2004; Germani

*et al.*, 2003). Moreover, Germani *et al.* (2003) found that increased VEGF expression within ischemic hind limb muscles of CD1 mice resulted in lower MyoD expression, which is consistent with our observations in the peridural scar tissue of the post-surgery animals. These authors hypothesized that VEGF might aid skeletal muscle regeneration by promoting the differentiation of myoblastic cells to more mature skeletal muscle fibres which no longer express MyoD (Germani *et al.*, 2003).

On comparing the RNA isolated from peridural scar tissue between 3 day, 21 day and 63 day post-surgery animals from all three groups, higher total RNA yields for the 3 day peridural scar tissues were obtained. This suggested a greater cellularity of the scar tissue during the early phase of the wound healing process. This finding is consistent with previous reports that discussed the cellular events leading to tissue healing (Adzick and Lorenz, 1994). A statistically significant lower total RNA yield was obtained from 21 day and 63 day peridural scar tissue (  $p$  value  $< 0.05$ ,  $n = 5$ ), which suggests that the scar matures with a higher proportion of ECM proteins and lower density of cells.

The texture of the peridural scar tissue had become progressively more fibrous in nature in the 63 day peridural scar tissue, as compared to the 3 day peridural scar tissue. Compared to 3 day peridural scar tissue, the 21 day and the 63 day peridural scar tissue exhibited considerably greater inconsistencies in both total RNA and total protein yields. This variability created problems in subsequent RNA and protein analysis of the late stage scar tissue samples, limiting our analysis to 3 day and 21 day animal groups.

Our RNA dot blot analysis indicated that Collagen type 1 ( $\alpha 2$ ) and Collagen type 3 ( $\alpha 1$ ) mRNAs were expressed at higher levels in the peridural scar tissue in comparison to Collagen type 4 ( $\alpha 1$ ) gene transcripts (see **Figure 19**). This is consistent with earlier

reports that type I and type III collagen are the predominant collagen types found in scar tissue (Allbrook, 1973; Bailey *et al.*, 1979; Best and Hunter, 2000; McMinn, 1967). In contrast, type IV collagen is predominantly formed in basement membranes and would be expected to be less abundant in scar tissue matrix (McMinn, 1967). Western blot analysis of the 3 day and 21 day peridural scar tissue homogenates showed the presence of type I collagen, fibronectin, and fibroblast markers such as hsp-47 and P4H (**Figure 15** and **Figure 16**). Collectively, the findings suggest the presence of both fibroblast cells and immature myoblast cells in peridural scar tissue.

#### **5.1.2. Systemic administration of OTC and quercetin may reduce cutaneous scar formation, and promote bone regrowth within the spinal laminae of the lumbar laminectomized rats**

Our initial qualitative observations on the extent of cutaneous wound repair (see **Section 4.1** and **Figure 9**) in the skin overlying the laminectomized area of the spine in 21 day and 63 day animal groups suggested that both OTC and quercetin treatments reduced scar formation at the site of the dermal incision, with fewer raised structures at the wound site and better restoration of skin pigmentation compared with the saline treated control rats (Cox, 2008). The histological appearance of the scar tissue as assessed by our research collaborators further suggested that OTC and quercetin treatment had beneficial effects on cutaneous wound repair. Furthermore, as described in **Section 4.1**, it appeared that both quercetin and OTC promoted improved bone regrowth in the underlying spinal laminae. However, the evidence that OTC and quercetin might have anti-scarring potential in rat cutaneous wounds is based entirely on subjective and qualitative assessments. Moreover, it does not directly address the issue of whether these

drugs influence peridural scar tissue formation.

Quantitative differences in the wet mass of the peridural scar tissue excised from saline, OTC and quercetin treated animals allow for a crude estimation of their relative effects on total scar tissue formation. At 3 days post-surgery, OTC treated animals showed no significant difference in scar tissue wet mass in comparison to saline-treated control animals. But at both 21 and 63 days post-surgery, OTC treated animals demonstrated a significantly lower mean wet mass as compared to peridural scars from saline treated control animals (see **Table 6**). Compared to saline treated rats, the OTC treated rats showed a 35% reduction in the wet mass for 21 day peridural scar tissue and a 27% reduction for 63 day peridural scar tissue

In contrast, quercetin treatment showed no consistent effects on peridural scar tissue wet weight. At 3 days post-surgery, the peridural scar tissue from quercetin-treated rats showed significantly higher wet mass compared to saline-treated control animals. However, at 21 days the quercetin treated animals showed a significantly lower peridural scar mass than controls (see **Table 6**), while at 63 day there was no significant difference between control and quercetin treated rats.

Collectively, these wet mass findings suggest that the OTC treated animals have reduced scar tissue mass as compared to the scar tissues obtained from either saline treated control rats or quercetin treated animals. This reduction in scar tissue wet mass could result from reduced accumulation of ECM proteins and/or polysaccharides in OTC treated scars or, alternatively, might result from reduced fluid retention due to improved venous flow in and around the scar tissues of OTC treated animals. Neither Western blot analysis nor RNA dot blot analysis demonstrated any significant reduction in mean levels

of collagen or fibronectin expression in OTC treated scar tissues relative to scar tissues from saline treated control - animals. We did not directly examine the presence of blood capillaries or venous outflow in the scar tissues of our experimental animals. However, Western blotting was performed to evaluate relative levels of VEGF protein, which might reflect angiogenic activity in these tissues. Due to large animal to animal variability in the expression levels of VEGF in both 3 and 21 day scar tissue samples, we were unable to establish any link between OTC treatment and improved angiogenesis. As such, the reasons for the reduced scar tissue wet mass in OTC treated animals remain to be determined. In future studies, it would be worthwhile to determine the dry weight of the scar tissues in addition to their wet weight, as this would shed insight as to whether OTC acts to reduce ECM deposition or fluid retention in the peridural scar.

### **5.1.3 Systemic administration of OTC and quercetin showed no significant treatment effects on collagen biosynthesis and/or abundance in the peridural scar tissue within the rat spinal lumbar laminectomy model.**

A collagen-specific histochemical procedure, the picosirius red polarization method, was used to determine the relative collagen abundance in the peridural scar tissue sections of 3 day and 21 day animals. In addition, the distribution of the sirius red stained fibrils within the tissue sections as visualized using circularly polarized light was correlated with the total collagen distribution profile of contiguous scar tissue sections as determined by FTIR spectroscopic mapping using a synchrotron light source. The FTIR spectroscopic imaging and picosirius red histochemical staining patterns revealed a high degree of correlation in detecting total collagen distribution and collagen fibrillar organization within the tissue sections, as was reported in our recent publication (Wiens

*et al.*, 2007).

The disadvantage of using synchrotron based FTIR mapping for collagen detection lies in the inherently time consuming nature of data acquisition and high equipment usage costs involved in mapping whole tissue sections. Moreover, the complex, overlapping spectral signatures of multiple biological components found within the tissue makes interpretation of FTIR spectral maps in tissue sections difficult, without first defining the spectral signatures of known biological components. Also, the FTIR spectral map is highly influenced by the orientation of collagen fibrils relative to the synchrotron light, which further contributes to the complexity of interpreting the FTIR spectral map generated from a heterogeneous tissue (Camacho *et al.*, 2001; Wiens *et al.*, 2007). In contrast, the picosirius red polarization method has the advantage of the simplicity of the histochemical staining procedure and image acquisitions using polarized light microscopy.

When the relative areas of picosirius red stainable collagen within histological sections of peridural scar tissue obtained from 3-day and 21-day animals were quantified using NIH Image J software, no statistically significant effects of either OTC or quercetin treatment on total collagen fibril abundance could be detected (see **Figure 14**). The picosirius red stainable collagen measurements showed that 3 day post-surgical scar tissues had a lower collagen area fraction as compared to 21 day post-surgical scar tissues within all treatment groups. This was consistent with FTIR map findings that showed reduced overall collagen levels in 3 day peridural scar tissue relative to 21 day scars (Wiens *et al.*, 2007). Large individual animal to animal variation was observed in the collagen levels within the scar tissues from individual animals within each treatment

group, including the saline control group, making it impossible to demonstrate any statistically significant treatment effects of either OTC or quercetin on overall collagen abundance in the peridural scar.

Similarly, western blot analysis revealed large animal to animal variation in the protein levels of collagen biosynthesis markers such as type I procollagen, hsp-47 and prolyl-4-hydroxylase (P4H), as well as in levels of fibronectin protein within the peridural scar tissue. Again, statistically significant changes in the levels of these proteins associated with OTC or quercetin treatment could not be demonstrated (**Figures 17-20**).

Using Pearson correlation coefficient analysis, I analyzed whether there was a correlation in the expression levels of the various collagen biosynthesis markers (viz. type I procollagen, hsp-47, and P4H) within the individual animals in each treatment group (see **Appendix 1**). This analysis was performed to test whether or not the animals that were high responders for one specific response parameter (e.g. type I collagen) showed a similarly high response to another specific response parameter (e.g. hsp-47 or P4H). Our analysis showed that in the 21 day OTC treatment group, those individual animals with relatively high levels of P4H expression also exhibited high hsp-47 protein levels, while those animals with low P4H expression had correspondingly low expression of hsp-47. This correlation was not observed in 3 day OTC treated animals or in 3 day and 21 day scar tissues from saline and quercetin treated animals. These findings suggest that as compared to quercetin and saline treatments, OTC might have the ability to balance expression levels of intracellular proteins involved in post-translational modification of collagen proteins, namely hsp-47, a procollagen chaperone protein, and P4H, an enzyme that catalyzes formation of 4-hydroxyproline that is essential for 3-D

folding of newly synthesized procollagen chains. Maintaining a proper balance between the proteins involved in post-translational modification of nascent procollagens is important, as it helps prevent accumulation of defective collagen fragments that may act as promoters of fibrotic scarring (Kofford *et al.*, 1997; Meier and Nanney, 2006a).

#### **5.1.4 Systemic administration of OTC and quercetin showed inconclusive results as to their treatment effects on TGF- $\beta$ 1 and TGF- $\beta$ 3 expression within the peridural scar tissue obtained from rat spinal lumbar laminectomy model.**

It has been hypothesized that the increased expression of TGF- $\beta$ 3 during the early phase of wound healing promotes increased cellular proliferation and differentiation following injury that leads to scarless healing (Shah *et al.*, 1995). In contrast, expression of TGF- $\beta$ 1 and TGF- $\beta$ 2 isoforms might have deleterious effects on wound repair by increasing scar formation (Frank *et al.*, 1996). We were unable to examine changes in TGF- $\beta$ 1 and - $\beta$ 3 mRNA levels using RNA dot blot analysis on peridural scar tissues of 3- and 21-day laminectomized rats, due to weak hybridization signals for both transcripts and high levels of background noise. TGF- $\beta$ 1 mRNA was barely detectable in scar tissues from 21-day post-surgery animal groups and the signal intensities were variable in 3-day post-surgery animal groups (see **Figure 21**). Consistent with the large animal to animal variation, densitometric analysis of the dot blots revealed no effects of the quercetin or OTC treatments on TGF- $\beta$ 1 mRNA levels (see **Figure 22**). Compared to TGF- $\beta$ 1 mRNA, TGF- $\beta$ 3 mRNA levels were conspicuously higher in both 3 day and 21 day peridural scar tissues. However, we were again unable to demonstrate any changes in the levels of TGF- $\beta$ 3 mRNA expression in OTC and quercetin treated animals relative to the saline control group.

**5.1.5. Effects of systemic administration of OTC and quercetin on mitogen-activated protein kinase signaling. OTC reduced both p38 MAPK and ERK activation in 21 day peridural scar tissue.**

Studies have reported that the ERK1/2, JNK and p38 MAPK signaling pathways are strongly stimulated after injury to skeletal muscle (Aronson *et al.*, 1998) and corneal tissue (Imayasu and Shimada, 2003; Li *et al.*, 2001; Sharma *et al.*, 2003). By western blot analysis, the 3 day peridural scar tissues exhibited only faint levels of active, dual phosphorylated p38 MAPK, while phosphorylated ERK1/2 was undetectable. In contrast, substantial levels of both phosphorylated p38 and phosphorylated ERK1/2 were detected in 21-day peridural scar tissue. This temporal pattern suggests that ERK and p38 MAPK activation are associated with the latter events of scar formation or wound repair in this system, rather than being a transient short-term response to tissue injury. This contrasts with the rapid, transient activation of ERK1/2 and p38 phosphorylation was observed in our wounded micromass co-cultures of FR fibroblasts and L8 myoblasts (see **Figures 54 and 55**). The different temporal dynamics of MAPK activation observed in our *in vivo* and *in vitro* wound repair models is probably attributable to the relatively complex nature of the *in vivo* peridural scar tissue compared to the *in vitro* micromass culture. In addition to fibroblasts myoblast and fibroblasts, peridural scar tissues contain macrophages, neutrophils and other inflammatory cell types. Proinflammatory cytokines released by these cells may have stimulated prolonged p38 and ERK1/2 activation. Moreover, chronic re-injury of the peridural tissue resulting from local destabilization of the laminectomized spinal column may have also contributed to the sustained activation of p38 and ERK1/2 MAPK observed at 3 and 21 days post-surgery. In contrast, the micromass co-cultures contained only myoblast and fibroblast cells in a controlled

environment that is devoid of inflammatory cell influences and chronic biomechanical stress.

Importantly, the 21 day peridural scar tissue from OTC treated rats showed significantly lower levels of both ERK activation and p38 MAPK activation when compared to scar tissue from saline treated control animals. In contrast, levels of phosphorylated ERK1/2 and p38 in peridural scar tissue from quercetin treated rats were similar to the saline control group. (see **Figure 25** and **26**). The reduction of ERK1/2 and p38 MAPK activation following OTC treatment was especially notable, as this was the only consistent tissue response to drug treatment that was observed in our *in vivo* spinal laminectomy model of peridural wound repair. The functional significance of altered MAPK signaling to the processes of scar formation and tissue healing in this model remains to be determined. It has been suggested that p38  $\alpha/\beta$  MAPK activation can function as a molecular switch for both satellite cell activation (Jones *et al.*, 2005) and subsequent differentiation of these satellite cells to muscle fibres to repair damaged muscle (Chen *et al.*, 2007). The reduced p38 MAPK activation is thought to be essential for regenerating muscles tissues lost at the wound site.

The reduced ERK1/2 and p38 MAPK activation levels in the OTC treated animals might also be due to the cytoprotective properties of OTC through improving cellular glutathione level. The improved cellular glutathione level may help attenuate effects of stress stimuli associated with biomechanical stress at the laminectomized region and inflammatory stimuli associated with muscle tissue healing (Kamencic *et al.*, 2001; Lee *et al.*, 2005; Ferreira *et al.*, 2009). Moreover, the ability of the ERK1/2 and p38-MAPK pathways to cross talk (Xiao *et al.*, 2002) suggests the possibility that specific inhibition

of either one of these pathway by OTC at molecular level could lead to synergistic inhibition of the other pathway (See **Appendix 3, A**).

High doses of quercetin have been reported to delay muscle differentiation through its pro-mitogenic activity that disrupts the differentiation program of myoblasts (Orzechowski *et al.*, 2001). Moreover high doses of quercetin also inhibit cell migration and proliferation of malignant cells (Huang *et al.*, 2005), vascular endothelial smooth muscle cells (Tan *et al.*, 2003) and osteoblasts (Nam *et al.*, 2008) through inhibition of MAPK signaling.

In this study, the phosphorylation levels of p38 MAPK and ERK1/2 were unchanged in peridural scar tissue from quercetin treated animals as compared to the saline control. An *in vitro* study demonstrated that quercetin inhibited both ERK1/2 and p38 MAPK activity in lipopolysaccharide treated RAW267.7 macrophage cells (Wadsworth *et al.*, 2001). However, another study observed that quercetin treatment did not affect either p38 MAPK or ERK1/2 activation in primary rat vascular smooth muscle cells *in vitro* (Perez-Vizcaino *et al.*, 2006). Collectively these findings suggest that quercetin might exert variable effects on the ERK1/2 and p38 MAPK signaling pathway in different cell types.

It is interesting to note that the 30  $\mu$ M concentration of quercetin used by Perez-Vizcaino *et al* (2006) was close to the dose (0.025 mmol/kg; or approximately 25  $\mu$ M) that was administered to animals in our *in vivo* experiments. However, their experiment demonstrated that at 30  $\mu$ M concentration, quercetin inhibited JNK activation in vascular smooth muscle cells, although it did not affect ERK or p38 MAPK. It could be possible that the 0.025-mmol/kg concentration of quercetin administered to the animals in our

study was not high enough to exert any effect on p38 MAPK or ERK1/2 activation within the peridural scar tissue *in vivo*. Due to time constraints, we did not explore the possible effects of quercetin and OTC on JNK activation in peridural scar tissue.

#### **5.1.6 Limitations of the spinal laminectomy wound repair model and possible reasons for the large animal to animal variation encountered.**

The rat spinal laminectomy model proved to be a very difficult system for quantifying molecular parameters of scar formation and wound repair. As noted above, experiments using this *in vivo* model of peridural scar formation revealed wide animal to animal variation in the expression levels of collagen biosynthesis markers and specific gene transcripts within each drug treatment group (OTC, quercetin, and saline).

This problem was also encountered by our collaborators who examined the accumulation of mast cells, activated macrophages, CD4 and CD8 T-lymphocytes within peridural scar tissue of the same rats (Cox, 2008). Similarly, a previous study involving a rabbit model of spinal laminectomy surgery failed to demonstrate any significant difference in levels of fibroblasts and immune cells within the peridural granulation tissue in animals treated with the non-steroidal anti-inflammatory drug- aceclofenac (Sandoval and Hernandez-Vaquero, 2008). This was attributed to huge animal to animal variation in the experimental model. Indeed, such variability may be a problem inherent to such a complex *in vivo* model of post-surgery wound healing that involves multiple cell types, and both incisional and excisional types of tissue injury.

Among humans, different individuals experience different levels of inflammation and scarring following tissue injury based on their ethnicity, health status, environmental exposure and diet (Bayat *et al.*, 2003; Robles and Berg, 2007). For example, the

incidence of keloidal scarring is determined by hereditary traits in humans, with greatest predominance in members of the African race (Bayat *et al.*, 2003; Robles and Berg, 2007).

Genetic differences may have contributed to variability in cellular and molecular parameters of scar formation among the individual animals used in our spinal laminectomy experiments. Although our study used rats of the same breed and gender (male Wistar rats), no special precautions were taken to ensure that all animals were derived from the same breeding line. Moreover, the small sample size used in our animal study might have also contributed to type II statistical error ( $\beta$  error) suggesting the lack of anti-scarring effects of quercetin and OTC in peridural tissues. In future drug development studies involving similar *in vivo* experimental models, it would be advisable to ensure that all animals employed are from the same genetic breeding line, and that the sample size is sufficiently large.

Secondly, the complexity of the surgically-induced wound repair model that we employed in our study is likely to have been a contributing factor to the animal to animal variation observed. The rat spinal laminectomy surgery involved multiple forms of incisional, excisional and blunt tissue trauma. This included damage to the vertebral bone laminae to expose the spinal cord, disruption of connective tissue around adjacent skeletal muscles and ruptured blood vessels. In such a model, it is very difficult to rigorously standardize the initial amount of tissue damage due to surgery among various animals in the test groups, which would lead to variable extents and rates of tissue inflammation, peridural scarring, and wound repair. Moreover, the instability generated in the spinal column as a result of ligament damage from surgery may have also

contributed to variability in the amount of scarring. In some animals this spinal destabilization and increased vertebral mobility may have caused biomechanical stress at the surgical site causing chronic re-injuring of the wound area, which could stimulate a prolonged inflammatory response. Thus, differences in the extent of ligament damage might have resulted in variability in animal responses and the degree of scarring. However, our experimental strategy was to select an animal model that mimicked peridural scarring following elective spinal surgery in a clinical setting, where some variability is unavoidable.

In regards to the quercetin treated animals, the method of drug delivery may have been an additional source of variability. Quercetin was administered intraperitoneally as a suspension in normal saline. When test animals were sacrificed for tissue analysis, the abdominal cavities of some quercetin-treated rats were observed to retain insoluble drug particles. Hence, there may have been substantial variability in the effective circulating dose of quercetin among different animals in the test group.

Finally, the specific doses of quercetin (0.025 mmol/kg) and OTC (1 mmol/kg) that were administered to the animals in our study may not have been the optimum doses for eliciting treatment effects on peridural scar formation. The specific OTC and quercetin doses that we employed were chosen based on earlier experiments by our collaborators; who had demonstrated their efficacy in restoring neurological function in rats subjected to surgically-induced spinal cord injury (Kamencic *et al.*, 2001; Schultke *et al.*, 2003). Subjective morphological observations suggested that these drug doses might also ameliorate associated cutaneous and peridural tissue healing, and therefore might be within a potentially therapeutic range for anti-scarring effects.

A more thorough set of dose response experiments and collection of peridural scar tissues at a greater number of post-surgical time points - might have revealed more consistent effects of OTC and quercetin at certain concentrations, and may have revealed some differences in gene and protein expressions that were missed in our study. However, such studies -would be prohibitively expensive, labour intensive and require a much large number of test animals. This highlights the need for a reliable, cost-effective *in vitro* organotypic wound repair model for preliminary drug screening studies including determination of effective drug concentrations. Hence, the remainder of my thesis research focused on developing a novel three-dimensional *in vitro* wound repair model utilizing fibroblast and myoblast cells in co-culture.

## **5.2. Outcomes of *in vitro* wound repair studies in a micromass co-culture model**

The predominantly inconclusive outcomes of the *in vivo* studies prompted me to initiate experiments aimed at developing a novel three-dimensional scaffold-free *in vitro* wound healing model that might mimic aspects of *in vivo* peridural scar formation and tissue repair. This *in vitro* model was used for testing the potential efficacy of OTC and quercetin as anti-fibrotic agents. Studies have hypothesized that excessive scarring/fibrosis in skeletal muscles tissues might be due to the interaction of injured muscle cells with fibroblast cells from the surrounding connective tissue (Ambrosio *et al.*, 2008; Clark, 1996; Lehto *et al.*, 1985a; Lehto *et al.*, 1985b; Sasse *et al.*, 1981). This cell-cell interaction may stimulate fibroblast cells to produce cytokines such as TGF- $\beta$ , interleukins and FGFs that can initiate muscle fibrosis and poor muscle regeneration. Our *in vivo* studies showed the presence of both immature myoblasts and fibroblast cells in

the peridural scar tissue. Therefore, we initially tried to isolate viable primary fibroblasts and myoblast cells from the abdominal skin of fetal rat and gluteus muscle of the adult rat respectively. These tissues were treated with trypsin-EDTA solution and collagenase for a period of 3 - 6 h at 37 °C to digest of extracellular matrix proteins and chelate Ca<sup>2+</sup> ions. The tissues were then gently agitated to dissociate cells and passed through sterile muslin filter to remove of large cell debris. The filtrant containing dissociated cell suspension were immediately inoculated into sterile DMEM-F12 culture medium containing 20% FBS, and subsequent passaged several times in sterile culture medium containing 10 % FBS over the period of four month, to isolate strongly adherent dermal fibroblasts and adult myoblast cells. We found that when micromass cultures of primary fibroblast and myoblast cultures were prepared, these cultures tended to show poor adherence to the culture plate. We suspect that the primary fibroblasts and myoblast cell cultures obtained from the fetal and adult tissues may not be pure cultures. The persistent problem that we encountered while isolating primary fibroblast or myoblast cells from both embryonic and adult rats was contamination with other primary cell types. Hence, we selected an *in vitro* model that incorporated a well-defined rat fibroblast and myoblast cell lines obtained from American Type Cell Culture (ATCC).

**5.2.1. Micromass cultures established with a seeding ratio of 1 part FR fibroblast and 3 parts L8 myoblast cells form a 3-D “microtissue” that expresses MyoD and fibroblast marker proteins.**

Micromass culture technology has been widely employed in developmental studies of bone and cartilage formation *in vitro*. Its potential utility in soft tissue regeneration and engineering applications was discussed in **Section 2.7**. The novelty of

our approach was the combination of cell types of two different lineages (myoblasts and fibroblast cells) in a high-density co-culture to generate a 3-D “microtissue” that is devoid of artificial scaffold. This microtissue was subjected to a single scrape wound to study the wound closure pattern following a laceration type injury, the interaction of myoblast and fibroblast cells, and molecular changes associated with scar formation and tissue repair.

The western blot data from our *in vivo* studies had indicated that peridural scar tissue contained MyoD positive myogenic cells, while the expression of P4H, a fibroblast marker protein suggested the additional presence of fibroblast cells (see **Figures 15, 16, 23**). Therefore, our micromass co-culture model of peridural tissue repair included L8 myoblast cells, a well characterized adult muscle derived cell line that expresses high levels of the myoblast marker, MyoD, and which has the ability to differentiate into skeletal muscle fibres when propagated in medium containing horse serum (Richler and Yaffe, 1970).

Our micromass co-cultures also included FR 3T3 cells, a well-characterized line of fibroblastic cells derived from fetal rat skin. Since FR 3T3 cells are of fetal origin they may exhibit a level of cellular plasticity initiated through direct cell-cell contact (Fukuhara *et al.*, 2003 and Lu *et al.*, 2005) or may produce chemical factors that could prevent de-differentiation of L8 myoblast in the co-culture condition. In initial experiments, we generated high-density micromass co-cultures by modulating the relative seeding densities of L8 myoblasts and FR fibroblast cells. It was demonstrated that a 1:3 ratio of FR fibroblasts to L8 myoblast cells developed a cohesive microtissue layer *in vitro*. The accumulation of picrosirius red stainable collagen and Alcian blue stainable

polysaccharides clearly demonstrated that the micromass co-culture is rich in the extracellular matrix components that contribute to microtissue formation (see **Figure 31**). Moreover, SEM images of the micromass co-culture may suggest the integration of the FR fibroblast and L8 myoblast cells into a 3-D microtissue structure *in vitro* (see **Figure 29**). SEM images of the 8 day post wounded culture suggest integration and compaction of cellular and extracellular matrix components in the healed micromass culture (see **Figure 30, Panel F**). Studies involving co-cultures of fibroblasts and hepatocytes have shown that the hepatocytes tend to aggregate to form a mass surrounded by fibroblast cell layer (Bhatia *et al.*, 1997; Khetani and Bhatia *et al.*, 2008). We cannot yet discount the possibility that some degree of cell sorting might also have occurred in our fibroblast:myoblast micromass co-culture system. A more detailed analysis using confocal fluorescent microscopy could be employed to resolve this issue.

Micromass cultures seeded at a 1:3 ratio of FR fibroblasts to L8 myoblasts were also able to best withstand a scrape wound manipulation without detaching from the culture dish. This ratio may have enabled optimal heterotypic cell interaction between the FR fibroblast and L8 myoblast cells to establish a cohesive microtissue layer with superior intercellular adhesion as well as cell-substrate adhesion properties.

Micromass cultures composed of FR fibroblasts alone quickly detached from the culture dishes after wounding. Cultures composed of L8 myoblasts alone were initially able to withstand the wound manipulation, but by 5 days of culture the cell layer curled up and detached from the culture dish. This may be due to the ability of L8 myoblast cells in homogenous micromass culture to differentiate into contractile myotubes as shown by the contraction of 8 day post wounded cultures (see **Figure 28**).

It was observed that MyHC and tropomyosin protein (markers of differentiated skeletal muscle fibres) were expressed in 3-day micromass cultures containing L8 myoblast cells alone (see **Fig 36**). The presence of fibroblast cells in 1:3 micromass co-cultures appeared to inhibit differentiation of the L8 myoblast cells into myotubes as confirmed by the absence of myogenic differentiation markers such as MyHC, OPN and tropomyosin in fibroblast: myoblast co-cultures (see **Figure 36**). Moreover, wounding of the micromass co-culture did not induce the expression of MyHC or OPN proteins (see **Figure 37**).

Previous studies have reported that the presence of fibroblast cells can prevent the differentiation of liver and chondrocyte cells *in vitro* (Bhatia *et al.*, 1997; Gerstenfeld *et al.*, 2003; Khetani and Bhatia, 2008; Lu *et al.*, 2005). The mechanisms by which fibroblast cells in co-culture might inhibit myoblast differentiation is unknown, but could involve soluble secreted agents such as growth factors and pro-mitogenic cytokines, or cell surface interactions mediated by integrins or other adhesion proteins.

### **5.2.2. Cell proliferation and preferential migration of fibroblast cells towards the wound site in wounded micromass co-cultures.**

Our data strongly suggest that the process of *in vitro* wound closure in our micromass co-culture model is primarily dependent on cell proliferation. We demonstrated that wound closure was effectively blocked by treating wounded cultures with 10 µg/mL mitomycin, (see **Figure 40-41**) a DNA cross-linking drug that has been shown to potently inhibit cell proliferation in a wide variety of different cell types without disrupting cell migration (Gottrup, 2000 and Stojadinovic *et al.*, 2005). Accordingly, migration of cells from the wound edges in the absence of concurrent cell

proliferation does not appear to be sufficient to promote closure of the wound gap in fibroblast:myoblast micromass co-cultures. However, a limitation of our study was that we did not directly confirm that mitomycin exposure inhibited DNA synthesis in our FR and L8 cell lines (e.g. by assaying bromodeoxyridine or <sup>3</sup>H-thymidine uptake into mitotically dividing cells). Also, we cannot fully exclude the possibility that mitomycin might have exerted some direct inhibitory effect on cell motility in our micromass cultures in addition to its presumed effect on cell proliferation. (Gottrup, 2000 and Stojadinovic *et al.*, 2005).

When FR fibroblast and L8 myoblast cells were labeled with DiI and DiO lipophilic dyes to track their migration in wounded micromass co-cultures, it was observed that fibroblast cells as well as some myoblast cells migrated into the wound gap (see **Figure 43**). However, quantitative analysis of the relative fluorescence intensities of DiI labeled FR fibroblast cells versus DiO labeled L8 myoblast cells suggests that the fibroblast cells preferentially localize to the region of wound site and wound edges (see **Figure 44**). Similar findings have been described for *in vivo* wound healing. Preferential fibroblast migration and proliferation at the wound site is necessary for providing matrix components that lead to eventual closure of the denuded region following dermal injury (Schreier *et al.*, 1993). Fibroblast cell migration and proliferation may also play a critical role in excessive scarring (Ambrosio *et al.*, 2008; Clark, 1996; Lehto *et al.*, 1985a; Lehto *et al.*, 1985b; Sasse *et al.*, 1981).

The growth factors PDGF and TGF- $\beta$  caused increased fibroblast migration in an *in vivo* incisional model of rat dermis wound repair (Pierce *et al.*, 1988) and TGF- $\beta$  signaling has been implicated in fibrotic scarring (Leask and Abraham, 2004). In our

experiments, TGF- $\beta$ 1 treatment of wounded micromass co-cultures caused accelerated wound closure (see **Figure 48-49**) with significantly increased migration of fibroblast cells and decreased migration of myoblast cells into the wound gap (see **Figures 50, 51**).

In micromass cultures composed of fibroblast cells alone, TGF- $\beta$ 1 treatment stimulated a dose-dependent increase in total DNA and total collagen levels (see **Figure 46**). In contrast, TGF- $\beta$ 1 led to a dose-dependent decrease in both total DNA and collagen levels in micromass cultures composed of L8 myoblasts alone (see **Figure 47**). Collectively, these findings suggest that the accelerated wound closure in the wounded micromass co-cultures exposed to exogenous TGF- $\beta$ 1 might be due to increased migration and proliferation of FR fibroblasts into the wound region as opposed to the L8 myoblast cells.

We also observed that treatment with relatively high concentrations (0.2 - 0.4 ng/mL) of TGF- $\beta$ 1 resulted in a curling up and eventual detachment of the micromass co-cultures from the culture plates (data not shown). L8 myoblast cells are reported to differentiate into contractile skeletal muscle fibres following exogenous TGF- $\beta$ 1 treatment (Endo and Nadal-Ginard, 1987). In addition to reducing L8 myoblast cell proliferation in the micromass co-culture, exogenous TGF- $\beta$ 1 treatment might also induce differentiation of myoblast cells because of the absence of pro-mitogenic stimuli. Due to time constraints, we could not examine the expression of MyHC, myogenin or tropomyosin in TGF- $\beta$ 1 treated cultures.

Collectively, these experiments suggest that cell proliferation plays an important role in the *in vitro* tissue repair of wounded micromass co-cultures. There is preferential migration of fibroblast cells into the wound site following injury, and exogenous TGF- $\beta$ 1

treatment promotes increased fibroblast migration and proliferation in the wounded micromass co-culture. These properties parallel features of *in vivo* wound repair (Clark *et al.*, 2004; Mustoe *et al.*, 1987).

**5.2.3. Endogenous TGF- $\beta$ 3 gene transcript levels were significantly higher compared to TGF- $\beta$ 1 gene transcripts in both wounded and corresponding unwounded cultures suggesting a possible link to *in vivo* peridural scar tissue.**

Semi-quantitative RT-PCR analysis indicated that the micromass co-cultures showed higher TGF- $\beta$ 3 mRNA levels relative to TGF- $\beta$ 1 transcript levels at all time points tested in both unwounded and wounded conditions (see **Figure 38, 39**). Specific TGF- $\beta$  isoforms such as TGF- $\beta$ 3 may exert either proliferative or anti-proliferative effects depending on cell type and oxygen levels *in vitro* (Halper *et al.*, 2005; Scheid *et al.*, 2002). In cultures of fetal fibroblast cells, physiologically low oxygen concentrations in culture media were shown to elevate TGF- $\beta$ 3 expression (Halper *et al.*, 2005; Scheid *et al.*, 2002). Accordingly, the relatively high endogenous TGF- $\beta$ 3 transcript levels in this *in vitro* co-culture might reflect the partially hypoxic conditions of the micromass culture system.

Endogenous TGF- $\beta$ 3 expression may provide mitogenic conditions that discourage L8 myoblast cells from differentiating into skeletal muscle fibres in the micromass co-cultures. In an earlier experiment, exogenous TGF- $\beta$ 1 treatment was found to decrease DNA levels of L8 myoblast cells in the micromass co-culture (see **Figure 47**) suggesting that high TGF- $\beta$ 1 levels in the culture media might induce differentiation of myoblast cells within the micromass co-culture.

Studies have shown that TGF- $\beta$ 3 can modulate the pro-fibrotic TGF- $\beta$ 1 signaling

during the wound healing process, suggesting its potential use in anti-scarring therapy (Occeleston *et al.*, 2008; Shah *et al.*, 1995). It was observed that TGF- $\beta$ 3 inhibited differentiation of MyoD expressing C3H10T1/2 cells and C2C12 myoblasts (Lafyatis *et al.*, 1991; Liu *et al.*, 2001). Thus, it can be postulated that high endogenous levels of TGF- $\beta$ 3 in the micromass co-culture might counteract the actions of TGF- $\beta$ 1 in promoting myoblast differentiation within this *in vitro* wound model. Due to limitations of the methods used to detecting TGF- $\beta$  isoforms in our experiments, this postulate could be explored in future using more sensitive molecular detection techniques

Interestingly, the relative expression of TGF- $\beta$  isoforms in the micromass co-culture paralleled the relative expression pattern of TGF- $\beta$ 3 versus TGF- $\beta$ 1 isoforms in the peridural scar tissue isolated from the laminectomized rats. This finding suggest that the artificial microtissue developed by co-culturing 1:3 ratio of FR fibroblast and L8 myoblast may have a molecular characteristics of *in vivo* peridural scar tissue.

#### **5.2.4. Gene and protein expression profiling of the wounded and corresponding unwounded micromass co-culture suggests a potential tool for future drug development studies.**

Semi-quantitative RT-PCR analysis was used to determine whether wounding of the micromass co-cultures resulted in altered expression of several genes involved in tissue repair. The expression of TGF- $\beta$ 1, TGF- $\beta$ 3, CD 44, hyaluronan synthase 1 and hsp-47 gene transcripts were significantly higher in 2 day post wounded cultures as compared to their corresponding unwounded cultures (see **Figure 38 and 39**). TGF- $\beta$ 3, RHAMM, hyaluronan synthase 1 and hsp-47 mRNA levels were also higher in 2 day post wounded cultures than in 4 or 8 day post wounded culture.

Hyaluronan synthases are involved in hyaluronan production which promotes cell motility through interaction with its cell surface receptors RHAMM and CD44 (Fraser *et al.*, 1997; Sherman *et al.*, 1994; Tolg *et al.*, 2006; Toole, 1990). Both CD44 and RHAMM also regulate cell proliferation by regulating cell cycle progression through G2M, which requires hyaluronan and growth factor-mediated ERK activation (Fraser *et al.*, 1997; Sherman *et al.*, 1994; Tolg *et al.*, 2006; Toole, 1990). Thus, the relatively high levels of RHAMM and Hyaluronan synthase 1 in 2 day post wounded micromass co-cultures might be associated with more rapid cell proliferation and cell motility at this time point as compared to 4 day and 8 day post wounded culture, when the wound site is covered by cells.

The expression of collagen, hsp-47 and hyaluronan synthase mRNAs is consistent with active biosynthesis of extracellular matrix collagens and polysaccharides in these cultures, as evidenced by their accumulation of both picrosirius red and alcian blue stainable matrix. The expression of TGF- $\beta$ 3 in 2 day post wounded micromass co-cultures was significantly higher than in corresponding unwounded cultures suggesting a potential role of TGF- $\beta$ 3 in regulating the biosynthesis of collagen and polysaccharides in the early *in vitro* wound repair process.

In all these experiments, the entire micromass culture (for both wounded and corresponding unwounded cultures) was used for preparing RNA as opposed to isolating RNA exclusively from cells located at the wound site. As such, it is possible that we failed to detect modest quantitative changes in gene transcript levels that were spatially restricted to cells within the wound site. Similarly, the magnitude of those wound-related changes in gene transcript levels that were detected might have been underestimated.

Possible approaches for determining spatially localized changes in gene transcript expression within the wound region would be laser capture microdissection to isolate the cells from the wound region for RT-PCR quantitation, or mRNA detection by whole-mount *in situ* hybridization. Undoubtedly, these approaches would provide valuable insight on localized changes in gene activation induced by wounding in our micromass co-culture model. However, time and resource constraints prevented us from initiating further experiments in this direction. Another potential limitation of our RT-PCR analysis was relying on GAPDH mRNA levels alone as an internal normalization control. It may be advantageous to include other constitutively expressed gene transcripts as normalization controls in future RT-PCR analyses to more accurately estimate relative changes in the mRNA levels of our various specific genes of interest.

Immunostaining experiments on wounded micromass co-cultures showed the presence of type I collagen protein at the wound site. Fibronectin was expressed at the wound edges as well as at the periphery of the micromass cultures and within the cells that migrate into the wound site (see **Figure 32**). However, the overall expression of fibronectin in the micromass co-culture appeared to be lower as compared to type I collagen, based on the much longer time taken for a positive color reaction to develop in the immunostaining procedure.

Types I, III and IV collagens are common collagen proteins that play an important role in the formation of tissue structures and production of type I collagen is a critical component of any tissue repair process (McMinn, 1967). The presence of type I collagen at the wound site within the wounded micromass co-cultures and higher levels of type I collagen as opposed to types III and IV collagen gene transcripts in the wounded

micromass co-culture suggests a predominant role of type I collagen in the *in vitro* tissue repair process. The presence of fibronectin together with type I collagen at the wound site is consistent with *in vivo* findings that both fibronectin and type I collagen are co-localized in scar tissue (Clark *et al.*, 1982; Clark *et al.*, 2004; McKeown-Longo and Mosher, 1984; Tamkun and Hynes, 1983).

#### **5.2.5. Modulation of p38 MAPK and ERK1/2 signaling pathways has differential effects on *in vitro* wound closure.**

The ERK1/2 and p38 MAPK signaling pathways are activated in epithelium and muscle tissue following injury (Sharma *et al.*, 2003; Yeow *et al.*, 2002). Western blot analyses revealed that active dual phosphorylated ERK1/2 was present both in wounded and unwounded FR: L8 cell micromass co-cultures (see **Figure 52**), though there was an increase in levels of ERK1 and ERK2 phosphorylation at 5 min post wounding compared to the corresponding unwounded culture.

Immunostaining suggested that the dual-phosphorylated ERK1/2 was most concentrated within the cells at the micromass culture wound edges, whereas total ERK1/2 protein was abundant throughout the wounded culture. This suggests that ERK1/2 activation is a component of the injury response in the micromass co-culture wound model (see **Figure 53**). Previous *in vitro* studies utilizing a 2-D skeletal muscle repair model have similarly reported that ERK1/2 expression is localized in the wound site in C2C12 muscle cell cultures (Yeow *et al.*, 2002).

The increased ERK1 and ERK2 phosphorylation in 5 min post-wounded cultures might lead to stimulation of cell proliferation and cell migration at the wound edges.

When the ERK1/2 signaling pathway was inhibited by treating the wounded micromass co-culture with 2  $\mu$ M of PD184352, there was a significant decrease in the rate of wound closure as compared to untreated cultures (see **Figure 57 and 58**). PD184352 is a highly specific inhibitor of MEK1 and MEK 2, the upstream MAPKKs that activate ERK1 and ERK2 in the ERK signaling cascade (Davies *et al.*, 2000). Western blot analysis confirmed that 2  $\mu$ M of PD184352 effectively inhibited phosphorylation of ERK1/2 in the micromass co-culture (see **Fig 56**).

Studies have suggested that ERK1/2 phosphorylation is important for maintaining functionality and metabolic dynamics during the wound healing process (Xiao *et al.*, 2002). Our findings suggest that ERK1/2 activation might be necessary for signaling cell proliferation and migration in the wounded micromass co-culture and that ERK activation is important for optimum wound closure of the wounded micromass co-culture.

Western blot analysis for active, dual phosphorylated p38 MAPK demonstrated a faint band in micromass co-cultures at 5 min after wounding, while immunostaining of the wounded micromass co-cultures revealed dual phosphorylated p38 MAPK at the wound edges at both 5 min and 1 day post wounding (see **Figure 54 and 55**). The absence of any detectable p38 MAPK phosphorylation in unwounded cultures at all time points might account for the lack of muscle fibre differentiation within the micromass co-cultures. Studies have shown that p38 MAP kinases play a regulatory role in the promotion of the expression of muscle-specific genes that are involved in muscle differentiation (Lluis *et al.*, 2006; Zetser *et al.*, 1999).

The activation of p38 MAPK in the micromass co-culture was brief following injury, which is contrary to the situation in a 2-D *in vitro* skeletal muscle wound model

where activation of p38 MAPK was observed at all time points (0-72 h) tested (Yeow *et al.*, 2002). However *in vivo* studies have shown that muscle injury initially results in activation of p38 that promotes MyoD expression, and that the accumulation of MyoD in the injured muscles causes a subsequent down regulation of p38 activity (Wu *et al.*, 2000). We observed that both unwounded and wounded cultures consistently expressed MyoD protein (see **Figure 36 and 37**) which might play a dynamic role in the regulation of p38 MAPK signaling in our system. The p38 MAPK activation was rapid and brief in 5 min post-injury cultures and phosphorylated p38 levels were low at subsequent time points. This transient expression pattern of phosphorylated p38 MAPK in our *in vitro* model, might suggest that wounding induced p38 activation, which could stimulate accumulation of MyoD protein. Once the MyoD protein reached a sufficient level, the p38 activation was inhibited. As such, our *in vitro* findings may be consistent with the *in vivo* studies conducted by Wu *et al* (2000).

When p38 MAPK signaling was inhibited by 10  $\mu$ M of SB202190 treatment in the wounded micromass co-cultures, it resulted in accelerated wound closure (see **Figure 60**). SB202190 is a highly specific inhibitor of p38 MAPK (Davies *et al.*, 2000) and western blots confirmed that 10  $\mu$ M of SB202190 effectively inhibited phosphorylation of p38 MAPK in micromass co-culture (see **Figure 59**). Studies have shown that during *in vivo* mammalian skeletal muscle healing, p38 MAPK might be necessary for optimum skeletal muscle regeneration at later stages of the tissue repair process. However, persistent activation of p38 MAPK in early skeletal muscle repair process may impair overall skeletal muscle healing (Nguyen and Witzke, 1997; Wu *et al.*, 2000).

The treatment of the wounded micromass co-culture with 100 ng/mL of

anisomycin resulted in delayed wound closure (see **Figure 60**). Anisomycin also caused eventual disruption of the integrity of the wounded micromass co-culture. A plausible reason for this disruption could be that protein synthesis is required to maintain the micromass culture integrity. Anisomycin interferes with protein synthesis by binding to 60S ribosomal subunits and blocking peptide bond formation (Ogawa *et al.*, 2004). This triggers cellular stress responses including activation of p38 and JNK signaling cascades (Khurana and Dey, 2003). It was observed that 100 ng/mL of anisomycin caused sustained expression of dual phosphorylated p38 MAPK protein in the micromass co-cultures (see **Figure 59**), which served as a positive control in our experiments for detecting dual phosphorylated p38 MAPK in western blots.

The observations made in our newly developed micromass co-culture based wound repair model suggest its superiority over other *in vitro* skeletal muscle wound models in its ability to closely mimic early *in vivo* skeletal muscle tissue injury response. Our experiments also showed that p38 MAPK inactivation resulted in accelerated wound closure, while sustained ERK1/2 inactivation delayed wound closure in the micromass co-culture. Collectively, these findings indirectly suggest that both p38 and ERK1/2 MAP kinases might be potential drug targets for wound healing modulators.

### **5.3. Quercetin and OTC treatment of wounded micromass co-culture of 1: 3 ratio of fibroblast and L8 myoblast cells suggest that they have differential effects on wound closure through their activity on MAPK signaling pathway, and modulating expression patterns of extracellular matrix gene transcripts.**

The final experiments utilized the 1:3 FR fibroblast: L8 myoblast micromass co-cultures to examine the effects of OTC and quercetin on *in vitro* wound repair. When wounded micromass co-cultures were treated with 40  $\mu$ M of quercetin, it promoted a

delay in wound closure as compared to untreated wounded cultures (see **Figures 67, 68 b**). The level of p38 MAPK was unaffected by quercetin treatment, while there was significant decrease in the level of active, phosphorylated ERK1/2 (see **Figures 70, 71**).

In contrast, treatment of the micromass co-cultures with 1.5 mM of OTC resulted in accelerated wound closure at the 1-4 day time points as compared to wounded cultures maintained in control medium (see **Figures 67 and 68 a**). It was observed that OTC significantly decreased both p38 MAPK and ERK1/2 activation (see **Figures 70-71**).

These observations indicate that p38 MAPK and ERK1/2 were consistent targets for OTC in both our *in vitro* micromass culture system and in our *in vivo* laminectomy model of peridural wound healing. In contrast, quercetin had no effect on p38 MAPK phosphorylation in either our *in vivo* or *in vitro* studies.

In micromass co-cultures, treatment with 40  $\mu$ M quercetin decreased ERK1/2 activation. On the contrary, when quercetin was administered to the animals *in vivo* at 0.025 mmol/kg, no change in ERK1/2 activation was observed within the peridural scar tissue as compared to saline treated control animals. The contrasting effects of quercetin on ERK1/2 activation *in vitro* versus *in vivo* might be attributed to the lower dose administered to animals *in vivo*. *In vitro* dose response studies on the effects of OTC and quercetin in micromass co-cultures showed changes in total DNA and total collagen staining starting at higher concentration (> 1.0 mM for OTC and > 25  $\mu$ M for quercetin) of these molecules (see **Figure 61-66**). Micromass co-cultures treated with 1.5 mM OTC or 40  $\mu$ M quercetin showed an inhibition of collagen biosynthesis and reduction in total DNA levels (see **Figures 61 and 64**). The doses of OTC (1.0 mmol/kg or 1.0 mM) and quercetin (0.025 mmol/kg or 25  $\mu$ M) that were administered in our live animal

experiments might not have been adequate for exerting detectable anti-scarring effects on the peridural tissue.

In addition, the *in vivo* peridural tissue healing process not only involves myoblast and fibroblast cells but also other cellular components, such as inflammatory cells, blood products, which might contribute to differential changes observed in ERK1/2 activation following quercetin treatment. Moreover, it should be noted that a xenobiotic, such as quercetin, when administered systemically can undergo first pass metabolism to form metabolites which can also influence local cellular responses (Hollman *et al.*, 1995; Huk *et al.*, 1998; Juurlink and Paterson, 1998; Theoharides *et al.*, 2001; Wang and Joseph, 1999). First pass metabolism was not replicated in our *in vitro* model; however it would be possible to directly test the effects of the drug's known first-pass metabolites on *in vitro* tissue repair.

Middleton *et al.* (2000) have reported that quercetin inhibits p38 MAPK activation and decreases stress proteins such as hsp70 in malignant tumor cells and UV/H<sub>2</sub>O<sub>2</sub> sensitized cells. This study showed that quercetin can exert its p38 MAPK inhibitory and anti-fibrotic activity on cells that have some degree of DNA damage caused by external stimuli. In our experiments, quercetin had no detectable effect on p38 MAPK activation; whereas OTC treatment affected both the p38 and ERK1/2 MAP kinase pathways in micromass co-culture of FR fibroblast and L8 myoblast cells.

To summarize, our *in vitro* data revealed that when micromass co-cultures are treated with 40  $\mu$ M quercetin or 1.5 mM OTC:

1. Quercetin treatment delayed wound closure *in vitro* and reduced ERK1/2 phosphorylation. A similar delay in wound closure was observed in cultures that

were treated with a specific ERK pathway inhibitor, PD184352. This suggests that quercetin's ability to inhibit ERK activity might be a mechanism through which it delays wound closure in the micromass co-culture model.

2. RT-PCR data revealed that transcript levels of the hyaluronan receptor CD44 were significantly higher in quercetin treated cultures at 2 day post wounding as compared to control untreated cultures at the same time point, while CD44 transcript levels were significantly lower in quercetin treated cultures at 4 day post wounding relative to controls. Transcript levels of HAS 1 and HAS 3, as well as hyaluronan receptor RHAMM were elevated in quercetin treated cultures as compared to untreated control cultures at both 2 and 4 days post-wounding. Thus quercetin may modulate the expression of RHAMM, HAS 1, HAS 3 and CD44 *in vitro*.
3. Picrosirius red staining showed that both OTC at 1.5 mM and quercetin at 40  $\mu$ M concentration significantly reduced collagen synthesis in micromass co-cultures.
4. OTC treatment accelerated wound closure in micromass co-cultures, and decreased p38-MAPK activity. More rapid wound closure was also observed in cultures that were treated with a specific p38-MAPK inhibitor SB202190. The ability of OTC to inhibit p38-MAPK activity might be a mechanism through which it accelerates wound closure in the micromass co-culture.
5. OTC treatment caused a slight decrease in ERK1/2 activation in the micromass co-culture at 5 min post-wounding and increased the rate of *in vitro* wound closure. In contrast, sustained ERK inhibition in the presence of PD184352 delayed wound closure in the micromass cultures. This suggests that the transient decline in ERK

phosphorylation elicited by OTC treatment was probably of insufficient duration to negatively affect the rate of wound closure.

6. Expression of mRNAs for hsp-47, a collagen-specific chaperone protein was increased in OTC treated cultures at 2 days post wounding as compared to untreated cultures. OTC treated cultures at 2 day post-wounding had decreased type I, III, IV collagen transcript levels, while only type IV and type I collagen transcript levels were found to be decreased at 4 day time-point. OTC at 1.5 mM concentration was found to reduce collagen biosynthesis in micromass co-cultures.

Collectively, the findings suggest that OTC may reduce collagen production during the early phase of *in vitro* wound healing. It is still unclear how the changes in various other gene transcript levels that we observed influence the process of wound closure in this *in vitro* model. A more comprehensive transcriptomic and proteomic analysis using modern microarray strategies might help uncover the exact molecular mechanisms through which OTC and quercetin exert their effects. Nevertheless, these RT-PCR experiments demonstrate the potential utility of our micromass co-culture wound repair model for evaluating the effects of candidate wound modulating drugs on specific gene expression profiles.

#### **5.4 As compared to quercetin, OTC might have significant potential as an anti-scarring drug through attenuation of p38 and ERK1/2 MAPK signaling mediated by a cytoprotective gene regulatory pathway.**

As discussed in **Section 5.1.5** and **5.3**, OTC was found to consistently affect p38 and ERK1/2 MAPK activation both *in vivo* and *in vitro*. Moreover, OTC was found to reduce collagen biosynthesis and improve wound closure *in vitro*. On the basis of these

findings, together with previous reports suggesting the cytoprotective effects of OTC, we propose a hypothetical model of the possible mechanism of OTC action on peridural wound repair. One might speculate that the ability of OTC to promote cellular glutathione synthesis helps to activate the expression of cytoprotective genes and/or cellular homeostatic mechanisms. This might in turn help prevent excessive collagen production and improper post-translational modifications. The consistent inhibition of p38 MAPK and ERK1/2 signaling pathway by OTC observed in our *in vitro* model may also suggest the synergistic potential of elevated cellular glutathione levels in attenuating MAP kinase pathways (see **Appendix 3, A**). OTC is metabolized by 5-oxoprolinase intracellularly into cysteine, a rate limiting amino acid in glutathione (GSH) synthesis, which favors improved intracellular GSH levels. The physiochemical properties of OTC, such as its hydrophilic nature, may favor conversion of OTC into GSH, rather than taurine or sulfates in myoblast cells (Banks and Stipanuk, 1994, Ferreira *et al.*, 2009). The increased intracellular GSH levels will in turn promote desired beneficial pharmacological and cellular effects. Based on these properties, we propose that OTC has potential as an anti-scarring agent through its ability to improve GSH levels that attenuate oxidative stress responses, by activating anti-oxidant and cytoprotective gene regulatory mechanisms by targeting the Nrf-2/Keap 1 complex (Zipper and Mulcahy, 2000; Yamamoto *et al.*, 2007) in myoblast and fibroblast cells. Activation of the Keap1/Nrf-2 pathway might cause the attenuation of the p38 and ERK1/2 MAPK pathways observed in our *in vivo* and *in vitro* experiments. However, other molecular mechanisms targeting activation of the antioxidant response element (ARE) and/or attenuation of NF- $\kappa$ B signaling that in turn attenuate p38 and ERK1/2 MAPK pathways cannot be ruled out (Balogun *et al.*, 2003;

Vayalil *et al.*,2007; Peng *et al.*, 2010).

Previous studies have demonstrated that quercetin and its metabolites might also cause activation of a cytoprotective gene regulatory pathway (Juurlink and Paterrson. 1998; Middleton *et al.*2000; Wadsworth *et al.* 2001) through multiple targets including activation of phase II enzymes (see **Appendix 3, B**). Inactivation of ERK1/2 and p38 MAPK pathway by quercetin could also be achieved through these cytoprotective mechanisms (Huk *et al.*, 1998; Theoharides *et al.*, 2001) . However, in our study we observed that quercetin did not affect p38 MAPK activation which was contrary to previous studies (Huk *et al.*, 1998; Middleton *et al.*, 2000; Phan *et al.*, 2003; Tan *et al.*, 2003; Nam *et al.*, 2008; Jiang *et al.*, 2008). Middleton *et al.* (2000) has shown that quercetin had potent anti-MAPK properties only on cells that had some level of DNA damage or are made susceptible through UV irradiation or hydrogen peroxide treatment. One possible explanation for the consistent expression of p38 MAPK in quercetin treated animals and wounded micromass cultures would have been that the cells tested in our study were normal and did not have any level of DNA damage, and this rendered quercetin impotent in exerting its anti-MAPK properties as observed in previous reports. Hence, our overall finding from *in vitro* and *in vivo* model appear to support the findings of Perez-Vizcaino *et al.* (2006), where it has been shown that quercetin did not affect either p38 or ERK1/2 activation in primary smooth muscle cells, and suggests that the quercetin might not affect either p38 or ERK1/2 signaling pathway in peridural scar tissues.

## 5.5. Conclusions

Our live animal studies using the spinal laminectomy wound repair model examined the effect of OTC and quercetin treatment on collagen accumulation in peridural scar tissues. Neither OTC nor quercetin treatment significantly altered picrosirius red stainable collagen levels in the tissue sections. Moreover, RNA dot blot and western blot analyses revealed no statistically significant changes in the expression of biomarkers of collagen biosynthesis (type I and III collagen, P4H, and hsp-47), possibly due to huge animal to animal variation within each of the drug treatment groups. Collectively, these whole animal studies yielded no substantial evidence to suggest that either OTC or quercetin was effective in reducing peridural scarring *in vivo*.

One positive outcome of our *in vivo* experiments was that we were able to successfully correlate the synchrotron FTIR spectral maps of collagen distribution and orientation in tissue sections with picrosirius red polarized light images. Western blot analyses indicated that the peridural scar tissue contained MyoD positive cells with an apparent absence of differentiated muscle fibres. The presence of fibroblast cells was suggested by the expression of a fibroblast marker protein, P4H. It was also observed that OTC consistently reduced both p38 MAPK and ERK1/2 activation in peridural scar tissue, while quercetin had no effect on either p38 MAPK or ERK1/2 activation.

Overall our *in vivo* experiments revealed numerous problems associated with the use of whole animal models, especially animal to animal variation that might be attributed to:

- i.) Use of a complex wound model system that incorporates both excisional and incisional forms of wounding.

- ii.) Use of animals from different genetic breeding lines.
- iii.) The complexity of the peridural wound healing process *in vivo*, which makes it difficult to predict the most appropriate biomarkers and metabolic parameters to assay in testing the efficacy of potential wound modulating drugs.
- iv.) The possibility that the doses of OTC and quercetin employed were not optimal for eliciting effects on peridural scarring.
- v.) The potentially variable pharmacological actions of drugs such as quercetin and OTC on different cell types *in vivo*. Their pharmacological efficacy might be masked in a heterogeneous tissue system such as the peridural wound tissue.

The second objective of my study was to develop a novel *in vitro* system that models peridural tissue repair in general and can be specifically applied to drug development studies on wound healing. We have demonstrated, for the first time, the potential utility of micromass co-culture technology towards developing a 3-D scaffold-free *in vitro* wound-healing model. We determined that a 1:3 seeding ratio of FR 3T3 fibroblast cells and L8 myoblast cells would form a 3-D microtissue *in vitro* that expressed myoblast and fibroblast markers such as MyoD, P4H, and  $\alpha$ -sma. The expression of fibroblast and myoblast biomarkers in the micromass co-culture system suggested molecular similarities to peridural tissue isolated from laminectomized rats.

The microtissue obtained was subjected to a single scrape and drug effects on wound closure rates could be quantified by the planimetry method. By labeling myoblast and fibroblast cells with fluorescent tracker dyes, we demonstrated preferential migration of fibroblast cells to the wound site.

The method validation studies using TGF- $\beta$ 1, modulators of MAPK signaling,

OTC and quercetin on this novel micromass co-culture model suggest its potential utility in rapid screening of candidate therapeutic agents for effects on the rate of wound closure. Thus, we describe for the first time the potential utility of micromass co-culture technology in wound healing and subsequent drug development research.

Studies on the micromass co-cultures revealed OTC and quercetin significantly reduced collagen biosynthesis *in vitro* in a dose-dependent manner. OTC accelerated the rate of wound closure while quercetin delayed the rate of wound closure in the wounded micromass co-cultures. OTC was found to inhibit both p38 and ERK1/2 MAP kinases during the early *in vitro* wound healing process, while quercetin inhibited ERK1/2 only. Thus, we demonstrated that OTC and quercetin may elicit distinct biological responses in the micromass co-culture wound repair model.

Collectively, both the micromass co-culture experiments and live animal studies suggest p38, ERK1 and ERK2 as potential molecular targets through which OTC might mitigate tissue fibrosis or scarring. Evidence from *in vitro* studies suggests that OTC might exert anti-scarring properties especially during the initial wound healing process through its inhibition of injury induced p38 MAPK activation that helps to promote accelerated wound closure. OTC was also found to decrease collagen gene transcript levels while quercetin seemed to modulate expression of the gene transcripts for hyaluronan receptors, RHAMM and CD44.

Our experiments suggest that quercetin may not be effective as an anti-scarring agent as it delays wound closure *in vitro*. In contrast, OTC may have some beneficial anti-scarring effects since it reduces collagen gene transcript levels and collagen deposition in micromass co-cultures and also accelerates wound closure *in vitro*.

## 5.6 Future directions

As in the case of any research, these experiments have raised more questions than answers and have opened up potentially fruitful avenues for future investigations. Our novel micromass co-culture wound repair model can be employed to determine changes in gene transcript and protein levels for other biomolecules implicated in tissue healing process such as integrins, JNK, SMADs, osteopontin, MMPs, Pax-7, and calcineurin. It has been suggested that integrins and JNK play a crucial role in myofibroblastic transition, while Pax 7 and SMADs are involved in regulating cell-cell interactions during skeletal muscle repair (Allbrook, 1973; Ambrosio *et al.*, 2009; Ambrosio *et al.*, 2008; Baker and Margolis, 1987; Best and Hunter, 2000).

The extent of myofibroblastic differentiation within our 3-D micromass co-culture system should be investigated, as previous *in vitro* studies have demonstrated myofibroblastic differentiation in the cutaneous wound using a two dimensional monolayer culture system (Amadeu *et al.*, 2003). It has been proposed that the Ca<sup>2+</sup> dependent cyclic AMP mediated signaling mechanism may play a crucial role in skeletal muscle injury as well as myofibroblastic transition, and differentiation (Allbrook, 1973; Ambrosio *et al.*, 2009; Ambrosio *et al.*, 2008; Baker and Margolis, 1987; Best and Hunter, 2000). Future investigations can explore the role of Ca<sup>2+</sup> dependent cyclic AMP mediated signaling mechanism in myofibroblastic transition utilizing our newly developed *in vitro* wound model.

Semi-quantitative RT-PCR technique was used to determine relative gene expression levels in our study. In the RT-PCR technique, the relative amplification efficiencies of the different gene transcripts in PCR could be influenced by differences in

primer's affinity for their target, differences in length of the amplicon, and the extent of amplification of competing non-specific PCR products. Hence, it would be important to confirm our findings using more rigorous methods such as quantitative real-time PCR. Moreover, in future experiments it would be important to specifically characterize changes in gene expression within cells localized at the wound site. This could be accomplished through application of laser directed microdissection technique, in conjunction with genomic, metabolomic & proteomic tools (e.g. tandem mass spectrometry, cDNA, and protein microarrays) to comprehensively analyze gene expression changes resulting from wounding and drug treatments. Confocal fluorescence microscopy can also be employed to better characterize drug effects on cell migration.

The utility of our micromass co-culture model for use in wound healing research should be validated using anti-scarring drugs with established efficacy such as Avotermin (a proprietary recombinant human TGF- $\beta$ 3 protein). Growth factor inhibitors that target TGF- $\beta$  signaling pathway (including TGF- $\beta$ 1 or CTGF antibodies) can also be tested. Moreover, the efficacy of novel candidate anti-scarring drugs should be tested alongside established anti-scarring drugs to assess their relative therapeutic potential.

Alternative research could involve testing the inflammatory response during *in vitro* repair in the micromass tissue layers. The inflammatory condition can be mimicked in the micromass co-culture system by incorporating conditioned media obtained from the cultures of macrophages or other inflammatory cells.

There is a clear potential to further refine the micromass model so that it would more closely mimic *in vivo* tissue repair. It would be possible to develop "tri-culture" or "tetra-culture" micromass system using three or four different cell types in combination

to more closely match the *in vivo* situation. In these systems, cell types such as endothelial cells, macrophages, and keratinocytes could be combined along with myoblast and fibroblast cells under micromass conditions. Of course, the more cell types that are incorporated into the micromass culture model to the study wound healing process, the more difficult it becomes to optimize culture conditions, and to interpret experimental outcomes of drug exposures or other treatments. Additionally, as an alternative to the FR fibroblast and L8 myoblast cell lines used in our study, it might be possible to use various other rat myoblast cell lines (e.g. L6; H9c2) and fibroblast cell lines (e.g. Rat2; C6) to develop micromass co-cultures.

The micromass wound model could also be modified by altering the type of wound inflicted on the culture such as inducing a punch wound using micropipette tip rather than a single scrape wound across the diameter of the micromass culture as utilized in this study. A focal punch wound might elicit a different wound healing response in the micromass culture in which it is easier to determine localized changes in protein and mRNA expression. Similarly a chemical injury could be inflicted on the micromass tissue layer, such as the application of NaOH crystals. Thus, our micromass co-culture model could be applied to the study of a wide range of wound healing responses.

The micromass co-culture technology developed in this study could be extended towards the utilization of human primary or immortalized cell lines as well as primary cells derived directly from human scar tissue. The primary advantage of using a human cell based micromass system is that the cultured “microtissues” might better mimic human tissue responses under *in vivo* conditions. These human microtissues could help to accelerate preclinical drug development research in a more cost-effective and efficient

manner. These microtissues can be used to test pharmacological (dose-response curve, absorption, distribution, metabolism, excretion and toxicity) and toxicological parameters of the potential therapeutic drug molecules by circumventing the need to use large number of animals during the initial pre-clinical screening and evaluation.

It should be possible to develop experimental microtissues from cells of cardiac, renal and hepatic origin by adapting the micromass co-culture strategy that was used in this study. This approach may help to increase the ease and precision of early drug screening and validation in a cost-efficient animal-free setting. This will also provide a vast window of opportunity for drug discovery and multiple drug analyses at tissue level. Moreover these experimental cardiac, renal and hepatic “microtissues” would have immense potential for future autologous tissue transplantation therapy too.

Our preliminary qualitative comparisons of cutaneous scar formation in laminectomized rats suggested that both quercetin and OTC might ameliorate cutaneous scarring after a laceration injury. This possibility should be investigated directly using a cutaneous wound healing model such as that described by Gottrup (2000), where duplicate skin incisions are inflicted on the back of a rat and the drug to be tested is applied to one wound while the other wound serves as matched control. Alternatively, a cutaneous punch wound model could be employed. The advantages of these *in vivo* approaches are better control of initial wound trauma, a more standardized wound healing response and the ability to use the same animal as test and control to reduce the influence of individual animal to animal variability.

A possible direction for future research could be to develop derivatives of quercetin that can be administered topically rather than the systemic delivery approach

employed in this study. Several avenues of multidisciplinary research could be pursued, such as development of topical drug delivery systems for quercetin, quercetin derivatives and OTC which would interest pharmaceutical scientists.

## REFERENCES

- Adamson, B., Schwarz, D., Klugston, P., Gilmont, R., Perry, L., Fisher, J., Lindblad, W., and Rees, R. (1996). Delayed repair: the role of glutathione in a rat incisional wound model. *J Surg Res* **62**, 159-64.
- Adzick, N. S., and Lorenz, H. P. (1994). Cells, matrix, growth factors, and the surgeon. The biology of scarless fetal wound repair. *Ann Surg* **220**, 10-8.
- Agmon, A., Yang, L. T., Jones, E. G., and O'Dowd, D. K. (1995). Topological precision in the thalamic projection to neonatal mouse barrel cortex. *J Neurosci* **15**, 549-61.
- Agren, M. S., Jorgensen, L. N., Andersen, M., Viljanto, J., and Gottrup, F. (1998). Matrix metalloproteinase 9 level predicts optimal collagen deposition during early wound repair in humans. *Br J Surg* **85**, 68-71.
- Ahn, S. T., and Mustoe, T. A. (1990). Effects of ischemia on ulcer wound healing: a new model in the rabbit ear. *Ann Plast Surg* **24**, 17-23.
- Ahrens, P. B., Solorsh, M., and Reiter, R. S. (1977). Stage-related capacity for limb chondrogenesis in cell culture. *Dev Biol* **60**, 69-82.
- Alaish, S. M., Bettinger, D. A., Olutoye, O. O., Gould, L. J., Yager, D. R., Davis, A., Crossland, M. C., Diegelmann, R. F., and Cohen, I. K. (1995). Comparison of the polyvinyl alcohol sponge and expanded polytetrafluoroethylene subcutaneous implants as models to evaluate wound healing potential in human beings. *Wound Repair Regen* **3**, 292-8.
- Allbrook, D. (1973). Muscle regeneration. *Physiotherapy* **59**, 240-7.
- Almeida, D. B., Prandini, M. N., Awamura, Y., Vitola, M. L., Simiao, M. P., Milano, J. B., Bordignon, K. C., Ache, M. P., and Ramina, R. (2008). Outcome following lumbar disc surgery: the role of fibrosis. *Acta Neurochir (Wien)* **150**, 1167-76.
- Almekinders, L. C., and Gilbert, J. A. (1986). Healing of experimental muscle strains and the effects of nonsteroidal antiinflammatory medication. *Am J Sports Med* **14**, 303-8.
- Amadeu, T. P., Coulomb, B., Desmouliere, A., and Costa, A. M. (2003). Cutaneous wound healing: myofibroblastic differentiation and *in vitro* models. *Int J Low Extrem Wounds* **2**, 60-8.
- Ambrosio, F., Kadi, F., Lexell, J., Fitzgerald, G. K., Boninger, M. L., and Huard, J. (2009). The effect of muscle loading on skeletal muscle regenerative potential: an update of current research findings relating to aging and neuromuscular pathology. *Am J Phys Med Rehabil* **88**, 145-55.

- Ambrosio, F., Li, Y., Usas, A., Boninger, M. L., and J, H. (2008). Muscle Repair after injury and disease. In "Musculoskeletal Tissue regeneration: Biological Materials and Methods" (W. Pietrzak, Ed.), pp. 459-480. Humana Press, Totowa, NJ, USA.
- Anderer, U., and Libera, J. (2002). *In vitro* engineering of human autogenous cartilage. *J Bone Miner Res* **17**, 1420-9.
- Annoni, G., Luvara, G., Arosio, B., Gagliano, N., Fiordaliso, F., Santambrogio, D., Jeremic, G., Mircoli, L., Latini, R., Vergani, C., and Masson, S. (1998). Age-dependent expression of fibrosis-related genes and collagen deposition in the rat myocardium. *Mech Ageing Dev* **101**, 57-72.
- Annunen, P., Autio-Harmainen, H., and Kivirikko, K. I. (1998). The novel type II prolyl 4-hydroxylase is the main enzyme form in chondrocytes and capillary endothelial cells, whereas the type I enzyme predominates in most cells. *J Biol Chem* **273**, 5989-92.
- Annunen, P., Helaakoski, T., Myllyharju, J., Veijola, J., Pihlajaniemi, T., and Kivirikko, K. I. (1997). Cloning of the human prolyl 4-hydroxylase alpha subunit isoform alpha(II) and characterization of the type II enzyme tetramer. The alpha(I) and alpha(II) subunits do not form a mixed alpha(I) alpha(II)beta2 tetramer. *J Biol Chem* **272**, 17342-8.
- Aota, S., Nagai, T., Olden, K., Akiyama, S. K., and Yamada, K. M. (1991). Fibronectin and integrins in cell adhesion and migration. *Biochem Soc Trans* **19**, 830-5.
- Apisariyakul, A., Chaichana, N., and Takemura, H. (1999). Dual effects of quercetin on contraction in cardiac and skeletal muscle preparations. *Res Commun Mol Pathol Pharmacol* **105**, 129-38.
- Arnold, L., Henry, A., Poron, F., Baba-Amer, Y., van Rooijen, N., Plonquet, A., Gherardi, R. K., and Chazaud, B. (2007). Inflammatory monocytes recruited after skeletal muscle injury switch into antiinflammatory macrophages to support myogenesis. *J Exp Med* **204**, 1057-69.
- Aronson, D., Wojtaszewski, J. F., Thorell, A., Nygren, J., Zangen, D., Richter, E. A., Ljungqvist, O., Fielding, R. A., and Goodyear, L. J. (1998). Extracellular-regulated protein kinase cascades are activated in response to injury in human skeletal muscle. *Am J Physiol* **275**, C555-61.
- Arsic, N., Zacchigna, S., Zentilin, L., Ramirez-Correa, G., Pattarini, L., Salvi, A., Sinagra, G., and Giacca, M. (2004). Vascular endothelial growth factor stimulates skeletal muscle regeneration *in vivo*. *Mol Ther* **10**, 844-54.
- Ausubel, F., Brent, R., Kingston, R., Moore, D., Seidman, J., Smith, J., and Struhl, K. (1994). "Current Protocols in Molecular Biology." John Wiley & Sons, New York.

- Babu, M., Diegelmann, R., and Oliver, N. (1992). Keloid fibroblasts exhibit an altered response to TGF-beta. *J Invest Dermatol* **99**, 650-5.
- Bailey, A. J., Shellswell, G. B., and Duance, V. C. (1979). Identification and change of collagen types in differentiating myoblasts and developing chick muscle. *Nature* **278**, 67-9.
- Baker, J. H., and Margolis, R. N. (1987). Calcium-activated protease activity in tenotomized muscle. *Muscle Nerve* **10**, 34-40.
- Balogun, E., Hoque, M., Gong, P., Killeen, E., Green, C. J., Foresti, R., Alam, J., and Motterlini, R. (2003). Curcumin activates the haem oxygenase-1 gene via regulation of Nrf2 and the antioxidant-responsive element. *Biochem J* **371**, 887-95.
- Banks, M. F., and Stipanuk, M. H. (1994). The utilization of N-acetylcysteine and 2-oxothiazolidine-4-carboxylate by rat hepatocytes is limited by their rate of uptake and conversion to cysteine. *J Nutr* **124**, 378-87.
- Bassleer, C., Gysen, P., Foidart, J. M., Bassleer, R., and Franchimont, P. (1986). Human chondrocytes in tridimensional culture. *In vitro Cell Dev Biol* **22**, 113-9.
- Bates, D. O., and Jones, R. O. (2003). The role of vascular endothelial growth factor in wound healing. *Int J Low Extrem Wounds* **2**, 107-20.
- Bayat, A., Arscott, G., Ollier, W. E., Ferguson, M. W., and McGrouther, D. A. (2003). "Aggressive keloid": a severe variant of familial keloid scarring. *J R Soc Med* **96**, 554-5.
- Bennett, N. T., and Schultz, G. S. (1993). Growth factors and wound healing: biochemical properties of growth factors and their receptors. *Am J Surg* **165**, 728-37.
- Best, T. M., and Hunter, K. D. (2000). Muscle injury and repair. *Phys Med Rehabil Clin N Am* **11**, 251-66.
- Bhadriraju, K., and Chen, C. S. (2002). Engineering cellular microenvironments to improve cell-based drug testing. *Drug Discov Today* **7**, 612-20.
- Bhalla, D. K. (1999). Evaluation of wound repair mechanisms with an *in vitro* cell culture model. *J Lab Clin Med* **134**, 331-2.
- Bhatia, S. N., Yarmush, M. L., and Toner, M. (1997). Controlling cell interactions by micropatterning in co-cultures: hepatocytes and 3T3 fibroblasts. *J Biomed Mater Res* **34**, 189-99.
- Bjorkerud, S., Bjorkerud, B., and Joelsson, M. (1994). Structural organization of reconstituted human arterial smooth muscle tissue. *Arterioscler Thromb* **14**, 644-51.

- Bloch, W., Huggel, K., Sasaki, T., Grose, R., Bugnon, P., Addicks, K., Timpl, R., and Werner, S. (2000). The angiogenesis inhibitor endostatin impairs blood vessel maturation during wound healing. *FASEB J* **14**, 2373-6.
- Bobick, B. E. (2006). Regulation of *in vitro* chondrogenesis by mitogen-activated protein kinases. In "Department of Anatomy & Cell biology", pp. 281. University of Saskatchewan, Saskatoon.
- Bobick, B. E., and Kulyk, W. M. (2004). The MEK-ERK signaling pathway is a negative regulator of cartilage-specific gene expression in embryonic limb mesenchyme. *J Biol Chem* **279**, 4588-95.
- Bock, O., and Mrowietz, U. (2002). [Keloids. A fibroproliferative disorder of unknown etiology]. *Hautarzt* **53**, 515-23.
- Boess, F., Kamber, M., Romer, S., Gasser, R., Muller, D., Albertini, S., and Suter, L. (2003). Gene expression in two hepatic cell lines, cultured primary hepatocytes, and liver slices compared to the *in vivo* liver gene expression in rats: possible implications for toxicogenomics use of *in vitro* systems. *Toxicol Sci* **73**, 386-402.
- Border, W. A., and Noble, N. A. (1994). Transforming growth factor beta in tissue fibrosis. *N Engl J Med* **331**, 1286-92.
- Bosch, P., Musgrave, D., Ghivizzani, S., Latterman, C., Day, C. S., and Huard, J. (2000). The efficiency of muscle-derived cell-mediated bone formation. *Cell Transplant* **9**, 463-70.
- Bradford, M. M. (1976). A rapid and sensitive method for the quantitation of microgram quantities of protein utilizing the principle of protein-dye binding. *Anal Biochem* **72**, 248-54.
- Bryan, B. A., Walshe, T. E., Mitchell, D. C., Havumaki, J. S., Saint-Geniez, M., Maharaj, A. S., Maldonado, A. E., and D'Amore, P. A. (2008). Coordinated vascular endothelial growth factor expression and signaling during skeletal myogenic differentiation. *Mol Biol Cell* **19**, 994-1006.
- Calderon, M., Lawrence, W. T., and Banes, A. J. (1996). Increased proliferation in keloid fibroblasts wounded *in vitro*. *J Surg Res* **61**, 343-7.
- Camacho, N. P., West, P., Torzilli, P. A., and Mendelsohn, R. (2001). FTIR microscopic imaging of collagen and proteoglycan in bovine cartilage. *Biopolymers* **62**, 1-8.
- Cannon, J. G., and St Pierre, B. A. (1998). Cytokines in exertion-induced skeletal muscle injury. *Mol Cell Biochem* **179**, 159-67.
- Carlberg, A. L., Pucci, B., Rallapalli, R., Tuan, R. S., and Hall, D. J. (2001). Efficient chondrogenic differentiation of mesenchymal cells in micromass culture by retroviral gene transfer of BMP-2. *Differentiation* **67**, 128-38.

- Carlson, B. M. (2005). Some principles of regeneration in mammalian systems. *Anat Rec B New Anat* **287**, 4-13.
- Carlson, C. J., Booth, F. W., and Gordon, S. E. (1999). Skeletal muscle myostatin mRNA expression is fiber-type specific and increases during hindlimb unloading. *Am J Physiol* **277**, R601-6.
- Cha, D., O'Brien, P., O'Toole, E. A., Woodley, D. T., and Hudson, L. G. (1996). Enhanced modulation of keratinocyte motility by transforming growth factor-alpha (TGF-alpha) relative to epidermal growth factor (EGF). *J Invest Dermatol* **106**, 590-7.
- Chazaud, B., Sonnet, C., Lafuste, P., Bassez, G., Rimaniol, A. C., Poron, F., Authier, F. J., Dreyfus, P. A., and Gherardi, R. K. (2003). Satellite cells attract monocytes and use macrophages as a support to escape apoptosis and enhance muscle growth. *J Cell Biol* **163**, 1133-43.
- Chen, S. E., Jin, B., and Li, Y. P. (2007). TNF-alpha regulates myogenesis and muscle regeneration by activating p38 MAPK. *Am J Physiol Cell Physiol* **292**, C1660-71.
- Chen, W. Y., and Abatangelo, G. (1999). Functions of hyaluronan in wound repair. *Wound Repair Regen* **7**, 79-89.
- Chin, G. S., Liu, W., Peled, Z., Lee, T. Y., Steinbrech, D. S., Hsu, M., and Longaker, M. T. (2001). Differential expression of transforming growth factor-beta receptors I and II and activation of Smad 3 in keloid fibroblasts. *Plast Reconstr Surg* **108**, 423-9.
- Chodon, T., Sugihara, T., Igawa, H. H., Funayama, E., and Furukawa, H. (2000). Keloid-derived fibroblasts are refractory to Fas-mediated apoptosis and neutralization of autocrine transforming growth factor-beta1 can abrogate this resistance. *Am J Pathol* **157**, 1661-9.
- Chomczynski, P., and Sacchi, N. (1987). Single-step method of RNA isolation by acid guanidinium thiocyanate-phenol-chloroform extraction. *Anal Biochem* **162**, 156-9.
- Clanton, T. L., Zuo, L., and Klawitter, P. (1999). Oxidants and skeletal muscle function: physiologic and pathophysiologic implications. *Proc Soc Exp Biol Med* **222**, 253-62.
- Clark, R. A. (1988). Potential roles of fibronectin in cutaneous wound repair. *Arch Dermatol* **124**, 201-6.
- Clark, R. A., Lanigan, J. M., DellaPelle, P., Manseau, E., Dvorak, H. F., and Colvin, R. B. (1982). Fibronectin and fibrin provide a provisional matrix for epidermal cell migration during wound reepithelialization. *J Invest Dermatol* **79**, 264-9.
- Clark, R. A., Lin, F., Greiling, D., An, J., and Couchman, J. R. (2004). Fibroblast invasive migration into fibronectin/fibrin gels requires a previously uncharacterized dermatan sulfate-CD44 proteoglycan. *J Invest Dermatol* **122**, 266-77.

- Clark, R. A., McCoy, G. A., Folkvord, J. M., and McPherson, J. M. (1997). TGF-beta 1 stimulates cultured human fibroblasts to proliferate and produce tissue-like fibroplasia: a fibronectin matrix-dependent event. *J Cell Physiol* **170**, 69-80.
- Clark, R. A. F. (1996). "The Molecular and Cellular Biology of Wound Repair." Plenum Press, New York.
- Clark, R. B. (2002). The role of PPARs in inflammation and immunity. *J Leukoc Biol* **71**, 388-400.
- Cochrane, C. A., Freeman, K. L., and Knottenbelt, D. C. (1996). Effect of growth factors on the characteristics of cells associated with equine wound healing and sarcoid formation. *Wound Repair Regen* **4**, 58-65.
- Collier, M. A., Brighton, C. T., Norrdin, R., Twardock, A. R., and Rendano, V. T. (1985). Direct current stimulation of bone production in the horse: preliminary study with a "gap healing" model. *Am J Vet Res* **46**, 610-21.
- Cotelle, N. (2001). Role of flavonoids in oxidative stress. *Curr Top Med Chem* **1**, 569-90.
- Cottrill, C. P., Archer, C. W., and Wolpert, L. (1987). Cell sorting and chondrogenic aggregate formation in micromass culture. *Dev Biol* **122**, 503-15.
- Cox, D. A. (1995). Transforming growth factor-beta 3. *Cell Biol Int* **19**, 357-71.
- Cox, N. (2008). The Anti-Inflammatory Potential of Quercetin and L-2-Oxothiazolidine-4-carboxylate (OTC) in Developing Scar Tissue. In "Department of Anatomy & Cell biology". University of Saskatchewan, Saskatoon.
- Croisier, J. L. (2004). Factors associated with recurrent hamstring injuries. *Sports Med* **34**, 681-95.
- Damsky, C. H., and Werb, Z. (1992). Signal transduction by integrin receptors for extracellular matrix: cooperative processing of extracellular information. *Curr Opin Cell Biol* **4**, 772-81.
- Davidson, J. M., and Breyer, M. D. (2003). Inflammatory modulation and wound repair. *J Invest Dermatol* **120**, 11-12.
- Davies, S. P., Reddy, H., Caivano, M., and Cohen, P. (2000). Specificity and mechanism of action of some commonly used protein kinase inhibitors. *Biochem J* **351**, 95-105
- De Vries, H. J., Mekkes, J. R., Middelkoop, E., Hinrichs, W. L., Wildevuur, C. R., and Westerhof, W. (1993). Dermal substitutes for full-thickness wounds in a one-stage grafting model. *Wound Repair Regen* **1**, 244-52.
- Dedieu, S., Dourdin, N., Dargelos, E., Poussard, S., Veschambre, P., Cottin, P., and Brustis, J. J. (2002). Calpain and myogenesis: development of a convenient cell culture model. *Biol Cell* **94**, 65-76.

- Dedkov, E. I., Kostrominova, T. Y., Borisov, A. B., and Carlson, B. M. (2003). MyoD and myogenin protein expression in skeletal muscles of senile rats. *Cell Tissue Res* **311**, 401-16.
- DeLise, A. M., Stringa, E., Woodward, W. A., Mello, M. A., and Tuan, R. S. (2000). Embryonic limb mesenchyme micromass culture as an *in vitro* model for chondrogenesis and cartilage maturation. *Methods Mol Biol* **137**, 359-75.
- Denker, A. E., Nicoll, S. B., and Tuan, R. S. (1995). Formation of cartilage-like spheroids by micromass cultures of murine C3H10T1/2 cells upon treatment with transforming growth factor-beta 1. *Differentiation* **59**, 25-34.
- di Mola, F. F., Friess, H., Riesle, E., Koliopanos, A., Buchler, P., Zhu, Z., Brigstock, D. R., Korc, M., and Buchler, M. W. (2002). Connective tissue growth factor is involved in pancreatic repair and tissue remodeling in human and rat acute necrotizing pancreatitis. *Ann Surg* **235**, 60-7.
- Diegelmann, R. F., and Evans, M. C. (2004). Wound healing: an overview of acute, fibrotic and delayed healing. *Front Biosci* **9**, 283-9.
- Donaldson, D. J., and Mahan, J. T. (1983). Fibrinogen and fibronectin as substrates for epidermal cell migration during wound closure. *J Cell Sci* **62**, 117-27.
- Dorsett-Martin, W. A. (2004). Rat models of skin wound healing: a review. *Wound Repair Regen* **12**, 591-9.
- Edwall-Arvidsson, C., and Wroblewski, J. (1996). Characterization of chondrogenesis in cells isolated from limb buds in mouse. *Anat Embryol (Berl)* **193**, 453-61.
- Ehrlich, H. P., Blewett, C., Krummel, T. M., and Cutroneo, K. R. (1996). Inhibition of wound closure by transforming growth factor-beta and dexamethasone in a fetal mouse limb organ culture model. *Wound Repair Regen* **4**, 482-8.
- Ehrlich, H. P., Desmouliere, A., Diegelmann, R. F., Cohen, I. K., Compton, C. C., Garner, W. L., Kapanci, Y., and Gabbiani, G. (1994). Morphological and immunochemical differences between keloid and hypertrophic scar. *Am J Pathol* **145**, 105-13.
- Ehrlich, H. P., and Needle, A. L. (1983). Wound healing in tight-skin mice: delayed closure of excised wounds. *Plast Reconstr Surg* **72**, 190-8.
- Eisenberg, C. A., Burch, J. B., and Eisenberg, L. M. (2006). Bone marrow cells transdifferentiate to cardiomyocytes when introduced into the embryonic heart. *Stem Cells* **24**, 1236-45.
- El-Ghalbzouri, A., Lamme, E. N., van Blitterswijk, C., Koopman, J., and Ponec, M. (2004). The use of PEGT/PBT as a dermal scaffold for skin tissue engineering. *Biomaterials* **25**, 2987-96.

- Endo, T., and Nadal-Ginard, B. (1987). Three types of muscle-specific gene expression in fusion-blocked rat skeletal muscle cells: translational control in EGTA-treated cells. *Cell* **49**, 515-26.
- Engert, J. C., Berglund, E. B., and Rosenthal, N. (1996). Proliferation precedes differentiation in IGF-I-stimulated myogenesis. *J Cell Biol* **135**, 431-40.
- Engstrom-Laurent, A. (1997). Hyaluronan in joint disease. *J Intern Med* **242**, 57-60.
- Falanga, V. (1993). Growth factors and wound healing. *Dermatol Clin* **11**, 667-75.
- Ferguson, M. W., and O'Kane, S. (2004). Scar-free healing: from embryonic mechanisms to adult therapeutic intervention. *Philos Trans R Soc Lond B Biol Sci* **359**, 839-50.
- Ferguson, M. W., Whitby, D. J., Shah, M., Armstrong, J., Siebert, J. W., and Longaker, M. T. (1996). Scar formation: the spectral nature of fetal and adult wound repair. *Plast Reconstr Surg* **97**, 854-60.
- Ferreira, L. F., Gilliam, L. A., and Reid, M. B. (2009). L-2-Oxothiazolidine-4-carboxylate reverses glutathione oxidation and delays fatigue of skeletal muscle *in vitro*. *J Appl Physiol* **107**, 211-6.
- Fleischmajer, R., MacDonald, E. D., Perlish, J. S., Burgeson, R. E., and Fisher, L. W. (1990). Dermal collagen fibrils are hybrids of type I and type III collagen molecules. *J Struct Biol* **105**, 162-9.
- Flint, O. P. (1983). A micromass culture method for rat embryonic neural cells. *J Cell Sci* **61**, 247-62.
- Florini, J. R., Ewton, D. Z., and Magri, K. A. (1991). Hormones, growth factors, and myogenic differentiation. *Annu Rev Physiol* **53**, 201-16.
- Frank, C., Shrive, N., Hiraoka, H., Nakamura, N., Kaneda, Y., and Hart, D. (1999). Optimisation of the biology of soft tissue repair. *J Sci Med Sport* **2**, 190-210.
- Frank, S., Madlener, M., and Werner, S. (1996). Transforming growth factors beta1, beta2, and beta3 and their receptors are differentially regulated during normal and impaired wound healing. *J Biol Chem* **271**, 10188-93.
- Fraser, J. R., Laurent, T. C., and Laurent, U. B. (1997). Hyaluronan: its nature, distribution, functions and turnover. *J Intern Med* **242**, 27-33.
- Fukae M, and Mechanic G.L. (1980). Maturation of collagenous tissue. Temporal sequence of formation of peptidyl lysine-derived cross-linking aldehydes and cross-links in collagen. *J Biol Chem* **255**, 6511-18.

- Fukuhara, S., Tomita, S., Yamashiro, S., Morisaki, T., Yutani, C., Kitamura, S., and Nakatani, T. (2003). Direct cell-cell interaction of cardiomyocytes is key for bone marrow stromal cells to go into cardiac lineage *in vitro*. *J Thorac Cardiovasc Surg* **125**, 1470-80.
- Funderburgh, J. L., Funderburgh, M. L., Mann, M. M., Corpuz, L., and Roth, M. R. (2001). Proteoglycan expression during transforming growth factor beta -induced keratocyte-myofibroblast transdifferentiation. *J Biol Chem* **276**, 44173-8.
- Funderburgh, M. L., Du, Y., Mann, M. M., SundarRaj, N., and Funderburgh, J. L. (2005). PAX6 expression identifies progenitor cells for corneal keratocytes. *FASEB J* **19**, 1371-3.
- Furukawa, K. S., Ushida, T., Sakai, Y., Suzuki, M., Tanaka, J., and Tateishi, T. (2001). Formation of human fibroblast aggregates (spheroids) by rotational culture. *Cell Transplant* **10**, 441-5.
- Garrett, W. E., Jr. (1990). Muscle strain injuries: clinical and basic aspects. *Med Sci Sports Exerc* **22**, 436-43.
- Garthoff, B. (2005). Alternatives to animal experimentation: the regulatory background. *Toxicol Appl Pharmacol* **207 Suppl2**: 388-92
- Germani, A., Di Carlo, A., Mangoni, A., Straino, S., Giacinti, C., Turrini, P., Biglioli, P., and Capogrossi, M. C. (2003). Vascular endothelial growth factor modulates skeletal myoblast function. *Am J Pathol* **163**, 1417-28.
- Gerstenfeld, L. C., Barnes, G. L., Shea, C. M., and Einhorn, T. A. (2003). Osteogenic differentiation is selectively promoted by morphogenetic signals from chondrocytes and synergized by a nutrient rich growth environment. *Connect Tissue Res* **44 Suppl 1**, 85-91.
- Ghassemifar, M. R., Ghassemifar, N., and Franzen, L. E. (1995). Macrophage-conditioned medium without serum enhances collagen gel contraction. *In vitro Cell Dev Biol Anim* **31**, 161-3.
- Glise, B., and Noselli, S. (1997). Coupling of Jun amino-terminal kinase and Decapentaplegic signaling pathways in Drosophila morphogenesis. *Genes Dev* **11**, 1738-47.
- Gottrup, F., Agren, M. S., and Karlsmark, T. (2000). Models for use in wound healing research: a survey focusing on *in vitro* and *in vivo* adult soft tissue. *Wound Repair Regen* **8**, 83-96.
- Green, J. A., Stockton, R. A., Johnson, C., and Jacobson, B. S. (2004). 5-lipoxygenase and cyclooxygenase regulate wound closure in NIH/3T3 fibroblast monolayers. *Am J Physiol Cell Physiol* **287**, C373-83.
- Grinnell, F., Billingham, R. E., and Burgess, L. (1981). Distribution of fibronectin during wound healing *in vivo*. *J Invest Dermatol* **76**, 181-9.

- Gruber, B. L. (2003). Mast cells in the pathogenesis of fibrosis. *Curr Rheumatol Rep* **5**, 147-53.
- Halper, J., Griffin, A., Hu, W., Jung, C., Zhang, J., Pan, H., Kisaalita, W. S., Foutz, T. L., and Frazier, K. S. (2005). *In vitro* culture decreases the expression of TGF(beta), Hsp47 and type I procollagen and increases the expression of CTGF in avian tendon explants. *J Musculoskelet Neuronal Interact* **5**, 53-63.
- Handschel, J. G., Depprich, R. A., Kubler, N. R., Wiesmann, H. P., Ommerborn, M., and Meyer, U. (2007). Prospects of micromass culture technology in tissue engineering. *Head Face Med* **3**, 4.
- Harimoto, M., Yamato, M., Hirose, M., Takahashi, C., Isoi, Y., Kikuchi, A., and Okano, T. (2002). Novel approach for achieving double-layered cell sheets co-culture: overlaying endothelial cell sheets onto monolayer hepatocytes utilizing temperature-responsive culture dishes. *J Biomed Mater Res* **62**, 464-70.
- Hattori, T., and Ide, H. (1984). Limb bud chondrogenesis in cell culture, with particular reference to serum concentration in the culture medium. *Exp Cell Res* **150**, 338-46.
- Hayashi, M., Matsuzaki, Y., and Shimonaka, M. (2009). Impact of plasminogen on an *in vitro* wound healing model based on a perfusion cell culture system. *Mol Cell Biochem* **322**, 1-13.
- Hertle, M. D., Kubler, M. D., Leigh, I. M., and Watt, F. M. (1992). Aberrant integrin expression during epidermal wound healing and in psoriatic epidermis. *J Clin Invest* **89**, 1892-901.
- Hertog, M. G., and Hollman, P. C. (1996). Potential health effects of the dietary flavonol quercetin. *Eur J Clin Nutr* **50**, 63-71.
- Higuchi, I., Hashiguchi, A., Matsuura, E., Higashi, K., Shiraishi, T., Hirata, N., Arimura, K., and Osame, M. (2007). Different pattern of HSP47 expression in skeletal muscle of patients with neuromuscular diseases. *Neuromuscul Disord* **17**, 221-6.
- Hill, M., Wernig, A., and Goldspink, G. (2003). Muscle satellite (stem) cell activation during local tissue injury and repair. *J Anat* **203**, 89-99.
- Hinton, J. L., Jr., Warejcka, D. J., Mei, Y., McLendon, R. E., Laurencin, C., Lucas, P. A., and Robinson, J. S., Jr. (1995). Inhibition of epidural scar formation after lumbar laminectomy in the rat. *Spine* **20**, 564-70; discussion 579-80.
- Hoem, D., Dalen, H., Andren-Sandberg, A., and Hostmark, J. (2002). Nonadhesive organ culture of human exocrine pancreatic cells with their stroma. *Pancreas* **25**, 71-7.
- Hoerstrup, S. P., Zund, G., Cheng, S., Melnitchouk, S., Kadner, A., Sodian, R., Kolb, S. A., and Turina, M. (2002). A new approach to completely autologous cardiovascular tissue in humans. *Asaio J* **48**, 234-8.

- Hoffman, L. M., and Kulyk, W. M. (1999). Alcohol promotes *in vitro* chondrogenesis in embryonic facial mesenchyme. *Int J Dev Biol* **43**, 167-74.
- Hollman, P. C., de Vries, J. H., van Leeuwen, S. D., Mengelers, M. J., and Katan, M. B. (1995). Absorption of dietary quercetin glycosides and quercetin in healthy ileostomy volunteers. *Am J Clin Nutr* **62**, 1276-82.
- Holm-Pedersen, P., and Zederfeldt, B. (1971). Granulation tissue formation in subcutaneously implanted cellulose sponges in young and old rats. *Scand J Plast Reconstr Surg* **5**, 13-6.
- Horikawa, M., Higashiyama, S., Nomura, S., Kitamura, Y., Ishikawa, M., and Taniguchi, N. (1999). Upregulation of endogenous heparin-binding EGF-like growth factor and its role as a survival factor in skeletal myotubes. *FEBS Lett* **459**, 100-4.
- Horsley, V., and Pavlath, G. K. (2003). Prostaglandin F<sub>2</sub>(alpha) stimulates growth of skeletal muscle cells via an NFATC2-dependent pathway. *J Cell Biol* **161**, 111-8.
- Hou, X. S., and Perrimon, N. (1997). The JAK-STAT pathway in *Drosophila*. *Trends Genet* **13**, 105-10.
- Huang, Y. T., Lee, L. T., Lee, P. P., Lin, Y. S., and Lee, M. T. (2005). Targeting of focal adhesion kinase by flavonoids and small-interfering RNAs reduces tumor cell migration ability. *Anticancer Res* **25**, 2017-25.
- Huk, I., Brovkovich, V., Nanobash Vili, J., Weigel, G., Neumayer, C., Partyka, L., Patton, S., and Malinski, T. (1998). Bioflavonoid quercetin scavenges superoxide and increases nitric oxide concentration in ischaemia-reperfusion injury: an experimental study. *Br J Surg* **85**, 1080-5.
- Hunt, T. K., Jawetz, E., Hutchison, J. G., and Dunphy, J. E. (1967). A new model for the study of wound infection. *J Trauma* **7**, 298-306.
- Hurme, T., Kalimo, H., Lehto, M., and Jarvinen, M. (1991). Healing of skeletal muscle injury: an ultrastructural and immunohistochemical study. *Med Sci Sports Exerc* **23**, 801-10.
- Hwang, C., Sinskey, A. J., and Lodish, H. F. (1992). Oxidized redox state of glutathione in the endoplasmic reticulum. *Science* **257**, 1496-502.
- Ignatz, R. A., Endo, T., and Massague, J. (1987). Regulation of fibronectin and type I collagen mRNA levels by transforming growth factor-beta. *J Biol Chem* **262**, 6443-6.
- Imayasu, M., and Shimada, S. (2003). Phosphorylation of MAP kinase in corneal epithelial cells during wound healing. *Curr Eye Res* **27**, 133-41.

- Itano, N., Sawai, T., Yoshida, M., Lenas, P., Yamada, Y., Imagawa, M., Shinomura, T., Hamaguchi, M., Yoshida, Y., Ohnuki, Y., Miyauchi, S., Spicer, A. P., McDonald, J. A., and Kimata, K. (1999). Three isoforms of mammalian hyaluronan synthases have distinct enzymatic properties. *J Biol Chem* **274**, 25085-92.
- Itskovitz-Eldor, J., Schuldiner, M., Karsenti, D., Eden, A., Yanuka, O., Amit, M., Soreq, H., and Benvenisty, N. (2000). Differentiation of human embryonic stem cells into embryoid bodies compromising the three embryonic germ layers. *Mol Med* **6**, 88-95.
- Jackson, K. A., Mi, T., and Goodell, M. A. (1999). Hematopoietic potential of stem cells isolated from murine skeletal muscle. *Proc Natl Acad Sci U S A* **96**, 14482-6.
- Jackson, M. J., Jones, D. A., and Edwards, R. H. (1984). Experimental skeletal muscle damage: the nature of the calcium-activated degenerative processes. *Eur J Clin Invest* **14**, 369-74.
- Jalali, M., and Bayat, A. (2007). Current use of steroids in management of abnormal raised skin scars. *Surgeon* **5**, 175-80.
- Jankowski, R. J., Deasy, B. M., Cao, B., Gates, C., and Huard, J. (2002). The role of CD34 expression and cellular fusion in the regeneration capacity of myogenic progenitor cells. *J Cell Sci* **115**, 4361-74.
- Jiang, Q., Cao, C., Zhou, C., Song, X., Healey, S., Kouttab, N., Chu, W., Xu, A., Bi, Z., and Wan, Y. (2008). Quercetin attenuates UV- and H<sub>2</sub>O<sub>2</sub>-induced decrease of collagen type I in cultured human lens epithelial cells. *J Ocul Pharmacol Ther* **24**, 164-74.
- Jiborn, H., Ahonen, J., and Zederfeldt, B. (1978). Healing of experimental colonic anastomoses. The effect of suture technic on collagen concentration in the colonic wall. *Am J Surg* **135**, 333-40.
- Jin, E. J., Park, J. H., Lee, S. Y., Chun, J. S., Bang, O. S., and Kang, S. S. (2006). Wnt-5a is involved in TGF-beta3-stimulated chondrogenic differentiation of chick wing bud mesenchymal cells. *Int J Biochem Cell Biol* **38**, 183-95.
- Jones, D. A., Jackson, M. J., McPhail, G., and Edwards, R. H. (1984). Experimental mouse muscle damage: the importance of external calcium. *Clin Sci (Lond)* **66**, 317-22.
- Jones, N. C., Tyner, K. J., Nibarger, L., Stanley, H. M., Cornelison, D. D., Fedorov, Y. V., and Olwin, B. B. (2005). The p38alpha/beta MAPK functions as a molecular switch to activate the quiescent satellite cell. *J Cell Biol* **169**, 105-16.
- Jorgensen, L. N., Kallehave, F., Christensen, E., Siana, J. E., and Gottrup, F. (1998). Less collagen production in smokers. *Surgery* **123**, 450-5.
- Jorgensen, L. N., Kallehave, F., Karlsmark, T., and Gottrup, F. (1996). Reduced collagen accumulation after major surgery. *Br J Surg* **83**, 1591-4.

- Junqueira, L. C., Bignolas, G., and Brentani, R. R. (1979). Picrosirius staining plus polarization microscopy, a specific method for collagen detection in tissue sections. *Histochem J* **11**, 447-55.
- Junqueira, L. C., and Montes, G. S. (1983). Biology of collagen-proteoglycan interaction. *Arch Histol Jpn* **46**, 589-629.
- Junqueira, L. C., Montes, G. S., Martins, J. E., and Joazeiro, P. P. (1983). Dermal collagen distribution. A histochemical and ultrastructural study. *Histochemistry* **79**, 397-403.
- Juurlink, B. H. (2001). Therapeutic potential of dietary phase 2 enzyme inducers in ameliorating diseases that have an underlying inflammatory component. *Can J Physiol Pharmacol* **79**, 266-82.
- Juurlink, B. H., and Paterson, P. G. (1998). Review of oxidative stress in brain and spinal cord injury: suggestions for pharmacological and nutritional management strategies. *J Spinal Cord Med* **21**, 309-34.
- Kafienah, W., Al-Fayez, F., Hollander, A. P., and Barker, M. D. (2003). Inhibition of cartilage degradation: a combined tissue engineering and gene therapy approach. *Arthritis Rheum* **48**, 709-18.
- Kale, S., Biermann, S., Edwards, C., Tarnowski, C., Morris, M., and Long, M. W. (2000). Three-dimensional cellular development is essential for *ex vivo* formation of human bone. *Nat Biotechnol* **18**, 954-8.
- Kamencic, H., Griebel, R. W., Lyon, A. W., Paterson, P. G., and Juurlink, B. H. (2001). Promoting glutathione synthesis after spinal cord trauma decreases secondary damage and promotes retention of function. *FASEB J* **15**, 243-250.
- Kami, K., and Senba, E. (2002). *In vivo* activation of STAT3 signaling in satellite cells and myofibers in regenerating rat skeletal muscles. *J Histochem Cytochem* **50**, 1579-89.
- Kamihira, M., Yamada, K., Hamamoto, R., and Iijima, S. (1997). Spheroid formation of hepatocytes using synthetic polymer. *Ann N Y Acad Sci* **831**, 398-407.
- Kasemkijwattana, C., Menetrey, J., Somogyl, G., Moreland, M. S., Fu, F. H., Buranapanitkit, B., Watkins, S. C., and Huard, J. (1998). Development of approaches to improve the healing following muscle contusion. *Cell Transplant* **7**, 585-98.
- Kaufmann, U., Martin, B., Link, D., Witt, K., Zeitler, R., Reinhard, S., and Starzinski-Powitz, A. (1999). M-cadherin and its sisters in development of striated muscle. *Cell Tissue Res* **296**, 191-8.
- Keller, B. P., Wille, J., van Ramshorst, B., and van der Werken, C. (2002). Pressure ulcers in intensive care patients: a review of risks and prevention. *Intensive Care Med* **28**, 1379-88.

- Keller, G. M. (1995). *In vitro* differentiation of embryonic stem cells. *Curr Opin Cell Biol* **7**, 862-9.
- Kelm, J. M., and Fussenegger, M. (2004). Microscale tissue engineering using gravity-enforced cell assembly. *Trends Biotechnol* **22**, 195-202.
- Kempuraj, D., Madhappan, B., Christodoulou, S., Boucher, W., Cao, J., Papadopoulou, N., Cetrulo, C. L., and Theoharides, T. C. (2005). Flavonols inhibit proinflammatory mediator release, intracellular calcium ion levels and protein kinase C theta phosphorylation in human mast cells. *Br J Pharmacol* **145**, 934-44.
- Khaoustov, V. I., Darlington, G. J., Soriano, H. E., Krishnan, B., Risin, D., Pellis, N. R., and Yoffe, B. (1999). Induction of three-dimensional assembly of human liver cells by simulated microgravity. *In vitro Cell Dev Biol Anim* **35**, 501-9.
- Kheradmand, F., Folkesson, H. G., Shum, L., Derynk, R., Pytela, R., and Matthay, M. A. (1994). Transforming growth factor-alpha enhances alveolar epithelial cell repair in a new *in vitro* model. *Am J Physiol* **267**, L728-38.
- Khetani, S. R., and Bhatia, S. N. (2008). Microscale culture of human liver cells for drug development. *Nat Biotechnol* **26**, 120-6.
- Khurana, A., and Dey, C. S. (2003). p38 MAPK interacts with actin and modulates filament assembly during skeletal muscle differentiation. *Differentiation* **71**, 42-50.
- Kiistala, U., and Mustakallio, K. K. (1964). In-Vivo Separation of Epidermis by Production of Suction Blisters. *Lancet* **1**, 1444-5.
- Kim, I., Mogford, J. E., Witschi, C., Nafissi, M., and Mustoe, T. A. (2003). Inhibition of prolyl 4-hydroxylase reduces scar hypertrophy in a rabbit model of cutaneous scarring. *Wound Repair Regen* **11**, 368-72.
- Kim, S.-H., Kang, B.-Y., Nam, G.-W., Lee, H.-K., Moon, S.-J., and Jang, I.-S. (2006). Composition for promoting production of hyaluronic acid containing kaempferol and quercetin. Amorepacific Corporation, 181, Hangang-ro 2-ga, Yongsan-gu, Seoul 140-777, Korea.
- Kinbara, T., Shirasaki, F., Kawara, S., Inagaki, Y., de Crombrughe, B., and Takehara, K. (2002). Transforming growth factor-beta isoforms differently stimulate proalpha2 (I) collagen gene expression during wound healing process in transgenic mice. *J Cell Physiol* **190**, 375-81.
- Kiritsy, C. P., Lynch, A. B., and Lynch, S. E. (1993). Role of growth factors in cutaneous wound healing: a review. *Crit Rev Oral Biol Med* **4**, 729-60.

- Kivirikko, K. I., Helaakoski, T., Tasanen, K., Vuori, K., Myllyla, R., Parkkonen, T., and Pihlajaniemi, T. (1990). Molecular biology of prolyl 4-hydroxylase. *Ann N Y Acad Sci* **580**, 132-42.
- Kivirikko, K. I., and Pihlajaniemi, T. (1998). Collagen hydroxylases and the protein disulfide isomerase subunit of prolyl 4-hydroxylases. *Adv Enzymol Relat Areas Mol Biol* **72**, 325-98.
- Klopp, L. S., Simon, B. J., Bush, J. M., Enns, R. M., and Turner, A. S. (2008). Comparison of a caprolactone/lactide film (mesofol) to two polylactide film products as a barrier to postoperative peridural adhesion in an ovine dorsal laminectomy model. *Spine* **33**, 1518-26.
- Knox, P., Crooks, S., and Rimmer, C. S. (1986). Role of fibronectin in the migration of fibroblasts into plasma clots. *J Cell Biol* **102**, 2318-23.
- Kofford, M. W., Schwartz, L. B., Schechter, N. M., Yager, D. R., Diegelmann, R. F., and Graham, M. F. (1997). Cleavage of type I procollagen by human mast cell chymase initiates collagen fibril formation and generates a unique carboxyl-terminal propeptide. *J Biol Chem* **272**, 7127-31.
- Konat, G. W. (1996). Generation of high efficiency ssDNA hybridization probes by linear polymerase chain reaction (LPCR). *Scanning Microsc Suppl* **10**, 57-60.
- Korff, T., and Augustin, H. G. (1998). Integration of endothelial cells in multicellular spheroids prevents apoptosis and induces differentiation. *J Cell Biol* **143**, 1341-52.
- Korff, T., Kimmina, S., Martiny-Baron, G., and Augustin, H. G. (2001). Blood vessel maturation in a 3-dimensional spheroidal coculture model: direct contact with smooth muscle cells regulates endothelial cell quiescence and abrogates VEGF responsiveness. *FASEB J* **15**, 447-57.
- Korthuis, R. J., Grisham, M. B., Zimmerman, B. J., Granger, D. N., and Taylor, A. E. (1988). Vascular injury in dogs during ischemia-reperfusion: improvement with ATP-MgCl<sub>2</sub> pretreatment. *Am J Physiol* **254**, H702-8.
- Kosonen, O., Kankaanranta, H., Uotila, J., and Moilanen, E. (2000). Inhibition by nitric oxide-releasing compounds of E-selectin expression in and neutrophil adhesion to human endothelial cells. *Eur J Pharmacol* **394**, 149-56.
- Kovacs, E. J. (1991). Fibrogenic cytokines: the role of immune mediators in the development of scar tissue. *Immunol Today* **12**, 17-23.
- Krummel, T. M., Michna, B. A., Thomas, B. L., Sporn, M. B., Nelson, J. M., Salzberg, A. M., Cohen, I. K., and Diegelmann, R. F. (1988). Transforming growth factor beta (TGF-beta) induces fibrosis in a fetal wound model. *J Pediatr Surg* **23**, 647-52.

- Ksiazek, K., Korybalska, K., Jorres, A., and Witowski, J. (2007). Accelerated senescence of human peritoneal mesothelial cells exposed to high glucose: the role of TGF-beta1. *Lab Invest* **87**, 345-56.
- Kukkola, L., Hieta, R., Kivirikko, K. I., and Myllyharju, J. (2003). Identification and characterization of a third human, rat, and mouse collagen prolyl 4-hydroxylase isoenzyme. *J Biol Chem* **278**, 47685-93.
- Kulyk, W. M., Franklin, J. L., and Hoffman, L. M. (2000). Sox9 expression during chondrogenesis in micromass cultures of embryonic limb mesenchyme. *Exp Cell Res* **255**, 327-32.
- Kulyk, W. M., and Hoffman, L. M. (1996). Ethanol exposure stimulates cartilage differentiation by embryonic limb mesenchyme cells. *Exp Cell Res* **223**, 290-300.
- Kuo, Y. R., Wu, W. S., Jeng, S. F., Huang, H. C., Yang, K. D., Sacks, J. M., and Wang, F. S. (2005). Activation of ERK and p38 kinase mediated keloid fibroblast apoptosis after flashlamp pulsed-dye laser treatment. *Lasers Surg Med* **36**, 31-7.
- Kuroda, K., and Tajima, S. (2004). HSP47 is a useful marker for skin fibroblasts in formalin-fixed, paraffin-embedded tissue specimens. *J Cutan Pathol* **31**, 241-6.
- Labarca, C., and Paigen, K. (1980). A simple, rapid, and sensitive DNA assay procedure. *Anal Biochem* **102**, 344-52.
- Lackler, K. P., Cochran, D. L., Hoang, A. M., Takacs, V., and Oates, T. W. (2000). Development of an *in vitro* wound healing model for periodontal cells. *J Periodontol* **71**, 226-37.
- Lafyatis, R., Lechleider, R., Roberts, A. B., and Sporn, M. B. (1991). Secretion and transcriptional regulation of transforming growth factor-beta 3 during myogenesis. *Mol Cell Biol* **11**, 3795-803.
- Lalani, T., Bhol, K., Khan, I. U., and Ahmed, A. R. (1998). The scarring processes in mucosal tissues after immune injury. *Semin Arthritis Rheum* **27**, 371-81.
- Layer, P. G., Robitzki, A., Rothermel, A., and Willbold, E. (2002). Of layers and spheres: the reaggregate approach in tissue engineering. *Trends Neurosci* **25**, 131-4.
- Lazarus, G. S., Cooper, D. M., Knighton, D. R., Percoraro, R. E., Rodeheaver, G., and Robson, M. C. (1994). Definitions and guidelines for assessment of wounds and evaluation of healing. *Wound Repair Regen* **2**, 165-70.
- Leeper, D., Ayliffe, G. A., and Gilchrist, B. (1996). Postoperative wound infection. *J Wound Care* **5**, 330-4.
- Leask, A., and Abraham, D. J. (2004). TGF-beta signaling and the fibrotic response. *FASEB J* **18**, 816-27.

- Ledley, F. D., Soriano, H. E., O'Malley, B. W., Jr., Lewis, D., Darlington, G. J., and Finegold, M. (1992). DiI as a marker for cellular transplantation into solid organs. *Biotechniques* **13**, 580, 582, 584-7.
- Lee, J. P., Jalili, R. B., Tredget, E. E., Demare, J. R., and Ghahary, A. (2005). Antifibrogenic effects of liposome-encapsulated IFN-alpha2b cream on skin wounds in a fibrotic rabbit ear model. *J Interferon Cytokine Res* **25**, 627-31.
- Lee, K. S., Park, H. S., Park, S. J., Kim, S. R., Min, K. H., Jin, S. M., Li, L., and Lee, Y. C. (2006). An antioxidant modulates expression of receptor activator of NF-kappaB in asthma. *Exp Mol Med* **38**, 217-29.
- Lee, K. S., Park, H. S., Park, S. J., Kim, S. R., Min, K. H., Jin, S. M., Park, K. H., Kim, U. H., Kim, C. Y., and Lee, Y. C. (2005). A prodrug of cysteine, L-2-oxothiazolidine-4-carboxylic acid, regulates vascular permeability by reducing vascular endothelial growth factor expression in asthma. *Mol Pharmacol* **68**, 1281-90.
- Lehto, M., Duance, V. C., and Restall, D. (1985). Collagen and fibronectin in a healing skeletal muscle injury. An immunohistological study of the effects of physical activity on the repair of injured gastrocnemius muscle in the rat. *J Bone Joint Surg Br* **67**, 820-8.
- Lehto, M., Sims, T. J., and Bailey, A. J. (1985). Skeletal muscle injury--molecular changes in the collagen during healing. *Res Exp Med (Berl)* **185**, 95-106.
- LeRoy, E. C., Trojanowska, M. I., and Smith, E. A. (1990). Cytokines and human fibrosis. *Eur Cytokine Netw* **1**, 215-9.
- Lescaudron, L., Peltekian, E., Fontaine-Perus, J., Paulin, D., Zampieri, M., Garcia, L., and Parrish, E. (1999). Blood borne macrophages are essential for the triggering of muscle regeneration following muscle transplant. *Neuromuscul Disord* **9**, 72-80.
- Levenberg, S., Rouwkema, J., Macdonald, M., Garfein, E. S., Kohane, D. S., Darland, D. C., Marini, R., van Blitterswijk, C. A., Mulligan, R. C., D'Amore, P. A., and Langer, R. (2005). Engineering vascularized skeletal muscle tissue. *Nat Biotechnol* **23**, 879-84.
- Li, W., Nadelman, C., Henry, G., Fan, J., Muellenhoff, M., Medina, E., Gratch, N. S., Chen, M., Han, J., and Woodley, D. (2001). The p38-MAPK/SAPK pathway is required for human keratinocyte migration on dermal collagen. *J Invest Dermatol* **117**, 1601-11.
- Li, X., Mohan, S., Gu, W., and Baylink, D. J. (2001). Analysis of gene expression in the wound repair/regeneration process. *Mamm Genome* **12**, 52-9.
- Li, Y., Foster, W., Deasy, B. M., Chan, Y., Prisk, V., Tang, Y., Cummins, J., and Huard, J. (2004). Transforming growth factor-beta1 induces the differentiation of myogenic cells into fibrotic cells in injured skeletal muscle: a key event in muscle fibrogenesis. *Am J Pathol* **164**, 1007-19.

- Lindblad, W. J. (2000). Animal models in wound healing research: do we need more? *Wound Repair Regen* **8**, 81-2.
- Liu, D., Black, B. L., and Derynck, R. (2001). TGF-beta inhibits muscle differentiation through functional repression of myogenic transcription factors by Smad3. *Genes Dev* **15**, 2950-66.
- Liu, H., Yin, Y., and Yao, K. (2007). Construction of chitosan-gelatin-hyaluronic acid artificial skin *in vitro*. *J Biomater Appl* **21**, 413-30.
- Liu, Y., Min, D., Bolton, T., Nube, V., Twigg, S. M., Yue, D. K., and McLennan, S. V. (2009). Increased matrix metalloproteinase-9 predicts poor wound healing in diabetic foot ulcers. *Diabetes Care* **32**, 117-9.
- Lluis, F., Perdiguero, E., Nebreda, A. R., and Munoz-Canoves, P. (2006). Regulation of skeletal muscle gene expression by p38 MAP kinases. *Trends Cell Biol* **16**, 36-44.
- Lovvorn, H. N., 3rd, Cass, D. L., Sylvester, K. G., Yang, E. Y., Crombleholme, T. M., Adzick, N. S., and Savani, R. C. (1998). Hyaluronan receptor expression increases in fetal excisional skin wounds and correlates with fibroplasia. *J Pediatr Surg* **33**, 1062-9; discussion 1069-70.
- Lu, H. F., Chua, K. N., Zhang, P. C., Lim, W. S., Ramakrishna, S., Leong, K. W., and Mao, H. Q. (2005). Three-dimensional co-culture of rat hepatocyte spheroids and NIH/3T3 fibroblasts enhances hepatocyte functional maintenance. *Acta Biomater* **1**, 399-410.
- Lumb, R. A., and Bulleid, N. J. (2002). Is protein disulfide isomerase a redox-dependent molecular chaperone? *Embo J* **21**, 6763-70.
- MacDonald, S. C., Fleetwood, I. G., Hochman, S., Dodd, J. G., Cheng, G. K., Jordan, L. M., and Brownstone, R. M. (2003). Functional motor neurons differentiating from mouse multipotent spinal cord precursor cells in culture and after transplantation into transected sciatic nerve. *J Neurosurg* **98**, 1094-103.
- Mariappan, M. R., Williams, J. G., Prager, M. D., and Eberhart, R. C. (1999). "Engineering" the wound-healing process. *IEEE Eng Med Biol Mag* **18**, 22-6.
- Marotta, M., and Martino, G. (1985). Sensitive spectrophotometric method for the quantitative estimation of collagen. *Anal Biochem* **150**, 86-90.
- Martin, P., and Leibovich, S. J. (2005). Inflammatory cells during wound repair: the good, the bad and the ugly. *Trends Cell Biol* **15**, 599-607.
- Martin, P., and Parkhurst, S. M. (2004). Parallels between tissue repair and embryo morphogenesis. *Development* **131**, 3021-34.

- Massague, J. (1990). The transforming growth factor-beta family. *Annu Rev Cell Biol* **6**, 597-641.
- Matta, S. G., Wobken, J. D., Williams, F. G., and Bauer, G. E. (1994). Pancreatic islet cell reaggregation systems: efficiency of cell reassociation and endocrine cell topography of rat islet-like aggregates. *Pancreas* **9**, 439-49.
- Maytin, E. V., Chung, H. H., and Seetharaman, V. M. (2004). Hyaluronan participates in the epidermal response to disruption of the permeability barrier *in vivo*. *Am J Pathol* **165**, 1331-41.
- McCroskery, S., Thomas, M., Maxwell, L., Sharma, M., and Kambadur, R. (2003). Myostatin negatively regulates satellite cell activation and self-renewal. *J Cell Biol* **162**, 1135-47.
- McCroskery, S., Thomas, M., Platt, L., Hennebry, A., Nishimura, T., McLeay, L., Sharma, M., and Kambadur, R. (2005). Improved muscle healing through enhanced regeneration and reduced fibrosis in myostatin-null mice. *J Cell Sci* **118**, 3531-41.
- McKeown-Longo, P. J., and Mosher, D. F. (1984). Mechanism of formation of disulfide-bonded multimers of plasma fibronectin in cell layers of cultured human fibroblasts. *J Biol Chem* **259**, 12210-5.
- McLennan, I. S. (1996). Degenerating and regenerating skeletal muscles contain several subpopulations of macrophages with distinct spatial and temporal distributions. *J Anat* **188** (Pt 1), 17-28.
- McMinn, R. M. (1967). The cellular morphology of tissue repair. *Int Rev Cytol* **22**, 63-145.
- Meier, K., and Nanney, L. B. (2006). Emerging new drugs for scar reduction. *Expert Opin Emerg Drugs* **11**, 39-47.
- Meier, K., and Nanney, L. B. (2006). Emerging new drugs for wound repair. *Expert Opin Emerg Drugs* **11**, 23-37.
- Meister, A. (1994). Glutathione, ascorbate, and cellular protection. *Cancer Res* **54**, 1969s-1975s.
- Mello, M. A., and Tuan, R. S. (1999). High density micromass cultures of embryonic limb bud mesenchymal cells: an *in vitro* model of endochondral skeletal development. *In vitro Cell Dev Biol Anim* **35**, 262-9.
- Menetrey, J., Kasemkijwattana, C., Day, C. S., Bosch, P., Vogt, M., Fu, F. H., Moreland, M. S., and Huard, J. (2000). Growth factors improve muscle healing *in vivo*. *J Bone Joint Surg Br* **82**, 131-7.
- Merly, F., Lescaudron, L., Rouaud, T., Crossin, F., and Gardahaut, M. F. (1999). Macrophages enhance muscle satellite cell proliferation and delay their differentiation. *Muscle Nerve* **22**, 724-32.

- Middleton, E., Jr., Kandaswami, C., and Theoharides, T. C. (2000). The effects of plant flavonoids on mammalian cells: implications for inflammation, heart disease, and cancer. *Pharmacol Rev* **52**, 673-751.
- Minamide, L. S., and Bamburg, J. R. (1990). A filter paper dye-binding assay for quantitative determination of protein without interference from reducing agents or detergents. *Anal Biochem* **190**, 66-70.
- Minta, M., Wilk, I., and Zmudzki, J. (2005). Inhibition of cell differentiation by quinolones in micromass cultures of rat embryonic limb bud and midbrain cells. *Toxicol In vitro* **19**, 915-9.
- Mitchell, P. O., Mills, T., O'Connor, R. S., Kline, E. R., Graubert, T., Dzierzak, E., and Pavlath, G. K. (2005). Sca-1 negatively regulates proliferation and differentiation of muscle cells. *Dev Biol* **283**, 240-52.
- Miyagawa, J., Higashiyama, S., Kawata, S., Inui, Y., Tamura, S., Yamamoto, K., Nishida, M., Nakamura, T., Yamashita, S., Matsuzawa, Y., and et al. (1995). Localization of heparin-binding EGF-like growth factor in the smooth muscle cells and macrophages of human atherosclerotic plaques. *J Clin Invest* **95**, 404-11.
- Moll, I. (2003). Human skin organ culture. *Methods Mol Med* **78**, 305-10.
- Montes, G. S., and Junqueira, L. C. (1991). The use of the Picrosirius-polarization method for the study of the biopathology of collagen. *Mem Inst Oswaldo Cruz* **86 Suppl 3**, 1-11.
- Montes, G. S., Krisztan, R. M., Shigihara, K. M., Tokoro, R., Mourao, P. A., and Junqueira, L. C. (1980). Histochemical and morphological characterization of reticular fibers. *Histochemistry* **65**, 131-41.
- Motoyama, J., and Eto, K. (1994). Antisense retinoic acid receptor gamma-1 oligonucleotide enhances chondrogenesis of mouse limb mesenchymal cells *in vitro*. *FEBS Lett* **338**, 319-22.
- Moulin, V., Auger, F. A., Garrel, D., and Germain, L. (2000). Role of wound healing myofibroblasts on re-epithelialization of human skin. *Burns* **26**, 3-12.
- Mummery, C., Ward-van Oostwaard, D., Doevendans, P., Spijker, R., van den Brink, S., Hassink, R., van der Heyden, M., Opthof, T., Pera, M., de la Riviere, A. B., Passier, R., and Tertoolen, L. (2003). Differentiation of human embryonic stem cells to cardiomyocytes: role of coculture with visceral endoderm-like cells. *Circulation* **107**, 2733-40.
- Muneoka, K., Allan, C. H., Yang, X., Lee, J., and Han, M. (2008). Mammalian regeneration and regenerative medicine. *Birth Defects Res C Embryo Today* **84**, 265-80.

- Muraglia, A., Corsi, A., Riminucci, M., Mastrogiacomo, M., Cancedda, R., Bianco, P., and Quarto, R. (2003). Formation of a chondro-osseous rudiment in micromass cultures of human bone-marrow stromal cells. *J Cell Sci* **116**, 2949-55.
- Mustoe, T. A., Pierce, G. F., Thomason, A., Gramates, P., Sporn, M. B., and Deuel, T. F. (1987). Accelerated healing of incisional wounds in rats induced by transforming growth factor-beta. *Science* **237**, 1333-6.
- Myllyharju, J. (2003). Prolyl 4-hydroxylases, the key enzymes of collagen biosynthesis. *Matrix Biol* **22**, 15-24.
- Myllyharju, J., and Kivirikko, K. I. (1997). Characterization of the iron- and 2-oxoglutarate-binding sites of human prolyl 4-hydroxylase. *Embo J* **16**, 1173-80.
- Naitoh, M., Hosokawa, N., Kubota, H., Tanaka, T., Shirane, H., Sawada, M., Nishimura, Y., and Nagata, K. (2001). Upregulation of HSP47 and collagen type III in the dermal fibrotic disease, keloid. *Biochem Biophys Res Commun* **280**, 1316-22.
- Nam, T. W., Yoo, C. I., Kim, H. T., Kwon, C. H., Park, J. Y., and Kim, Y. K. (2008). The flavonoid quercetin induces apoptosis and inhibits migration through a MAPK-dependent mechanism in osteoblasts. *J Bone Miner Metab* **26**, 551-60.
- Nanney, L. B., Caldwell, R. L., Pollins, A. C., Cardwell, N. L., Opalenik, S. R., and Davidson, J. M. (2006). Novel approaches for understanding the mechanisms of wound repair. *J Invest Dermatol Symp Proc* **11**, 132-9.
- Narmoneva, D. A., Vukmirovic, R., Davis, M. E., Kamm, R. D., and Lee, R. T. (2004). Endothelial cells promote cardiac myocyte survival and spatial reorganization: implications for cardiac regeneration. *Circulation* **110**, 962-8.
- Nedelec, B., Ghahary, A., Scott, P. G., and Tredget, E. E. (2000). Control of wound contraction. Basic and clinical features. *Hand Clin* **16**, 289-302.
- Nguyen, L. M., and Witzke, J. D. (1997). Mammalian wound repair environment does not permit skeletal muscle regeneration. *Wound Repair Regen* **5**, 39-46.
- Nietfeld, J. J., and Kemp, A. (1981). The function of ascorbate with respect to prolyl 4-hydroxylase activity. *Biochim Biophys Acta* **657**, 159-67.
- Nikolaou, P. K., Seaber, A. V., Glisson, R. R., Ribbeck, B. M., and Bassett, F. H., 3rd. (1986). Anterior cruciate ligament allograft transplantation. Long-term function, histology, revascularization, and operative technique. *Am J Sports Med* **14**, 348-60.
- Nwomeh, B. C., Liang, H. X., Cohen, I. K., and Yager, D. R. (1999). MMP-8 is the predominant collagenase in healing wounds and nonhealing ulcers. *J Surg Res* **81**, 189-95.

- Nwomeh, B. C., Liang, H. X., Diegelmann, R. F., Cohen, I. K., and Yager, D. R. (1998). Dynamics of the matrix metalloproteinases MMP-1 and MMP-8 in acute open human dermal wounds. *Wound Repair Regen* **6**, 127-34.
- Oberringer, M., Meins, C., Bubel, M., and Pohlemann, T. (2007). A new *in vitro* wound model based on the co-culture of human dermal microvascular endothelial cells and human dermal fibroblasts. *Biol Cell* **99**, 197-207.
- Occleston, N. L., O'Kane, S., Goldspink, N., and Ferguson, M. W. (2008). New therapeutics for the prevention and reduction of scarring. *Drug Discov Today* **13**, 973-81.
- Ochoa, O., Sun, D., Reyes-Reyna, S. M., Waite, L. L., Michalek, J. E., McManus, L. M., and Shireman, P. K. (2007). Delayed angiogenesis and VEGF production in CCR2<sup>-/-</sup> mice during impaired skeletal muscle regeneration. *Am J Physiol Regul Integr Comp Physiol* **293**, R651-61.
- Ogawa, T., Hayashi, T., Kyoizumi, S., Kusunoki, Y., Nakachi, K., MacPhee, D. G., Trosko, J. E., Kataoka, K., and Yorioka, N. (2004). Anisomycin downregulates gap-junctional intercellular communication via the p38 MAP-kinase pathway. *J Cell Sci* **117**, 2087-96.
- Oikarinen, A., Makela, J., Vuorio, T., and Vuorio, E. (1991). Comparison on collagen gene expression in the developing chick embryo tendon and heart. Tissue and development time-dependent action of dexamethasone. *Biochim Biophys Acta* **1089**, 40-6.
- Ojha, N., Roy, S., He, G., Biswas, S., Velayutham, M., Khanna, S., Kuppusamy, P., Zweier, J. L., and Sen, C. K. (2008). Assessment of wound-site redox environment and the significance of Rac2 in cutaneous healing. *Free Radic Biol Med* **44**, 682-91.
- Ojingwa, J. C., and Isseroff, R. R. (2003). Electrical stimulation of wound healing. *J Invest Dermatol* **121**, 1-12.
- Okada, S., Nakauchi, H., Nagayoshi, K., Nishikawa, S., Miura, Y., and Suda, T. (1992). *In vivo* and *in vitro* stem cell function of c-kit- and Sca-1-positive murine hematopoietic cells. *Blood* **80**, 3044-50.
- Okubo, H., Matsushita, M., Kamachi, H., Kawai, T., Takahashi, M., Fujimoto, T., Nishikawa, K., and Todo, S. (2002). A novel method for faster formation of rat liver cell spheroids. *Artif Organs* **26**, 497-505.
- O'Leary, R., and Wood, E. J. (2003). A novel *in vitro* dermal wound-healing model incorporating a response to mechanical wounding and repopulation of a fibrin provisional matrix. *In vitro Cell Dev Biol Anim* **39**, 204-7.
- Olsen, D. R., and Uitto, J. (1989). Differential expression of type IV procollagen and laminin genes by fetal vs adult skin fibroblasts in culture: determination of subunit mRNA steady-state levels. *J Invest Dermatol* **93**, 127-31.

- Ondarza, R. N. (1989). Enzyme regulation by biological disulfides. *Biosci Rep* **9**, 593-604.
- Orzechowski, A., Grzelkowska, K., Karlik, W., and Motyl, T. (2001). Effect of Quercetin and DMSO on Skeletal Myogenesis from C2C12 Skeletal Muscle Cells with Special Reference to PKB/Akt Activity, Myogenin and Bcl-2 Expression. *Basic Appl Myol* **11**, 31-44.
- Ozer, A. F., Oktenoglu, T., Sasani, M., Bozkus, H., Canbulat, N., Karaarslan, E., Sungurlu, S. F., and Sarioglu, A. C. (2006). Preserving the ligamentum flavum in lumbar discectomy: a new technique that prevents scar tissue formation in the first 6 months postsurgery. *Neurosurgery* **59**, ONS126-33; discussion ONS126-33.
- Pallin, B., Ahonen, J., Rank, F., and Zederfeldt, B. (1975). Granulation tissue formation in viscose cellulose sponges of different design. *Acta Chir Scand* **141**, 697-701.
- Passi, A., Sadeghi, P., Kawamura, H., Anand, S., Sato, N., White, L. E., Hascall, V. C., and Maytin, E. V. (2004). Hyaluronan suppresses epidermal differentiation in organotypic cultures of rat keratinocytes. *Exp Cell Res* **296**, 123-34.
- Pavlath, G. K., and Horsley, V. (2003). Cell fusion in skeletal muscle--central role of NFATC2 in regulating muscle cell size. *Cell Cycle* **2**, 420-3.
- Pearson, D. S., Kulyk, W. M., Kelly, G. M., and Krone, P. H. (1996). Cloning and characterization of a cDNA encoding the collagen-binding stress protein hsp47 in zebrafish. *DNA Cell Biol* **15**, 263-72.
- Peng, Z., Geh, E., Chen, L., Meng, Q., Fan, Y., Sartor, M., Shertzer, H. G., Liu, Z. G., Puga, A., and Xia, Y. (2010) Inhibitor of kappaB kinase beta regulates redox homeostasis by controlling the constitutive levels of glutathione. *Mol Pharmacol* **77**, 784-92.
- Perez-Vizcaino, F., Bishop-Bailley, D., Lodi, F., Duarte, J., Cogolludo, A., Moreno, L., Bosca, L., Mitchell, J. A., and Warner, T. D. (2006). The flavonoid quercetin induces apoptosis and inhibits JNK activation in intimal vascular smooth muscle cells. *Biochem Biophys Res Commun* **346**, 919-25.
- Phan, T. T., Lim, I. J., Chan, S. Y., Tan, E. K., Lee, S. T., and Longaker, M. T. (2004). Suppression of transforming growth factor beta/smad signaling in keloid-derived fibroblasts by quercetin: implications for the treatment of excessive scars. *J Trauma* **57**, 1032-7.
- Phan, T. T., Lim, I. J., Sun, L., Chan, S. Y., Bay, B. H., Tan, E. K., and Lee, S. T. (2003). Quercetin inhibits fibronectin production by keloid-derived fibroblasts. Implication for the treatment of excessive scars. *J Dermatol Sci* **33**, 192-4.
- Phan, T. T., Wang, L., See, P., Grayer, R. J., Chan, S. Y., and Lee, S. T. (2001). Phenolic compounds of *Chromolaena odorata* protect cultured skin cells from oxidative damage: implication for cutaneous wound healing. *Biol Pharm Bull* **24**, 1373-9.

- Pierce, G. F., Mustoe, T. A., Senior, R. M., Reed, J., Griffin, G. L., Thomason, A., and Deuel, T. F. (1988). *In vivo* incisional wound healing augmented by platelet-derived growth factor and recombinant c-sis gene homodimeric proteins. *J Exp Med* **167**, 974-87.
- Pietta, P. G. (2000). Flavonoids as antioxidants. *J Nat Prod* **63**, 1035-42.
- Pimorady-Esfahani, A., Grounds, M. D., and McMEnamin, P. G. (1997). Macrophages and dendritic cells in normal and regenerating murine skeletal muscle. *Muscle Nerve* **20**, 158-66.
- Pluchino, S., Quattrini, A., Brambilla, E., Gritti, A., Salani, G., Dina, G., Galli, R., Del Carro, U., Amadio, S., Bergami, A., Furlan, R., Comi, G., Vescovi, A. L., and Martino, G. (2003). Injection of adult neurospheres induces recovery in a chronic model of multiple sclerosis. *Nature* **422**, 688-94.
- Plumb, J. A., Milroy, R., and Kaye, S. B. (1989). Effects of the pH dependence of 3-(4,5-dimethylthiazol-2-yl)-2,5-diphenyl-tetrazolium bromide-formazan absorption on chemosensitivity determined by a novel tetrazolium-based assay. *Cancer Res* **49**, 4435-40.
- Poss, K. D., Wilson, L. G., and Keating, M. T. (2002). Heart regeneration in zebrafish. *Science* **298**, 2188-90.
- Qu-Petersen, Z., Deasy, B., Jankowski, R., Ikezawa, M., Cummins, J., Pruchnic, R., Mytinger, J., Cao, B., Gates, C., Wernig, A., and Huard, J. (2002). Identification of a novel population of muscle stem cells in mice: potential for muscle regeneration. *J Cell Biol* **157**, 851-64.
- Rahban, S. R., and Garner, W. L. (2003). Fibroproliferative scars. *Clin Plast Surg* **30**, 77-89.
- Rando, T. A. (2001). Role of nitric oxide in the pathogenesis of muscular dystrophies: a "two hit" hypothesis of the cause of muscle necrosis. *Microsc Res Tech* **55**, 223-35.
- Rantanen, J., Ranne, J., Hurme, T., and Kalimo, H. (1995). Denervated segments of injured skeletal muscle fibers are reinnervated by newly formed neuromuscular junctions. *J Neuropathol Exp Neurol* **54**, 188-94.
- Raya, A., Koth, C. M., Buscher, D., Kawakami, Y., Itoh, T., Raya, R. M., Sternik, G., Tsai, H. J., Rodriguez-Esteban, C., and Izpisua-Belmonte, J. C. (2003). Activation of Notch signaling pathway precedes heart regeneration in zebrafish. *Proc Natl Acad Sci U S A* **100 Suppl 1**, 11889-95.
- Raynaud, F., Carnac, G., Marcilhac, A., and Benyamin, Y. (2004). m-Calpain implication in cell cycle during muscle precursor cell activation. *Exp Cell Res* **298**, 48-57.
- Razzaque, M. S., and Taguchi, T. (1999). The possible role of colligin/HSP47, a collagen-binding protein, in the pathogenesis of human and experimental fibrotic diseases. *Histol Histopathol* **14**, 1199-212.

- Reed, B. H., Wilk, R., and Lipshitz, H. D. (2001). Downregulation of Jun kinase signaling in the amnioserosa is essential for dorsal closure of the *Drosophila* embryo. *Curr Biol* **11**, 1098-108.
- Reid, B., Song, B., McCaig, C. D., and Zhao, M. (2005). Wound healing in rat cornea: the role of electric currents. *FASEB J* **19**, 379-86.
- Reid, W. D., and MacGowan, N. A. (1998). Respiratory muscle injury in animal models and humans. *Mol Cell Biochem* **179**, 63-80.
- Reish, R. G., and Eriksson, E. (2008). Scar treatments: preclinical and clinical studies. *J Am Coll Surg* **206**, 719-30.
- Reno, C., Marchuk, L., Sciore, P., Frank, C. B., and Hart, D. A. (1997). Rapid isolation of total RNA from small samples of hypocellular, dense connective tissues. *Biotechniques* **22**, 1082-6.
- Rice-Evans, C. A., and Miller, N. J. (1996). Antioxidant activities of flavonoids as bioactive components of food. *Biochem Soc Trans* **24**, 790-5.
- Richler, C. and D. Yaffe (1970). "The *in vitro* cultivation and differentiation capacities of myogenic cell lines." *Dev Biol* 23(1): 1-22.
- Robles, D. T., and Berg, D. (2007). Abnormal wound healing: keloids. *Clin Dermatol* **25**, 26-32.
- Robson, M. C., Mustoe, T. A., and Hunt, T. K. (1998). The future of recombinant growth factors in wound healing. *Am J Surg* **176**, 80S-82S.
- Roman, C. D., Choy, H., Nanney, L., Riordan, C., Parman, K., Johnson, D., and Beauchamp, R. D. (2002). Vascular endothelial growth factor-mediated angiogenesis inhibition and postoperative wound healing in rats. *J Surg Res* **105**, 43-7.
- Ronot, X., Doisy, A., and Tracqui, P. (2000). Quantitative study of dynamic behavior of cell monolayers during *in vitro* wound healing by optical flow analysis. *Cytometry* **41**, 19-30.
- Rothermel, A., and Layer, P. G. (2001). Photoreceptor plasticity in reaggregates of embryonic chick retina: rods depend on proximal cones and on tissue organization. *Eur J Neurosci* **13**, 949-58.
- Ruthamann, A., and Terwelp, U. (1979). Disaggregation and Reaggregation of Cells of the Primitive Metazoon *Trichoplax adhaerens*. *Differentiation* **13**, 185-198.
- Sakai, Y., Naruse, K., Nagashima, I., Muto, T., and Suzuki, M. (1996). Short-term hypothermic preservation of porcine hepatocyte spheroids using UW solution. *Cell Transplant* **5**, 505-11.

- Samuels, P., and Tan, A. K. (1999). Fetal scarless wound healing. *J Otolaryngol* **28**, 296-302.
- Sanchez Alvarado, A. (2004). Regeneration and the need for simpler model organisms. *Philos Trans R Soc Lond B Biol Sci* **359**, 759-63.
- Sandoval, M. A., and Hernandez-Vaquero, D. (2008). Preventing peridural fibrosis with nonsteroidal anti-inflammatory drugs. *Eur Spine J* **17**, 451-5.
- Sasse, J., von der Mark, H., Kuhl, U., Dessau, W., and von der Mark, K. (1981). Origin of collagen types I, III, and V in cultures of avian skeletal muscle. *Dev Biol* **83**, 79-89.
- Scheid, A., Wenger, R. H., Schaffer, L., Camenisch, I., Distler, O., Ferenc, A., Cristina, H., Ryan, H. E., Johnson, R. S., Wagner, K. F., Stauffer, U. G., Bauer, C., Gassmann, M., and Meuli, M. (2002). Physiologically low oxygen concentrations in fetal skin regulate hypoxia-inducible factor 1 and transforming growth factor-beta3. *FASEB J* **16**, 411-3.
- Schiaffino, S., Reggiani, C. (1994). Myosin isoforms in mammalian skeletal muscle. *J Appl Physiol.* **77**, 493-501.
- Schreier, T., Degen, E., and Baschong, W. (1993). Fibroblast migration and proliferation during *in vitro* wound healing. A quantitative comparison between various growth factors and a low molecular weight blood dialysate used in the clinic to normalize impaired wound healing. *Res Exp Med (Berl)* **193**, 195-205.
- Schultke, E., Kendall, E., Kamencic, H., Ghong, Z., Griebel, R. W., and Juurlink, B. H. (2003). Quercetin promotes functional recovery following acute spinal cord injury. *J Neurotrauma* **20**, 583-91.
- Schultz, E., and Jaryszak, D. L. (1985). Effects of skeletal muscle regeneration on the proliferation potential of satellite cells. *Mech Ageing Dev* **30**, 63-72.
- Seale, P., and Rudnicki, M. A. (2000). A new look at the origin, function, and "stem-cell" status of muscle satellite cells. *Dev Biol* **218**, 115-24.
- Seale, P., Sabourin, L. A., Girgis-Gabardo, A., Mansouri, A., Gruss, P., and Rudnicki, M. A. (2000). Pax7 is required for the specification of myogenic satellite cells. *Cell* **102**, 777-86.
- Sen, C. K., Khanna, S., Babior, B. M., Hunt, T. K., Ellison, E. C., and Roy, S. (2002). Oxidant-induced vascular endothelial growth factor expression in human keratinocytes and cutaneous wound healing. *J Biol Chem* **277**, 33284-90.
- Seppa, H., Grotendorst, G., Seppa, S., Schiffmann, E., and Martin, G. R. (1982). Platelet-derived growth factor in chemotactic for fibroblasts. *J Cell Biol* **92**, 584-8.
- Serbedzija, G. N., Bronner-Fraser, M., and Fraser, S. E. (1989). A vital dye analysis of the timing and pathways of avian trunk neural crest cell migration. *Development* **106**, 809-16.

- Serini, G., and Gabbiana, G. (1996). Modulation of alpha-smooth muscle actin expression in fibroblasts by transforming growth factor-beta isoforms: an *in vivo* and *in vitro* study. *Wound Repair Regen* **4**, 278-87.
- Shaffer, J. J., Taylor, S. C., and Cook-Bolden, F. (2002). Keloidal scars: a review with a critical look at therapeutic options. *J Am Acad Dermatol* **46**, S63-97.
- Shah, M., Foreman, D. M., and Ferguson, M. W. (1995). Neutralisation of TGF-beta 1 and TGF-beta 2 or exogenous addition of TGF-beta 3 to cutaneous rat wounds reduces scarring. *J Cell Sci* **108** ( Pt 3), 985-1002.
- Sharma, G. D., He, J., and Bazan, H. E. (2003). p38 and ERK1/2 coordinate cellular migration and proliferation in epithelial wound healing: evidence of cross-talk activation between MAP kinase cascades. *J Biol Chem* **278**, 21989-97.
- Shen, W., Prisk, V., Li, Y., Foster, W., and Huard, J. (2006). Inhibited skeletal muscle healing in cyclooxygenase-2 gene-deficient mice: the role of PGE2 and PGF2alpha. *J Appl Physiol* **101**, 1215-21.
- Shephard, P., Martin, G., Smola-Hess, S., Brunner, G., Krieg, T., and Smola, H. (2004). Myofibroblast differentiation is induced in keratinocyte-fibroblast co-cultures and is antagonistically regulated by endogenous transforming growth factor-beta and interleukin-1. *Am J Pathol* **164**, 2055-66.
- Sherman, L., Sleeman, J., Herrlich, P., and Ponta, H. (1994). Hyaluronate receptors: key players in growth, differentiation, migration and tumor progression. *Curr Opin Cell Biol* **6**, 726-33.
- Shi, Y., and Massague, J. (2003). Mechanisms of TGF-beta signaling from cell membrane to the nucleus. *Cell* **113**, 685-700.
- Shimizu, T., Yamato, M., Kikuchi, A., and Okano, T. (2003). Cell sheet engineering for myocardial tissue reconstruction. *Biomaterials* **24**, 2309-16.
- Shoshan, V., Campbell, K. P., MacLennan, D. H., Frodis, W., and Britt, B. A. (1980). Quercetin inhibits Ca<sup>2+</sup> uptake but not Ca<sup>2+</sup> release by sarcoplasmic reticulum in skinned muscle fibers. *Proc Natl Acad Sci U S A* **77**, 4435-8.
- Simon, H. G., Nelson, C., Goff, D., Laufer, E., Morgan, B. A., and Tabin, C. (1995). Differential expression of myogenic regulatory genes and Msx-1 during dedifferentiation and redifferentiation of regenerating amphibian limbs. *Dev Dyn* **202**, 1-12.
- Singer, A. J., and McClain, S. A. (2006). Development of a porcine incisional wound model and novel scarring scales. *Wound Repair Regen* **14**, 492-7.

- Smerdu, V., Karsch-Mizrachi, I., Campione, M., Leinwand, L., Schiaffino, S. (1994). Type IIx myosin heavy chain transcripts are expressed in type IIb fibers of human skeletal muscle. *Am J Physiol* **267** (6 Pt 1), C1723-28
- Sonnet, C., Lafuste, P., Arnold, L., Brigitte, M., Poron, F., Authier, F. J., Chretien, F., Gherardi, R. K., and Chazaud, B. (2006). Human macrophages rescue myoblasts and myotubes from apoptosis through a set of adhesion molecular systems. *J Cell Sci* **119**, 2497-507.
- Soo, C., Hu, F. Y., Zhang, X., Wang, Y., Beanes, S. R., Lorenz, H. P., Hedrick, M. H., Mackool, R. J., Plaas, A., Kim, S. J., Longaker, M. T., Freymiller, E., and Ting, K. (2000). Differential expression of fibromodulin, a transforming growth factor-beta modulator, in fetal skin development and scarless repair. *Am J Pathol* **157**, 423-33.
- Sperelakis, N. (1978). Cultured heart cell reaggregate model for studying cardiac toxicology. *Environ Health Perspect* **26**, 243-67.
- Spicer, A. P., and McDonald, J. A. (1998). Characterization and molecular evolution of a vertebrate hyaluronan synthase gene family. *J Biol Chem* **273**, 1923-32.
- Spicer, A. P., and Tien, J. Y. (2004). Hyaluronan and morphogenesis. *Birth Defects Res C Embryo Today* **72**, 89-108.
- St Pierre, B. A., and Tidball, J. G. (1994). Differential response of macrophage subpopulations to soleus muscle reloading after rat hindlimb suspension. *J Appl Physiol* **77**, 290-7.
- Stewart, E. A., Friedman, A. J., Peck, K., and Nowak, R. A. (1994). Relative overexpression of collagen type I and collagen type III messenger ribonucleic acids by uterine leiomyomas during the proliferative phase of the menstrual cycle. *J Clin Endocrinol Metab* **79**, 900-6.
- Stipcevic, T., Piljac, J., and Vanden Berghe, D. (2006). Effect of different flavonoids on collagen synthesis in human fibroblasts. *Plant Foods Hum Nutr* **61**, 29-34.
- Stojadinovic, O., Brem, H., Vouthounis, C., Lee, B., Fallon, J., Stallcup, M., Merchant, A., Galiano, R. D., and Tomic-Canic, M. (2005). Molecular pathogenesis of chronic wounds: the role of beta-catenin and c-myc in the inhibition of epithelialization and wound healing. *Am J Pathol* **167**, 59-69.
- Straface, G., Aprahamian, T., Flex, A., Gaetani, E., Biscetti, F., Smith, R. C., Pecorini, G., Pola, E., Angelini, F., Stigliano, E., Castellot, J. J., Jr., Losordo, D. W., and Pola, R. (2008). Sonic Hedgehog Regulates Angiogenesis and Myogenesis During Post-Natal Skeletal Muscle Regeneration. *J Cell Mol Med*. [Epub ahead of print]
- Styszynski, A., Wieczorowska-Tobis, K., Podkowka, R., Breborowicz, A., and Oreopoulos, D. G. (2006). Effects of glutathione supplementation during peritoneal dialysis. *Adv Perit Dial* **22**, 88-93.

- Sullivan, T. P., Eaglstein, W. H., Davis, S. C., and Mertz, P. (2001). The pig as a model for human wound healing. *Wound Repair Regen* **9**, 66-76.
- Swann, D. A., Garg, H. G., Jung, W., and Hermann, H. (1985). Studies on human scar tissue proteoglycans. *J Invest Dermatol* **84**, 527-31.
- Szpaderska, A. M., Walsh, C. G., Steinberg, M. J., and DiPietro, L. A. (2005). Distinct patterns of angiogenesis in oral and skin wounds. *J Dent Res* **84**, 309-14.
- Szpaderska, A. M., Zuckerman, J. D., and DiPietro, L. A. (2003). Differential injury responses in oral mucosal and cutaneous wounds. *J Dent Res* **82**, 621-6.
- Taguchi, T., and Razzaque, M. S. (2007). The collagen-specific molecular chaperone HSP47: is there a role in fibrosis? *Trends Mol Med* **13**, 45-53.
- Tajbakhsh, S., Vivarelli, E., Cusella-De Angelis, G., Rocancourt, D., Buckingham, M., and Cossu, G. (1994). A population of myogenic cells derived from the mouse neural tube. *Neuron* **13**, 813-21.
- Takamiya, M., Saigusa, K., and Aoki, Y. (2002). Immunohistochemical study of basic fibroblast growth factor and vascular endothelial growth factor expression for age determination of cutaneous wounds. *Am J Forensic Med Pathol* **23**, 264-7.
- Takashima, A., Billingham, R. E., and Grinnell, F. (1986). Activation of rabbit keratinocyte fibronectin receptor function *in vivo* during wound healing. *J Invest Dermatol* **86**, 585-90.
- Tamkun, J. W., and Hynes, R. O. (1983). Plasma fibronectin is synthesized and secreted by hepatocytes. *J Biol Chem* **258**, 4641-7.
- Tan, W. F., Lin, L. P., Li, M. H., Zhang, Y. X., Tong, Y. G., Xiao, D., and Ding, J. (2003). Quercetin, a dietary-derived flavonoid, possesses antiangiogenic potential. *Eur J Pharmacol* **459**, 255-62.
- Taylor, R. S., Van Buyten, J. P., and Buchser, E. (2005). Spinal cord stimulation for chronic back and leg pain and failed back surgery syndrome: a systematic review and analysis of prognostic factors. *Spine* **30**, 152-60.
- Theoharides, T. C., Alexandrakis, M., Kempuraj, D., and Lytinas, M. (2001). Anti-inflammatory actions of flavonoids and structural requirements for new design. *Int J Immunopathol Pharmacol* **14**, 119-127.
- Thibeault, S. L., Rousseau, B., Welham, N. V., Hirano, S., and Bless, D. M. (2004). Hyaluronan levels in acute vocal fold scar. *Laryngoscope* **114**, 760-4.

- Thuillier, P., Brash, A. R., Kehrer, J. P., Stimmel, J. B., Leesnitzer, L. M., Yang, P., Newman, R. A., and Fischer, S. M. (2002). Inhibition of peroxisome proliferator-activated receptor (PPAR)-mediated keratinocyte differentiation by lipoxygenase inhibitors. *Biochem J* **366**, 901-10.
- Tidball, J. G. (1995). Inflammatory cell response to acute muscle injury. *Med Sci Sports Exerc* **27**, 1022-32.
- Tidball, J. G., and Wehling-Henricks, M. (2007). Macrophages promote muscle membrane repair and muscle fibre growth and regeneration during modified muscle loading in mice *in vivo*. *J Physiol* **578**, 327-36.
- Tolg, C., Hamilton, S. R., Nakrieko, K. A., Kooshesh, F., Walton, P., McCarthy, J. B., Bissell, M. J., and Turley, E. A. (2006). Rhamm-/- fibroblasts are defective in CD44-mediated ERK1,2 mitogenic signaling, leading to defective skin wound repair. *J Cell Biol* **175**, 1017-28.
- Tomic-Canic, M., Mamber, S. W., Stojadinovic, O., Lee, B., Radoja, N., and McMichael, J. (2007). Streptolysin O enhances keratinocyte migration and proliferation and promotes skin organ culture wound healing *in vitro*. *Wound Repair Regen* **15**, 71-9.
- Toole, B. P. (1990). Hyaluronan and its binding proteins, the hyaladherins. *Curr Opin Cell Biol* **2**, 839-44.
- Toumi, H., F'Guyer, S., and Best, T. M. (2006). The role of neutrophils in injury and repair following muscle stretch. *J Anat* **208**, 459-70.
- Uaesoontrachoon, K., Yoo, H. J., Tudor, E. M., Pike, R. N., Mackie, E. J., and Pagel, C. N. (2008). Osteopontin and skeletal muscle myoblasts: association with muscle regeneration and regulation of myoblast function *in vitro*. *Int J Biochem Cell Biol* **40**, 2303-14.
- Uchida, K., Shiraishi, M., Naito, Y., Torii, Y., Nakamura, Y., and Osawa, T. (1999). Activation of stress signaling pathways by the end product of lipid peroxidation. 4-hydroxy-2-nonenal is a potential inducer of intracellular peroxide production. *J Biol Chem* **274**, 2234-42.
- van Luyn, M. J., Tio, R. A., Gallego y van Seijen, X. J., Plantinga, J. A., de Leij, L. F., DeJongste, M. J., and van Wachem, P. B. (2002). Cardiac tissue engineering: characteristics of in unison contracting two- and three-dimensional neonatal rat ventricle cell (co)-cultures. *Biomaterials* **23**, 4793-801.
- van Zuijlen, P. P., Angeles, A. P., Kreis, R. W., Bos, K. E., and Middelkoop, E. (2002). Scar assessment tools: implications for current research. *Plast Reconstr Surg* **109**, 1108-22.
- Vayalil, P. K., Iles, K. E., Choi, J., Yi, A. K., Postlethwait, E. M., and Liu, R. M. (2007). Glutathione suppresses TGF-beta-induced PAI-1 expression by inhibiting p38 and JNK MAPK and the binding of AP-1, SP-1, and Smad to the PAI-1 promoter. *Am J Physiol Lung Cell Mol Physiol* **293**, L1281-92.

- Viljanto, J. (1976). Cellstic: A device for wound healing studies in man. Description of the method. *J Surg Res* **20**, 115-9.
- Vuolteenaho, K., Moilanen, T., and Moilanen, E. (2008). Non-steroidal anti-inflammatory drugs, cyclooxygenase-2 and the bone healing process. *Basic Clin Pharmacol Toxicol* **102**, 10-4.
- Wadsworth, T. L., McDonald, T. L., and Koop, D. R. (2001). Effects of Ginkgo biloba extract (EGb 761) and quercetin on lipopolysaccharide-induced signaling pathways involved in the release of tumor necrosis factor-alpha. *Biochem Pharmacol* **62**, 963-74.
- Wang, C., Thor, A. D., Moore, D. H., 2nd, Zhao, Y., Kerschmann, R., Stern, R., Watson, P. H., and Turley, E. A. (1998). The overexpression of RHAMM, a hyaluronan-binding protein that regulates ras signaling, correlates with overexpression of mitogen-activated protein kinase and is a significant parameter in breast cancer progression. *Clin Cancer Res* **4**, 567-76.
- Wang, H., and Joseph, J. A. (1999). Structure-activity relationships of quercetin in antagonizing hydrogen peroxide-induced calcium dysregulation in PC12 cells. *Free Radic Biol Med* **27**, 683-94.
- Wang, J. F., Olson, M. E., Winkfein, R. J., Kulyk, W. M., Wright, J. B., and Hart, D. A. (2002). Molecular and cell biology of porcine HSP47 during wound healing: complete cDNA sequence and regulation of gene expression. *Wound Repair Regen* **10**, 230-40.
- Wang, Y., Belflower, R. M., Dong, Y. F., Schwarz, E. M., O'Keefe, R. J., and Drissi, H. (2005). Runx1/AML1/Cbfa2 mediates onset of mesenchymal cell differentiation toward chondrogenesis. *J Bone Miner Res* **20**, 1624-36.
- Wang, Z. L., Inokuchi, T., Ikeda, H., Baba, T. T., Uehara, M., Kamasaki, N., Sano, K., Nemoto, T. K., and Taguchi, T. (2002). Collagen-binding heat shock protein HSP47 expression during healing of fetal skin wounds. *Int J Oral Maxillofac Surg* **31**, 179-84.
- Warren, G. L., O'Farrell, L., Summan, M., Hulderman, T., Mishra, D., Luster, M. I., Kuziel, W. A., and Simeonova, P. P. (2004). Role of CC chemokines in skeletal muscle functional restoration after injury. *Am J Physiol Cell Physiol* **286**, C1031-6.
- Watanabe, K., and Yamaguchi, Y. (1996). Molecular identification of a putative human hyaluronan synthase. *J Biol Chem* **271**, 22945-8.
- Watzka, S. B., Lucien, J., Shimada, M., Edwards, V., Yeger, H., Hannigan, G., and Coles, J. G. (2000). Selection of viable cardiomyocytes for cell transplantation using three-dimensional tissue culture. *Transplantation* **70**, 1310-7.

- Wenk, J., Foitzik, A., Achterberg, V., Sabiwalsky, A., Dissemond, J., Meewes, C., Reitz, A., Brenneisen, P., Wlaschek, M., Meyer-Ingold, W., and Scharffetter-Kochanek, K. (2001). Selective pick-up of increased iron by deferoxamine-coupled cellulose abrogates the iron-driven induction of matrix-degrading metalloproteinase 1 and lipid peroxidation in human dermal fibroblasts *in vitro*: a new dressing concept. *J Invest Dermatol* **116**, 833-9.
- Whittaker, P., Kloner, R. A., Boughner, D. R., and Pickering, J. G. (1994). Quantitative assessment of myocardial collagen with picosirius red staining and circularly polarized light. *Basic Res Cardiol* **89**, 397-410.
- Whittaker, P., and Przyklenk, K. (2009). Fibrin architecture in clots: a quantitative polarized light microscopy analysis. *Blood Cells Mol Dis* **42**, 51-6.
- Wiens, R., Rak, M., Cox, N., Abraham, S., Juurlink, B. H., Kulyk, W. M., and Gough, K. M. (2007). Synchrotron FTIR microspectroscopic analysis of the effects of anti-inflammatory therapeutics on wound healing in laminectomized rats. *Anal Bioanal Chem* **387**, 1679-89.
- Wildi, S., Kleeff, J., Mayerle, J., Zimmermann, A., Bottinger, E. P., Wakefield, L., Buchler, M. W., Friess, H., and Korc, M. (2007). Suppression of transforming growth factor beta signalling aborts caerulein induced pancreatitis and eliminates restricted stimulation at high caerulein concentrations. *Gut* **56**, 685-92.
- Wilgus, T. A., Ferreira, A. M., Oberyszyn, T. M., Bergdall, V. K., and Dipietro, L. A. (2008). Regulation of scar formation by vascular endothelial growth factor. *Lab Invest* **88**, 579-90.
- Williams, J. T., Southerland, S. S., Souza, J., Calcutt, A. F., and Cartledge, R. G. (1999). Cells isolated from adult human skeletal muscle capable of differentiating into multiple mesodermal phenotypes. *Am Surg* **65**, 22-6.
- Winkler, B. S., Orselli, S. M., and Rex, T. S. (1994). The redox couple between glutathione and ascorbic acid: a chemical and physiological perspective. *Free Radic Biol Med* **17**, 333-49.
- Woessner, J. F., Jr., and Boucek, R. J. (1961). Connective tissue development in subcutaneously implanted polyvinyl sponge. I. Biochemical changes during development. *Arch Biochem Biophys* **93**, 85-94.
- Wolfman, N. M., McPherron, A. C., Pappano, W. N., Davies, M. V., Song, K., Tomkinson, K. N., Wright, J. F., Zhao, L., Sebald, S. M., Greenspan, D. S., and Lee, S. J. (2003). Activation of latent myostatin by the BMP-1/tolloid family of metalloproteinases. *Proc Natl Acad Sci U S A* **100**, 15842-6.
- Wu, Z., Woodring, P. J., Bhakta, K. S., Tamura, K., Wen, F., Feramisco, J. R., Karin, M., Wang, J. Y., and Puri, P. L. (2000). p38 and extracellular signal-regulated kinases regulate the myogenic program at multiple steps. *Mol Cell Biol* **20**, 3951-64.

- Xaymardan, M., Gibbins, J. R., and Zoellner, H. (2002). Adipogenic healing in adult mice by implantation of hollow devices in muscle. *Anat Rec* **267**, 28-36.
- Xiao, Y. Q., Malcolm, K., Worthen, G. S., Gardai, S., Schiemann, W. P., Fadok, V. A., Bratton, D. L., and Henson, P. M. (2002). Cross-talk between ERK and p38 MAPK mediates selective suppression of pro-inflammatory cytokines by transforming growth factor-beta. *J Biol Chem* **277**, 14884-93.
- Yager, D. R., Zhang, L. Y., Liang, H. X., Diegelmann, R. F., and Cohen, I. K. (1996). Wound fluids from human pressure ulcers contain elevated matrix metalloproteinase levels and activity compared to surgical wound fluids. *J Invest Dermatol* **107**, 743-8.
- Yamamoto, N., Sawada, H., Izumi, Y., Kume, T., Katsuki, H., Shimohama, S., and Akaike, A. (2007). Proteasome inhibition induces glutathione synthesis and protects cells from oxidative stress: relevance to Parkinson disease. *J Biol Chem* **282**, 4364-72.
- Yamamoto, T., Kozawa, O., Tanabe, K., Akamatsu, S., Matsuno, H., Dohi, S., and Uematsu, T. (2001). Involvement of p38 MAP kinase in TGF-beta-stimulated VEGF synthesis in aortic smooth muscle cells. *J Cell Biochem* **82**, 591-8.
- Yannas, I. V., Lee, E., and Ferdman, A. (1990). Biodegradable templates for the regeneration of tissues. United States Patent 4947840, issued on 14 August 1990.
- Yarrow, J. C., Perlman, Z. E., Westwood, N. J., and Mitchison, T. J. (2004). A high-throughput cell migration assay using scratch wound healing, a comparison of image-based readout methods. *BMC Biotechnol* **4**, 21.
- Yeow, K., Cabane, C., Turchi, L., Ponzio, G., and Derijard, B. (2002). Increased MAPK signaling during *in vitro* muscle wounding. *Biochem Biophys Res Commun* **293**, 112-9.
- Yoon, J., Shim, W. J., Ro, Y. M., and Lim, D. S. (2005). Transdifferentiation of mesenchymal stem cells into cardiomyocytes by direct cell-to-cell contact with neonatal cardiomyocyte but not adult cardiomyocytes. *Ann Hematol* **84**, 715-21.
- Zetser, A., Gredinger, E., and Bengal, E. (1999). p38 mitogen-activated protein kinase pathway promotes skeletal muscle differentiation. Participation of the Mef2c transcription factor. *J Biol Chem* **274**, 5193-200.
- Zhao, B., Cooper, L. J., Brahma, A., MacNeil, S., Rimmer, S., and Fullwood, N. J. (2006). Development of a three-dimensional organ culture model for corneal wound healing and corneal transplantation. *Invest Ophthalmol Vis Sci* **47**, 2840-6.
- Zhu, J., Li, Y., Shen, W., Qiao, C., Ambrosio, F., Lavasani, M., Nozaki, M., Branca, M. F., and Huard, J. (2007). Relationships between transforming growth factor-beta1, myostatin, and decorin: implications for skeletal muscle fibrosis. *J Biol Chem* **282**, 25852-63.

Zimmermann, W. H., and Eschenhagen, T. (2003). Cardiac tissue engineering for replacement therapy. *Heart Fail Rev* **8**, 259-69.

Zipper, L. M., and Mulcahy, R. T. (2000). Inhibition of ERK and p38 MAP kinases inhibits binding of Nrf2 and induction of GCS genes. *Biochem Biophys Res Commun* **278**, 484-92.

## Appendix 1

### Pearson Correlation Coefficient analysis of Western blot data

#### 3 day Saline treated animal group

	<b>Col 1</b>	<b>P4H</b>	<b>hsp-47</b>	<b>fibronectin</b>	<b>VEGF</b>	<b>MyoD</b>
<b>Animal 1</b>	0.48	1	0.022647	1.2	0.48	0.90653
<b>Animal 2</b>	1.21	1.01	0.872961	1.1	0.2	0.996609
<b>Animal 3</b>	0.97	0.94	0.858557	0.1	0.45	0.905149
<b>Animal 4</b>	0.18	0.9	0.76962	0.43	0.1	0.798078
<b>Animal 5</b>	0.18	0.95	0.598568	0.32	0.3	0.899026
<b>Animal 6</b>	0.1	0.99	0.535552	0.54	0.31	0.804432

#### Correlations

		<b>Col_1</b>	<b>P4H</b>	<b>hsp47</b>	<b>fibronectin</b>	<b>VEGF</b>	<b>MyoD</b>
<b>Col1</b>	Pearson Correlation	1	.356	.401	.267	.163	<b>.831*</b>
	Sig. (2-tailed)		.489	.431	.609	.757	.041
	N	6	6	6	6	6	6
<b>P4H</b>	Pearson Correlation	.356	1	-.401	.749	.369	.554
	Sig. (2-tailed)	.489		.431	.087	.472	.254
	N	6	6	6	6	6	6
<b>Hsp-47</b>	Pearson Correlation	.401	-.401	1	-.520	-.553	.116
	Sig. (2-tailed)	.431	.431		.290	.255	.827
	N	6	6	6	6	6	6
<b>fibronectin</b>	Pearson Correlation	.267	.749	-.520	1	.050	.455
	Sig. (2-tailed)	.609	.087	.290		.926	.365
	N	6	6	6	6	6	6
<b>VEGF</b>	Pearson Correlation	.163	.369	-.553	.050	1	.229
	Sig. (2-tailed)	.757	.472	.255	.926		.662
	N	6	6	6	6	6	6
<b>MyoD</b>	Pearson Correlation	<b>.831*</b>	.554	.116	.455	.229	1
	Sig. (2-tailed)	.041	.254	.827	.365	.662	
	N	6	6	6	6	6	6

\*. Correlation is significant at the 0.05 level (2-tailed).

3 day OTC treated animal group

	<b>Col 1</b>	<b>P4H</b>	<b>hsp47</b>	<b>fibronectin</b>	<b>VEGF</b>	<b>MyoD</b>
<b>Animal 1</b>	0.39	0.71	0.572898	1.1	0.5	0.80435
<b>Animal 2</b>	0.29	1	0.734155	0.9	0.6	0.863152
<b>Animal 3</b>	0.59	0.54	0.519904	0.9	0.9	0.612262
<b>Animal 4</b>	0.2	0.92	0.333608	0.1	0.2	0.900981
<b>Animal 5</b>	0.16	0.99	0.304175	0.09	0.5	0.989166
<b>Animal 6</b>	0.23	0.45	0.541185	0.1	0.2	0.965582

**Correlations**

		<b>Col_1</b>	<b>P4H</b>	<b>Hsp-47</b>	<b>fibronectin</b>	<b>VEGF</b>	<b>MyoD</b>
<b>Col 1</b>	Pearson Correlation	1	-.517	.402	.756	.797	<b>-.976**</b>
	Sig. (2-tailed)		.293	.430	.082	.058	.001
	N	6	6	6	6	6	6
<b>P4H</b>	Pearson Correlation	-.517	1	-.191	-.101	-.058	.379
	Sig. (2-tailed)	.293		.717	.849	.913	.458
	N	6	6	6	6	6	6
<b>Hsp-47</b>	Pearson Correlation	.402	-.191	1	.714	.327	-.328
	Sig. (2-tailed)	.430	.717		.111	.527	.526
	N	6	6	6	6	6	6
<b>fibronectin</b>	Pearson Correlation	.756	-.101	.714	1	.697	-.733
	Sig. (2-tailed)	.082	.849	.111		.124	.098
	N	6	6	6	6	6	6
<b>VEGF</b>	Pearson Correlation	.797	-.058	.327	.697	1	-.792
	Sig. (2-tailed)	.058	.913	.527	.124		.061
	N	6	6	6	6	6	6
<b>MyoD</b>	Pearson Correlation	<b>-.976**</b>	.379	-.328	-.733	-.792	1
	Sig. (2-tailed)	.001	.458	.526	.098	.061	
	N	6	6	6	6	6	6

\*\* . Correlation is significant at the 0.01 level (2-tailed).

3 day quercetin treated animal group

	<b>Col 1</b>	<b>P4H</b>	<b>hsp47</b>	<b>fibronectin</b>	<b>VEGF</b>	<b>MyoD</b>
<b>Animal 1</b>	0.51	0.66	0.197129	0.95	0.5	0.702755
<b>Animal 2</b>	1.4	0.75	0.547358	1	0.6	0.900551
<b>Animal 3</b>	0.75	1	0.758774	1	0.7	0.847534
<b>Animal 4</b>	0.45	0.66	0.394814	0.2	0.2	0.835191
<b>Animal 5</b>	0.37	0.89	0.852326	0.25	0.1	0.647527
<b>Animal 6</b>	0.51	0.5	0.908006	0.1	0.2	0.647262

**Correlations**

		<b>Col 1</b>	<b>P4H</b>	<b>Hsp-47</b>	<b>fibronectin</b>	<b>VEGF</b>	<b>MyoD</b>
<b>Col 1</b>	Pearson Correlation	1	.152	-.077	.642	.674	.727
	Sig. (2-tailed)		.774	.885	.170	.142	.102
	N	6	6	6	6	6	6
<b>P4H</b>	Pearson Correlation	.152	1	.212	.455	.411	.330
	Sig. (2-tailed)	.774		.686	.365	.419	.523
	N	6	6	6	6	6	6
<b>Hsp-47</b>	Pearson Correlation	-.077	.212	1	-.418	-.284	-.317
	Sig. (2-tailed)	.885	.686		.409	.586	.540
	N	6	6	6	6	6	6
<b>fibronectin</b>	Pearson Correlation	.642	.455	-.418	1	<b>.946**</b>	.560
	Sig. (2-tailed)	.170	.365	.409		.004	.248
	N	6	6	6	6	6	6
<b>VEGF</b>	Pearson Correlation	.674	.411	-.284	<b>.946**</b>	1	.655
	Sig. (2-tailed)	.142	.419	.586	.004		.158
	N	6	6	6	6	6	6
<b>MyoD</b>	Pearson Correlation	.727	.330	-.317	.560	.655	1
	Sig. (2-tailed)	.102	.523	.540	.248	.158	
	N	6	6	6	6	6	6

\*\* . Correlation is significant at the 0.01 level (2-tailed).

21 day Saline treated animal groups

	<b>Col 1</b>	<b>P4H</b>	<b>Hsp-47</b>	<b>fibronectin</b>	<b>VEGF</b>	<b>MyoD</b>
<b>Animal 1</b>	1.65	0.57	0.007813	0.8	0.2	0.632793
<b>Animal 2</b>	1.15	0.7	0.516958	0.75	0.35	0.64736
<b>Animal 3</b>	0.61	0.17	0.951516	0.4	1	0.71688
<b>Animal 4</b>	0.21	0.61	1.106112	0.11	0.92	0.504014
<b>Animal 5</b>	0.83	0.84	0.562478	0.08	0.8	0.389074

**Correlations**

		<b>Col 1</b>	<b>P4H</b>	<b>Hsp-47</b>	<b>fibronectin</b>	<b>VEGF</b>	<b>MyoD</b>
<b>Col 1</b>	Pearson Correlation	1	-.206	-.755	.596	-.474	-.153
	Sig. (2-tailed)		.695	.083	.212	.342	.772
	N	6	6	6	6	6	6
<b>P4H</b>	Pearson Correlation	-.206	1	-.323	-.035	-.503	-.109
	Sig. (2-tailed)	.695		.532	.947	.309	.837
	N	6	6	6	6	6	6
<b>Hsp-47</b>	Pearson Correlation	-.755	-.323	1	-.696	<b>.851*</b>	-.130
	Sig. (2-tailed)	.083	.532		.124	.032	.806
	N	6	6	6	6	6	6
<b>fibronectin</b>	Pearson Correlation	.596	-.035	-.696	1	-.825*	.650
	Sig. (2-tailed)	.212	.947	.124		.043	.163
	N	6	6	6	6	6	6
<b>VEGF</b>	Pearson Correlation	-.474	-.503	<b>.851*</b>	<b>-.825*</b>	1	-.423
	Sig. (2-tailed)	.342	.309	.032	.043		.403
	N	6	6	6	6	6	6
<b>MyoD</b>	Pearson Correlation	-.153	-.109	-.130	.650	-.423	1
	Sig. (2-tailed)	.772	.837	.806	.163	.403	
	N	6	6	6	6	6	6

\*. Correlation is significant at the 0.05 level (2-tailed).

21 day OTC treated animal group

	<b>Col 1</b>	<b>P4H</b>	<b>Hsp-47</b>	<b>fibronectin</b>	<b>VEGF</b>	<b>MyoD</b>
<b>Animal 1</b>	0.55	0.22	0.751364	0.08	0.5	0.393865
<b>Animal 2</b>	1.15	0.28	0.816673	0.41	0.4	0.44936
<b>Animal 3</b>	0.69	0.15	0.781308	0.44	0.2	0.536934
<b>Animal 4</b>	0.51	0.56	0.989381	0.08	0.53	0.746584
<b>Animal 5</b>	1.56	0.63	0.990881	0.26	0.9	0.758056
<b>Animal 6</b>	1.55	0.89	0.988054	0.38	0.92	0.607397

**Correlations**

		<b>Col 1</b>	<b>P4H</b>	<b>Hsp-47</b>	<b>fibronectin</b>	<b>VEGF</b>	<b>MyoD</b>
<b>Col 1</b>	Pearson Correlation	1	.662	.527	.510	.751	.302
	Sig. (2-tailed)		.152	.283	.301	.085	.560
	N	6	6	6	6	6	6
<b>P4H</b>	Pearson Correlation	.662	1	<b>.908*</b>	-.024	<b>.897*</b>	.650
	Sig. (2-tailed)	.152		.012	.964	.015	.162
	N	6	6	6	6	6	6
<b>Hsp-47</b>	Pearson Correlation	.527	<b>.908*</b>	1	-.122	.773	<b>.892*</b>
	Sig. (2-tailed)	.283	.012		.818	.072	.017
	N	6	6	6	6	6	6
<b>fibronectin</b>	Pearson Correlation	.510	-.024	-.122	1	-.133	-.169
	Sig. (2-tailed)	.301	.964	.818		.802	.749
	N	6	6	6	6	6	6
<b>VEGF</b>	Pearson Correlation	.751	<b>.897*</b>	.773	-.133	1	.526
	Sig. (2-tailed)	.085	.015	.072	.802		.283
	N	6	6	6	6	6	6
<b>MyoD</b>	Pearson Correlation	.302	.650	<b>.892*</b>	-.169	.526	1
	Sig. (2-tailed)	.560	.162	.017	.749	.283	
	N	6	6	6	6	6	6

\*. Correlation is significant at the 0.05 level (2-tailed).

21 day quercetin treated animal group

	<b>Col 1</b>	<b>P4H</b>	<b>Hsp-47</b>	<b>fibronectin</b>	<b>VEGF</b>	<b>MyoD</b>
<b>Animal 1</b>	0.69	0.41	1.101024	0.13	0.6	0.744669
<b>Animal 2</b>	0.62	0.35	0.739451	0.13	0.4	0.520345
<b>Animal 3</b>	1.68	0.28	0.745268	0.08	0.6	0.428783
<b>Animal 4</b>	0.55	0.15	0.112771	0.4	0.15	0.646695
<b>Animal 5</b>	1.95	0.9	0.993065	0.64	0.99	0.643122

**Correlations**

		<b>Col 1</b>	<b>P4H</b>	<b>Hsp-47</b>	<b>fibronectin</b>	<b>VEGF</b>	<b>MyoD</b>
<b>Col 1</b>	Pearson Correlation	1	.572	.297	.476	<b>.850*</b>	-.375
	Sig. (2-tailed)		.235	.568	.340	.032	.464
	N	6	6	6	6	6	6
<b>P4H</b>	Pearson Correlation	.572	1	.660	.578	.744	.274
	Sig. (2-tailed)	.235		.154	.230	.090	.599
	N	6	6	6	6	6	6
<b>Hsp-47</b>	Pearson Correlation	.297	.660	1	-.163	.610	.205
	Sig. (2-tailed)	.568	.154		.758	.198	.697
	N	6	6	6	6	6	6
<b>fibronectin</b>	Pearson Correlation	.476	.578	-.163	1	.475	.302
	Sig. (2-tailed)	.340	.230	.758		.341	.561
	N	6	6	6	6	6	6
<b>VEGF</b>	Pearson Correlation	<b>.850*</b>	.744	.610	.475	1	-.022
	Sig. (2-tailed)	.032	.090	.198	.341		.967
	N	6	6	6	6	6	6
<b>MyoD</b>	Pearson Correlation	-.375	.274	.205	.302	-.022	1
	Sig. (2-tailed)	.464	.599	.697	.561	.967	
	N	6	6	6	6	6	6

\*. Correlation is significant at the 0.05 level (2-tailed).

## Appendix 2

### Pearson Correlation Coefficient analysis for RNA dot blot data

#### 3 day Saline treated animal group

	Col 1( $\alpha$ 2)	Col 3 ( $\alpha$ 1)	Col 4( $\alpha$ 1)	TGF- $\beta$ 1	TGF- $\beta$ 3
<b>Animal 1</b>	1.182907	0.915435	0.272722	0.797609	0.23623
<b>Animal 2</b>	1.061624	0.7258	0.238535	0.888919	0.481482
<b>Animal 3</b>	0.476795	0.699922	0.456184	0.442193	0.571203
<b>Animal 4</b>	0.527858	0.640204	0.218011	0.053365	0.385466
<b>Animal 5</b>	0.592655	0.727128	0.176038	0.013754	0.421831
<b>Animal 6</b>	0.434129	0.638079	0.208718	0.111956	0.261611

#### Correlations

		Col 1( $\alpha$ 2)	Col 3 ( $\alpha$ 1)	Col 4( $\alpha$ 1)	TGF- $\beta$ 1	TGF- $\beta$ 3
<b>Col 1(<math>\alpha</math>2)</b>	Pearson Correlation	1	<b>.822*</b>	-.096	<b>.858*</b>	-.242
	Sig. (2-tailed)		.045	.856	.029	.644
	N	6	6	6	6	6
<b>Col 3 (<math>\alpha</math>1)</b>	Pearson Correlation	<b>.822*</b>	1	.104	.654	-.339
	Sig. (2-tailed)	.045		.844	.159	.510
	N	6	6	6	6	6
<b>Col 4(<math>\alpha</math>1)</b>	Pearson Correlation	-.096	.104	1	.333	.554
	Sig. (2-tailed)	.856	.844		.519	.255
	N	6	6	6	6	6
<b>TGF-<math>\beta</math>1</b>	Pearson Correlation	<b>.858*</b>	.654	.333	1	.072
	Sig. (2-tailed)	.029	.159	.519		.893
	N	6	6	6	6	6
<b>TGF-<math>\beta</math>3</b>	Pearson Correlation	-.242	-.339	.554	.072	1
	Sig. (2-tailed)	.644	.510	.255	.893	
	N	6	6	6	6	6

\*. Correlation is significant at the 0.05 level (2-tailed).

3 day OTC treated animal group

	<b>Col 1(<math>\alpha</math>2)</b>	<b>Col 3 (<math>\alpha</math>1)</b>	<b>Col 4(<math>\alpha</math>1)</b>	<b>TGF-<math>\beta</math>1</b>	<b>TGF-<math>\beta</math>3</b>
<b>Animal 1</b>	0.789886	0.841988	0.268747	0.198041	0.087223
<b>Animal 2</b>	1.10997	0.874313	0.32999	0.328455	0.101627
<b>Animal 3</b>	0.87796	0.784144	0.29549	0.129893	0.16222
<b>Animal 4</b>	0.766323	0.63338	0.26886	0.172031	0.318604
<b>Animal 5</b>	0.933822	0.801254	0.269984	0.174131	0.504125
<b>Animal 6</b>	0.788143	0.777029	0.222838	0.215698	0.459215

**Correlations**

		<b>Col 1(<math>\alpha</math>2)</b>	<b>Col 3 (<math>\alpha</math>1)</b>	<b>Col 4(<math>\alpha</math>1)</b>	<b>TGF-<math>\beta</math>1</b>	<b>TGF-<math>\beta</math>3</b>
<b>Col 1(<math>\alpha</math>2)</b>	Pearson Correlation	1	.631	.797	.682	-.271
	Sig. (2-tailed)		.179	.058	.135	.603
	N	6	6	6	6	6
<b>Col 3 (<math>\alpha</math>1)</b>	Pearson Correlation	.631	1	.394	.535	-.402
	Sig. (2-tailed)	.179		.439	.274	.430
	N	6	6	6	6	6
<b>Col 4(<math>\alpha</math>1)</b>	Pearson Correlation	.797	.394	1	.425	-.672
	Sig. (2-tailed)	.058	.439		.401	.144
	N	6	6	6	6	6
<b>TGF-<math>\beta</math>1</b>	Pearson Correlation	.682	.535	.425	1	-.294
	Sig. (2-tailed)	.135	.274	.401		.572
	N	6	6	6	6	6
<b>TGF-<math>\beta</math>3</b>	Pearson Correlation	-.271	-.402	-.672	-.294	1
	Sig. (2-tailed)	.603	.430	.144	.572	
	N	6	6	6	6	6

3 day quercetin treated animal group

	<b>Col 1(<math>\alpha</math>2)</b>	<b>Col 3 (<math>\alpha</math>1)</b>	<b>Col 4(<math>\alpha</math>1)</b>	<b>TGF-<math>\beta</math>1</b>	<b>TGF-<math>\beta</math>3</b>
<b>Animal 1</b>	0.82493	0.987679	0.253081	0.45282	0.135093
<b>Animal 2</b>	0.801673	1.050476	0.283341	0.258012	0.291367
<b>Animal 3</b>	1.184472	1.20092	0.130312	0.039712	0.339177
<b>Animal 4</b>	0.888079	0.84331	0.224868	0.023602	0.427502
<b>Animal 5</b>	0.959709	0.839985	0.196381	0.293294	0.833568
<b>Animal 6</b>	0.723855	0.720947	0.146545	0.272166	0.717922

**Correlations**

		<b>Col 1(<math>\alpha</math>2)</b>	<b>Col 3 (<math>\alpha</math>1)</b>	<b>Col 4(<math>\alpha</math>1)</b>	<b>TGF-<math>\beta</math>1</b>	<b>TGF-<math>\beta</math>3</b>
<b>Col 1(<math>\alpha</math>2)</b>	Pearson Correlation	1	.668	-.475	-.564	-.075
	Sig. (2-tailed)		.147	.341	.244	.888
	N	6	6	6	6	6
<b>Col 3 (<math>\alpha</math>1)</b>	Pearson Correlation	.668	1	.062	-.222	-.677
	Sig. (2-tailed)	.147		.907	.673	.140
	N	6	6	6	6	6
<b>Col 4(<math>\alpha</math>1)</b>	Pearson Correlation	-.475	.062	1	.408	-.485
	Sig. (2-tailed)	.341	.907		.422	.329
	N	6	6	6	6	6
<b>TGF-<math>\beta</math>1</b>	Pearson Correlation	-.564	-.222	.408	1	-.059
	Sig. (2-tailed)	.244	.673	.422		.911
	N	6	6	6	6	6
<b>TGF-<math>\beta</math>3</b>	Pearson Correlation	-.075	-.677	-.485	-.059	1
	Sig. (2-tailed)	.888	.140	.329	.911	
	N	6	6	6	6	6

21 day Saline treated animal group

	<b>Col 1(<math>\alpha</math>2)</b>	<b>Col 3 (<math>\alpha</math>1)</b>	<b>Col 4(<math>\alpha</math>1)</b>	<b>TGF-<math>\beta</math>1</b>	<b>TGF-<math>\beta</math>3</b>
<b>Animal 1</b>	0.908181	0.898813	0.561958	0.095241	0.372181
<b>Animal 2</b>	0.362339	0.530395	0.279121	0.02433	0.179155
<b>Animal 3</b>	1.073714	1.038854	0.83908	0.024347	0.449923
<b>Animal 4</b>	0.812988	0.998869	0.613319	0.075691	0.70089
<b>Animal 5</b>	0.491259	0.843626	0.345556	0.027657	0.477643

**Correlations**

		<b>Col 1(<math>\alpha</math>2)</b>	<b>Col 3 (<math>\alpha</math>1)</b>	<b>Col 4(<math>\alpha</math>1)</b>	<b>TGF-<math>\beta</math>1</b>	<b>TGF-<math>\beta</math>3</b>
<b>Col 1(<math>\alpha</math>2)</b>	Pearson Correlation	1	<b>.888<sup>*</sup></b>	<b>.962<sup>**</sup></b>	.013	.537
	Sig. (2-tailed)		.018	.002	.980	.271
	N	6	6	6	6	6
<b>Col 3 (<math>\alpha</math>1)</b>	Pearson Correlation	<b>.888<sup>*</sup></b>	1	<b>.886<sup>*</sup></b>	-.053	<b>.831<sup>*</sup></b>
	Sig. (2-tailed)	.018		.019	.921	.041
	N	6	6	6	6	6
<b>Col 4(<math>\alpha</math>1)</b>	Pearson Correlation	<b>.962<sup>**</sup></b>	<b>.886<sup>*</sup></b>	1	-.221	.583
	Sig. (2-tailed)	.002	.019		.674	.224
	N	6	6	6	6	6
<b>TGF-<math>\beta</math>1</b>	Pearson Correlation	.013	-.053	-.221	1	.004
	Sig. (2-tailed)	.980	.921	.674		.994
	N	6	6	6	6	6
<b>TGF-<math>\beta</math>3</b>	Pearson Correlation	.537	<b>.831<sup>*</sup></b>	.583	.004	1
	Sig. (2-tailed)	.271	.041	.224	.994	
	N	6	6	6	6	6

\*. Correlation is significant at the 0.05 level (2-tailed).

\*\* . Correlation is significant at the 0.01 level (2-tailed).

21 day OTC treated animal group

	<b>Col 1(<math>\alpha</math>2)</b>	<b>Col 3 (<math>\alpha</math>1)</b>	<b>Col 4(<math>\alpha</math>1)</b>	<b>TGF-<math>\beta</math>1</b>	<b>TGF-<math>\beta</math>3</b>
<b>Animal 1</b>	0.494146	0.613201	0.32647	0.101966	0.672425
<b>Animal 2</b>	0.725564	0.764158	0.462515	0.057863	0.456295
<b>Animal 3</b>	0.704049	0.708877	0.309812	0.063957	0.545579
<b>Animal 4</b>	1.106218	0.944009	0.72592	0.050554	0.809321
<b>Animal 5</b>	0.593757	0.728231	0.386317	0.033035	0.656581
<b>Animal 6</b>	0.841547	0.71912	0.382391	0.019847	0.742962

**Correlations**

		<b>Col 1(<math>\alpha</math>2)</b>	<b>Col 3 (<math>\alpha</math>1)</b>	<b>Col 4(<math>\alpha</math>1)</b>	<b>TGF-<math>\beta</math>1</b>	<b>TGF-<math>\beta</math>3</b>
<b>Col 1(<math>\alpha</math>2)</b>	Pearson Correlation	1	<b>.911*</b>	<b>.849*</b>	-.458	.494
	Sig. (2-tailed)		.012	.032	.361	.319
	N	6	6	6	6	6
<b>Col 3 (<math>\alpha</math>1)</b>	Pearson Correlation	<b>.911*</b>	1	<b>.948**</b>	-.391	.374
	Sig. (2-tailed)	.012		.004	.443	.465
	N	6	6	6	6	6
<b>Col 4(<math>\alpha</math>1)</b>	Pearson Correlation	<b>.849*</b>	<b>.948**</b>	1	-.207	.469
	Sig. (2-tailed)	.032	.004		.693	.348
	N	6	6	6	6	6
<b>TGF-<math>\beta</math>1</b>	Pearson Correlation	-.458	-.391	-.207	1	-.250
	Sig. (2-tailed)	.361	.443	.693		.633
	N	6	6	6	6	6
<b>TGF-<math>\beta</math>3</b>	Pearson Correlation	.494	.374	.469	-.250	1
	Sig. (2-tailed)	.319	.465	.348	.633	
	N	6	6	6	6	6

\*. Correlation is significant at the 0.05 level (2-tailed).

21 day quercetin treated animal group

	<b>Col 1(<math>\alpha</math>2)</b>	<b>Col 3 (<math>\alpha</math>1)</b>	<b>Col 4(<math>\alpha</math>1)</b>	<b>TGF-<math>\beta</math>1</b>	<b>TGF-<math>\beta</math>3</b>
<b>Animal 1</b>	0.317662	0.439117	0.155278	0.061763	0.278716
<b>Animal 2</b>	0.329453	0.513709	0.331661	0.055727	0.455142
<b>Animal 3</b>	0.270706	0.460615	0.225728	0.050907	0.349767
<b>Animal 4</b>	0.911584	0.926608	0.503845	0.079827	0.517295
<b>Animal 5</b>	0.912142	0.764158	0.424319	0.093002	0.447622

**Correlations**

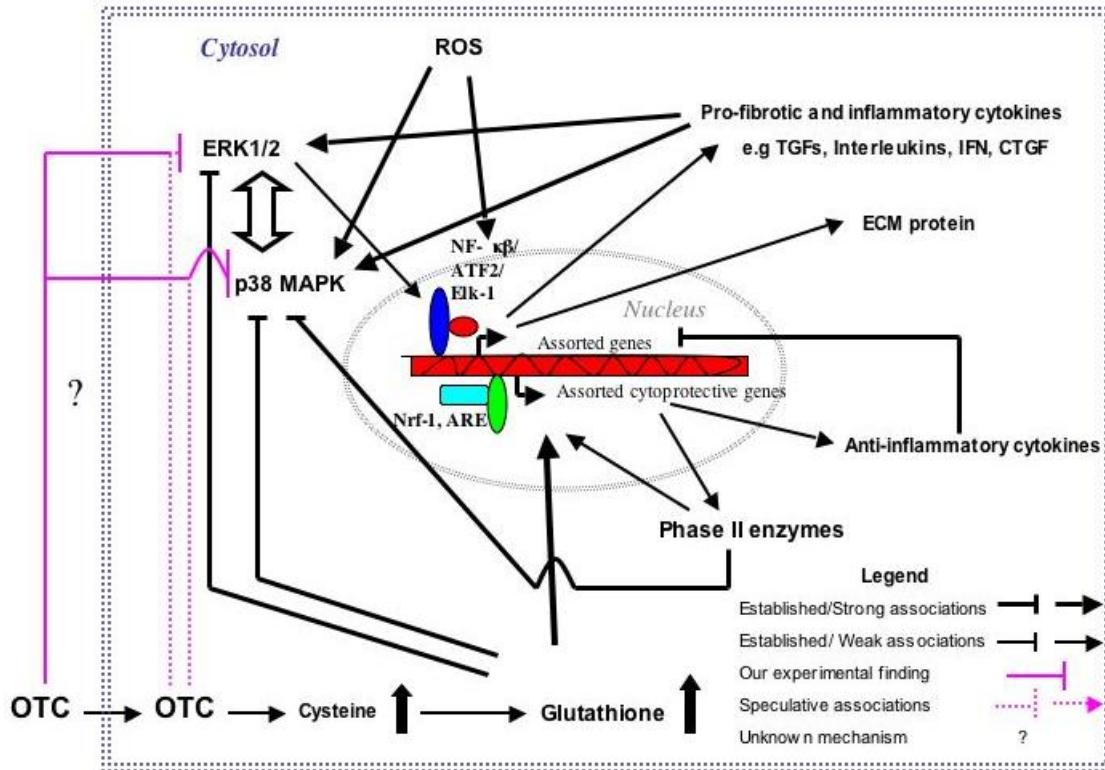
		<b>Col 1(<math>\alpha</math>2)</b>	<b>Col 3 (<math>\alpha</math>1)</b>	<b>Col 4(<math>\alpha</math>1)</b>	<b>TGF-<math>\beta</math>1</b>	<b>TGF-<math>\beta</math>3</b>
<b>Col 1(<math>\alpha</math>2)</b>	Pearson Correlation	1	<b>.958**</b>	.622	.402	.581
	Sig. (2-tailed)		.003	.188	.430	.226
	N	6	6	6	6	6
<b>Col 3 (<math>\alpha</math>1)</b>	Pearson Correlation	<b>.958**</b>	1	.692	.354	.622
	Sig. (2-tailed)	.003		.128	.492	.187
	N	6	6	6	6	6
<b>Col 4(<math>\alpha</math>1)</b>	Pearson Correlation	.622	.692	1	-.379	.043
	Sig. (2-tailed)	.188	.128		.459	.935
	N	6	6	6	6	6
<b>TGF-<math>\beta</math>1</b>	Pearson Correlation	.402	.354	-.379	1	<b>.870*</b>
	Sig. (2-tailed)	.430	.492	.459		.024
	N	6	6	6	6	6
<b>TGF-<math>\beta</math>3</b>	Pearson Correlation	.581	.622	.043	<b>.870*</b>	1
	Sig. (2-tailed)	.226	.187	.935	.024	
	N	6	6	6	6	6

\*\* . Correlation is significant at the 0.01 level (2-tailed).

\* . Correlation is significant at the 0.05 level (2-tailed).

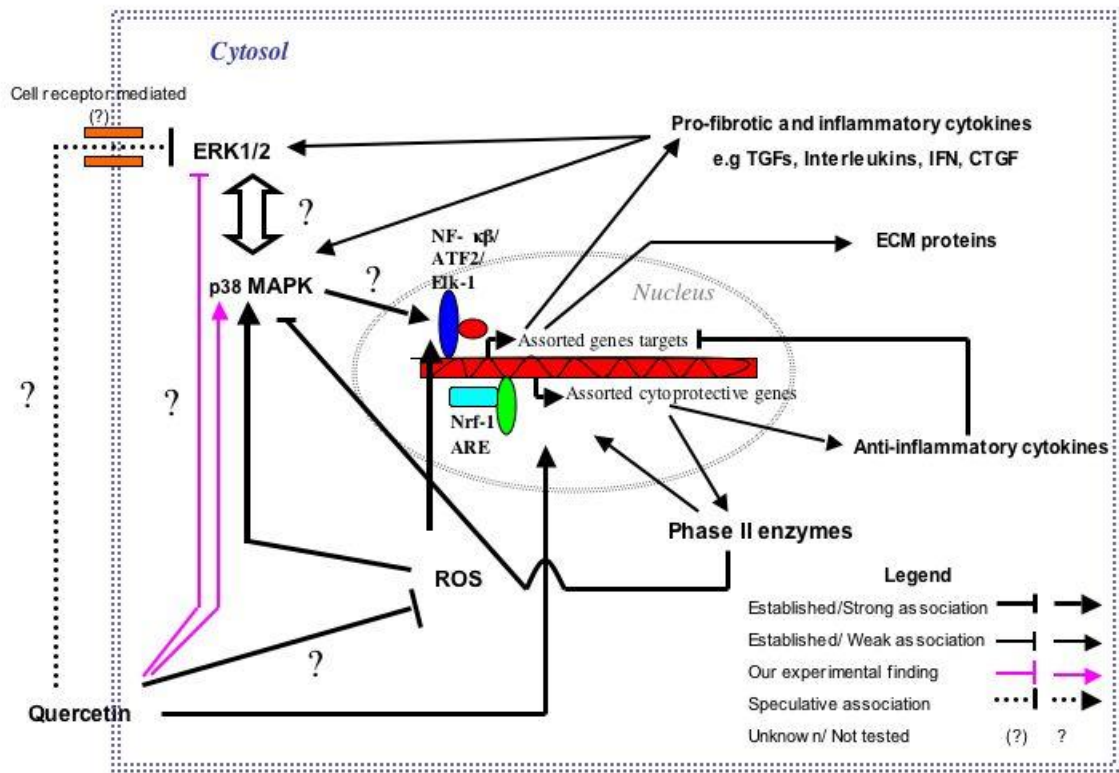
## Appendix 3

### A. Illustration suggesting why OTC might have consistently inhibited p38 MAPK and ERK1/2 signaling pathway in our *in vivo* and *in vitro* models.



In Section 2.4.1.2, we reviewed that OTC is a procysteine compound that is converted into the amino acid, cysteine, by the action of 5-oxoprolinase and this cysteine is then converted to glutathione (GSH) by  $\gamma$ -glutamylcysteine synthase within the cell. Studies have shown that OTC treatment elevates intracellular glutathione levels. Increased intracellular GSH levels have been shown to inactivate ERK and p38 MAPK signaling pathway. Moreover, GSH inhibited NF- $\kappa$ B transcription factor, which leads to activation of antioxidant response element (ARE) and Nrf-1 transcription factor. The activation of ARE and Nrf-1 promotes the expression of cytoprotective and anti-inflammatory cytokine genes, which help attenuate pro-inflammatory gene expression. Our experiments on both *in vivo* and *in vitro* model suggest consistency of OTC in inactivating ERK1/2 and p38 MAPK signaling pathway. This might be due to the ability of increased GSH level to inhibit both ERK1/2 and p38 MAPK signaling pathways simultaneously and we speculate that OTC through an alternate cytosolic pathway might induce synergistic p38 and ERK1/2 MAPK inhibitory action.

**B. Illustration suggesting the potential mechanism by which quercetin might inhibit p38 MAPK and ERK1/2 signaling pathway in our *in vitro* model**



In **Section 2.4.1.1**, we reviewed that quercetin is a naturally occurring flavanoid that has both antioxidant and antiproliferative properties. In our micromass co-culture wound model, 40  $\mu$ M quercetin treatment was found to significantly reduce phosphorylated (active) ERK1/2, while having no significant effect on p38 MAPK activation (see **Figure 70** and **71**). This may suggest that p38 MAPK activation could have promoted NF- $\kappa$ B transcription mediated signaling, which in turn promoted cytokine production. These cytokines might have been detrimental in the initiation of cell proliferative signals associated with physiochemical changes and cellular injury response *in vitro*. In addition, the quercetin inhibited ERK1/2 signaling pathway (which can also promote cell proliferation), that may have further contributed to the delay in wound closure. We speculate that quercetin might have blocked cell receptor mediated ERK1/2 signaling pathway, which would have further contributed to reduced phosphorylated (active) ERK1/2 in our *in vitro* model system.

## APPENDIX 4

### **Article published as peer-reviewed abstract or research paper**

**Abraham, S.**, Cox, N., Weins, R., Rak, M., Gough, K.M., Juurlink, B.H.J., Kulyk, W.M. (2006). Quercetin and L-2-oxothiazolidine-4-carboxylate (OTC) reduce peridural scar formation following spinal laminectomy surgery in a rat model. *The AAPS Journal*, Vol 8 (S1): 108. [http://www.aapsj.org/abstracts/NBC\\_2006/NBC06-000108.pdf](http://www.aapsj.org/abstracts/NBC_2006/NBC06-000108.pdf) (Meeting abstract)

Cox, N., **Abraham, S.**, Weins, R., Rak, M., Gough, K.M., Kulyk, W.M., Juurlink, B.H.J. (2006). The anti-inflammatory potential of Quercetin and L-2-oxothiazolidine-4-carboxylate (OTC) in scar tissue. *The FASEB Journal*, 20: LB5 (Meeting abstract)

Weins, R., Rak, M., Cox, N., **Abraham, S.**, Juurlink, B.H.J., Kulyk, W.M., Gough, K.M. (2007). Synchrotron FTIR Microspectroscopic analysis of the effects of anti-inflammatory therapeutics on wound healing in Laminectomized rats. *Analytical & Bioanalytical Chemistry*, 387:1679-89, doi: 10.1007/s00216-006-1095-9 (Research article)

**Abraham, S.**, Basiri, M., Cox, N., Juurlink, B.H.J., Kulyk, W.M. (2008). Development of a novel co-culture based *in-vitro* model system to study wound scarring. *The AAPS Journal*, Vol 10 (S1): 714. [http://www.aapsj.org/abstracts/NBC\\_2008/NBC08-000714.PDF](http://www.aapsj.org/abstracts/NBC_2008/NBC08-000714.PDF) (Meeting abstract)

### **Referred Paper and Poster presentation**

**Abraham, S.**, Cox, N., Weins, R., Rak, M., Gough, K.M., Juurlink, B.H.J., Kulyk, W.M. Quercetin and L-2-oxothiazolidine-4-carboxylate (OTC) reduce peridural scar formation following spinal laminectomy surgery in a rat model. *2006 AAPS National Biotechnology Conference, Boston, MA, USA*

Cox, N., **Abraham, S.**, Weins, R., Rak, M., Gough, K.M., Kulyk, W.M., Juurlink, B.H.J. The anti-inflammatory potential of Quercetin and L-2-oxothiazolidine-4-carboxylate (OTC) in scar tissue. *2006 Experimental Biology Conference, San Francisco, CA, USA*

**Abraham, S.**, Basiri, M., Juurlink, B.H.J., Kulyk, W.M. Development of a novel co-culture based *in-vitro* model system to study wound scarring. *2008 AAPS National Biotechnology Conference, Toronto, ON, Canada*